# COMPOSITIONAL CHANGE OF MELTWATER INFILTRATING FROZEN GROUND

GRO LILBAEK

2009

# COMPOSITIONAL CHANGE OF MELTWATER INFILTRATING FROZEN GROUND

A Thesis Submitted to
the College of Graduate Studies and Research
in Partial Fulfillment of the Requirements
for the Degree of Doctor of Philosophy
in the Department of Geography and Planning
(Centre for Hydrology)
University of Saskatchewan
Saskatoon, Canada

by

GRO LILBÆK

# PERMISSION TO USE

In presenting this thesis in partial fulfilment of the requirements for a Postgraduate degree from the University of Saskatchewan, I agree that the Libraries of this University may make it freely available for inspection. I further agree that permission for copying of this thesis in any manner, in whole or in part, for scholarly purposes may be granted by the professor who supervised my thesis work or, in their absence, by the Head of the Department or the Dean of the College in which my thesis work was done. It is understood that any copying or publication or use of this thesis or parts thereof for financial gain shall not be allowed without my written permission. It is also understood that due recognition shall be given to me and to the University of Saskatchewan in any scholarly use which may be made of any material in my thesis.

Requests for permission to copy or to make other use of material in this thesis in whole or part should be addressed to:

Head of the Department of Geography and Planning
University of Saskatchewan
Saskatoon, Saskatchewan
S7N 5C8, Canada

# ABSTRACT

Meltwater reaching the base of the snowpack may either infiltrate the underlying stratum, run off, or refreeze, forming a basal ice layer. Frozen ground underneath a melting snowpack constrains infiltration promoting runoff and refreezing. Compositional changes in chemistry take place for each of these flowpaths as a result of phase change, contact between meltwater and soil, and mixing between meltwater and soil water. Meltwater ion concentrations and infiltration rate into frozen soils both decline rapidly as snowmelt progresses. Their temporal association is highly non-linear and the covariance must be compensated for in order to use time-averaged values to calculate chemical infiltration over a melt event. This temporal covariance is termed 'enhanced infiltration' and represents the additional ion load that infiltrates due to the timing of high meltwater ion concentration and infiltration rate. Both theoretical and experimental assessments of the impact of enhanced infiltration showed that it causes a greater ion load to infiltrate leading to relative dilute runoff water. Sensitivity analysis showed that the magnitude of enhanced infiltration is governed by initial snow water equivalent, average melt rate, and meltwater ion concentration factor. Based on alterations in water chemistry due to various effects, including enhanced infiltration, three major flowpaths could be distinguished: overland flow, organic interflow, and mineral interflow. Laboratory experiments were carried out in a temperature-controlled environment to identify compositional changes in water from these flowpaths. Samples of meltwater, runoff, and interflow were filtered and analyzed for major anions and cations. Chemical signatures for each flowpath were determined by normalizing runoff and interflow concentrations using meltwater concentrations. Results showed that changes in ion concentrations were most significant for $H^+$, $NO_3^-$, $NH_4^+$, $Mg^{2+}$, and $Ca^{2+}$. Repeated flushes of meltwater through each interflowpath caused a washout of ions. In the field, samples of soil water and ponding water were collected daily from a Rocky Mountain hillslope during snowmelt. Their normalized chemical compositions were compared to the laboratory-identified signatures to evaluate the flowpath. The majority of the flowpaths sampled had chemical signatures, which indicated mineral interflow, only 10% showed unmixed organic interflow.

# ACKNOWLEDGEMENTS

To My Family

Who Helped Making This Journey an Adventure

# TABLE OF CONTENTS

# LIST OF TABLES

# LIST OF FIGURES

# LIST OF SYMBOLS

$A$        Area [m$^2$]

$B$        Fraction of ice in a unit mass of wet snow (usually 0.95 to 0.97)

$c$        Speed of light [$3 \cdot 10^8$ m s$^{-1}$]

$c_i$        Specific heat of ice [kJ kg$^{-1}$ K$^{-1}$]

$C$        Location coefficient [dimensionless]

$C_i(t)$        Concentration of an ion $i$ at time $t$ [meq m$^{-3}$]

$C_i(0)$        Initial concentration of an ion $i$ in the snowpack [meq m$^{-3}$]

$CF$        Concentration factor; $CF = C_i(t)/C_i(0)$ [(meq m$^{-3}$) (meq m$^{-3}$)$^{-1}$]

$CF_{max}$        Concentration factor of the initial meltwater [(meq m$^{-3}$) (meq m$^{-3}$)$^{-1}$]

$d$        Depth of ring insertion [m]

$d_s$        Depth of snowpack [m]

$dU/dt$        Change in internal energy of the snowpack [W m$^{-2}$]

$dz/dt$        Rate of ice growth [m s$^{-1}$]

$E$        Evaporation rate [kg s$^{-1}$ m$^{-2}$]

$ER$        Enrichment ratio; $ER$=RW/SW [(meq m$^{-3}$) (meq m$^{-3}$)$^{-1}$]

$ER_{max}$        Greatest enrichment ratio [(meq m$^{-3}$) (meq m$^{-3}$)$^{-1}$]

$f(t)$        Infiltration rate [kg s$^{-1}$ m$^{-2}$]

$F$        Cumulative mass of water infiltrating [kg m$^{-2}$]

$F_i$        Cumulative load of an ion that infiltrates [meq m$^{-2}$]

$g$        Acceleration of gravity [m s$^{-2}$]

$G$        dimensionless factor

$H_l$        Steady pressure head [m]

$i$        Van't Hoff factor; equal to the number of moles of ions per mole of electrolyte

$ICB$        Ion charge balance [dimensionless]

$k$        Leaching coefficient [dimensionless]

$k_f$        Molal freezing point constant [ºC kg mol$^{-1}$], [ºC $m^{-1}$]

$K$        Saturated hydraulic conductivity [m s$^{-1}$]

$K_a$      Dielectric constant, can also be written $\varepsilon_r$

$K_{a\text{-}field}$      Measured $K_a$ in the field

$K_{adj}$      Adjusted $K_a$ to a standard temperature (25 ºC)

$K_f$      Molal freezing point constant [ºC kg mol$^{-1}$], [ºC $m^{-1}$]

$K_{fs}$      Field saturated hydraulic conductivity [m s$^{-1}$]

$L$      Length of TDR probe [m]

$L_f$      Latent heat of fusion [kJ kg$^{-1}$]

$m$      Molality of the dissolved solute [mol kg$^{-1}$]

$M$      Melt rate [kg m$^{-2}$ s$^{-1}$]

$\overline{M}$      Average melt rate [kg m$^{-2}$ s$^{-1}$]

$M_s$      Dry mass of solid; i.e. mineral soil or organic material [kg]

$n$      Porosity [dimensionless]

$n$      Number of samples

$NEI$      Normalized enhanced infiltration [(meq m$^{-2}$) (meq m$^{-2}$)$^{-1}$]

$NR_i$      Normalized infiltration excess ion load [(meq m$^{-2}$) (meq m$^{-2}$)$^{-1}$]

$1-NR_i$      Reduction in infiltration excess ion load [(meq m$^{-2}$) (meq m$^{-2}$)$^{-1}$]

$p_w$      Pressure of water [m]

$P$      Water available for infiltration, i.e. snow meltwater [kg m$^{-2}$]

$P_i$      Meltwater ion load [meq m$^{-2}$]

$Q$      Rate of heat released by the growth of the basal ice layer [kg m$^{-2}$ s$^{-1}$]

$Q_E$      Latent heat flux [W m$^{-2}$]

$Q_G$      Ground heat flux [W m$^{-2}$]

$Q_H$      Sensible heat flux [W m$^{-2}$]

$Q_M$      Energy available for melting a unit volume of snow [W m$^{-2}$]

$Q_N$      Net radiation (longwave and shortwave) [W m$^{-2}$]

$Q_R$      Advective heat flux (derived from precipitation)

$r$      Radius of the inner ring of a double infiltrometer

$R$      Infiltration excess water; i.e. water ponding at the surface or runs off at the surface [kg m$^{-2}$]

$R_i$      Infiltration excess ion load [meq m$^{-2}$]

$S$      TDR rod spacing [m]

$\Delta S$      Change in storage [$m^3\ m^{-2}\ m^{-1}$]

$S^*$      Effective water saturation of snow [$m^3\ m^{-3}$]

$S_0$      Soil moisture at the surface [$mm^3\ mm^{-3}$]

$S_I$      Average soil saturation (water + ice) of the top 0.4 m of the soil [$mm^3\ mm^{-3}$]; $S_I = \theta/\phi$. In Equation 2.3 it is only for the top 0.3 m

$S_w$      Effective water saturation immediately above the wetting front [$m^3\ m^{-3}$]

$SWE$      Initial snow water equivalent [$kg\ m^{-2}$]

$SWE_m$      Snow meltwater [mm]

$t, t_n, t_{n-1}$      Time [s, h, or d]

$t_1, t_2$      Time [s, h, or d]

$t_o$      Infiltration opportunity time in hours [h]; estimated as $t_o = SWE/\overline{M}$

$t/t_o$      Fraction of infiltration opportunity time

$t_r$      Travel time for an electromagnetic wave [s]

$T_I$      Average initial soil temperature within the top 0.4 m of the soil [K]

$T_s$      Snow temperature immediately below the wetting front [K]

$\Delta T_f$      Freezing point depression [$^{o}$C]

$u$      Vertical meltwater flux [$m^3\ m^{-2}\ s^{-1}$]

$V_t$      Total sample volume [$m^3$]

$z$      Depth [m]

### Greek Letters

$\alpha$      Soil texture parameter [$m^{-1}$]

$\varepsilon_r$      Dielectric constant or permittivity; can also be written $K_a$

$d\xi/dt$      Rate of movement of a one-dimensional wetting front [$mm\ h^{-1}$]

$\phi$      Soil porosity [$mm^3\ mm^{-3}$]

$\phi_s$      Snow porosity [$mm^3\ mm^{-3}$]

$\kappa_s$      Permeability of snow [$m\ s^{-1}$]

$\mu_w$      Viscosity of water [$kg\ m^{-1}\ s^{-1}$]

$\omega$      Gravimetric soil moisture content [$g\ g^{-1}$]

θ        Average volumetric soil moisture (water + ice) [$mm^3$ $mm^{-3}$]; in Equation 5.5 it refers to the average volumetric soil moisture at the beginning of infiltration

$\rho_b$        Dry bulk density [$kg\ m^{-3}$]

$\rho_i$        Density of ice [$kg\ m^{-3}$]

$\rho_s$        Density of snow [$kg\ m^{-3}$]

$\rho_s$        Soil particle density [$kg\ m^{-3}$]

$\rho_w$        Density of water [$kg\ m^{-3}$]

*Abbreviations*

ABS        Acrylonitrile butadiene styrene

Ave        Average

BI        Overland flow due to formation of a basal ice layer

BW        Runoff water, which had sustained contact with a basal ice layer

CEL        Cryospheric environmental laboratory, located at Centre for Hydrology, University of Saskatchewan

DDI        Deionized distilled water

DI        Distilled water

DOC        Dissolved organic carbon

HDPE        High density polyethylene

JD        Julian Day

LAI        Leaf area index

LDPE        Low density polyethylene

MIF        Mineral interflow

MIF*        Mineral interflow with evidence of substantial organic contact

MSW        Mineral soil water

MW        Runoff water, which had sustained contact with a mineral soil layer

n.d.        Below detection limits

OIF        Organic interflow

OSW    Organic soil water; OSW* is organic soil water collected at the overland flow installation

OW    Runoff water, which had sustained contact with an organic layer

PE    Polyethylene

PW    Ponding water; PW-site refers to ponding water at the observation site; PW-snow refers to ponding water on top of snow/ice; and PW-soil refers to ponding water on top of soil

RMSD   Root mean square difference

RW    Runoff water, which had sustained contact with either a basal ice layer, an organic layer, or a mineral soil layer

Stdev   Standard deviation

SW    Snowmelt water, which had not sustained contact with the underlying stratum

TC    Thermocouples

TDR   Time domain reflectometry

# CHAPTER 1

# INTRODUCTION

The seasonal snowcover accumulates ions as wet and dry deposition over the course of winter, releasing them rapidly at the time of spring snowmelt. This is a major event in terrestrial and aquatic ecosystems (Jones, 1999) that has been related to episodic acidification of lakes and streams (Davies *et al*., 1987; Ikuta *et al*., 1999; Schindler, 1999) and to changes in soil chemistry and microbiology (Abrahams *et al*., 1989). Ion fractionation and preferential elution of ions in snowpacks take place during melt, resulting in a 2- to 7-fold enrichment of major ions in the initial meltwater and characteristic sequences of peak ion concentration in meltwater (Johannessen and Henriksen, 1978; Tranter, 1991). As melting proceeds, meltwater ion concentrations decrease exponentially; up to 80% of the solute within a snowpack may be eluted within the initial third of the melt period. This leads to a change in the proportional ion composition of the snowpack and meltwater during snowmelt.

In land surfaces typical of many cold regions, meltwater at the base of the snowpack can be partitioned into ponded water, basal ice, overland flow, organic layer storage, organic interflow, and/or infiltration to frozen mineral soils (Figure 1.1). Partitioning depends on factors such as duration and rate of snowmelt, soil temperature, available pore space, macropores, hillslope gradient, depressional storage availability, hydraulic conductivity of the frozen organic layer, and the infiltrability of the frozen mineral soil (Romanov *et al*., 1974; Gray *et al*., 1985b; Zhao *et al*., 1997). The various flowpaths attenuate and delay the flow to different extents (Kirkby, 1988). Infiltrated water can be stored as soil moisture (frozen or liquid), drained as mineral interflow, or percolate deeper to become part of the groundwater system. The water can remain stored in the soil for long periods and then eventually contribute to evaporation or relatively slow groundwater or interflow contributions to streamflow. Surface flow and organic
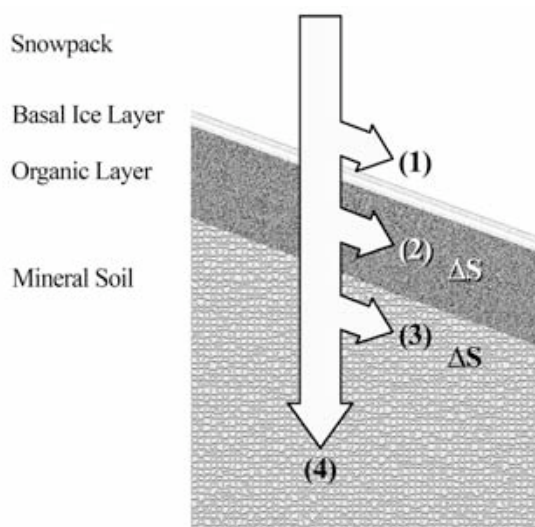
*Figure 1.1. Below a melting snowpack, meltwater is partitioned into (1) ponded water, basal ice storage, and overland flow, (2) organic layer storage (ΔS) and interflow, (3) infiltration to frozen mineral soils with subsequent storage (ΔS) or interflow and (4) percolation to groundwater.*

interflow and storage are termed 'infiltration excess' and primarily end up as rapid runoff, even where there is a well developed organic layer (Carey and Woo, 2001; Quinton and Pomeroy, 2006). In areas with seasonally frozen ground or permafrost, infiltration excess often dominates during snowmelt (e.g. Pomeroy and Brun, 2001).

Better understanding of the influence hydrological processes and pathways have on the fate of chemicals, deposited either as snow or directly on the ground surface is essential to evaluate the effect that meltwater chemistry may have on ecosystems (Stein *et al*., 1986; Maulé and Stein, 1990; Iida *et al*., 2000; Tranter and Jones, 2001; Quinton and Pomeroy, 2006). Soil interflow, during infiltration of snowmelt water, can become highly concentrated and when mixed with infiltration excess water can dramatically change surface water chemistry (Peters and Driscoll, 1987). Thus, partitioning of the snowmelt chemical load via infiltration is important in determining the aquatic or terrestrial sink for ions and the timing of ion delivery to water bodies.

Temporal and spatial variation in snow accumulation and melt between slopes within a basin as a result of variations in aspect, gradient, and vegetation may lead to asynchronous runoff generation (Davis, 1991; Woo, 2005). The runoff water may reach the channel network through various flowpaths which alters the chemical composition

differently; however, the processes which regulate the solute chemistry of the snow meltwater and its modification before entering the hydrological network are not very well understood (Christophersen *et al.*, 1984; Stottlemyer *et al.*, 1997; Campbell *et al.*, 2004; Quinton and Pomeroy, 2006). Being able to model the mass of water that infiltrates frozen ground (Gray *et al.*, 1985b; Zhao *et al.*, 1997) is important since the degree to which meltwater infiltrates the soil is considered a great regulator of the solute added to streams and lakes (Stottlemyer *et al.*, 1997).

There have been several studies of the compositional change in stream and lake water chemistry that can be observed during spring melt (e.g. Maulé and Stein, 1990; Shanley and Chalmer, 1999; Jones and Pomeroy, 2001); however, streams and lakes accumulate the compositional changes within a whole watershed and are therefore most often used to evaluate large-scale processes and the overall influences that chemical alterations will have on ecosystems. Still, the influence and the different processes that take place once meltwater gets in contact with frozen soil are not very well understood (Maulé and Stein, 1990; Shanley and Chalmer, 1999). The chemical interactions are complex due to the presence of a mixture of liquid water and ice containing solvent, the exclusion of impurities from ice during freezing, and changes in thermal gradients, which controls the movement of the water (e.g. Kane and Stein, 1983; Grant, 2000). Studying chemical processes that take place on the scale of a hillslope might elucidate some of the mechanisms governing chemical changes in spring streamflow.

***Parts of this thesis have previously been published as:***

Lilbæk G and Pomeroy JW. 2007. Modelling enhanced infiltration of snowmelt ions into frozen soil. *Hydrological Processes* **21**: 2641-2649. DOI: 10.1002/hyp.6788; erratum in 10.1002/hyp.6905.

Lilbæk G and Pomeroy JW. 2008. Ion enrichment of snowmelt runoff water caused by basal ice formation. *Hydrological Processes* **22**: 2758-2766. DOI: 10.1002/hyp.7028.

# CHAPTER 2

# BACKGROUND

In the northern hemisphere, more than 50% of the land surface receives precipitation in the form of snow each year (Groisman and Davies, 2001), compared to only ~2% of the land surface in the southern hemisphere, excluding Antarctica (Brown and Goodison, 2005). Some areas rely on this annual snowcover to recharge soil moisture and groundwater storage through infiltration and replenishment of reservoirs, lakes, and rivers through runoff. When melting initiates, the soil underneath the melting snowcover may be frozen, limiting infiltration, as part or all of the pore water has turned into ice (Komarov and Makarova, 1973). Frozen ground can be found in areas where the air temperature is below the freezing point for parts of the year and a large part of the annual precipitation falls as snow (e.g. Pomeroy and Brun, 2001). In the northern hemisphere (20º N to 90º N), 24% of the exposed land surface is covered with permafrost (frozen ground that has remained at or below 0°C for at least two consecutive years; van Everdingen, 1998) and 55-60% experience seasonally frozen ground (Figure 2.1) (Brown *et al*., 1997; Zhang *et al*., 2000). Parts of Canada, Greenland, Norway, and Russia are among the regions in the northern hemisphere where seasonally frozen ground or permafrost occurs.

## 2.1 Snowpacks

Snow crystals are formed high in the atmosphere where the temperature is below 0 ºC and supercooled water droplets can be found along with atmospheric particles (aerosols) suitable as condensation nuclei (Schemenauer *et al*., 1981). These nuclei consist mainly of clay, sea salt, and/or organic debris in form of combustion products (i.e. $NO_x$ and $SO_2$) and hygroscopic chemical compounds (e.g. Davis, 1991; Tranter and Jones, 2001).

*Figure 2.1. The extent of permafrost in the northern hemisphere (UNEP/GRID-Arendal, 2007).*

As supercooled water droplets condense onto an aerosol an ice crystal is formed. Continuous growth of the ice crystals occurs either by vapour transport, which produces snow crystals, or by collision with other supercooled water droplets, which results in hail or graupel particles. As the crystals become heavier their downward velocity increases. At some point, the internal lift forces of the cloud are overcome by Earth's gravity and the crystals fall from the cloud to the ground (e.g. Schemenauer *et al*., 1981).

Snowpacks are often formed from several snowfall events (Langham, 1981). Variations in meteorological conditions such as e.g. air temperature, humidity, and wind speed during each event influence on the type of snow crystal formed (LaChapelle, 1969). The wind speed near the ground surface at time of deposition determines how the arriving crystals are packed. Their combined effect results in a highly stratified snowpack (Langham, 1981). Following deposition, redistribution of snow by wind and surface melt due to solar radiation may result in further stratification as the surfaces are covered by subsequent snowfall events.

## 2.1.1 Metamorphism

Different temperature and humidity conditions exist near the ground surface than in the atmosphere, such that crystals are no longer stable and as a result undergo metamorphism (e.g. LaChapelle, 1969; Langham, 1981). This causes the individual snow crystals to reduce their free surface energy leading to a thermodynamically more favourable state; they metamorphose towards a spherical shape (LaChapelle, 1969; Langham, 1981). Snow metamorphism is influenced by variables such as the snowpack's density, porosity, temperature and temperature gradient, and in particular the amount of liquid water filling the snow pore space (e.g. Davis, 1991; Pomeroy and Brun, 2001). In 1990, an international classification system of seasonal snow on the ground was created based on fundamental principles, representing both crystal form and formation process (Table 2.1) (Colbeck *et al*., 1990).

Following deposition, before a significant temperature gradient has been established, the crystals start to round (type 3a-c in Table 2.1) (e.g. Langham, 1981; Colbeck, 1986). Initially, the snow crystals are reduced to well-bonded, rounded grains through mass transfer due to vapour pressure differences across the surface of the individual crystals. Later, vapour pressure differences between grains result in mass transfer from grains with a higher vapour pressure (smaller grains) to grains with a lower vapour pressure (larger grains). The process is referred to as 'equilibrium metamorphism' as it only occurs in snowpacks that have a relatively uniform temperature. It is most rapid at temperatures near 0 ºC and can therefore be observed when the snowpack becomes isothermal just prior to melt; the rate of change diminishing in intensity as the temperature decreases.

Variations in snowpack temperature with depth are common following deposition and typically develop because of radiative cooling of the snow surface, warm and/or wet soils, and the low thermal conductivity of the snowpack (e.g. Pomeroy and Brun, 2001). The variation in temperature causes changes in the saturation water vapour pressure, which results in sublimating snow to be transferred across the air-filled pore space from the lower (warmer) sides of pore spaces and condensing on the upper (colder) side of the space (Langham, 1981; Colbeck *et al*., 1990). Consequently, cold crystals in the upper snowpack grow at the expense of warmer crystals in the lower snowpack. The process is

*Table 2.1. International classification of snow crystals (adapted from Colbeck et al., 1990, by Pomeroy and Brun, 2001).*

| | Basic classification | Shape | Process classification |
|---|---|---|---|
| 1 | Precipitation particles | a) Columns<br>b) Needles<br>c) Plates<br>d) Stellar dendrites<br>e) Irregular crystals<br>f) Graupel<br>g) Hail<br>h) Ice pellets | a-g) Cloud-derived falling snow<br>h) frozen rain |
| 2 | Decomposing and fragmented precipitation particles | a) Partly rounded particles<br>b) Packed shard fragments | a) Freshly deposited snow<br>b) Wind-packed snow |
| 3 | Rounded grains | a) Small rounded particles<br>b) Large rounded particles<br>c) Mixed forms | a-c) Dry equilibrium forms |
| 4 | Faceted crystals | a) Solid hexagonal<br>b) Small faceted<br>c) Mixed forms | a) Solid kinetic growth form<br>b) Early kinetic growth form<br>c) Transitional form |
| 5 | Cup-shaped crystals and depth hoar | a) Cup crystal<br>b) Columns of depth hoar<br>c) Columnar crystals | a) Hollow kinetic crystal<br>b) Columns of a)<br>c) Final growth stage |
| 6 | Wet grains | a) Clustered rounded grains<br>b) Rounded polcrystals<br>c) Slush | a) No melt-freeze cycles<br>b) Melt-freeze cycles<br>c) Poorly bounded single crystals |
| 7 | Feathery crystals | a) Surface hoar crystals<br>b) Cavity hoar | a) Kinetic growth in air<br>b) Kinetic growth in cavities |
| 8 | Ice masses | a) Ice layer<br>b) Ice column<br>c) Basal ice | a) Refrozen water above less-permeable layer<br>b) Frozen flow finger<br>c) Frozen ponded water |
| 9 | Surface deposits and crusts | a) Rime<br>b) Rain crust<br>c) Sun crust, firn-spiegel<br>d) Wind crust<br>e) Melt-freeze crust | a) Surface accretion<br>b) Freezing rain on snow<br>c) Refrozen sun-melted snow<br>d) Wind-packed snow<br>e) Crust of melt-freeze grains |

referred to as 'temperature gradient metamorphism' or 'kinetic metamorphism' and result in faceting of the crystals. When the temperature gradient is small (<10 ºC m$^{-1}$), the snow grains grow large without developing a well-defined crystal habit (type 3c, 4b, and 4c in Table 2.1). However, when the gradient is large (>10 ºC m$^{-1}$), the crystals may develop either a solid form (type 4a) or if the gradient is very strong they develop a cup or cone shaped crystals, which are known as 'depth hoar' (type 5b) since they frequently

grow in the lower layers of a cold snowpack (LaChapelle, 1969; Langham, 1981; Colbeck *et al.*, 1990). If followed by a reduction in the temperature gradient, rounded crystal forms will develop (type 4c).

The liquid water content in the snowpack increases as the temperature of the snowpack rises to the melting point. This causes the rate of grain growth to increase (e.g. Langham, 1981; Davis, 1991) and the individual grains to become rounder as they melt at their extremities first (e.g. Colbeck, 1987; Pomeroy and Brun, 2001). Consequently, the presence of free water affects the evolution and physical properties of snow crystals and layers drastically (e.g. Langham, 1981; Pomeroy and Brun, 2001). The process is referred to as 'wet snow metamorphism' and with time, individual grains will either grow or be reduced, resulting in a snowpack that is comprised of coarse-grained particles of nearly uniform size (type 6a in Table 2.1) (Langham, 1981; Marsh, 1991). Refreezing of meltwater within the snowpack causes several grains to grow together and form an aggregate (type 6b). This process is also referred to as 'melt-freeze metamorphism' or 'firnification' (e.g. Langham, 1981) and may take place on a diurnal basis, during periods where the temperature of the surroundings changes between frost and thaw, or when meltwater percolates into the cold, dry snow.

Some processes take place only at the surface of the snowpack (type 7a and 9a-e), e.g. formation of surface hoar, sun or wind crusts, and melt-freeze layer. These features affect the behaviour of the snowpack greatly when they become incorporated into the snowpack by subsequent burial.

The general effects of metamorphism are a change in grain shape and size, which leads to a better packing of the snow grains and therefore an increase in snowpack density; and an increase of the porosity of the snowpack, which causes the permeability to increase and thus also an increase of the meltwater flux through the snowpack (Langham, 1981; Waldner *et al.*, 2004). Consequently, metamorphism is a major difference between water movement through a typical porous media and a snowpack.

## 2.1.2 Flow Through Snow

Melting of the snowpack depends on the net heat exchange between the snow and its surrounding environment. It may take place at air temperatures below 0 °C due to

impurities in the ice or when solar radiation is sufficiently intense (e.g. Langham, 1981; Pomeroy and Brun, 2001). The energy balance for of any snowpack can be written as

$$Q_M = Q_N + Q_H + Q_E + Q_P + Q_G - \frac{dU}{dt} \tag{2.1}$$

where $Q_M$ is the energy available for melting a unit volume of snow [W m$^{-2}$], $Q_N$ is the net radiation (long- and shortwave) [W m$^{-2}$], $Q_H$ is the sensible heat flux [W m$^{-2}$], $Q_E$ is the latent heat flux [W m$^{-2}$], $Q_G$ is the ground heat flux [W m$^{-2}$], $Q_R$ is the advective heat flux (derived from precipitation) [W m$^{-2}$], and $dU/dt$ is the change in internal energy of the snowpack [W m$^{-2}$]. For an isothermal snowpack at 0 ºC, $dU/dt=0$ as all energy inputs are directed toward snowmelt (e.g. Pomeroy and Brun, 2001). Based on the energy balance the melt rate can be estimated from

$$SWE_m = \frac{Q_M}{\rho_w \cdot L_f \cdot B} \tag{2.2}$$

where $SWE_m$ is the snow meltwater [mm], $\rho_w$ is the density of water [kg m$^{-3}$], $L_f$ is the latent heat of fusion [333.5 kJ kg$^{-1}$], and $B$ is the fraction of ice in a unit mass of wet snow (usually 0.95 to 0.97) (e.g. Pomeroy and Brun, 2001).

The major processes controlling meltwater flux through snow are heat flux [W m$^{-2}$ s$^{-1}$] and mass flux [kg m$^{-2}$ s$^{-1}$] (e.g. Marsh, 1991). They influence processes such as metamorphism of snow grains, refreezing of meltwater within the snowpack, and development of wetting fronts. The processes either impede or accelerate the meltwater flux and associated energy fluxes; as the snowpack ripens the impact of each process changes.

### *Wetting Fronts*

Snow is a porous medium and so capillary forces together with gravitational forces control the infiltration of meltwater into dry snow (e.g. Wankiewicz, 1979; Langham, 1981). Initially, meltwater fills pore spaces to satisfy the irreducible water content of the pores; this is strongly held in the capillaries and on the pore walls. Once 5-10% of the pore space is filled, the meltwater becomes mobile and gravitational forces become important. According to Marsh and Woo (1984), more than 50% of the surface melt is

used to supply the irreducible water content in a dry, cold snowpack (T <0 ºC) from the time melting initiates until meltwater reaches the base of the snowpack.

As meltwater percolates through the snowpack a wetting front develops, dividing the snowpack into a wet snow zone, where mass flux and latent heat flux are transferred by the water flow, and a dry snow zone, where energy is transferred by conduction along temperature gradients (e.g. Marsh, 2005). Energy is transferred across this wetting front by the release of latent heat as meltwater refreezes.

The downward rate of movement of a horizontal one-dimensional wetting front, $d\xi/dt$ [m$^3$ s$^{-1}$] (Equation 2.3), was found by Colbeck (1976) to depend on the meltwater flux, $u$ [m$^3$ s$^{-1}$ m$^{-2}$], and the effective water saturation, $S_w$ [m$^3$ m$^{-3}$], immediately above the front, the snow temperature immediately below the front, $T_s$ [ºK], the snow porosity, $\phi_s$ [m$^3$ m$^{-3}$], the densities of ice and water, $\rho_i$ [kg m$^{-3}$] and $\rho_w$ [kg m$^{-3}$], the latent heat of fusion, $L_f$ [kJ kg$^{-1}$], and the specific heat of ice, $c_i$ [kJ kg$^{-1}$ ºK$^{-1}$].

$$\frac{d\xi}{dt} = \frac{u}{(\phi_s \cdot S_I) - (\phi - 1)\left(\dfrac{T_s \cdot \rho_i}{(L_f / C_i)\rho_w}\right)} \quad (2.3)$$

For an unsaturated, isothermal (at 0 ºC) snowpack, the vertical water flux, $u$ [m$^3$ s$^{-1}$ m$^{-2}$], can be estimated based on Darcian flow for unsaturated media, where $\kappa_s$ [m$^2$] is the permeability of the snow, $\mu_w$ [kg m$^{-1}$ s$^{-1}$] is the viscosity of water, $dp_w/dz$ is the pressure gradient [kg m$^{-2}$ s$^{-2}$], and $\rho_w g$ is the gravitational gradient [kg m$^{-2}$ s$^{-2}$] (Wankiewicz, 1979)

$$u = -\left[\frac{\kappa_s}{\mu_w}\right]\left[\frac{dp_w}{dz} + \rho_w g\right] \quad (2.4)$$

Colbeck and Davidson (1973) found from drainage tests that $\kappa_s$ is a power function of the effective saturation of snow, $S^*$ [m$^3$ m$^{-3}$]. For the vertical flux in a snowpack the pressure gradient will be <2% of the gravitational gradient (e.g. Marsh, 2005) and can therefore be ignored; thus, $u$ can be calculated as

$$u = \frac{\kappa_s \cdot S^{*3} \cdot \rho_w g}{\mu_w} \quad (2.5)$$

The depth to which meltwater penetrates into the snowpack depends on factors such as snow temperature, its structural characteristics, and the flux of the water (e.g. Pfeffer *et al*., 1990). As the wetting front reaches snow with a temperature below 0 ºC, refreezing can occur, causing release of latent heat (e.g. Marsh, 1991). This release of latent heat results in an increase in the temperature of the surrounding snowpack and is sometimes the most important factor for warming up the lower layers of a cold snowpack (Marsh and Woo, 1984).

A large temperature gradient between the meltwater (T=0 ºC) and the colder surrounding snow can cause an ice body to be formed when the meltwater refreezes (e.g. Marsh, 1991). The freezing of the meltwater within the snowpack results in a reduction of the meltwater flux (Marsh, 1991). However, if the refrozen particles are large, the ice layer may still be permeable. Continuous, steady freezing results in a thick ice layer, which may block meltwater flowpaths. These ice bodies can form horizontally along stratigraphic horizons within the snowpack (Type 8a in Table 2.1), vertically within flow fingers (Type 8b in Table 2.1), and/or at the base of the snowpack as basal ice layers (Type 8c in Table 2.1) (e.g. Marsh, 1991). Ice structures may vary spatially from a few centimetres to several metres in width (e.g. Marsh and Woo, 1984a; Marsh, 1991).

***Preferential Flowpaths***

Percolation of meltwater through the snowpack is a non-uniform process that, in addition to heat and mass flux, is strongly influenced by meso-structural characteristics such as snow density, ice lenses or layers, and stratification (Wankiewicz, 1979; Colbeck, 1981). The meteorological conditions during individual precipitation events and snow metamorphism after deposition result in highly stratified snowpacks (Langham, 1981). Together with formation of ice bodies within the snowpack (Type 8a-b in Table 2.1), the natural instability of the flow leads to formation of preferential flowpaths (or flow fingers) within the snowpack (e.g. Wankiewicz, 1979; Marsh, 1991). These flowpaths concentrate water into a smaller cross-sectional area; once formed, meltwater may continue enlarging the path through refreezing as well as from the pressure of the flow itself. Ultimately, the presence of liquid water increases the rate of grain growth, which increases permeability and thereby amplifies the water flow

(Waldner *et al.*, 2004). With time, percolating meltwater will move along these preferred channels rather than in the full cross-sectional area as a classical wetting front (e.g. Wankiewicz, 1979).

The processes controlling the development of preferential flowpaths are not well understood (Marsh, 2005). An attempt to explain flow finger development was provided by Wankiewicz (1979) with the FINA model; Flow Impeding, Neutral, or Accelerating. This model describes the interaction of snow layer boundaries on water flux based on the relationship between gravity flow pressures ($p_w$) in two adjacent layers (Figure 2.2A):

- *Neutral horizon, N*: exists where the gravity flow pressures for the two layers are almost equal ($p_{w1} \approx p_{w2}$). This boundary has no effect on the meltwater flow.

- *Accelerating horizon, A*: exists where the gravity flow pressure in the overlying layer is higher than that in the underlying ($p_{w1} > p_{w2}$), accelerating the passage of
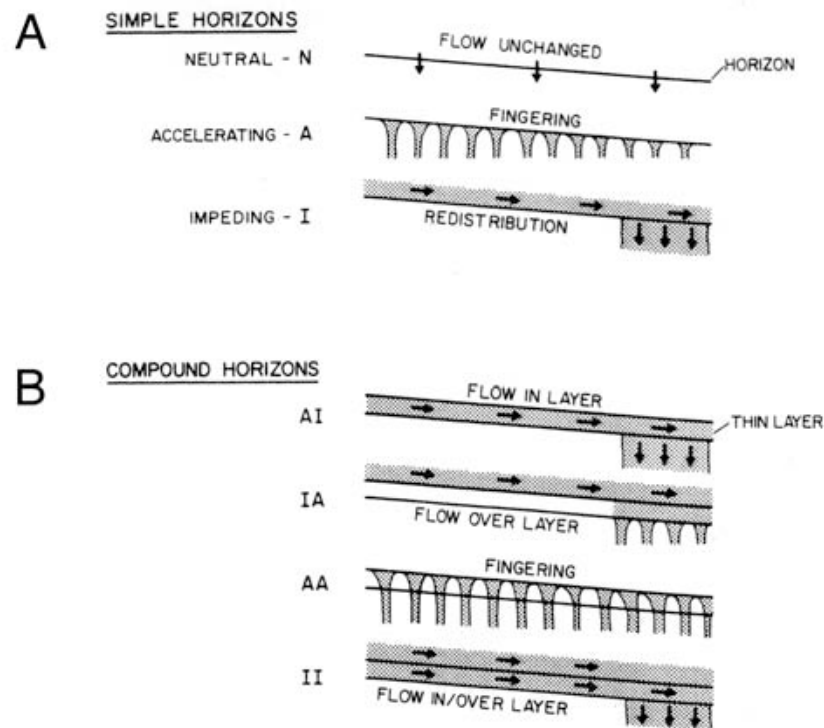


*Figure 2.2. Flow patterns within a snowpack produced by sloping stratigraphic horizons according to the FINA model (from Wankiewicz, 1979). A) The influence of a single horizon on meltwater flow. B) The influence from a combination of the horizons.*

the wetting front to the underlying snow. This causes the wetting front to become unstable and flow fingers are formed allowing meltwater to percolate into the underlying dry, cold snow, ahead of the main wetting front.

- *Impeding horizon, I*: exists where gravity flow pressure in the overlying layer is lower than that of the underlying layer ($p_{w1} < p_{w2}$). Meltwater will be held back until the gravitational flow pressure for the underlying layer has been reached, slowing down the water flux. A sloping horizon will cause flow to occur along the horizon, redistributing the meltwater.

The snowpack may consist of multiple layers and therefore boundaries (horizons), which leads to a complex flow through the snowpack (Colbeck, 1972; Wankiewicz, 1979). Figure 2.2B shows how combined horizons influence meltwater flow; i.e both impeding and accelerating horizons lead to a concentration of the vertical flow.

Formation of flow fingers has been observed in both arctic and temperate snowpacks (e.g. Colbeck, 1972; Marsh and Woo, 1984a; Williams and Melack, 1989; Harrington *et al*., 1996; Pfeffer and Humphrey, 1996). Field studies by Pfeffer and Humphrey (1996) showed that a fine- to coarse-grained boundary resulted in an impeding horizon, and a coarse- to fine-grained boundary resulted in a neutral boundary. However, the influence that a horizon has on the flow depends strongly on the meltwater flux (Wankiewicz, 1979). The boundary between new, fine grained snow and old, coarse grained snow will at low flow rates form an impeding horizon whilst at high flow rates it will accelerate the flow. At the base of the snowpack, the boundary between the snow and the ground will be an accelerating horizon during low flow rates and an impeding horizon at high flow rates.

The result of the formation of these preferential flowpaths are a reduction in the lag time from when melting starts until meltwater is eluted at the base of the snowpack (Kattlemann, 1986) causing elution of meltwater to initiate at different times in different places (e.g. Williams and Melack, 1989; Marsh, 1991; Harrington *et al*., 1996).

A model to describe the flux in these preferential flows was developed by Marsh and Woo (1984b). Meltwater fluxes at the finger front and at the background front were estimated based on the portion of total area that the fingers covered, and the proportion of total flow in the fingers as derived from observations. Recent models of meltwater

flow through snow are based on numerical solutions derived from basic physics (Marsh, 2005); however, the ability to measure the physical properties of snow needed for these models, limits their use. Similarly, a better understanding of the physical processes controlling water flux is needed to develop a completely physically based model. A reason for the limitations in the knowledge is partly due to the difficulties of carrying out experiments in a snowpack with a temperature at the melting point (Marsh, 1991). Better techniques for measurement of the changes in the snowpacks properties (i.e. hydraulic properties such as porosity and permeability) are generally needed (Marsh, 2005).

### 2.1.3 Meltwater Chemistry

The supercooled water droplets in the atmosphere, which form the ice crystals that later become snow on the ground, scavenge gases and aerosols from the surrounding air (Davis, 1991; Tranter and Jones, 2001). As the ice crystals grow, chemical species are continuously incorporated into the snow crystals by scavenging of gases and aerosols. The greater surface area of the snow crystals and the slower falling velocity through the atmosphere makes snow a greater scavenger of particulate material than are raindrops of equal mass. Consequently, snow is a better indicator of the presence of pollutants in the atmosphere.

The chemical composition of the snow reaching the ground surface depends on factors such as the origin of the scavenged air masses, the altitude of deposition, and meteorological conditions during precipitation (e.g. Davies *et al.*, 1992). Marine air masses contain large quantities of $Na^+$ and $Cl^-$ (Tranter *et al.*, 1986) whereas air masses from industrial areas produce snow with high concentrations of acid anions such as $NO_3^-$ and $SO_4^{2-}$ (Davies *et al.*, 1984). Snow deposited on top of mountains often has lower ion concentrations than snow in valleys due to the shorter decent and thereby time for scavenging and adsorption of aerosols and gases (e.g. Tranter and Jones, 2001). In addition, dry climates have been found to have more aerosols present than humid climates.

Compositional changes of the snowpack take place after the snow has reached the ground. Processes that will change the chemical composition are: ventilation, which

causes an exchange of gases and particles between the top part of the snow and the air; atmospheric dry deposition, which is strongly affected by the proximity of polluting sources (i.e. industrial areas); redistribution of the snow by wind; and differential scavenging by vegetation (e.g. Tranter and Jones, 2001). These processes do not occur evenly over an area resulting in spatial variation in the chemical composition of the snowpack over short distances.

### *Fractionated Elution*

Snowpack metamorphism and refreezing of meltwater within the snowpack relocate incorporated ions to quasi-liquid layers on the grain surface and between grains (Colbeck, 1981). This partitioning, or ion exclusion, occurs because the individual ions lack the ability to become incorporated into the crystal lattice of ice (e.g. Colbeck 1981; Davies *et al.*, 1987; Tranter and Jones, 2001). The ability is related to the ions' hydrated radii and capability to form hydrogen bonds. For instance, ions such as $Na^+$ and $Cl^-$ are incorporated more readily into the ice crystal lattice than are $NO_3^-$ and $SO_4^{2-}$.

The thickness of the quasi-liquid layer diminishes as the temperature drops, leading to an increase in solute concentrations within the layer due to continued ion exclusion. As a result of the induced freezing point depression, this layer will be present even at very low temperatures. Thus, throughout melt, soluble impurities in the quasi-liquid layers on both snow crystals and ice layers within the snowpack can be readily mixed with percolating meltwater, enhancing the ion concentrations (e.g. Bales *et al.*, 1989).

Studies show that the combination of preferential flowpaths and concentration of solutes in the quasi-liquid layer results in ion concentrations, which exceeds the concentrations in the matrix flow (e.g. Colbeck, 1981; Williams and Melack, 1991; Marsh and Pomeroy, 1999). On average, the meltwater released at the base of the snowpack has an initial 2- to 7-fold enrichment in ion concentrations compared to the bulk composition of the parent snowpack (e.g. Johannessen and Henriksen, 1978; Tranter, 1991). Greater enrichments (>20) have been observed too (e.g. Tsiouris *et al.*, 1985; Bales *et al.*, 1989; Tranter, 1991).

As melt progresses, the ion concentrations in the meltwater decrease (Figure 2.3). Typical ion elution curves show an initial enrichment followed by a rapid decrease until the meltwater is depleted relative to the parent snowpack (e.g. Johannessen and Henriksen, 1978); this is referred to as ion fractionation. Most of the enrichment occurs during the first one-third of the total melt period and has been found to be influenced by ion distribution within the parent snowpack, melt-freeze cycles, rain-on-snow events, snow depth, and preferential flow through the snowpack (e.g. Colbeck, 1981; Davies *et al.*, 1982; Marsh and Pomeroy, 1999). Species in the upper part of the snowpack will be eluted prior to species in the lower part of the snowpack (e.g. Bales *et al.*, 1989); melt-freeze-cycles enhances meltwater enrichment as a result of ion exclusion during refreezing (e.g. Colbeck, 1981; Jones, 1985; Tsiouris *et al.*, 1985); rain-on-snow events lead to a greater production of free water than during melt alone causing a more rapid drainage through the snowpack, resulting in less contact time with the snow and therefore a more transient acidification event (Jones *et al.*, 1989). Consequently, snow meltwater chemistry may be strongly influenced by processes occurring weeks or months prior to melt (Cragin *et al.*, 1996) and combined with the spatial variability in onset of snowmelt the result may be either an exaggeration of the apparent magnitude and duration of the ion pulse, or conversely an attenuation of the ion pulse (e.g. Williams and Melack, 1991).
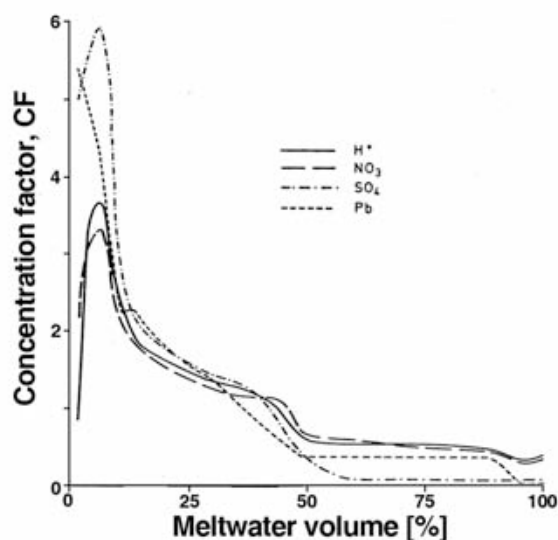


*Figure 2.3. Example of ion elution curves (from Johannessen and Henriksen, 1978).*

The ion fractionation does not take place at the same rate for all ions. Some are eluted preferentially compared to others (e.g. Johannessen and Henriksen, 1978; Brimblecombe *et al*., 1986; Tranter *et al*., 1986), which leads to a change in the proportional ion composition of the snowpack and meltwater during snowmelt. There is no general elution sequence, but the prevailing tendencies in both field and laboratory studies are for $NO_3^-$ and $SO_4^{2-}$ to be preferentially eluted compared to $Cl^-$ (i.e. $NO_3^-$, $SO_4^{2-} > Cl^-$); $Ca^{2+}$ is preferentially eluted compared to $Mg^{2+}$ (i.e. $Ca^{2+} > Mg^{2+}$); and $Na^+$ is the last of the major ions to become depleted (e.g. Tranter, 1991; Cragin *et al*., 1996). Brimblecombe *et al*. (1985) found that the variations in anion concentrations during melt were greater than for cations. The reason for this variation in elution sequence has been widely discussed (e.g. Tranter, 1991) and has been hypothesized to mainly be a result of the difference in the distribution of solute within the snowpack and within the individual snow crystals.

### 2.1.4  Basal Ice Formation

Once meltwater reaches the base of the snowpack ponding may occur if the melt rate exceeds the infiltration rate and runoff rate. Where there is sufficient heat flow into the soil ($T_{soil} < 0$ ºC), the result is formation of a basal ice layer (type 8c in Table 2.1) (Woo and Heron, 1981). Basal ice formation is most common early in melt over saturated or very cold frozen soils and has been observed in glacial environments, where it is referred to as superimposed ice (e.g. Wakahama *et al*., 1976), as well as in non-glacial arctic (e.g. Woo *et al*., 1982; Marsh and Woo, 1984a), boreal (e.g. Stein *et al*., 1994), and alpine environments (personal observations during this research).

The rate of heat released by the growth of the basal ice layer, $Q$ [kg m$^{-2}$ s$^{-1}$], can be approximated as:

$$Q \ = \ (\rho_i - \rho_s) \cdot L_f \cdot \frac{dz}{dt}$$
(2.6)

where $\rho_i$ and $\rho_s$ are the respective densities of the basal ice and the snowpack [kg m$^{-3}$], $L_f$ is the latent heat of fusion [333 kJ kg$^{-1}$], and *dz/dt* is the rate of ice growth [m s$^{-1}$] (Woo and Heron, 1981).

Several studies have looked at the importance of basal ice formation on meltwater routing in both environments (e.g. Wakahama *et al*., 1976; Jones and Pomeroy, 2001). Formation of a basal ice layer acts analogous to a switch in the flowpathway, causing a soil with unlimited or limited infiltrability to become a restricting soil where no infiltration occurs and all water ends up as runoff (Gray *et al*., 1985b).

The influence that a growing basal ice layer has on runoff chemistry was inferred by Jones and Pomeroy (2001) as they observed considerable increases in stream water $NO_3^-$ concentrations as the percentage of concrete frost in a boreal forest watershed increased to 75%. Concrete frost was assumed to be associated with basal ice formation. However, to the knowledge of the author no studies have examined the influence of basal ice layer formation on runoff chemistry for all major ions. Based on processes known to occur as ice is formed within the snowpack it is hypothesized that ion exclusion takes place during basal ice formation and that an enriched brine forms on the basal ice surface, which mixes with meltwater in contact with it. This hypothesis is tested in Chapter 6.

## 2.2    Meltwater Partitioning

Infiltration is the process by which water enters a stratum and may occur through the entire surface uniformly or through preferential flowpaths (e.g. Hillel, 1998). The maximum infiltration rate at which a given stratum can absorb water is equal to its infiltrability, which is a function of input rate, duration, physiographical conditions (e.g. slope and aspect), and soil properties (Dingman, 2002). Macropores increase the rate at which water and its solutes can infiltrate and move through a stratum (Beven and Germann, 1982). They may originate from e.g. biological activity (e.g. decayed plant roots, worm holes, animals), geological activity (e.g. fractures, differences in media), freeze-thaw cycles, or farm management practice. The fractional volume of macropores may be quite small, however, the effects that they may have on flow phenomena such as infiltration, drainage, and transportation of solutes in saturated or near-saturated conditions can be significant (e.g. Hillel, 1998).

Underneath a melting snowpack, the infiltrability of the stratum, whether it is frozen or unfrozen, determines the partitioning of meltwater into infiltration, overland

flow, and ponding (e.g. Hillel, 1998; Zhao and Gray, 1999). The biggest difference between infiltration to unfrozen and frozen soil is the presence of ice as a solid phase (e.g. Kane and Stein, 1983). Thus, the rate and volume of snowmelt runoff depends not only on the melt intensity and amount of water in the snowpack, but also on the physical and thermodynamic properties of the underlying stratum; i.e. the initial distribution of soil moisture (water and ice) and temperature within the profile, the depth and nature of freezing, and the spatial variations in infiltration (Alexeev *et al*., 1972; Zhao and Gray, 1997; Gray *et al*., 2001). Consequently, the infiltrability influences the timing and spatial distribution of surface runoff (Hillel, 1998). Knowledge of the infiltrability of soils is important for agricultural, economical, and ecological reasons as it reduces direct runoff and thereby peak flow (Male and Gray, 1981).

Infiltration of meltwater into an unfrozen stratum will occur in a similar manner as that of rainfall or ponding water (Male and Gray, 1981). When the total water content (water and ice) in a frozen substratum is low and/or the frost depth is less than 0.15 m, infiltration will behave as for an unfrozen stratum (e.g. Pomeroy and Brun, 2001). Due to the volume change from liquid water to solid ice, a water saturation of 91.7% results in a fully ice saturated frozen media in which no further flow can occur (Andersland *et al*., 1996). This causes an unsaturated frozen stratum to be less permeable than an unfrozen stratum with similar saturation. Forested areas with mineral soils and organic layers are more likely to experience porous (granular or stalactite) frost, which impedes but does not restrict infiltration, than the presence of impermeable, concrete frost (e.g. Pierce *et al*., 1958; Barry *et al*., 1990). This is due to the generally low soil moisture content at time of freeze-up. Nevertheless, concrete frost has been observed in forested areas by e.g. Stein *et al*. (1994), Jones and Pomeroy (2001), and in the present study (see Chapter 7).

Impeding horizons within the soil, due to the soil texture or the presence of ice, may prevent the infiltrating water from percolating to the groundwater. Instead the water may flow laterally down-slope as interflow (e.g. Dingman, 2002); this can take place in both the organic layer and the mineral soil. In forested environments, flow through laterally orientated macropores from plant roots and burrowing animals may dominate (Weiler *et al*., 2005).

When the rate of water supplied to the surface exceeds the infiltrability of the stratum water will accumulate on the surface (Freeze and Cherry, 1978). The initial water will pond due to geometric irregularities in the ground surface. When the depressional storage in these irregularities has been filled, surface-storage capacity has been reached, and runoff can initiate; this process is also referred to as the 'fill and spill' principle. Surface runoff (or overland flow) represents the portion of the supplied water that is neither absorbed by nor accumulates on the surface of the stratum but flows down slope across the surface (Hillel, 1998).

## 2.3    Infiltration to Frozen Soil

Movement of water in various porous media at different saturations has been studied for decades (Hillel, 1998). Research has primarily focused on flow in unfrozen media, however, infiltration curves for seasonally frozen soils have the same shape as infiltration curves for unfrozen soils (e.g. Kuznik and Bezmenov, 1963; Komarov and Makarova, 1973). They show that as water enters the soil, the effective saturation increases, causing an increase in the liquid permeability and a decrease in the capillary pressure gradient (e.g. Hillel, 1998). Consequently, infiltration can be divided into two flow regimes: a transient period where the rate of infiltration decreases rapidly followed by a quasi-steady-state where changes in infiltration and heat transfer are relatively constant (Figure 2.4).
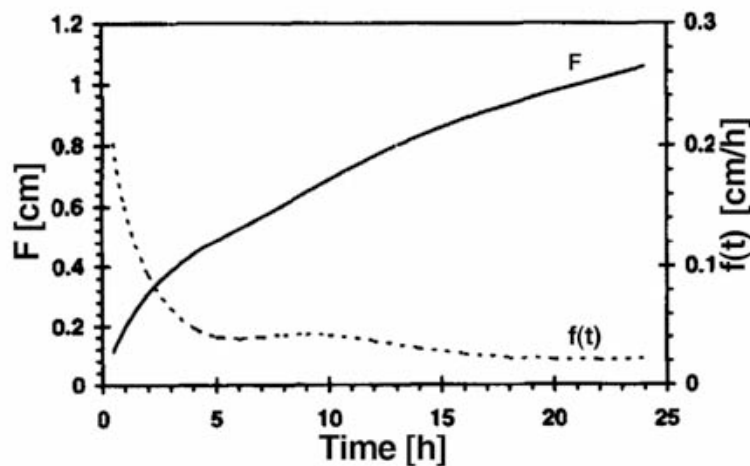


*Figure 2.4. Change in infiltration rate, f(t) [cm h⁻¹], as found by Zhao et al. (1997) for frozen soil. F is the cumulative mass of water that infiltrates [cm].*

Although the first research on infiltration into frozen ground and its influence on runoff was dominated by Russian scientists (e.g. Kuznik and Bezmenov, 1963; Alexeev *et al*., 1972; Komarov and Makarova, 1973; Motovilov, 1978), recent studies have also been carried out in Canada (e.g. Lin and Gray, 1971; Lewkowicz and French, 1982; Granger *et al*., 1984; Gray *et al*., 1985b; Maulé and Stein, 1990; Zhao *et al*., 1997; Zhao and Gray, 1999; Gray *et al*., 2001); USA (e.g. Kane and Stein, 1983; Shanley and Chalmers, 1999; Meijer, 2002); Sweden (e.g. Engelmark, 1984; Nyberg *et al*., 2001; Stähli *et al*., 2001; Lindström *et al*., 2002); Norway (e.g. French *et al*., 1999); and Austria (e.g. Jaesche *et al*., 2003). Common for all studies is the importance of understanding the partitioning of spring snowmelt water between infiltration and runoff and thereby being able to predict the timing and duration of spring flood.

### 2.3.1 Flow in Frozen, Unsaturated Soil

Infiltration to frozen soil is controlled by the structural, hydrological, and thermophysical characteristics of the soil (i.e. the initial moisture content (ice and water) and its distribution), meteorological conditions, the heat flux of the infiltrating water, the soil-ice-water system's temperature profile, and the induced freezing point depression due to solute concentrations (e.g. Kuznik and Bezmenov, 1963; Komarov and Makarova, 1973; Romanov *et al*., 1974). Changes in any of these parameters may lead to changes in the infiltration rate. Tao and Gray (1994) later suggested that the infiltration process is least sensitive to frozen soil temperature.

The laws of physics dictate that water flow will occur towards areas with a lower state of energy (Hillel, 1998). Thus, as long as the energy of the snowpack's meltwater is greater than the energy in the soil water will infiltrate cold, unsaturated soils (e.g. Wiggert *et al*., 1997; Zhao *et al*., 1997). If the heat balance is reversed, i.e. the temperature of the soil is below the freezing point, the infiltrating water will refreeze in the soil, blocking pore spaces (e.g. Woo and Steer, 1983).

Kachinskiy addressed the importance of heat transfer during refreezing of water in the soil in 1927 (in Kuznik and Bezmenov, 1963). He found that frozen soil underneath a snowpack only thaws because of the infiltration of meltwater. During the early stage of infiltration, the addition of mainly conductive energy causes an increase in the

internal energy and melting of the ice within the soil (Zhao *et al*., 1997). As the wetting front reaches a layer of ice within the soil, the conductive heat transfer rate and the energy change rate due to the phase change becomes zero and as a result the temperature of the surrounding is increased. During this transient phase, more than 60% of the conducted energy is used to melt the ice; the remaining energy is used to raise the temperature of the surrounding soil  (Zhao *et al*., 1997). As the infiltration reaches a quasi-steady-state, heat is added to the control volume by latent energy released by freezing of liquid water. Zhao *et al*. (1997) found that more than 90% of this latent heat is conducted deeper into the soil.

Two theories of water movement through frozen soil prevailed in 1983 (Kane and Stein, 1983). The first theory was that water creeps along the pore walls, through the unfrozen water film existing on the surface of the soil particles, in as similar way as in unfrozen soil. The unfrozen water is present due to their solute concentrations, which induces a freezing point depression. The second theory is referred to as 'regelation', where heat transfer with phase change is thought to be the mechanism responsible for inducing fluid movement. As infiltrating water reaches the freezing front within the soil, refreezing occur and latent heat is released. In order to allow additional freezing to occur, the released heat is conducted through the formed ice lens or layer, towards the colder surface (downstream in direction of heat flow), where some melting of the ice occurs. According to Horiguchi and Miller (1980), Darcy's law can be used to quantify both theories.

Macropores (e.g. cracks, worm holes, and dead root passages) are important when determining the permeability of frozen soil (Komarov and Makarova, 1973). The capillary pores are considered secondary since they will be completely filled with ice, at least in the narrowings. Measurements of the hydraulic conductivity, *K*, of frozen, unsaturated soils show that *K* decreases substantially with a slight reduction in the soil temperature below 0 ºC and with the existence of ice lenses within the soil (Burt and Williams, 1976; Horiguchi and Miller, 1980).

Infiltration ceases when the soil pores are sealed by ice, blocking further movement (Woo and Steer, 1983; Wiggert *et al*., 1997). Until the meltwater supply is exhausted or until the ground temperature is raised to 0 ºC, refreezing of infiltrating

water continues to provide heat to the ground (Woo and Steer, 1983). The depth of frozen soil is affected by the timing of when soil freezing initiates and the snowcover is formed (Osokin *et al.*, 2000). Frost depth will be greater when soil freezing initiates prior to the formation of the snowpack; if there is only a short delay, the frost depth might be limited due to insulation by the snowpack.

## 2.3.2   Redistribution of Soil Moisture

Redistribution of soil moisture is important when quantifying the moisture content in frozen soil, as the changes in soil moisture over the course of winter directly affect the infiltration that can take place and thereby the soil water recharge from the snowpack (Kane and Stein, 1983; Granger *et al.*, 1984). As the soil water freezes, formation of ice results in the water being confined in progressively smaller spaces. This causes a decrease in Gibb's free energy of water, which causes migration of water to the freezing zone (Williams and Smith, 1989). Thus, within the soil, water moves from the unfrozen to frozen zone due to the pressure differences imposed by the temperature and local hydraulic gradients, i.e. caused by the freezing process in frozen soils (Male and Gray, 1981; Kane and Stein, 1983; Gray *et al.*, 1985a). The magnitude of the migration is directly related to the moisture content; being greatest for light textured, wet soils (Gray *et al.*, 1985a). In soils that are dry at the time of freeze-up, the migration of water is negligible. Water migrates above and below the freezing front seen as a decrease in moisture content in the upper part of the soil (0-0.3 m) and an increase in the lower part of the soil (Gray *et al.*, 1985a).

Ice lenses will develop when the soil is moisture-rich and has a transmission rate high enough to supply enough water to the freezing front so that the release of latent heat prohibits advancement of the freezing front. The moisture migration and freezing may result in soil heaving (Baker, 2003). If a strong thermal gradient exists and the soil has low water content, limiting the released latent heat upon freezing, then the freezing front will advance without developing ice lenses. This migration of water towards a freezing front has been found to complicate the computation of infiltration (e.g. Komarov and Makarova, 1973).

### 2.3.3  Modelling Infiltration

The importance of being able to model the partitioning of meltwater between infiltration and runoff has lead to several numerical models. Prior to 1978, the general view of the physical processes taking place during infiltration to frozen soils was based on a relatively few experiments (Motovilov, 1978). Models consisted of a system of equations describing the transport of heat and water in a porous frozen media. Motovilov (1978) improved these models by including the approximate hydrological and thermophysical characteristics of the soil.

Gray *et al*. (1985) considered the changes in a frozen soil's infiltrability during the thawing and divided infiltration into three regimes based on the soil surface infiltrability defined by Granger *et al*., (1984). *Unlimited infiltrability* exists when all water released at the soil's surface infiltrates (Figure 2.5). Large, surface-connected, air-filled macropores, which are capable of infiltrating most or all of the rainfall or meltwater, are essential in this regime. The flow is predominantly gravity flow. *Restricted infiltrability* exists when there is a lack of macro pores and/or if impermeable ice near or on top of the soil surface impedes infiltration. The amount of infiltration is negligible and most water ends up as runoff or evaporates. *Limited infiltrability* exists when a partitioning of water between infiltrating and surface runoff takes place. During limited infiltrability,
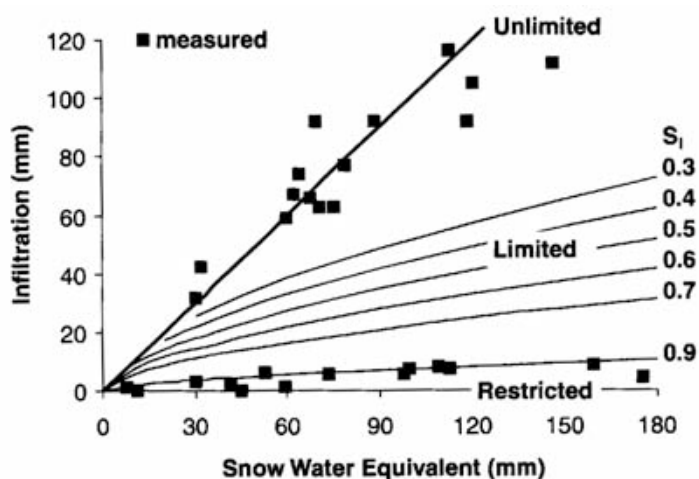


*Figure 2.5. Cumulative infiltrating mass, F [mm], versus snow water equivalent, SWE [mm], for unlimited, limited, and restricted frozen soils (from Gray et al., 1985b). $S_I$ denotes the saturation of the soil; 1 equals saturated conditions and 0 equals dry conditions.*

infiltration depends primarily on the snow water equivalent (*SWE*), its melt rate, and the unfrozen and frozen water content of the soil. In this regime, capillary flow dominates.

The first model that employed the different infiltrability regimes assumed that unlimited infiltrability resulted in no runoff since all meltwater infiltrates and restricted infiltrability resulted in all runoff since none of the meltwater infiltrates (Gray *et al.*, 1985b). The cumulative mass that infiltrates a frozen prairie soil during limited infiltrability conditions, *F*, was initially believed to depend primarily on the snow water equivalent, *SWE*, and the average water and ice content of the top 0.3 m of the soil at the time of melt, $S_I$,

$$F = 5 \cdot (1 - S_I) \cdot SWE^{0.584} \tag{2.7}$$

During the 1990s, the number of frozen soil studies increased significantly; the ratio between field studies and models increased too. Models kept evolving and it became more common to verify models using collected field data. In 1999, Zhao and Gray derived a parametric equation describing cumulative infiltration into frozen unsaturated soils of limited infiltrability

$$F = C \cdot S_o^{2.92} \cdot (1 - S_I)^{1.64} \cdot \left(\frac{273.15 - T_I}{273.15}\right)^{-0.45} \cdot t_o^{0.44} \tag{2.8}$$

where *C* is a constant, $S_o$ is the surface saturation or moisture content at the soil surface [mm$^3$ mm$^{-3}$], $S_I$ is the average soil saturation of the top 40 cm of the soil layer at the start of infiltration [mm$^3$ mm$^{-3}$], $T_I$ is the average initial temperature of the top 0.4 m of the soil [K], and $t_o$ is the infiltration opportunity time [h]. The equation assumes quasi-steady flow, constant surface saturation, homogeneous soil, and that the vertical distribution of soil moisture and soil temperature at the start of infiltration is uniform and constant. The sensitivity of the different components in the model is discussed in Gray *et al.* (2001).

Unlike rainfall, snowmelt often lasts for several days or even weeks. Thus, when predicting runoff and infiltration quantities, use of the equilibrium infiltration rate for the entire melt period does not produce significant errors (Kane and Stein, 1983) since quasi-steady flow occurs after 5-6 hours (Zhao *et al.*, 1997).

Most models, which predict water percolation and transportation of water-aided solutions through the unsaturated zone, are based on a combination of Darcy's law with a convective-dispersive equation (Wallach *et al*., 1999). Such models assume that transport of the bulk solution occurs at one velocity, which is inconsistent with field observations. Often they show a very quick release from the surface to the groundwater after the first rainfall. The difficulty of modelling this fast transport through the unsaturated soil is due, in part, to the presence of preferential flowpaths, which may result from the instability of a wetting front and/or macropores, as well as the complicated network of interconnected pathways in the soil, which can transmit solutions at varying velocities (Hillel, 1998; Wallach *et al*., 1999). When solutions are transmitted through these pores, the velocity may be even higher than those predicted by Darcy's law (Hillel, 1998; Wallach *et al*., 1999). Discrepancies between observations and modelling indicate that there is still a great need to study frozen ground and the partitioning of waters (e.g. Barry *et al*., 1990).

## 2.4    Compositional Changes due to Flowpath

Studies of episodic acidification of streams and lakes have shown decreases in pH of between 1 and 3 units during spring melt (e.g. Johannessen and Henriksen, 1978; Tranter, 1991; Laudon *et al*., 2000). This episodic acidification influences both terrestrial and aquatic environments; particularly in areas with a limited capacity to neutralize acids (e.g. Schöndorf and Herrmann, 1987; Bales *et al*., 1989; Bales and Harrington, 1995; Wigington *et al*., 1996; Laudon *et al*., 2000; Wellington and Driscoll, 2004). Small changes in the acidity of a stream or lake may have major effect on the fish habitat, i.e. malformation of fish embryos due to the stress (Roberge and Plamondon, 1987; USEPA, 1995; Wiginton *et al*., 1996; Helliwell *et al*., 1998; Ikuta *et al*., 1999; Wellington and Driscoll, 2004). In areas with limited buffering capacity even fish kills have been observed during snowmelt (Leivestad and Muniz, 1976; Johannessen and Henriksen, 1978).

Changes in flowpaths during any hydrological event (rainfall or snowmelt) are an important determinant of the characteristics of the compositional changes in the chemistry of the receiving environment (e.g. Peters and Driscoll, 1989; Wigington *et al*.,

1996). Until the late 1980s, it was believed that acidification of streams and lakes during spring melt originated solely from the fractionated elution of snowmelt water. However, the constituent runoff water for these acidic shocks comprises both meltwater from the snowpack and water expelled from soils by infiltrating meltwater (Peters and Driscoll, 1987; Rachel *et al*., 1987; Maulé and Stein, 1990; Laudon *et al*., 2000; Tranter and Jones, 2001; Quinton and Pomeroy, 2006). Consequently, the acidity that eventually reaches the stream or lake waters is dependent upon flowpath and dilution by pre-event groundwater.

An understanding of source area and timing of runoff generation is essential for modelling and managing aquatic systems (e.g. McEachern *et al*., 2005). Studies have showed that pipe flow through macropores at the organic-mineral interface can have a significant impact on lake chemistry, and thereby aquatic biota, over short time periods (Roberge and Plamondon, 1987; Tranter *et al*., 1994). The rapid flow through the macropores induces less contact with the mineral soil and therefore less solute derived from soils in the snowmelt water. In addition, the temperature of the snowmelt water is 0 ℃, compared with 2-3 ℃ for groundwater, causing the density of the runoff water to be lower than the density of groundwater; consequently, when snowmelt runoff water is released to a lake, it will stay at the surface and little or no mixing will occur (Roberge and Plamondon, 1987).

Studies of the influence of frozen soils on flowpath and chemical alteration have been carried out in both boreal and arctic regions; however, the understanding of the different chemical processes that takes place once meltwater infiltrates frozen ground is very limited. Research has mainly focused on in-stream chemistry changes due to surface runoff (e.g. Duysings *et al*., 1983; Obradovic and Sklash, 1986; Maulé and Stein, 1990; Helliwell *et al*., 1998; Shanley and Chalmers, 1999; Laudon *et al*., 2000; Jones and Pomeroy, 2001; Anderson and Dietrich, 2001; Shanley *et al*., 2002; Quinton and Pomeroy, 2006). Other studies include: N losses during snowmelt (e.g. Tranter and Jones 2001; Fitzhugh *et al*., 2003; Quinton and Pomeroy, 2006), movement of insoluble contaminants in frozen soil (e.g. Andersland *et al*., 1996; Wiggert *et al*., 1997; French *et al*., 1999; Grant, 2000), and variation in isotope chemistry to interpret sources for stream water (e.g. Maulé and Stein, 1990; Buttle *et al*., 1995; Shanley *et al*., 2002; Taylor *et al*.,

2002; Sugimoto *et al*., 2003; McEachern *et al*., 2005; Murray and Buttle, 2005). Quinton and Pomeroy (2006) found that the composition of meltwater changed markedly as it flowed through soil to the stream due to mixing with soil matrix water and interaction with the soils. However, they also observed that the degree of alteration in the runoff water was strongly correlated to the extent of concrete frost in the stratum.

The chemical interaction that can take place when meltwater comes in contact with a frozen organic layer or mineral soil is complex. The dominant controls on the changes in chemical composition with flowpath in both frozen and unfrozen ground are: the stratum's chemical composition, weathering, micro-organisms, the N-cycle, carbonate equilibria, redox reactions, and ion exchange (e.g. Ollier, 1975; Borggaard and Elberling, 2004). Different processes may be important in affecting the water quality in various soil layers (Christophersen *et al*., 1984). Ion exchange may be the dominating process in the upper soil horizons which are rich in organic matter, whilst weathering may be the dominant process in the deeper layers of the mineral soil (e.g. Borggaard and Elberlign, 2004). Soil drying will concentrate solute in the water films on soil particle surfaces; these films readily mix with subsequent soil water flow originating from rainfall or snowmelt (Quinton and Pomeroy, 2006). Since water tends to flow through the largest soil pores, changes in chemical composition only require mixing with a small highly concentrated water volume close to the macropore (e.g. Christophersen *et al*., 1984). However, macropores may conduct water rapidly through an unsaturated, frozen matrix with minimal mixing with the matrix pore water (Espeby, 1990).

Most chemical processes in the soil are driven by pH (e.g. Freeze and Cherry, 1979), as chemical reactions are $H^+$ generating under oxidizing (or aerobic) conditions and $H^+$ consuming under reducing (or anaerobic) conditions. Microbes mediate the majority of the redox reactions that occur in the soil (Borggaard and Elberling, 2004). Once all the dissolved oxygen is gone there are usually still considerable amounts of organic carbon left for oxidation (e.g. Freeze and Cherry, 1979). Consequently, the microbes use other oxidizing agents; for instance, initially $NO_3^-$ is reduced to $N_2(g)$. When all $NO_3^-$ is gone, Fe(III) is reduced to Fe(II); and when all Fe(III) is gone, $SO_4^{2-}$ is reduced to $H_2S$ and $H_2S^-$.

Tracers are suitable tools for investigating runoff generation processes; especially conservative tracers (Hoeg *et al.*, 2000). Often a combination of chemical tracers (i.e. $Cl^-$, $Mg^{2+}$, and total $SiO_2$) and isotopic tracers (i.e. $^2H$ and $^{18}O$) is used to reduce the uncertainties experienced when information is available from only a single tracer. The natural tracer selected to determine a flowpath must be significant for, and locally available in, the area where work is carried out (Clow and Sueker, 2000); tracers vary with landscape and basin. Buttle and Peters (1997) carried out an experiment in which they assumed that $Si^{4+}$ was a good indicator for contact with the mineral soil due to quick reaction with the layer. However, the infiltrating water followed preferential flowpaths and so only minimal reactions with the mineral soil took place.

### *Behaviour of Major Ions*

Snowmelt water is a major factor in the availability and redistribution of nutrients and solute in a forested area (Jones and Pomeroy, 2001). Based on the findings in previous studies, expected alterations of the concentration of the individual major ions occurring when meltwater infiltrates a frozen organic layer (organic interflow) or frozen mineral soil (mineral interflow) are described in the following paragraphs and shown in Table 2.2.

Natural waters are often acidic (pH ≈ 5.7) due to $CO_2$ equilibrium with the atmosphere (e.g. Fetter, 1994). The following reactions take place as $CO_2$ dissolves in water

$$CO_2(g) \;\; + \;\; H_2O \;\; \Leftrightarrow \;\; H_2CO_3 \tag{2.9}$$
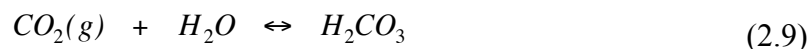
*Table 2.2. Expected alterations in chemical composition when meltwater infiltrates a frozen forest organic layer (organic interflow) or calcareous mineral soil (mineral interflow). Arrows pointing up and down denote relative increases and decreases; hyphens denote no significant changes.*

| Ion | $H^+$ | $Cl^-$ | $SO_4^{2-}$ | $NO_3^-$ | $NH_4^+$ | $Na^+$ | $K^+$ | $Mg^{2+}$ | $Ca^{2+}$ | DOC |
|---|---|---|---|---|---|---|---|---|---|---|
| Organic interflow | ↑ | – | – | ↓ | ↑ | ↑ | ↑ | – | – | ↑ |
| Mineral interflow | ↓ | – | – | ↓ | ↓ | ↑ | ↑ | ↑ | ↑ | ↑ |

$$H_2CO_3 \quad \leftrightarrow \quad HCO_3^- \quad + \quad H^+ \tag{2.10}$$

$$HCO_3^- \quad \leftrightarrow \quad CO_3^{2-} \quad + \quad H^+ \tag{2.11}$$

Another important source of $CO_2$, and thereby acidity ($H^+$), is oxidation of organic material by microbes (e.g. Fetter, 1994). A typical reaction is the oxidation of carbohydrate, $CH_2O$,

$$CH_2O \quad + \quad O_2 \quad \leftrightarrow \quad CO_2 \quad + \quad H_2O \tag{2.12}$$
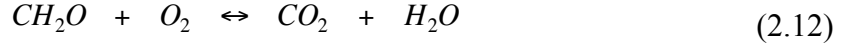
Consequently, in the organic layer, alterations of the infiltrating meltwater will be a result of mixing between dilute meltwater and acidic matrix water produced by the decomposition of organic material. In areas prone to acidic precipitation the alterations will be due to an acid-acid mixing.

Dissolution of $CaCO_3$ is an important buffer in many environments due to the resulting slightly alkaline solution:

$$CaCO_3(s) \quad \leftrightarrow \quad Ca^{2+} \quad + \quad CO_3^{2-} \tag{2.13}$$

$$H_2O \quad + \quad CO_3^{2-} \quad \leftrightarrow \quad HCO_3^- \quad + \quad OH^- \tag{2.14}$$

$$H_2O \quad + \quad HCO_3^- \quad \leftrightarrow \quad H_2CO_3 \quad + \quad OH^- \tag{2.15}$$
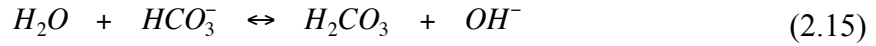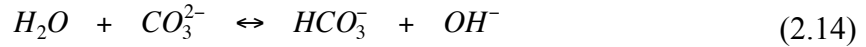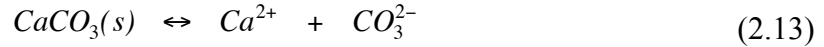
A system that contains dissolved $CaCO_3$ in equilibrium with the atmosphere will have a pH of 8.4 (e.g. Fetter, 1994). Many natural waters have a pH between 6 and 8 resulting in most carbonate being present as bicarbonate ($HCO_3^-$). Thus, the buffering capacity of the mineral soil layer determines the compositional change of the infiltrating water. Soil water in calcareous soils, such as those found in the eastern parts of the Canadian Rocky Mountains, is expected to be basic and alterations will be a result of acid-base mixing.

Chloride, $Cl^-$, is considered to be a conservative tracer and so is not released or adsorbed by minerals or vegetation (e.g. Grimaldi *et al.*, 2004). It is mainly derived from marine deposition (NaCl) and anthropogenic pollution (HCl) (e.g. Tranter and Jones, 2001; Meybeck *et al.*, 2005). The concentration of $Cl^-$ in the residual soil water as plants and trees take up water is often used as an indicator of residence time within unfrozen soils. However, the root growth of most plants and germination of most seeds are

restricted when soil temperatures are below +5 ºC (Kimmins, 2004). Thus, significant changes in $Cl^-$ concentrations are not expected in the organic interflow and the mineral interflow when the ground is frozen (e.g. Stottlemyer *et al.*, 1997; Stottlemyer and Toczydlowski, 1999). An increase in concentration could result from dissolution of ions located on the surfaces of the pore walls as water evaporated from the layers prior to freeze-up (Quinton and Pomeroy, 2006).

Sulphate, $SO_4^{2-}$, originates primarily from marine deposits ($MgSO_4$ and $CaSO_4$) (e.g. Meybeck *et al.*, 2005) and from industrial sources as oxidation of $SO_2$ gas (e.g. Tranter and Jones, 2001). In the presence of sulphur-oxidizing bacteria, $SO_4^{2-}$ may also origin from oxidation of pyrite ($FeS_2$), which many types of clay contain in low concentrations (Borggard and Elberling, 2004). In aerobic soils, $SO_4^{2-}$ is the stable form; anaerobic conditions cause $SO_4^{2-}$ to be reduced to $H_2S$ and $H_2S^-$ (e.g. Fetter, 1994). Changes in $SO_4^{2-}$ concentrations are assumed to be limited in either aerobic or anaerobic conditions in frozen soils as bacterial activity is restricted in cold conditions (Peters and Driscoll, 1987; Stottlemyer *et al.*, 1997; Jones and Pomeroy, 2001). Slight increases in concentration may be observed due to washout of dry deposition (Stottlemyer and Toczydlowski, 1999) as well as dissolution of ions from the pore walls (Quinton and Pomeroy, 2006).

Many forested areas have a deficit in inorganic nitrogen, N, which will result in a quick removal of N from the meltwater due to microbiological activity (Jones, 1999). During the snowmelt period, changes in nitrate, $NO_3^-$, and ammonium, $NH_4^+$, concentrations in the soil water will depend on a combination of snowmelt input, biological uptake, over-winter nitrification, and mineralization in the soil (Stottlemyer *et al.*, 1997). In general, oxidizing conditions results in nitrification (Equation 2.16), which leads to an increase in $NO_3^-$ concentration and a decrease in $NH_4^+$ concentration (e.g. Freeze and Cherry, 1979). Reducing conditions, on the other hand, cause a decrease in $NO_3^-$ concentrations due to denitrification (Equation 2.17) and an increase in $NH_4^+$ concentrations due to N fixation followed by mineralization (equation 2.18). Denitrification is of great importance in wetlands and flooded areas, as N becomes the electron acceptor during redox reactions instead of $O_2$ (e.g. Meybeck *et al.*, 2005).

Decomposition of humus by micro-organisms causes N to become readily available for denitrification.

$$2O_2 \;+\; NH_4^+ \;\leftrightarrow\; NO_3^- \;+\; 2H^+ \;+\; H_2O \qquad\qquad (2.16)$$

$$5CH_2O \;+\; 4NO_3^- \;\leftrightarrow\; 2N_2 \;+\; 5HCO_3^- \;+\; H^+ \;+\; 2H_2O \qquad (2.17)$$

$$N_2(g) \;\xrightarrow{\;bacteria\;}\; NH_2 \;\xrightarrow{\;bacteria\;}\; NH_4 \qquad\qquad (2.18)$$
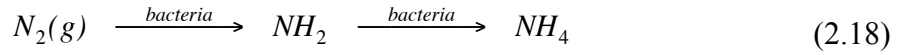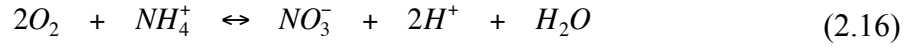
During the summer, biological activity may immobilize most or all $NO_3^-$ input, whereas reduced biological activity during winter and spring may result in a mobilization of the anion (e.g. Rascher *et al.*, 1987; Jones, 1999). Residence time in the soil will also have a major influence on the concentrations of $NO_3^-$ and $NH_4^+$ in the organic and mineral interflow. Short residence times due to a rapid flow rate will result in a relatively higher concentrations of $NO_3^-$ than a long residence time, since biological uptake will be limited; long residence times will result in greater opportunity for microbiological communities to immobilize N or denitrify it (Jones and Pomeroy, 2001). In areas with a surplus of inorganic N, uptake in the soil will cause the $NO_3^-$ concentration in the runoff water to be higher than in the meltwater due to nitrification (e.g. Rascher *et al.*, 1987; Peters and Driscoll, 1989). Concentrations in the organic interflow may be slightly higher compared to the mineral interflow due to a higher porosity and therefore the possibility of a more rapid flow; however, this strongly depends on whether there is a deficit or surplus of N in the environment and on biological uptake in the organic layers. A decrease in the $NH_4^+$ concentration in organic and mineral interflow waters is expected due to nitrification (Stottlemyer and Toczydlowski, 1999).

Sodium, $Na^+$, originates mainly from marine deposits (NaCl) but may also originate from mineral weathering (clays and feldspars), ion exchange, and leaching from unfrozen litter (Jones and Pomeroy, 2001; Borggaard and Elberling, 2004). Changes in $Na^+$ concentration are often used for estimation of meltwater routing as it considered a relatively conservative ion (Jones and Pomeroy, 2001). Thus, a relative increase in $Na^+$ concentration for the organic and mineral interflow is assumed as a result of ion exchange.

Potassium may either be of organic origin (i.e. biosolids, plant breakdown, or manure) or inorganic origin (i.e. weathering of micas and feldspars) and is an essential component of plant nutrition (Havlin *et al*., 1999). Plants readily take up $K^+$ where it remains soluble, as it does not become a structural component of organic compounds, like $NO_3^-$. Consequently, organic matter does not have to undergo mineralizing reactions in order to release $K^+$ and will therefore be readily soluble in rain, snowmelt, and/or soil water. However, since plant and microbiological activity are limited in frozen soil (e.g. Jones, 1999; Kimmins, 2004), changes in interflow water concentrations are assumed limited due to biological uptake. A relative increase in the cation concentration in the interflow relative to the meltwater may be observed as a result of $K^+$ leaching from unfrozen litter decomposition concentration in the organic interflow (Havlin *et al*., 1999) and/or as a result of cation exchange in either the organic or the mineral interflow (e.g. Borggaard and Elberling, 2004). A decrease in the mineral interflow concentration could be a result of fixation of $K^+$ in-between clay minerals (2:1 clays), as these are not readily released back into solution. Stottlemyer *et al*. (1997) showed that an increase in the $K^+$ concentration of the snow meltwater in the later parts of the melt season may occur due to leaching of soluble $K^+$ from the debris within the snowpack, leaching from the canopy, and/or leaching from shrubs.

The majority of $Mg^{2+}$ is derived from marine deposits (Meybeck *et al*., 2005) whereas $Ca^{2+}$ is mainly derived from weathering of sedimentary, igneous, and metamorphic rocks (e.g. Fetter, 1994). Calcium and $Mg^{2+}$ concentrations can be high in the snow due to wind transport from locally exposed calcareous bedrock. Leaching from unfrozen litter may increase the ion concentrations in the organic interflow (Jones and Pomeroy, 2001) and dissolution of $CaCO_3$ (equation 2.13) due to continuous contact with the calcareous soil is assumed to increase the concentrations in the mineral interflow (Borggaard and Elberling, 2004). Ion exchange in both organic and mineral layers may cause a decrease in $Mg^{2+}$ and $Ca^{2+}$ concentrations, as the ions will be preferentially retained at exchange sites relative to $Na^+$ and $K^+$ (e.g. Borggard and Elberling, 2004). Consequently, changes in the concentrations are expected to be limited for the organic interflow and to result in increasing concentrations in the mineral interflow.

Dissolved organic carbon (DOC) originates from plant litter breakdown, root exudates, and decomposition of organic matter (e.g. Borggaard and Elberling, 2004). It is an important component in mineral weathering and dissolution of plant nutrients due to its acidic nature (e.g. equation 2.12). During reducing conditions, it is an important component in denitrification, iron reduction, and sulphate reduction (e.g. Freeze and Cherry, 1979). The concentration of DOC in snow is very low making DOC a good indicator for contact with the organic layer. Consequently, a large increase in DOC concentration is assumed for the organic interflow. An increase in concentration is also assumed for the mineral interflow due to the content of organic matter in the top most part of the mineral soil layer (e.g. Borggaard and Elberling, 2004); however, this increase is assumed to be much less than that of the organic interflow.
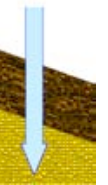
# CHAPTER 3

# OBJECTIVES

In many snow covered regions with seasonally frozen ground, seven flowpaths can be hypothesized that are affected by the infiltration regime of the frozen ground and contact with organic and/or mineral soil layers. Table 3.1 shows a schematic overview of these flowpaths. Knowledge of the partitioning of meltwater discharge from the snowpack between infiltration and runoff is important as it impacts nutrient and contaminant delivery to surrounding terrestrial and aquatic ecosystems (e.g. Rascher *et al*., 1987; Abrahams *et al*., 1989; Jones, 1999).

Snow processes and chemistry, i.e. metamorphism, formation of preferential flowpaths, refreezing, and ion fractionation, have been well studied due to their implication on the timing and magnitude of runoff (e.g. Marsh, 2005). In order to link

*Table 3.1. Schematic overview of the theoretical flowpaths constituting the three flowpaths that are hypothesized distinguishable based on compositional changes in chemistry. The light blue line underneath the arrows in flowpath 1 and 4 illustrates an ice layer.*

| Flowpath # | 1 | 2 | 3 | 4 | 5 | 6 | 7 |
|---|---|---|---|---|---|---|---|
| *Snowpack* *Organic Layer* *Mineral Soil* | | | | | | | |
| **'Soil Contact'** | No Contact | ———— Contact ———— | | | ———— Contact ———— | | |
| **Infiltration Regime** | Restricted | ———— Limited ———— | | | ——— Limited ——— | | Unlimited |
| **Flowpath Type** | Overland Flow | Overland Flow | – Organic Interflow – | | – Mineral Interflow – | | Infiltration |

the chemical composition of meltwater to that of stream water, understanding the chemical transformations that may occur along hydrological flowpaths is also important (e.g. Peters and Driscoll, 1989). Though the interaction between meltwater discharge and the underlying stratum is poorly understood (e.g. Rascher *et al.*, 1987; Quinton and Pomeroy, 2006); most research has focused on chemical alteration due to contact with unfrozen ground (e.g. Peters and Driscoll, 1989). Similarly, studies of basal ice formation and its impact on runoff water routing and chemistry are limited (e.g. Wakahama *et al.*, 1976; Jones and Pomeroy 2001) and many have been carried out only in Arctic regions with distinctive energy and melt regimes (e.g. Marsh and Woo, 1984a). As a result, this thesis will primarily consider the alterations in chemical composition of meltwater due to contact with a basal ice layer, a frozen forest organic layer, and a frozen mineral soil.

Contact between meltwater and the organic and/or mineral soil layer and mixing between meltwater and matrix water will alter the ion content and concentrations of surface runoff, interflow, and infiltrate. The chemical alteration of snowmelt water upon release from the snowpack is hypothesized to depend on: i) matrix water solution, ii) biochemical reactions, and iii) mixing of waters. These processes can vary with flowpath, residence time, and mixing with old matrix water.

In areas, where a thin, well-developed organic layer overlies a calcareous mineral soil, it is hypothesized that as soon as contact with the layer occurs, chemical change takes place. No contact with a substrate is hypothesized only to occur when an ice layer is formed at the base of the snowpack, preventing contact; saturation of the underlying stratum will not restrict contact. Consequently, only three major flowpaths are hypothesized to be distinguishable based on chemical alteration:

- *Overland flow,* where a continuous basal ice layer at the bottom of the snowpack results in a restricted infiltration regime; all meltwater ends up as surface runoff and no contact between meltwater and soil surface occurs (flowpath 1 in Table 3.1). The chemical alteration of meltwater is hypothesized to depend on the spatial variability in the elution rate from the snowpack, refreezing of meltwater, and whether it is a melting or a growing basal ice layer. It is hypothesized that ion exclusion takes place during formation of a basal ice layer, forming an

enriched quasi-liquid layer on its surface, which will readily mix with runoff meltwater and increase the concentrations of some ions.

- *Organic interflow*, a limited infiltration regime, where the infiltrating meltwater is only in contact with the organic layer (flowpath 2 to 4 in Table 3.1). The compositional change due to contact between infiltrating water, the layer, and existing soil water is hypothesized to be dominated by the acidic regime of the organic layer. If the organic layer is fully saturated, meltwater ends up as surface runoff (flowpath 2); however, alterations will still occur since contact with the organic layer exists. Flowpath 3 is a result of flow through macropores, which channels the infiltrated water rapidly through the layer, minimizing residence time and surface area of contact, and limiting the possibility of chemical change. An ice layer at the interface between the organic layer and the mineral soil may restrict the organic interflow and result in additional chemical alterations due to ion exclusion as the ice layer is formed (flowpath 4).

- *Mineral interflow*, where contact with the mineral soil is hypothesized to cause rapid alteration of the chemical composition as a result of its buffering capacity (flowpath 5 to 7 in Table 3.1). The infiltration regime may be either limited or unlimited, depending on the mineral soil's degree of saturation. Flowpath 5 is present if saturated conditions or concrete frost in the mineral soil limit infiltration, resulting in flow along the interface between the organic layer and the mineral soil. Flowpath 6 is present where the top most layer of the mineral soil is unsaturated, or thawing, allowing infiltration, which leads to a horizontal flow over the underlying, saturated frozen soil. Saturation of this layer will result in flowpath 5. The only scenario where an unlimited infiltration regime is present is if all the water percolates deeper into the vadoze zone (flowpath 7), where it eventually may become part of groundwater flow.

Partitioning of infiltrating water may take place at any flowpath interface due to a difference in infiltration rate between the layers. In the field, the flowpaths may be more complex and runoff at any one point on the slope may consist of a mixing of water from

all the theoretical flowpaths; however, this is hypothesized to be recognized as mineral interflow.

Being able to distinguish between the different flowpaths is important due to the impacts that they may have on aquatic and terrestrial ecosystems. Runoff over a basal ice layer will be rapid. The solute concentrations in the meltwater will often be dilute; however, the delivery of the ions is fast. Thus, in areas prone to acidic precipitation the environmental impact may be severe. Organic layers often have a high porosity and thereby have the ability to transmit water as interflow rapidly from hillslope to water body compared to mineral soils (e.g. Carey and Woo, 2001). The matrix water in the organic layer is often acidic due to a high content of organic acids; thus, the impact of the rapid delivery of ion to the ecosystems may be grave. In an environment where precipitation is acidic and the buffering capacity of the mineral soil is high, the impact on the ecosystem from mineral interflow will be limited. A decrease in the flow rate, due to different hydraulic conditions in the three flowpaths, allows longer opportunity time for chemical alteration.

The objective of this thesis is to better understand how flowpaths in frozen soil and their flow celerity alter water chemistry. This understanding may aid in larger efforts to use chemistry to differentiate between surface flow, flow in the organic layer, and flow in mineral soil. It may also help apportion snow ion load between the aquatic and terrestrial ecosystems. This overall objective can be met by addressing three sub-objectives:

i. To better understand the rate and magnitude of chemical change of snowmelt runoff and interflow along a hillslope,

ii. To better understand the effects of mixing of snowmelt and matrix water in frozen soils; and

iii. To better understand changes in runoff chemistry due to exclusion of ions during refreezing above or infiltration of ion load into frozen ground.

# CHAPTER 4

# METHODOLOGY

Laboratory and field experiments were conducted to evaluate the objectives of this thesis. Field observations were supported by laboratory experiments to elucidate uncertainties associated with field investigations; i.e. timing of snowmelt and sampling.

## 4.1    Preparation of Equipment

Before use, all equipment and sampling bottles were rinsed with plenty of distilled (DI) or deionized distilled water (DDI) where after they were left to soak in fresh DI or DDI water for at least 24 hours. A Barnstead Megapure System with a high capacity disposable deionizer cartridge (#D400499) produced the DDI; it was located in the Soil Science Department, University of Saskatchewan. In the field, materials were cleaned between usages with DI water from a Millipore 3 reverse osmosis water purification system located at the University of Calgary, Kananaskis Field Station, Alberta.

During experiments, equipment was rinsed in-between usages and left to soak over night. Rinsed materials that were not used right away were left to air-dry upside-down where after they were stored wrapped in plastic (PE) to prevent contamination. Sterile Ultrafree™ latex gloves (Cardinal Health; 2D72F7I) were worn at all times to prevent contamination.

## 4.2    Cryospheric Environmental Laboratory

Laboratory experiments were carried out in a temperature-controlled cryospheric environmental laboratory (CEL) located at Centre for Hydrology, University of Saskatchewan. The CEL contains a dual refrigerating system (Heatcraft, BZ series) with stable cooling capacity from +7.5 to −30 ºC (±2 ºC); experiments were carried out

within the range –5 to +7.5 ºC. The CEL is sealed to prevent contamination of samples from dust and atmospheric particulates. The floor area was 18 $m^2$ with a free height of ~2 m.

The CEL was used for experiments that examined enhanced infiltration into frozen soil and compositional changes of meltwater as a result of contact with a basal ice layer, an organic layer, or mineral soil.

## 4.3    Enhanced Infiltration

Enhanced infiltration was demonstrated and evaluated both theoretically and in the laboratory to evaluate the possible magnitude of the enhancement of ion infiltration due to covariance between infiltration rate in frozen soil and ion concentration in the meltwater released at the base of a melting snowpack (Chapter 5). Field-testing was attempted at the observation site described in section 4.5.1.

### 4.3.1   Demonstration Scenarios

Four sites, all located in western Canada, were used to demonstrate the theory of enhanced infiltration and assess its sensitivity to various environmental conditions (Figure 4.1). At all four demonstration sites, a large part of the annual precipitation falls as snow and soils are frozen at the time of snowmelt. Using field-based meteorology, soil and snow conditions to evaluate the model proposed in Chapter 5 is considered an appropriate first step in assessing the importance of enhanced infiltration over a wide range of environmental conditions. The four sites are:

- A *Prairie site*, located in St. Denis National Wildlife Area (52º 02' N 106º 06' W) in south-central Saskatchewan. This area is cultivated for cereal grains and oilseeds or left to hay and native pasture and has a gently rolling terrain with fine loamy textured soil underlain by clay-rich glacial till (van der Kamp *et al.*, 2003);

- A *Boreal Forest site*, located in Prince Albert National Park (53º 53' N 106º 07' W), central Saskatchewan. The site is in the southern boreal forest and has a terrain that consists of gently rolling slopes with vegetation consisting of 15-25

*Figure 4.1. Location of four demonstration sites used to evaluate enhanced infiltration: a Prairie site, a Boreal Forest site, a Mountain Forest site, and a Tundra site. See site descriptions in the text.*

m tall jack pine and aspen stands together with 10-12 m tall black spruce stands (Pomeroy *et al.*, 1997). The understory consists of deciduous bushes and sphagnum moss; an organic layer overlies sandy loam textured soils, developed on thick glacial deposits;

- A *Mountain Forest site*, located in the Marmot Creek Research Basin (50º 56' N 115º 08' W) in the Kananaskis River Valley of the Rocky Mountains, Alberta. The site has a ~20º inclination, facing almost due east, and a vegetation that is dominated by mature lodge-pole pine with an average trunk density varying from ~0.3 to ~0.6 trunks m$^{-2}$. Ground cover consists mostly of grass and litter, with sparse deciduous shrubs. The mineral soil consists of sandy loam with a high content of silt and clay and is overlain by a poorly developed organic layer with a general thickness between 0.03 and 0.05 m;

- A *Tundra site*, located in Wolf Creek Research Basin, Yukon (60° 32' N 135° 18' W), on the northern fringe of the Coast Mountains in the zone of discontinuous permafrost (Quinton *et al.*, 2005; McCartney *et al.*, 2006). The

soil consists of glacial till overlain by <0.14 m organic layer. The tundra is shrub tundra with vegetation dominated by *Salix* and *Alnus*.

Soil, snow, and melt properties for each site are summarized in Table 4.1. $C$ is a dimensionless location coefficient; $S_0$ is the soil moisture at the surface [mm$^3$ mm$^{-3}$]; $S_I$ is the average soil saturation (water + ice) of the top 0.4 m of the soil [mm$^3$ mm$^{-3}$]; $\phi$ is the porosity of the soil [mm$^3$ mm$^{-3}$]; $T_I$ is the average initial soil temperature within the top 0.4 m of the soil [K]; $SWE$ is the snow water equivalent [kg m$^{-2}$]; $C_i(0)$ is the initial sulphate concentration in the snowpack [meq m$^{-3}$]; $M$ is the melt rate [kg m$^{-2}$ s$^{-1}$]; $t_o$ is the infiltration opportunity time in hours [h]; $k$ is a dimensionless leaching factor; and

Table 4.1. *Soil, snow, and melt properties for four demonstration sites. Parameter values were obtained from literature and field data. Initial bulk snow ion concentrations, $C_i(0)$, were all for SO$_4^{2-}$. Melting was assumed to occur 12 hours/day at the Prairie and Tundra sites and for 8 hours/day at the forested sites. Values for k were chosen based on CF$_{max}$ values presented in previous studies (e.g. Tranter, 1991).*

| | PARAMETER | SITES | | | |
|---|---|---|---|---|---|
| | | **ST. DENIS** | **PRINCE ALBERT NATIONAL PARK** | **MARMOT CREEK** | **WOLF CREEK** |
| | | Sask. PRAIRIE | Sask. BOREAL FOREST | Alta. MOUNTAIN FOREST | Yukon SHRUB TUNDRA |
| *Soil Properties* | **C** | 2.1 [1] | 1.14 [1*] | 1.14 [6] | 1.14 [6*] |
| | **$S_0$** [mm$^3$ mm$^{-3}$] | 1.00 [2] | 1.00 [2] | 1.00 [2] | 1.0 [2] |
| | **$\phi$** [mm$^3$ mm$^{-3}$] | 0.45 [3] | 0.44 [3] | 0.44 [3] | 0.44 [3] |
| | **$S_I$** [mm$^3$ mm$^{-3}$] | 0.60 [4] | 0.57 [1*] | 0.68 [8] | 0.80 [10] |
| | **$T_I$** [°K] | 269.0 [1] | 270.0 [1*] | 271.0 [8*] | 272.0 [10] |
| *Snow Properties* | **SWE** [kg m$^{-2}$] | 85.0 [4] | 50.0 [5*] | 40.0 [8*] | 146.0 [9] |
| | **$C_i(0)$** [meq m$^{-3}$] | 12.0 [4] | 10.0 [5*] | 15.0 [8*] | 7.5 [10] |
| *Melt Properties* | **M** [kg m$^{-2}$ d$^{-1}$] | 4.5 [4] | 3.5 [5*] | 1.9 [8*] | 7.7 [9] |
| | **Melt Length** [d] | 19.0 [4] | 14.0 [4] | 21.0 [4] | 19.0 [4] |
| | **$t_0$** [h] | 226.7 [2] | 114.3 [2] | 168.4 [2] | 227.5 [2] |
| | **k** | 0.04 [4] | 0.04 [4] | 0.04 [4] | 0.04 [4] |
| | **CF$_{max}$** | 4.4 [4] | 3.0 [4] | 2.6 [4] | 6.7 [4] |

[1] Zhao and Gray, 1999; [2] Assumption based on Gray *et al.*, 2001; [3] Clapp and Hornberger 1978; [4] Field data 2006; [5] Pomeroy *et al.*, 1997; [6] Pomeroy *et al.*, 1999; [7] Assumption based on Zhao and Gray, 1999; [8] Field data 2005; [9] Pomeroy *et al.*, 2006; and [10] Carey and Woo, 2001.

$CF_{max}$ is the concentration factor in the initial meltwater, defined as the ratio between the ion concentration in the meltwater to that in the bulk snowpack [(meq m$^{-3}$) (meq m$^{-3}$)$^{-1}$]. Further descriptions of these parameters are given in Chapter 5.

Parameter values were obtained from literature and field data collected by the authors and colleagues except for the value of $k$, which was based on previously reported $CF_{max}$ values (e.g. Tranter, 1991). Porosity values based on the mineral soil texture at each site were used; values were obtained from Clapp and Hornberger (1978). Surface saturation, $S_o$, was assumed equal to 1.0 at each site due to the low infiltration rate of a frozen soil and the high likelihood of ponding above the soil (Gray *et al*., 2001).

In chapter 5, examples are presented to demonstrate enhanced infiltration with $k$ held constant at 0.04 for all four sites, causing $CF_{max}$ to vary between 2.6 and 6.7. Holding $k$ constant throughout the melt period for various sites is possible because the parameter depends on a wide variety of factors such as snowpack flowpaths, distribution of solute in snow, melt-freeze cycles, rain-on-snow, and the possibility of biological activity (e.g. Tranter, 1991).

## 4.3.2 Laboratory Experiments

Laboratory experiments were carried out in the CEL to assess whether enhanced infiltration could be identified in a small-scale laboratory experiment. The experimental setup consisted of a 0.46 m long frozen soil column with a surface area of 0.004 m$^2$ (Figure 4.2A). Each column consisted of an acrylonitrile butadiene styrene (ABS) pipe with a 1 mm mesh at the base. The column was filled with 30 mm of coarse quartz gravel (particle size was ~2-3 mm) to prevent the overlying soil from exiting the column, ~0.32 m of homogenized, dried, and ground loamy soil collected at a forested site in the Marmot Creek Research Basin, Kananaskis Valley, AB (50º 56' N, 115º 08' W), and ~0.11 m of an in-situ soil sample from the same field site. The column was placed on top of ~70 mm of filter sand (particle size was ~1 mm) to allow air to escape freely during the infiltration experiments.
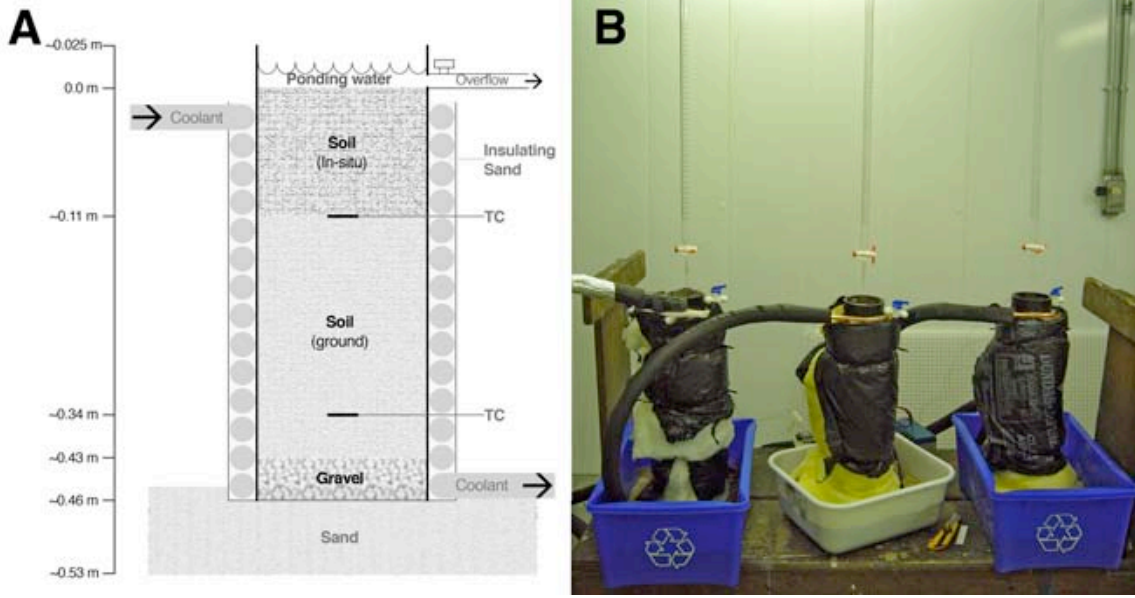
*Figure 4.2. A) Schematic drawing of soil column setup (not to scale). B) Three columns with burettes over top were set up in the cryospheric environmental laboratory (CEL).*

Type-E thermocouples (TC) were placed at two depths within the column to monitor the temperature of the soil: one at the interface between the in-situ soil sample and the homogenized soil, and one towards the base of the column (~0.34 m). The accuracy of the TC was ±0.1 ºC within the applied temperature range (Campbell Scientific, 2007). Temperatures were recorded every 10 s by a Campbell Scientific CR21X datalogger. In the first experiment the values were averaged and logged hourly; in the following two experiments, the values were averaged and logged every 10 min.

Copper pipe was coiled tightly around the ABS pipe and connected to a temperature-controlled refrigerated bath (RTE-DD8, Neslab). This allowed circulation of coolant, which was used to maintain frozen soil conditions during experiments. Filter sand was used to fill the voids between the coils. Insulation was wrapped around the outside of each column for further insulation.

Three experiments were carried out, differing with respect to initial average soil saturation, $S_I$ [mm$^3$ mm$^{-3}$], which was estimated from average volumetric soil moisture, $\theta$ [mm$^3$ mm$^{-3}$], and average soil porosity, $\phi$, as $S_I = \theta/\phi$. Each experiment was conducted simultaneously on three soil columns (Figure 4.2B). One experiment was conducted on air-dried soil, which hygroscopic water content (~2%) was determined using standard

oven-drying method (Levitt and Young, 2008). Average $S_I$ for the dry soil was 0.06 mm$^3$ mm$^{-3}$ (dry conditions). Two experiments were conducted on wetted soil: an unsaturated and a saturated experiment. Wetting of the soil columns were done by allowing water to enter from the base, by capillary forces; the columns were placed on a layer of filter sand to ease the process. Water depth was ~0.3 m for eight days. Hereafter, the columns used in the unsaturated experiment were allowed to drain by gravity at room temperature for three days. Time constraints dictated this time period and thereby the average initial soil saturation of 0.83 mm$^3$ mm$^{-3}$. To ensure saturated conditions of the columns used in the saturated experiment, water was ponded on top of the columns 24 h prior to experimental use; average $S_I$ was 0.97 mm$^3$ mm$^{-3}$. Volumetric soil moisture in the columns were determined by weight; assuming a density of the water of 1000 kg m$^{-3}$.

The dry and saturated conditions were selected to represent the boundaries for the effect of enhanced infiltration during infiltration to frozen soil and the infiltrability cases described as "unlimited" and "restricted" by Granger *et al*. (1984). For the dry soil, infiltration was assumed unlimited because the pore space was free of ice. For the saturated soil, infiltration was presumed restricted as a result of ice in the pore spaces. The unsaturated conditions represented a situation in-between, where part of the pore space was filled with ice, limiting infiltration.

The soil columns were allowed to freeze for a minimum of 12 hours at a room temperature of −2 ℃ (±2 ℃). Circulation of coolant took place during this period too, allowing a rapid freezing (< 4 h); the temperature of the coolant was −2 ℃ (±2 ℃). The experimental setup caused the freezing of the soil to occur from the sides as well as top and bottom. This is not like in nature, where freezing generally occurs from the top; in areas where permafrost exists, freezing of the soil can also progress from below. The method of soil freezing will influence the migration of soil moisture that takes place during freezing of the soil (e.g. Male and Gray, 1981; Kane and Stein, 1983; Williams and Smith, 1989). However, redistribution of soil moisture is considered negligible in extremely dry soils (i.e. the dry experiment) and only limited migration was expected in the unsaturated and saturated soil columns due to their high $S_I$ (e.g. Gray *et al*., 1984).

The temperature in the CEL was increased just prior to initiation of the experiments. Average room temperature during experiments was +1.6 ºC (±1.2 ºC). Small adjustments (±2 ºC) of the coolant temperature were made throughout the experiments to ensure frozen soil conditions; these adjustments were based on the TC readings within the soil columns. Total experimental time for each column was 12 hours.

To simulate preferential ion elution from an overlying snowpack, chloride solutions with decreasing concentrations with time were added to the soil surface (Figure 4.3). Burettes (100 ml) were used for the application; rates varied between 0.001 kg s$^{-1}$ m$^{-2}$ (3.6 mm h$^{-1}$) and 0.020 kg s$^{-1}$ m$^{-2}$ (72 mm h$^{-1}$); the average rate was 0.010 kg s$^{-1}$ m$^{-2}$ (36 mm h$^{-1}$). This range of rates was strongly influenced by the burettes themselves; however, an overflow valve (4 mm in diameter) prevented ponding greater than ~10 mm. An increasing ponding depth, and thereby head, would result in changing infiltration conditions as time progressed (i.e. enhance the rate of infiltration for the water). Thus, the maximum head was chosen to resemble field conditions. The chloride concentration decreased exponentially from ~81400 meq m$^{-3}$ (~2890 ppm) to ~4060
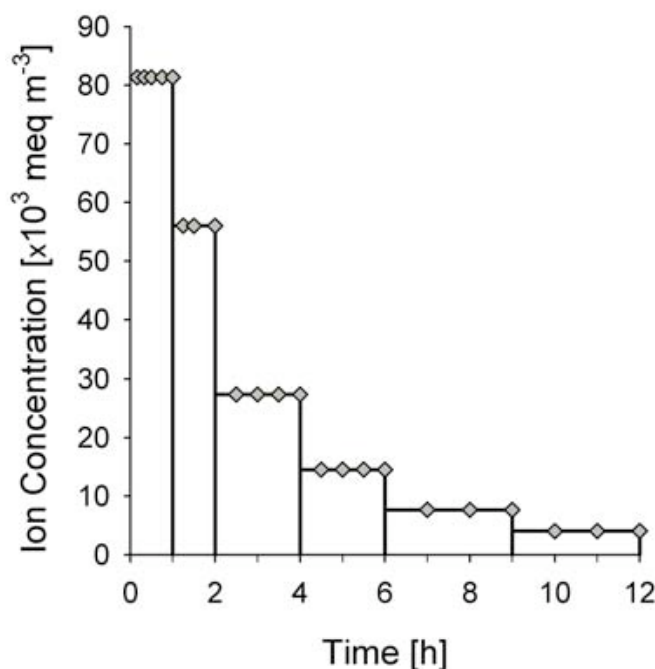


*Figure 4.3. Changes in the applied chloride concentration over time (line). The diamonds represents when sampling occurred.*

meq m$^{-3}$ (~145 ppm) during the 12 hours. Solutions were spiked compared to normal snow concentrations to achieve an enhanced indication of changes in ion load. The solutions were at room temperature (~2℃) when they were added. In each experiment, initial addition of solution to the soil surfaces of column 2 and 3 were delayed 25 and 50 minutes, respectively, due to the timing of sample collection.

Infiltration excess water was collected using a syringe at increasing time intervals (Figure 4.3). All water was collected each time to determine the mass of water that had infiltrated the soil. Samples were stored at 3 ℃ until analysed (<24 h).

## 4.4    Flowpath Signatures

An insulated box, with a cooling system at the base, controlled snowmelt and basal cooling to examine the compositional change of meltwater for each of the hypothesized flowpaths (Figure 4.4). Expanded polystyrene plates were used as insulation. Inside surfaces of the box, i.e. base and sides, were covered by polyethylene to prevent contamination.

The front of the box had a slit along the base for collection of runoff water (RW), which had sustained contact with a basal ice layer, an organic layer, or mineral soil layer. An acrylonitrile butadiene styrene (ABS) half-pipe (50 mm diameter) was placed with its base ~30 mm above the slit opening for extraction of meltwater before basal contact (SW). The half-pipe covered a tenth of the base area. The base consisted of a
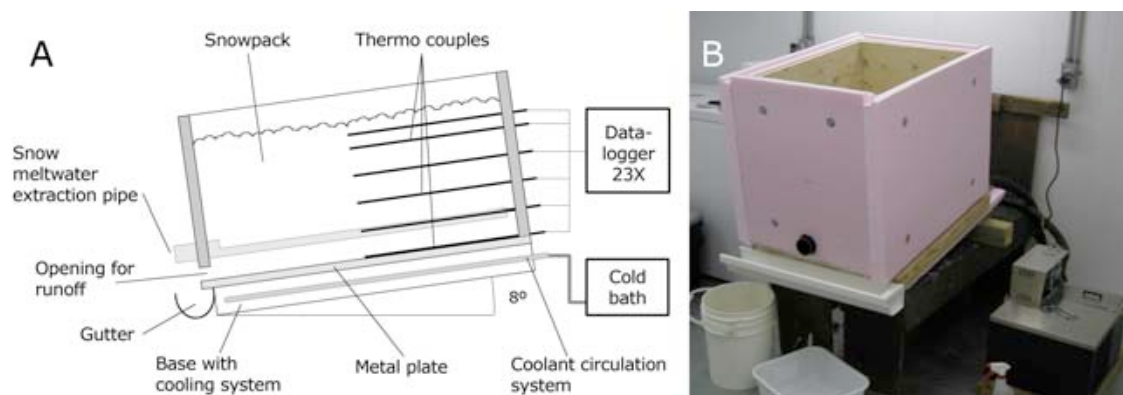


*Figure 4.4. A) Schematic drawing of the experimental box and its instrumentation (not to scale). B) The actual box placed in the temperature-controlled cryospheric environmental laboratory (CEL).*

metal plate, which was underlain by a cooling system that was connected to a temperature controlled refrigerated bath (RTE-DD8, Neslab). The entire apparatus was tilted 8º so that water drained freely into collectors.

Variations in snowpack temperature were measured using type-E and –T TCs; they were placed at the base and 10, 20, 30, 40, and 45 cm above the base. A type-K TC was used to measure the temperature of the coolant. The accuracy of the individual TC are ±1.75% for type-T, ±1.25% for type-E, and ±2.25% for type-K within the applied temperature ranges (Campbell Scientific, 2007) or ±0.1 ºC for most of the measurements. Temperatures were sampled every 10 s; averaged temperatures were recorded every 15 minutes by a Campbell Scientific CR23X datalogger.

Experiments were conducted using snow from a site located within the limits of Saskatoon, Saskatchewan, Canada, a city of just over 200,000 with a cold continental climate and little industry, and two sites located in rural areas 15 km outside of city limits, in a hay meadow. Snow was collected within a few days of snowfall and composed of loose 1-2 mm crystals; metamorphism was not pronounced. Snow was stored at –20 ºC until used in experiments.

To homogenize the snowpack, the snow was sieved with an 8 mm mesh (HDPE). The depth of the snowpack ranged between ~0.4 and ~0.45 m at the beginning of the experiments, giving a total snow volume between 0.13 and 0.15 $m^3$ within the box. The initial densities of the snowpacks ranged between ~215 kg $m^{-3}$ and ~440 kg $m^{-3}$. The snow was then left to reach thermal equilibrium at a room temperature of –2 ºC; coolant temperature ranged between –5 °C and –2 °C in each experiment, respectively. Once thermal equilibrium was reached, the room temperature was increased to +5 ºC or +7.5 ºC. Small adjustments (±3 ºC) of the coolant temperature were made throughout each experiment to ensure frozen conditions at the base of the box. These adjustments were made based on the TC readings at the base of the snowpack.

Experiments differing with respect to the layer underneath the snowpack were carried out to identify the compositional change of runoff water (RW) in unmixed flowpaths due to contact with either a growing basal ice layer, an organic layer, or a mineral soil layer. During melt, water samples (RW and SW) were collected

simultaneously twice a day. The volumes of melt- and runoff water as well as the changes in snow depth were observed throughout melt.

### 4.4.1  Basal Ice Layer

Keeping the base temperature below zero ensured formation of an ice layer at the base of the snowpack. Once meltwater reached the base of the snowpack refreezing occurred, forming an ice layer. Three experiments (BI-1, -2, and -3) were conducted varying with respect to snowpack density, melt rate, and temperature at the base of the snowpack. In BI-1 the initial snow density, $\rho_s$, was 350 kg m$^{-3}$, average melt rate, $\overline{M}$, was 3.6 kg m$^{-2}$ s$^{-1}$, and the average temperature at the base of the snowpack was –2 ºC; in BI-2, $\rho_s$ was 410 kg m$^{-3}$, $\overline{M}$ was 6.8 kg m$^{-2}$ s$^{-1}$, and the average base temperature was –0.5 ºC; and in BI-3, $\rho_s$ was 215 kg m$^{-3}$, $\overline{M}$ was 7.8 kg m$^{-2}$ s$^{-1}$, and the average base temperature was –0.2 ºC.

### 4.4.2  Organic Layer

The base of the box was covered by a ~60 mm thick organic layer, which consisted of five sections (0.14 x 0.48 m$^2$), which were collected in-situ at a forested field site in the Marmot Creek Research Basin, AB (50º 56' N, 115º 08' W), in the fall of 2005 (Figure 4.5A). Samples were stored and kept frozen (≤–5 ºC) in wooden boxes until the experiments were carried out, to limit alterations in the organic layer.

The samples were placed with their lengths perpendicular to the general flow direction to eliminate preferential flow along their connecting edges. The sections were arranged so they looked like a continuous organic layer, comprised of decomposed litter and deadfall covered with moss and/or litter (Figure 4.5B). Prior to applying the organic material to the box the individual samples were rinsed for mineral soil to prevent its influence on the chemistry of the interflow water.

The temperature at the base of the organic layer was kept below zero throughout the experiments. The TC at 10 cm height above the base was used as an indicator for conditions at the surface of the layer. A total of three experiments (OIF-1, -2, and -3) were carried out, differing in snow density, melt rate, base temperature, and organic

*Figure 4.5. A) One of the five sections of which the organic layer was comprised. B) The organic layer at the base of the box was made to look natural.*

layer moisture content. In OIF-1, $\rho_s$ was 290 kg m$^{-3}$, $\overline{M}$ was 8.3 kg m$^{-2}$ s$^{-1}$, the average temperature at the base of the snowpack was –0.8 ºC, and the initial gravimetric moisture content, $\omega$, was 0 g g$^{-1}$; in OIF-2, $\rho_s$ was 297 kg m$^{-3}$, $\overline{M}$ was 8.9 kg m$^{-2}$ s$^{-1}$, the average temperature at the base of the snowpack was –0.9 ºC, and initial $\omega$ was 2.7 g g$^{-1}$; in OIF-3, $\rho_s$ was 400 kg m$^{-3}$, $\overline{M}$ was 11.8 kg m$^{-2}$ s$^{-1}$, the average temperature at the base of the snowpack was ~0 ºC, and initial $\omega$ was 2.8 g g$^{-1}$;

### 4.4.3 Mineral Soil Layer

Loamy soil was collected in the fall of 2005 at the field site in the Marmot Creek Research Basin, AB, and stored at room temperature (~20 ºC) in plastic bins; undisturbed sampling was not possible.

During storage, the soil air-dried and became hard due to the high content of silt and clay. To add the mineral soil to the box, in addition to making it resemble a natural soil layer, the soil was saturated with excess snow meltwater from previous experiments. The wetted soil was then homogenized by stirring. The soil was added to the base of the box in an even layer approximately 75 mm thick (Figure 4.6A). A type-E TC was placed
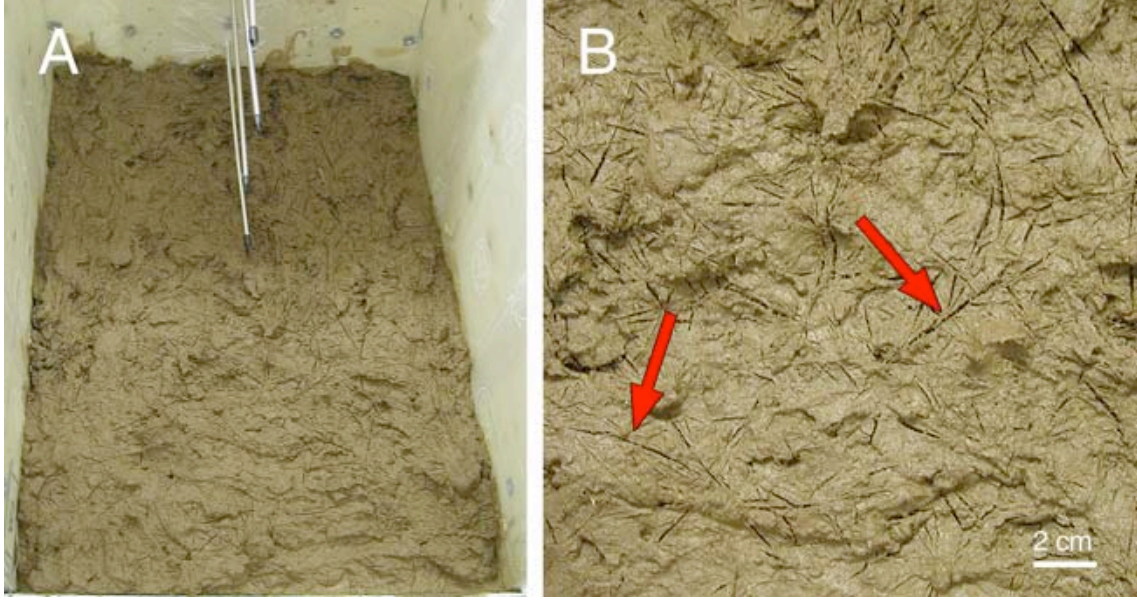
*Figure 4.6. A) View of the mineral soil cover at the base of the box. B) Close-up of macropores (arrows); area is 0.2 x 0.2 m².*

within the soil layer, ~50 mm above the base. The soil was left to settle in the box for a month at +15 ºC, as well as allowing excess water to evaporate. Following, macro-pores were added artificially to the soil layer by exposing it to freeze-thaw cycles. Verification that this methodology worked was done visually (Figure 4.6B).

Two experiments (MIF-1 and -2) were carried out varying in snow density, melt rate, base temperature, and initial soil moisture content. In MIF-1, $\rho_s$ was 430 kg m$^{-3}$, $\overline{M}$ was 8.2 kg m$^{-2}$ s$^{-1}$, the average temperature at the base of the snowpack was –0.2 ºC, and initial $\omega$ was 0.2 g g$^{-1}$; in MIF-2, $\rho_s$ was 442 kg m$^{-3}$, $\overline{M}$ was 14.2 kg m$^{-2}$ s$^{-1}$, the average temperature at the base of the snowpack was –0.1 ºC, and initial $\omega$ was 0.3 g g$^{-1}$. Repairs to the soil layer had to be made after terminating MIF-1 as 'soil slides' had taken place along the front of the box during the experiment. To ensure the presence of macropores, the layer was re-exposed to two freeze-thaw cycles.

## 4.5    Field Observations

The field site where observations were carried out was part of the Marmot Creek Research Basin (50º 56' N, 115º 08' W) located in the Kananaskis River valley, in the eastern part of the Canadian Rocky Mountains, approximately 80 km west of Calgary,
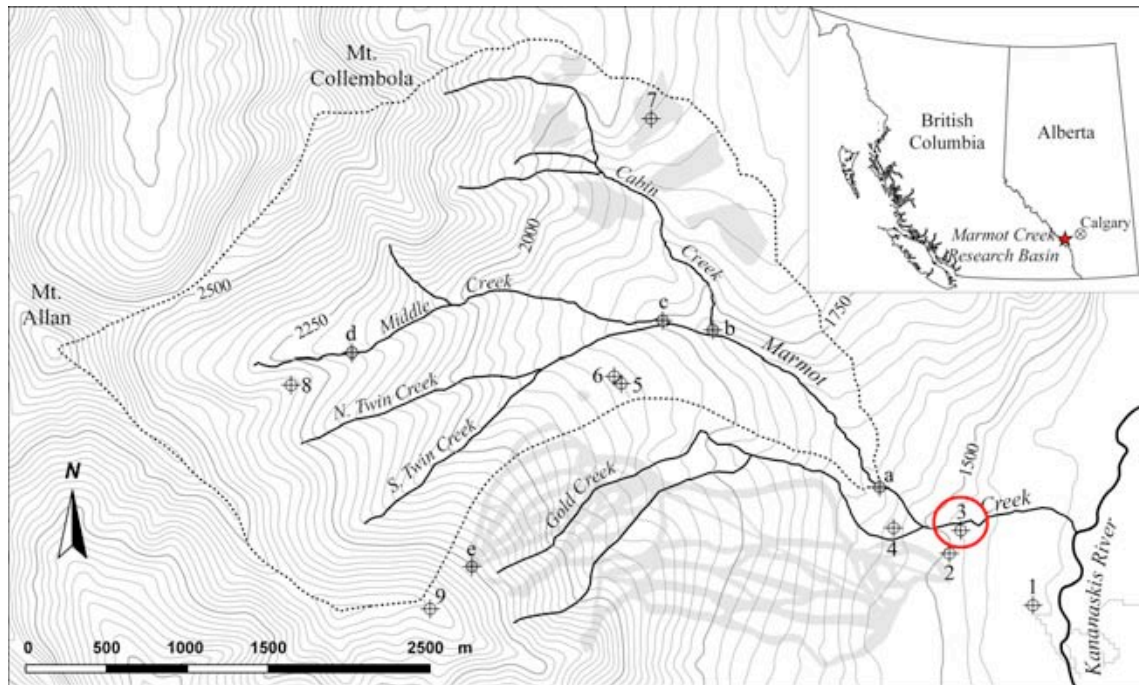
*Figure 4.7. Topographic map of the Marmot Creek Research Basin (contour interval is 25 m); map insert shows location within western Canada (by Chris DeBeer, 2008). The red circle mark the observation slope where field data was collected. Numbers 1-9 mark meteorological stations within the basin as of 2008; a-e marks other study sites within the basin (not used in this research).*

Alberta (Figure 4.7). The basin covers an area of 9.4 km$^2$ and consists of three sub-basins (Twin Creek, Middle Creek, and Cabin Creek) with a confluence area below (Kirby and Ogilvie, 1969). The terrain ranges in elevation from 1425-2800 masl and is typical of eastern slopes of the Canadian Rockies. The basin has an overall easterly aspect with an average slope of 39% (or 21º).

The regional climate consists of long, cold winters and wet, cool summers (Kirby and Ogilvie, 1969; Swanson *et al*., 1986). Temperature range and amount of precipitation vary with elevation, aspect, and slope. Annual precipitation is ~650 mm of which ~60% falls as snow (based on Kirby and Ogilvie (1969), Swanson *et al*. (1986), and measurements at the Kananaskis Field Station, ~20 km north of the basin, from 1975-2007). There are no permanent glaciers or snowpacks in the basin. Accumulation patterns are fairly consistent from year to year (Storr, 1967) with an annual water yield from the basin that is about half of the annual precipitation (Golding and Hillman, 1981). The water balance and geology of the basin suggest that there are little or no

subsurface losses or gains on Marmot Creek (Stevenson, 1967); more resent observations suggest that Cabin Creek leaks water to groundwater flow, which leaves the basin as but that these flows are very small (e.g. Swanson *et al.*, 1986). The phreatic divide follows the surface topography of the basin closely.

More than half of the basin is covered with forest. In 1969, 48% of the basin was covered with alpine non-productive forest, rock, and meadow (Kirby and Ogilvie, 1969); the rest was considered a productive forest, which consisted mainly of 210-310 years old trees. The majority of this area (91%) was covered with spruce, fir, and pine species. At lower elevations the lodge-pole pine was mixed with spruce and aspen. Forest cutting in 1970s and 1980s (e.g. Swanson *et al.*, 1986) may have changed these percentages. A more complete review of the basin vegetation can be found in Kirby and Ogilvie (1969).

The soil cover of the basin consists mainly of well-drained glacial (till and glaciofluvial material) and postglacial deposits (talus, scree, and alluvium). The minimum infiltration rates of the deposits (unfrozen conditions) have been found to vary from $2.8 \cdot 10^{-5}$ kg s$^{-1}$ m$^{-2}$ (1.7 mm h$^{-1}$) to $4.2 \cdot 10^{-5}$ kg s$^{-1}$ m$^{-2}$ (2.5 mm h$^{-1}$) (Stevenson, 1967), which are higher than the reported intensities of most rainfall and snowmelt events in the area (Ferner, 1984; historic data from Environment Canada); extreme daily rainfall intensity for the period 1971 to 2007 was 93 mm (~3.9 mm h$^{-1}$). Consequently, most of the infiltrating water reaches streams via subsurface flow (Golding and Hillman, 1981; Swanson *et al.*, 1986). The depth of the glacial deposits varies between 18 and 30 m for large parts of the basin; however, an impeding clay layer is situated at 0.30-0.45 m depth (Golding and Hillman, 1981; Ferner, 1984; Swanson et al., 1986). Bedrock outcrops can be found along stream channels and in the upper part of the basin. In the forested areas, the soil is well developed (Ferner, 1984).

The basin was established as an experimental watershed in 1962 as part of the East Slopes Watershed Research Program (Ferner, 1984). Previous research included the influence of clear cutting and thinning of the forest (e.g. Swanson et al., 1986); hydrological and physical parameters of the forest floor under different forest cover types (e.g. Beje, 1969; Golding and Hillman, 1981); and surface water and groundwater

quality (Thomas, 1963; Gale, 1964, 1965, 1966). The basin was re-established as a research watershed in 2004 after a hiatus of ~20 years.

### 4.5.1 Observation Site

Observations were carried out on a forested east-facing slope in the lower part of the basin (~1475 masl). Total slope length was estimated to be more than 150 m; a hiking trail crossed the slope about half way down. Consequently, the study area was located approximately half way down-slope to achieve as large an undisturbed upslope area as possible. A topographical map of the site was generated from topographic surveys made using a Sokkia SET 610 surveyor's level (Figure 4.8A). An 8 by 8 grid with 5 m spacing was set up for this. The map shows that the slope has a concave shape that faces almost due east with an inclination varying between 19º and 22º.

### *Vegetation*

The forest cover was dominated by 10-15 m tall lodge-pole pine with an average trunk diameter of 0.1 m. The number of fallen trees was generally low; however, in the south-eastern part of the area the density of fallen trees was so high that it was impossible to walk there. Digital hemispherical images were recorded at 13 points across the site to
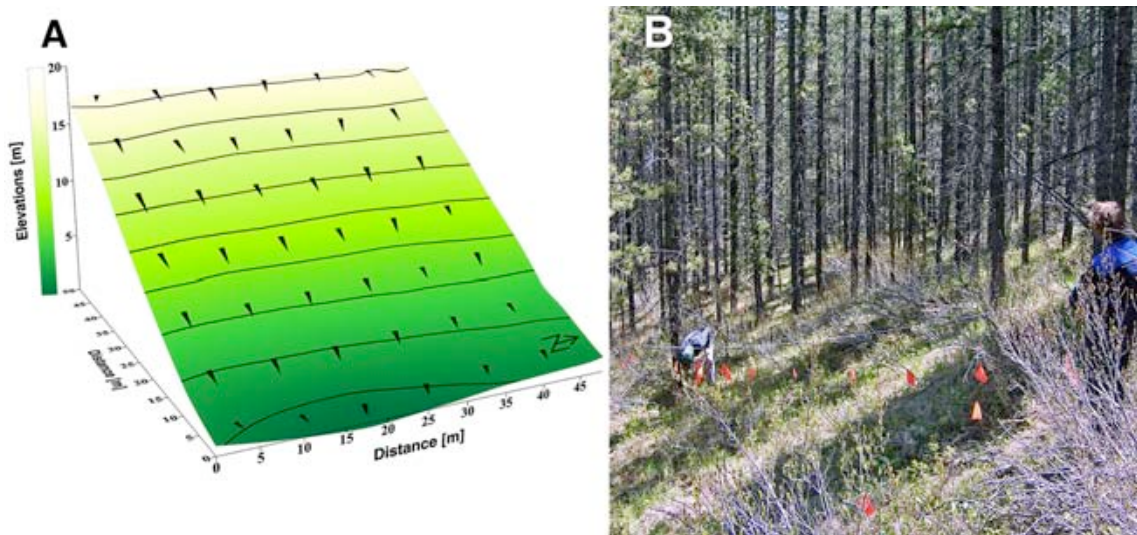


*Figure 4.8. A) Topographic map of the study site; the contour interval is 2 m and the ratio between height and distance is 1.5. B) Picture of the slope looking towards southeast, across the experimental area.*

examine the structure of the canopy; the methodology is described in Appendix A. Each image was processed using 'Gap Light Analyzer 2.0' to determine leaf area index, LAI [leaf surface area per unit ground area], and canopy openness [%] across the slope (Frazer *et al.*, 1999). LAI varied from 1.4 in the northwest part of the area to 1.7 in the southeast part (Figure 4.9A); average LAI was 1.6 ±0.9. Similarly, the openness of the canopy structure varied from 19% to 27%; averaging 21% ±1.8% (Figure 4.9A).

The groundcover consisted mostly of grass, moss, and litter with a few shrubs (Figure 4.8B). Most of the shrubs were located in the north-western part of the area where there were almost no trees. The organic layer varied in thickness from 0.03 to 0.05 m with a maximum thickness of 0.2 m observed in the southern part of the area.
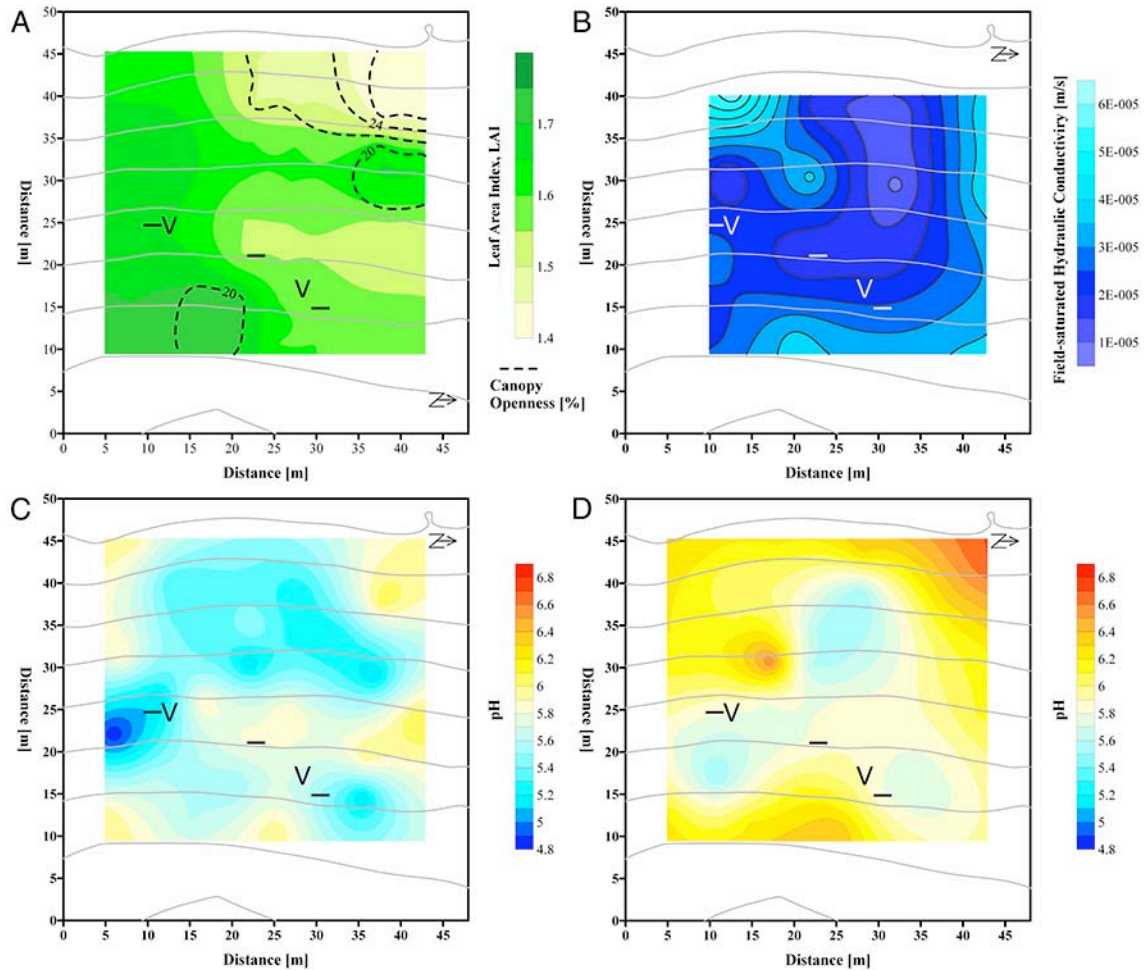


*Figure 4.9. A) Leaf area index, LAI, and canopy openness [%] across the study site. B) Field-saturated hydraulic conductivity, $K_{fs}$ [m s$^{-1}$]. C and D) Variations in pH for the organic layer and the mineral soil, respectively. The V-shape and horizontal line refer to instrumentation at the site (section 4.5.2).*

*Soil Properties*

Dry bulk density, porosity, soil texture, and infiltration rates were measured at multiple points throughout the study site. All properties were estimated for unfrozen conditions.

Undisturbed soil samples were collected at 64 points; collection was done using a 'soil sampler' with a known volume. The sample volume was double-checked by pouring quartz sand into the sampling hole and measuring the volume of sand added. This was done since an intact soil sample can be hard to obtain due to the presence of roots and rocks; often the lower part was missing. However, this was assumed not to bias the samples, as there was no visible difference in the soil texture of the missing soil. Volumes were obtained for both the organic and the mineral soil layer. After collection each soil sample was split into its organic material and mineral soil and bagged; each sample was double-bagged.

Dry bulk density, $\rho_b$ [kg m$^3$], was determined for both the organic layer and the mineral soil using standard methodology (Hillel, 1998). Samples were dried at 105 ºC for 24 hours, $M_s$ [kg], for mineral soil and at 65 ºC for organic layer. $\rho_b$ was calculated as the dry mass of solid, organic or mineral, to the total volume of the sample, $V_t$ [m$^3$],

$$\rho_b \quad = \quad \frac{M_s}{V_t} \tag{4.1}$$

Average $\rho_b$ was 1223 kg m$^{-3}$ ($\pm$318 kg m$^{-3}$) for the mineral soil and 238 kg m$^{-3}$ ($\pm$166 kg m$^{-3}$) for the organic layer.

Soil porosity, $n$, was estimated across the experimental area for the mineral soil using the estimated $\rho_b$ and an assumed soil particle density, $\rho_s$, of 2650 kg m$^{-3}$ for the whole area (Hillel, 1998)

$$n \quad = \quad \left(1 - \frac{\rho_b}{\rho_s}\right) \tag{4.2}$$

The results showed little variation in soil porosity across the slope. Average porosity was 0.54 ($\pm$0.12).

Soil texture was estimated for 12 samples collected across the slope using the standard methodology (USDA, 1993). A known volume of soil was added to a graduated cylinder and mixed with DDI water. The soil was left to settle in the cylinder

for ~24 h. The percentage distribution of sand, silt, and clay content were calculated and soil class was determined. Results showed that the soil on the slope consisted of 42% ±7% sand, 44% ±8% silt, and 14% ±6% clay giving it a loam texture, which corresponded well to the $\rho_b$ found for the area (e.g. Hillel, 1998).

Double-ring infiltrometers were used to determine the one-dimensional, vertical, steady state infiltration rate, $f(t)$ [kg s$^{-1}$ m$^{-2}$], at the interface between the unfrozen organic layer and mineral soil. The theory behind the method as well as a description of the methodology can be found in Appendix B. Sixteen measurements were carried out across the observation site and $f(t)$ ranged from $2.2 \cdot 10^{-5}$ kg s$^{-1}$ m$^{-2}$ (1.3 mm h$^{-1}$) to $1.4 \cdot 10^{-4}$ kg s$^{-1}$ m$^{-2}$ (8.4 mm h$^{-1}$); average $f(t)$ was $6.7 \cdot 10^{-5}$ kg s$^{-1}$ m$^{-2}$ (4.0 mm h$^{-1}$). These results were slightly higher than those found for the basin by Stevenson (1967).

Field-saturated hydraulic conductivities, $K_{fs}$ [m s$^{-1}$], were estimated based on the field quasi-steady infiltration rates. The term 'field saturated hydraulic conductivity' is used since air may be entrapped in the soil during this type of infiltration and lead to an underestimation compared to the 'saturated' hydraulic conductivity in completely saturated soils (Mertens *et al*., 2002; Reynolds *et al*., 2002). Results showed that $K_{fs}$ varied between $8.3 \cdot 10^{-6}$ m s$^{-1}$ and $5.8 \cdot 10^{-5}$ m s$^{-1}$. Figure 4.9B illustrates the variation in $K_{fs}$ across the slope; calculations are shown in Appendix B. The measurements show a log-normal distribution, which is similar to previous observations in forested areas (e.g. Watson and Luxmoore, 1986; Wilson and Luxmoore, 1988; Sauer and Logsdon, 2002).

### *Soil pH*

Standard methods were used to determine soil pH of the mineral soil and organic layer (USDA, 1993). For the mineral soil a 1:1 ratio between soil and DDI water was used; 10 g of dried, ground soil to 10 ml of water. For the organic layer a 1:5 ratio was used; 5 g of organic material to 25 ml of DDI water. The mixtures were stirred and allowed to stand before measurements were made; standing time was 30 minutes for the mineral mixture and 2 hours for the organic mixture. An Orion 290A meter with an Orion low maintenance triode was used to determine pH. Prior to the measurements the mixture was stirred once more.

Soil pH was determined at 30 points across the slope for both the organic layer and the mineral soil. The pH range for the organic layer was 4.8–6.1 with an average of 5.4 (Figure 4.9C); the range for the mineral layer was 5.5–6.7 with an average of 6.0 (Figure 4.9D).

## 4.5.2 Instrumentation

The northern area of the study site was instrumented with thermocouples (TC) and time domain reflectometers (TDR) within the organic layer and the mineral soil (Figure 4.10). For collection of meltwater, overland flow, and soil water, garden edges and lysimeters were installed across the slope in areas which were not obstructed immediately upslope by vegetation. All installations were carried out in the fall of 2005.

### *Soil Temperature and Moisture Content*
Type-T TCs (accuracy of ±0.1 °C; Campbell Scientific, 2007) were installed at three locations, approximately 12 m apart, for continuous measurement of the temperature within the organic layer and the mineral soil (Figure 4.10). At each site there was one measurement within the organic layer and one 5 cm below the mineral interface. At the
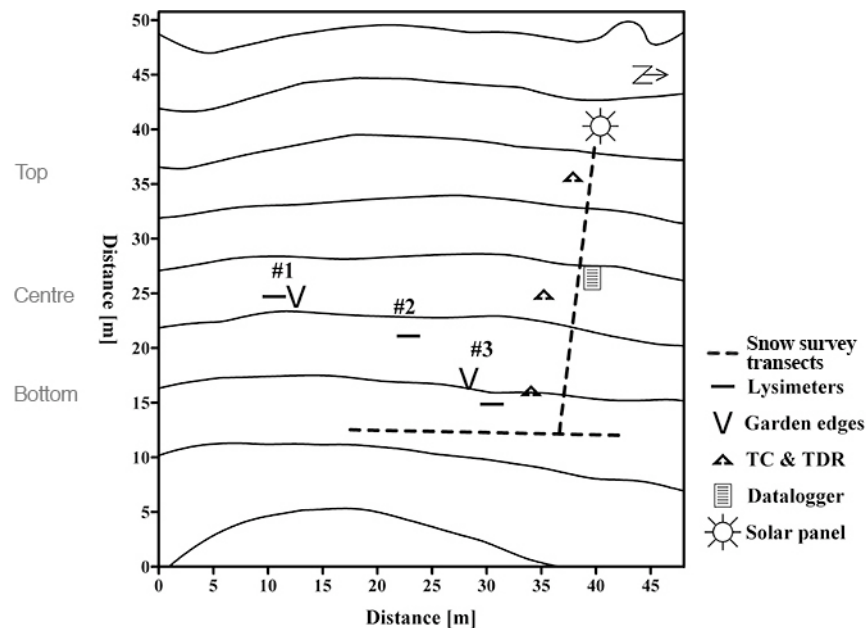


*Figure 4.10. The positioning of instrumentation at the study site. Solid lines show the relative elevation; contour interval is 2 m.*

centre site, additional measurements were carried out at the interface between the organic layer and the mineral soil, and at 5, 10, and 20 cm below the interface. A schematic overview of the setup is given in Table 4.2.

The temperature of the soil alone does not indicate that the soil is frozen. The presence of liquid water in frozen soil also depends on the concentration of soluble salts, which induces a freezing point depression (Cary and Mayland, 1972), as well as the soil moisture content at the time of freeze-up, which influences the infiltrability of the soil (e.g. Komarov ad Makarov, 1973; Kane and Stein, 1983).

The soil's liquid water content was measured using TDR probes which were installed at the same locations and depths as soil temperature probes, except at the centre location where only four probes were installed; in the organic layer, at the interface, and 5 and 15 cm below the interface (Table 4.2).

The probes consisted of two parallel stainless steel rods, 0.15 m long, which were placed 50 mm apart. All probes were installed parallel to the surface, measuring water content over a 70 mm thick layer. Since the probe rods are antennas, which both transmit and receive electromagnetic signals, installation was done ~23 cm apart from each other to avoid interference. A Campbell Scientific TDR100 was used as the pulse wave generator as well as receiver. A description of the theory and methodology of TDR is given in Appendix C.

Both soil temperatures and soil moisture contents were measured, averaged, and recorded by a Campbell Scientific Canada CR10X datalogger. Soil temperatures were averaged and recorded hourly and moisture contents every 4 hours. The data was used to

*Table 4.2. Schematic overview of the positioning of thermocouples (TC) and time domain reflectors (TDR) at the study site.*

| Slope position | Top | | Centre | | Base | |
|---|---|---|---|---|---|---|
| | TC | TDR | TC | TDR | TC | TDR |
| Organic Layer | * | * | * | * | * | * |
| Interface | | | * | * | | |
| Mineral Soil, 5 cm | * | * | * | * | * | * |
| Mineral Soil, 10 cm | | | * | | | |
| Mineral Soil, 15 cm | | | | * | | |
| Mineral Soil, 20 cm | | | * | | | |

evaluate the freezing history of the soil in late fall and to evaluate spatial variability in the freezing and thawing of the soil.

### *Overland Flow*

Garden edges (HDPE) were dug into the ground in a V-shape to redirect surface runoff and organic interflow through a HDPE plastic funnel with an attached Nalgene® premium tube (LAB/FDA/USP VI Grade) into a HDPE Nalgene® sampling bottle (Figure 4.11A). Installation was done at two locations on the slope (Figure 4.10). The edges, funnels, and tubes were installed during fall 2005; the sampling containers (1 and 3.8 l) were not installed until just before snowmelt in 2007.

### *Soil Water*

Zero tension lysimeters were constructed for drainage of soil water samples from within the soil profile. They were composed of acrylonitrile butadiene styrene (ABS) half-pipes; 0.05 m in diameter and ~0.16 m long. Installation was done by driving them into the soil at designated depths, parallel to the soil surface. Water was drained from the pipe into a sampling container.

Three transects were established for soil water collection (short solid lines on Figure 4.10). Each of these transects had three soil lysimeters in the organic layer, 0 mm; two lysimeters 50 mm below the interface between the organic and mineral layer; and two lysimeters 0.15 m below the interface (Figure 4.11B). The centre transect had
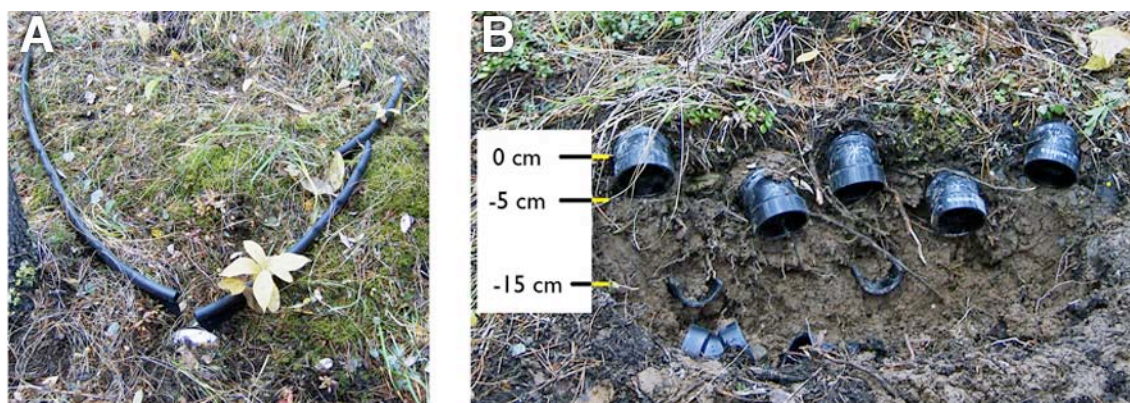


*Figure 4.11. A) Installed garden edges for collection of overland flow and/or organic interflow. The white spot at the bottom is the funnel, which redirects the water into a bottle. B) Installed zero tension soil lysimeters.*

additional lysimeters in the organic layer and 50 mm below it. The transect widths varied from 0.6 to 1.0 m, ensuring that no lysimeter was directly below another lysimeter.

### 4.5.3  Sampling Procedures

During snowmelt, snowpack characteristics and soil infiltrability were determined along two transects. The transect positions were selected to minimize snowpack interference within the upland area of sample collection and thereby flow on the slope (Figure 4.10). One transect was placed perpendicular to the slope, stretching north-south below the sampling area; the other was placed parallel to the slope (east-west) in the north part of the experimental area.

Snow surveying was carried out prior to snowmelt and daily during snowmelt to observe changes in the snowpack. The survey consists of (1) measurement of snowpack depth [m]; and (2) characterization of grain shape, grain size [mm], density [kg m$^{-3}$], and thickness [m] for individual snow layers. Melting and/or compaction of the snow cause decreases in the depth of the snowpack; snowfall causes increases in depth of the snowpack.

The depth of concrete frost in the soil was measured daily during snowmelt to determine the infiltrability of the soil. A graduated metal rod (10 mm in diameter) was forced into the ground surface by hand to measure penetration depth, indicating the presence of impermeable ice (Quinton *et al.*, 2005).

Snow and water samples were collected throughout melt and stored in LDPE Zip-Lock® bags until filtration could take place. All samples were transferred to a freezer (–20 ºC) for storage within 1 h of sampling to minimize compositional change in chemistry. Filtration of samples did not take place until just prior to analysis (see section 4.6), at which point their volumes were determined too, using a graduated cylinder. Sampling procedure and frequency for each sample type were:

- Snow, S, was sampled daily using a clean plastic shovel to avoid contamination.

- Precipitation, P, was collected in a dishpan that was placed on top of the existing snow just prior to snowmelt. Surface area of the dishpan was ~0.08 m$^2$.

Sampling was done whenever new snow, rain, or fall-though snow was present. The dishpan was rinsed with DI water after each sampling.

- Overland flow, OLF, was collected twice a day when water was present.

- Organic soil water, OSW, and mineral soil water, MSW, were collected twice a day, when enough water was present. Water extracted from similar soil horizons at each lysimeter transect was composite.

- Ponding water, PW, was observed in the excavated area in front of the soil lysimeter transects on top of the mineral soil as well as in the vicinity of the experimental site. The latter was either ponding directly on the soil surface, at the bottom of the snowpack, or on top of an ice layer. The ponded water, if present, was sampled with a clean 60 ml HDPE syringe to which a clean Tygon® tube was attached. If enough water was present, one full volume was used to wash the syringe before the actual sampling. When the ponding water volume was less than 60 ml, no extra cleaning of the syringe took place. Between each sample, the syringe was rinsed with DI water.

## 4.6    Storage of Samples

All snow and water samples collected during the laboratory and field experiments were filtered through a 0.4 μm Nuclepore® filter paper with a vacuum pump. If filtration was not possible within the first few hours after sampling, samples were stored frozen (<–20ºC) until filtration was possible.

The filtered samples were divided into three or four aliquots, depending on the analyses that were to be made, and transferred into clean Nalgene® polypropylene (PP) sample containers. Aliquots analyzed for $Na^+$, $K^+$, $Mg^{2+}$, $Ca^{2+}$, and DOC were acidified with $H_2SO_4$ to a pH<2 to prevent changes in their chemical composition prior to analyses. No preservatives were added for $Cl^-$, $SO_4^{2-}$, $NO_3^-$, or $NH_4^+$; however, samples were stored frozen as a precaution. In-between filtering and analyses, samples were stored below –20 ºC.

Transportation from the Kananaskis Field Station back to the University of Saskatchewan took place in an electrical cooler, which contained several cold packs to

ensure frozen conditions and thereby minimize possible chemical alteration while transported.

## 4.7 Analytical Methods

All samples were analyzed for their concentrations of major anions ($Cl^-$, $NO_3^-$, and $SO_4^{2-}$) and cations ($H^+$, $Na^+$, $K^+$, $NH_4^+$, $Mg^{2+}$, and $Ca^{2+}$). In addition, some samples were analyzed for dissolved organic carbon (DOC) since this was assumed to be a good indicator for contact with the organic layer. All concentrations were converted to meq $m^{-3}$ for comparison; except the concentrations of DOC, which was reported as g $m^{-3}$.

### Hydrogen, $H^+$

Prior to filtration, pH was measured using an Orion 290A meter with an Orion low maintenance triode (Ag/AgCl internal reference system and built-in thermistor for automatic temperature compensation). A three-point calibration was made using buffers at pH 4.01, pH 7.00, and pH 10.01. The temperature of the samples, measured by the pH triode, was between 18 and 20 ºC when measurements were carried out. Values were converted into $H^+$ concentrations. Conversion may lead to errors since the activity of the hydrogen ion may be affected by other ions (Fishman and Friedman, 1989); for most waters a reproducibility and accuracy of $\pm 0.1$ eq $m^{-3}$ can be assumed.

### Chloride, $Cl^-$

For the enhanced infiltration experiment (Chapter 5), chloride concentrations were measured using an Orion 290A meter with a chloride combination electrode (Orion 9617B). Detection sensitivity of the electrode was found to be 3 mV over 10 readings. Triplicate readings were done on all water samples, allowing <1.5 mV differences between readings. Calibration curves had correlation coefficients of 0.99. Drift in electrode readings were checked every 10 samples and were <10%.

In all other experiments, ion chromatography (Dionex ICS-2000) was used for $Cl^-$ analysis. Analysis was carried out at the Saskatchewan Research Council laboratory in Saskatoon, Saskatchewan. Standard analytical methodology according to American Public Health Association (APHA; Eaton and Franson, 2005) was used. The water

sample was injected into a stream of eluent (15 mM l$^{-1}$ KOH) and passed through an IonPac-AG17 guard column; sample injection volume was 25 μl. Sample loop was 25 μl and eluent flow rate was 1 ml min$^{-1}$. Reporting detection limit was 2.8 meq m$^{-3}$.

### Sulphate, SO$_4^{2-}$

Inductively coupled plasma atomic emission spectroscopy (ICP-AES) was used for SO$_4^{2-}$ analysis. Analyses were carried out at the Saskatchewan Research Council laboratory in Saskatoon, Saskatchewan. Standard analytical methodology according to APHA was used (Eaton and Franson, 2005). The aqueous sample was introduced into an argon-based, high temperature radio-frequency plasma. Energy transfer from the plasma to the sample causes atomization and ionization of target elements. The calibration curve was checked for drifts every five samples. Reporting detection limit was 2.1 meq m$^{-3}$.

### Sodium, Na$^+$, potassium, K$^+$, magnesium, Mg$^{2+}$, and calcium, Ca$^{2+}$

Flame spectroscopy was used for the detection of Na$^+$, K$^+$, Mg$^{2+}$, and Ca$^{2+}$ concentrations. Measurements were done with a SpectrAA 220 atomic absorption instrument (Varian). Emission spectroscopy was used for Na$^+$ and K$^+$ and absorption spectroscopy was used for Mg$^{2+}$ and Ca$^{2+}$. All samples and standards were diluted with a lanthanum solution (~3 g l$^{-1}$) in an approximate sample-to-lanthanum ratio of 1:26. This was done to ensure better ionization and thereby detection of the ion concentrations. An acetylene-oxide flame was used for atomization of the water samples for detection of Na$^+$, K$^+$, and Mg$^{2+}$. For better detection of Ca$^{2+}$ concentrations, a nitrous oxide-acetylene high temperature flame was used.

Measurements were integrated over two 3 seconds intervals and averaged; relative standard deviation between these readings were <5%. Calibration was done using a blank and three standard samples. Drifting was checked every 20 samples for Mg$^{2+}$ and Ca$^{2+}$ and every 15 samples for Na$^+$ and K$^+$, as drifting is more common for the latter ions; drifting of <10% was accepted. Detection sensitivity for distilled deionized water was found to be ±0.3 meq m$^{-3}$ for Na$^+$, ±0.9 meq m$^{-3}$ for K$^+$, ±0.5 meq m$^{-3}$ for Mg$^{2+}$,

and $\pm1.7$ meq m$^{-3}$ for Ca$^{2+}$. Analyses were carried out at the lab for soil testing, Agriculture and Agri-food Canada, University of Saskatchewan.

### Nitrate, NO$_3^-$, and ammonium, NH$_4^+$

Detection of NO$_3^-$ and NH$_4^+$ concentrations were carried out using colorimetric methods on a Technicon AutoAnalyzer II; standard methodology was used (Technicon 1972, 1973). Reagent and sample were mixed, causing a chemical reaction, forming the colour complexes necessary for the specific determination; blue for NH$_4^+$ and red for NO$_3^-$. A colorimeter measures the intensity and amount of light absorbed as the liquid flows along an optical path and phototubes. The method is based on the law of Beer-Lambert, which states that the absorbance (optical density) of a substance is directly proportional to the concentration of the substance. Analyses were carried out in the Department of Soil Science, University of Saskatchewan. Recalibration of base line was done every 30 samples; checking for drift was carried out every 6 samples. Detection limits were 0.2 meq m$^{-3}$ for NH$_4^+$ and 0.1 meq m$^{-3}$ for NO$_3^-$.

### Dissolved organic carbon, DOC

Analysis for dissolved organic carbon (DOC) was carried out on a Dohrmann Phoenix 8000 Carbon Analyzer. Standard analytical method according to APHA was used (Eaton and Franson, 2005). Inorganic carbon was removed from the samples in the form of CO$_2$ by treating them with phosphoric acid. The remaining organic carbon in the samples was treated with sodium persulphate and UV light to release it as CO$_2$. The gas was measured with a non-dispersive infrared detector. Analyses were carried out at Saskatchewan Research Council laboratory in Saskatoon, Saskatchewan; reporting detection limit was 0.2 g m$^{-3}$.

## 4.8    Accuracy and Precision

Blind samples for quality assurance and control, ~10% of total number of samples collected, comprised of duplicate water samples. If they were not within $\pm15\%$ of any measured parameter, samples were re-analyzed.

The ion charge balance, *ICB*, was calculated for each sample as

$$ICB = \frac{\left( \sum cation\ equivalents - \sum anion\ equivalents \right)}{\left( \sum cation\ equivalents + \sum anion\ equivalents \right)} \tag{4.1}$$

Accepted error depends on the total ion concentrations in the sample; low concentrations increase the acceptable error as small variations in concentrations produce large calculated errors. Fishman and Friedman (1989) suggest following acceptable error values: For samples with a total (cations plus anions) milliequivalent per litre [meq l$^{-1}$] value of 20, the acceptable error is 2%; for samples with total value of 7 meq l$^{-1}$, the acceptable error is 3%; and for samples with a total meq l$^{-1}$ value of 0.9 the error may be as high as 12%.

Total values of milliequivalent per litre ranged between 0.1 and 2.3 meq l$^{-1}$ for the analyzed samples. For most samples, the acceptable error was at least 12%. However, a greater *ICB* was observed for a majority of the samples, as not all major ions were analyzed; carbonate species might have been present at the pH range (6.3-8.2) encountered (e.g. Maupetit and Davies, 1991).

# CHAPTER 5

# ENHANCED SOLUTE INFILTRATION

The mass of water that can infiltrate a soil, $F$ [kg m$^{-2}$], is equal to the difference between the mass of water available for infiltration, $P$ [kg m$^{-2}$], and the mass of water that will end up as runoff or ponding at the surface, $R$ [kg m$^{-2}$],

$$F \;=\; P \;-\; R \tag{5.1}$$

For a melting snowpack, $P$ will be equal to the eluting meltwater flow from the base of the snowpack, which will be a function of the change in snowpack depth, $dSWE/dt$ [kg s$^{-1}$ m$^{-2}$], and evaporation rate, $E$ [kg s$^{-1}$ m$^{-2}$],

$$\frac{dP}{dt} \;=\; \frac{dSWE}{dt} \;-\; E \tag{5.2}$$

For a shallow snowpack, where storage is negligible, the daily change in $SWE$ and $E$ will be approximately equal to the melt rate, $M$ [kg s$^{-1}$ m$^{-2}$],

$$\left( \frac{dSWE}{dt} \;-\; E \right)_{daily} \;\approx\; M \tag{5.3}$$

Previous studies have shown that both the depth of infiltration into unsaturated frozen soils and the rate of ion elution from the snowpack depend on the depth of the snowpack and the snowmelt rate (Stein *et al*., 1986; Tranter, 1991; Zhao and Gray, 1997). Studies of ion load and concentration in runoff water from snowmelt over frozen soils have shown dramatic changes in ion retention and release that are correlated with the frozen moisture content of soils and infiltrability (Jones and Pomeroy, 2001). However, there are no known studies or theories that link the physical process of frozen soil infiltration to preferential elution of ions from melting snow. The objective is to propose a solute infiltration model and assess its sensitivity to various environmental

conditions using data from four demonstration sites located in western Canada as well as from a small-scale controlled laboratory experiment. The proposed model will describe the partitioning of snowmelt solute into infiltration excess and into infiltration to unsaturated frozen mineral soils as a function of the ion concentration in the parent snow, snow water equivalent, melt rate, soil porosity, soil temperature, and volumetric soil moisture content. The model assumes the meltwater solute is conservative and fully mixed and that limited infiltration occurs, in which there are neither substantive macropores nor impeding basal ice layers.

## 5.1   Model

The cumulative mass of water that infiltrates into an unsaturated frozen soil, $F$ [kg m$^{-2}$], is a function of heat and mass transfer processes and phase changes between water and ice in the soil (Zhao *et al.*, 1997). The variation in infiltration rate with time, *f(t)* [kg s$^{-1}$ m$^{-2}$], in frozen soils has been found to be similar to that of unfrozen soil; it decreases exponentially with time. Infiltration rate, *f(t)*, is related to $F$ as

$$\int_0^t f(t)\,dt \;=\; F \tag{5.4}$$

Zhao and Gray (1997) derived a simple parametric relationship from a physically-based mass transfer scheme (Zhao *et al.*, 1997) that describes $F$ as a function of the following conditions at the start of infiltration of meltwater; surface saturation, $S_0$ [mm$^3$ mm$^{-3}$], average saturation (water and ice) in the top 40 cm of soil, $S_I$ [mm$^3$ mm$^{-3}$], estimated from average volumetric soil moisture, $\theta$ [mm$^3$ mm$^{-3}$], and soil porosity, $\phi$, as $S_I = \theta/\phi$, soil temperature in the top 40 cm of soil, $T_I$ [K], and the infiltration opportunity time, $t_o$ [h]. Cumulative infiltration, $F$, to mineral soils of various textures can be estimated from following parametric equation (Zhao and Gray, 1999) for frozen unsaturated mineral soils that have no impeding layer above such as basal ice and contain no substantive macropores

$$F = C \cdot S_o^{2.92} \cdot \left(1 - S_I\right)^{1.64} \cdot \left(\frac{273.15 - T_I}{273.15}\right)^{-0.45} \cdot t_o^{0.44} \tag{5.5}$$

Gray *et al*. (2001) found that $F$ is limited by the water storage potential of the soil (available porosity) and depends on a coefficient, $C$ which is influenced by the vertical profile of saturation in the upper 0.4 m of soil. $C$ was found experimentally for prairie and boreal forest soils to be 2.10 and 1.14, respectively, and these values represent the strong overwinter desiccation of prairie soils compared to less severe desiccation of forest soils. Infiltration opportunity time, $t_o$, can be approximated as the time required to melt the snowpack, $t$, which depends on the snow water equivalent (snow accumulation), $SWE$ [kg m$^{-2}$] and average melt rate over the melt period, $\overline{M}$ [kg m$^{-2}$ s$^{-1}$]. Assuming that snowmelt is continuous and storage and evaporation are small, t can be estimated as

$$t_o \quad \approx \quad t \quad = \quad \frac{SWE}{\overline{M}} \tag{5.6}$$

Gray *et al*. (2001) suggest more exact solutions to Equation 5.6 based on techniques for estimating the duration of active meltwater delivery to the soil surface under conditions when snowmelt is not continuous.

Use of Zhao and Gray's equation to estimate infiltration to mineral soils under an organic layer is appropriate when the organic layer rapidly transfers water to the mineral soil surface. This assumption is robust where the organic layer is thin or porosity is high or organic layer macropores are abundant.

Ion concentration in meltwater, $C_i(t)$ [meq m$^{-3}$], during an interval meltwater discharge period $t_{n-1}$ to $t_n$ can be found from Stein *et al*.'s (1986) expression, Equation 5.7, which is governed by the initial ion concentration in the bulk snowpack, $C_i(0)$ [meq m$^{-3}$], initial snow water equivalent, $SWE$ [kg m$^{-2}$], average melt rate for the whole melt period, $\overline{M}$ [kg m$^{-2}$ s$^{-1}$], and a dimensionless leaching coefficient, $k$.

$$C_i(t) \quad = \quad \frac{C_i(0)}{\overline{M} \cdot (t_n - t_{n-1})} \cdot \left(\left(SWE - (\overline{M} \cdot t_{n-1})\right) \cdot e^{-k \cdot \overline{M} \cdot t_{n-1}} - \left(SWE - (\overline{M} \cdot t_n)\right) \cdot e^{-k \overline{M} t_n}\right)$$

$$\tag{5.7}$$

A concentration factor, $CF$ [(meq m$^{-3}$) (meq m$^{-3}$)$^{-1}$], defined as the ratio between the ion concentration in the meltwater to that in the bulk snowpack ($CF = C_i(t)/C_i(0)$; Johannessen and Henriksen, 1978), is often used to illustrate the variation in meltwater's ion concentration during snowmelt. Ion enrichment is shown for $CF$ values $>1$. Initial meltwaters generally show the greatest enrichment, $CF_{max}$, whose magnitude is mainly a function of time, $\overline{M}$, and $k$ (Equation 5.7). The rate of change in $C_i(t)$ is strongly affected by $k$.

The cumulative load of an ion that infiltrates into frozen unsaturated soil underneath a snowpack, $F_i$ [meq m$^{-2}$], is a function of the ion concentration in the meltwater released at the base of the snowpack, $C_i(t)$, infiltration rate, $f(t)$, and water density, $\rho_w$ [kg m$^{-3}$]; thus,

$$F_i = \int_o^t C_i(t) \cdot \frac{f(t)}{\rho_w} \ dt \qquad\qquad (5.8)$$

During the snowmelt event, $F_i$ can be estimated from a combination of frozen soil infiltration and preferential elution expressions using Equations 5.4-5.8.

***Enhanced Infiltration***

As seen in Equations 5.4, 5.5, and 5.7 the infiltration rate, $f(t)$, and meltwater ion concentration, $C_i(t)$, both decline rapidly with time. High concentrations during high infiltration rates result in greater cumulative ion infiltration than if concentration and infiltration were time invariant (Figure 5.1). The resulting temporal association between $C_i(t)$ and $f(t)$ is highly non-linear and a covariance term must be added in order to use time averaged values of ion concentration and infiltration rate in calculating chemical infiltration. Time averaged ion concentration and infiltration are far easier and more reliable to estimate than are concentrations at some time or infiltration rates. Thus, the solution to F$_i$ in Equation 5.8 can be found from the product of time, $t$, and the time averaged values of ion concentration and infiltration rate, $\overline{C_i}$ and $\overline{f}/\rho$, plus the covariance between the instantaneous values of $C_i(t)$ and $f(t)$.
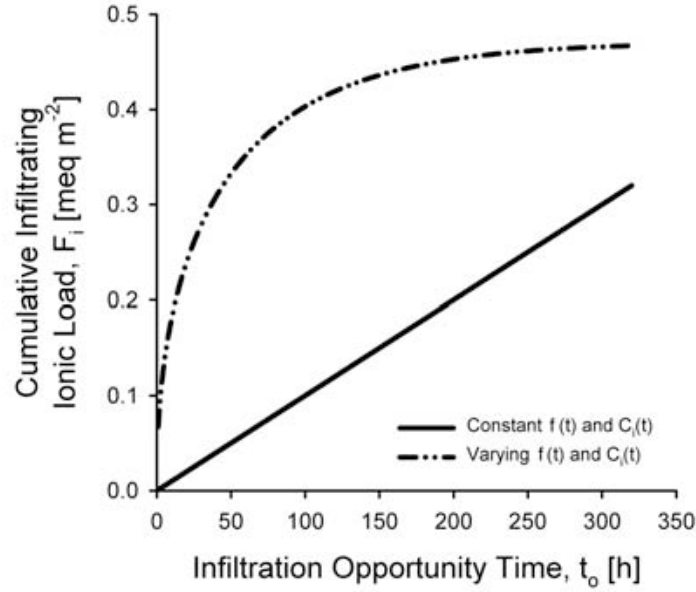
*Figure 5.1. The cumulative load of an ion that infiltrates frozen soil if infiltration rate, f(t), and ion concentration, Cᵢ(t), are held constant with time and if both parameters vary with time, respectively.*

$$F_i \;=\; \frac{\overline{C_i} \cdot \overline{f} \cdot t}{\rho} + \text{cov}\big[C_i(t), f(t)\big] \;=\; \frac{\overline{C_i} \cdot F}{\rho} + \text{cov}\big[C_i(t), f(t)\big] \qquad (5.9)$$

The covariance term is positive as both meltwater ion concentration and infiltration rate decrease with time. It represents the additional load of ion that infiltrates during snowmelt due to the temporal association between ion concentration and infiltration rate (Figure 5.1). This covariance term is labelled the *enhanced infiltration* of an ion.

An exact analytical solution of Equation 5.8 is not straightforward because both infiltration rate and ion concentration are functions of time. Equation 5.8 was therefore integrated over time using 1-hour increments of *t* in a numerical solution.

## 5.1.1  Model Sensitivity

### *Sensitivity of Enhanced Infiltration to Parameters*
Model results suggest that enhanced infiltration is more sensitive to changes in snow and snowmelt properties than to changes in soil properties. The degree of ion

enrichment in the meltwater, *CF*, and the initial snow water equivalent, *SWE*, influenced enhanced infiltration more than other parameters. To illustrate and compare enhanced infiltration, the cumulative enhanced ion infiltration due to covariance was normalized, *NEI* [(meq m$^{-2}$) (meq m$^{-2}$)$^{-1}$], as the ratio between the cumulative enhanced infiltration and cumulative ion infiltration estimated from time-averaged ion concentration and cumulative infiltration (no covariance)

$$
NEI \;=\; \frac{\text{cov}\left[C_i(t), f(t)\right]}{\left(\dfrac{\overline{C_i \cdot F}}{\rho}\right)} \;=\; \frac{F_i - \left(\dfrac{\overline{C_i \cdot F}}{\rho}\right)}{\left(\dfrac{\overline{C_i \cdot F}}{\rho}\right)}
\tag{5.10}
$$

Figure 5.2 shows the effect of changes in single parameters on the cumulative ion infiltration, $F_i$, and *NEI*. A 15 mm increase in *SWE* resulted in an increase of the infiltration opportunity time and therefore an increase in $F_i$ (Figure 5.2A). The change in *SWE* also resulted in a proportional increase in *NEI* of ~15% (Figure 5.2B). A 0.01 increase of *k* increased *CF* by 0.85, resulting in increasing $F_i$ (Figure 5.2C) and a 22-27% increase in *NEI* (Figure 5.2D). The relative increase in $F_i$ and *NEI* as *k* increased was not constant, but diminished with increasing *k*. Infiltration opportunity time was sensitive to melt rate; increasing $\overline{M}$ resulted in decreasing $F_i$ (Figure 5.2E). However, *NEI* was constant as $\overline{M}$ increased (Figure 5.2F). Increasing the initial ion concentration in the snowpack, $C_i(0)$, increased $F_i$ (Figure 5.2G), but did not change *NEI* substantially (<1%) (Figure 5.2H).

Enhanced solute infiltration resulted in reduced ion load in infiltration excess water. Infiltration excess ion load, $R_i$ [meq m$^{-2}$], can be estimated as the difference between ion load in the meltwater leaving the snowpack, $P_i$ [meq m$^{-2}$], and infiltrating ion load, $F_i$,

$$
R_i \;=\; P_i \;-\; F_i
\tag{5.11}
$$

where $P_i$ is found from the melt rate and ion concentration in meltwater integrated over the melt period
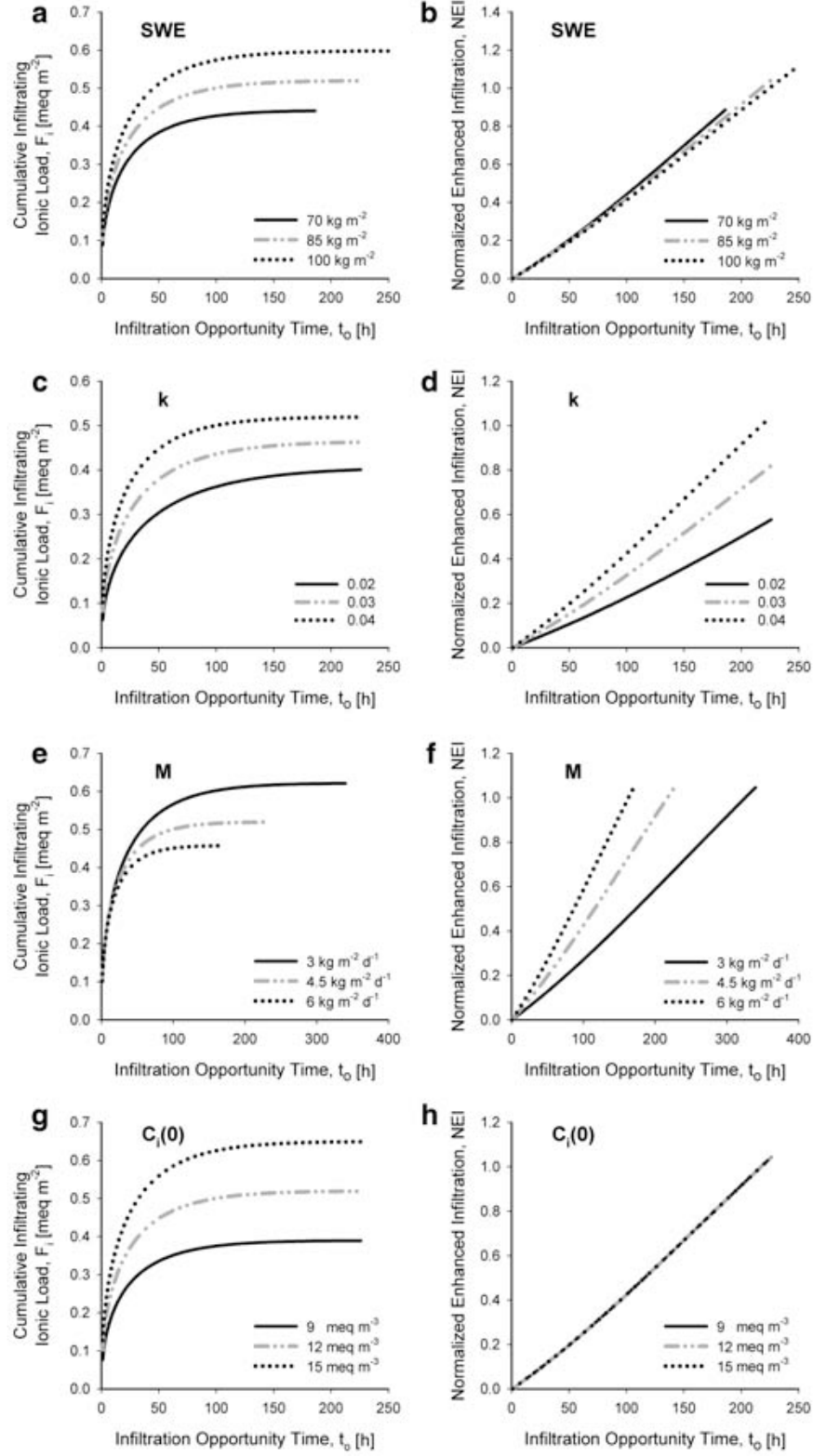
*Figure 5.2. The influence of changes in single parameters on cumulative ion load infiltration, $F_i$, and normalized enhanced infiltration, NEI.*

$$P_i = \int_{o}^{t} C_i(t) \cdot \overline{M} \; dt \qquad\qquad (5.12)$$

Subsequently, increased *SWE* and/or *k* will decrease the ion load in infiltration excess water, whereas changes in $\overline{M}$ and $C_i(0)$ will have little influence.

From previous studies it is known that *CF* is greatly influenced by *SWE* and $\overline{M}$ (e.g. Bales *et al.*, 1989; Tranter, 1991). Increasing *SWE* and/or slow melt rates results in longer percolation times through the snowpack and greater opportunity to incorporate in eluent the enriched meltwater at the surface of the snow crystals. *CF* is also strongly affected by the leaching coefficient, *k*, layering in the snowpack, and preferential flowpaths (Marsh and Pomeroy, 1999).

### *Ion Infiltration and Enhanced Infiltration at Demonstration Sites*

Cumulative ion infiltration, $F_i$, was strongly affected by the soil, snow, and snowmelt properties at the four demonstration sites described in section 4.3.1 (Figure 5.4). Two $F_i$ groups were identified: i) Prairie and ii) others. Largest $F_i$ was at the Prairie site, with values more than twice those of the other sites; ~0.4 meq m$^{-2}$ higher. The high $F_i$ was an outcome of the combination of high *SWE*, $C_i(0)$, and $CF_{max}$ together with double the mass of infiltrating water, *F* (See Table 4.1). This doubling of *F* was a result of the value of *C*, which was twice that of the other sites, together with the low initial soil moisture content, θ. The values of $F_i$ for the other sites were within 0.13 meq m$^{-2}$ of each other. Lowest $F_i$ was obtained for the Tundra as a result of the higher *SWE* and $\overline{M}$ combined with the lower $C_i(0)$ and initial soil moisture content, θ. The general ranking of $F_i$ was Prairie > Mountain Forest > Boreal Forest > Tundra.

At all four demonstration sites, the non-linear relationship between *f(t)* and $C_i(t)$ (Figure 5.3A) caused an initially rapid increase in enhanced infiltration, reaching a maximum in the initial third of the melt period (Figure 5.3B). As both *f(t)* and $C_i(t)$ approached quasi-steady-states with increasing time, enhanced infiltration decreased rapidly except for the Mountain Forest site, which only decreased slightly. The combination of low $CF_{max}$ and shallow snowpack was the reason for this.
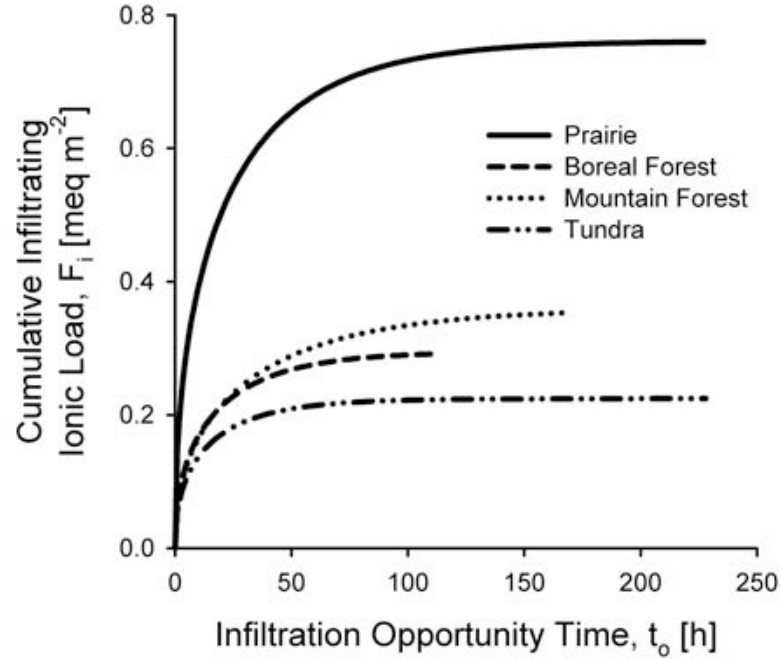
*Figure 5.4. Cumulative ion infiltration, $F_i$, as a function of time.*

Peak enhanced infiltration ranged between 0.9 and 2.5 μeq m$^{-2}$, ranking Prairie > Boreal Forest > Tundra > Mountain Forest. Over the course of melt the range of enhanced infiltration subsequently diminished to 0.2–0.9 μeq m$^{-2}$ and ranking position shifted for the Mountain Forest and Tundra. The timing of high ion concentration and
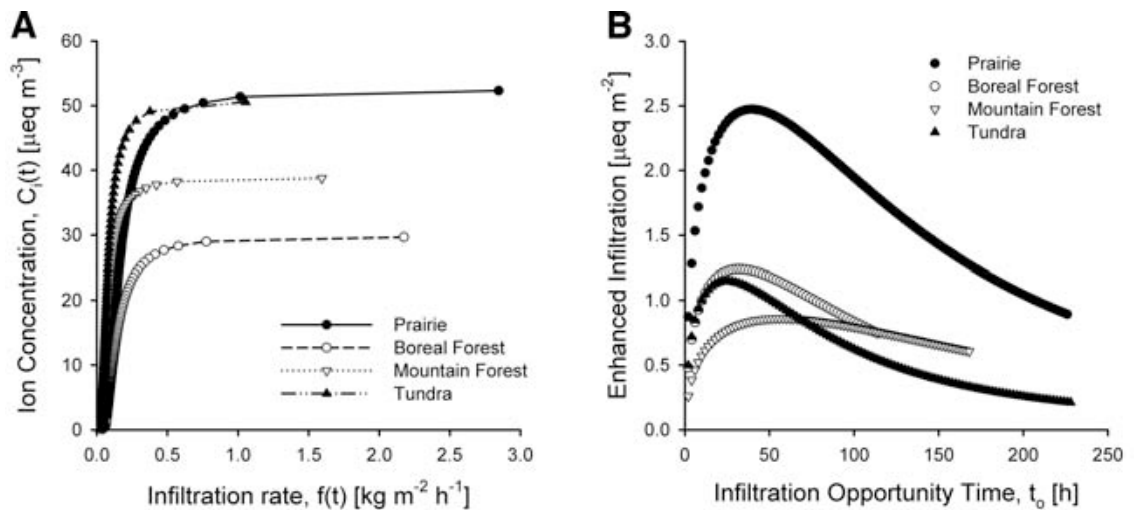


*Figure 5.3. A) The relationship between infiltration rate, f(t) and ion concentration, $C_i$(t). B) Variation in enhanced infiltration of ions over the snowmelt period.*
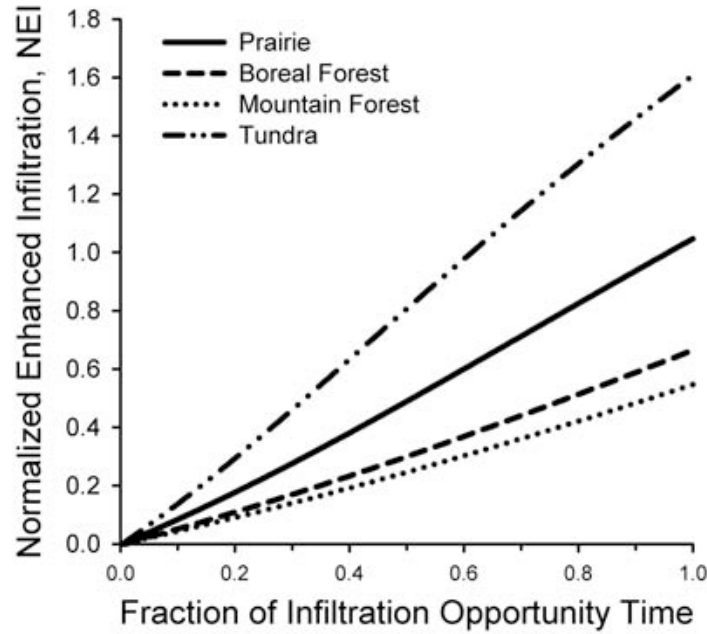
*Figure 5.5. Variations in normalized enhanced infiltration, NEI, at four demonstration sites over the course of the melt.*

infiltration rate caused a higher peak enhanced infiltration for the Tundra than the Mountain Forest. However, the lower $C_i(0)$ and $F$ for the Tundra caused the greater decrease in enhanced infiltration over the course of the melt.

The normalized enhanced infiltration, *NEI*, is shown in Figure 5.5 as a function of the fractional infiltration opportunity time ($t/t_o$). *NEI* increased approximately linearly with fractional time at all demonstration sites. The rate of increase in *NEI* with time was primarily a function of $\overline{M}$, *SWE*, and $CF_{max}$ differences amongst sites (also see Figure 5.5). The rate of increase ranked Tundra > Prairie > Boreal Forest > Mountain Forest. *NEI* increased from 0.36 after the initial third of the melt to 1.60 by the end of the melt for the Tundra and from 0.16 to 0.55 for the Mountain Forest. In all cases there was a substantial enhancement of ion infiltration by the end of melt.

The normalized infiltration excess ion load, $NR_i$, is defined as $R_i$ (Equation 5.11) divided by the difference between meltwater ion load, $P_i$, and ion infiltration, $F_i$, due only to time averaged ion concentration and cumulative infiltration (no covariance), where

$$NR_i \quad = \quad \frac{R_i}{P_i - \left(\dfrac{\overline{C_i \cdot F}}{\rho}\right)} = \frac{P_i - F_i}{P_i - (F_i - Cov(C_i(t), f(t)))} \quad = \quad \frac{R_i}{R_i + Cov(C_i(t), f(t))}$$

$$(5.13)$$

Thus, $NR_i$ is a function of the enhanced infiltration and the infiltration excess ion load. Reductions in the infiltration excess ion load due to enhanced ion infiltration ($1-NR_i$) give an indication of the importance of the process to runoff generation and hence it's impact on aquatic chemistry. Figure 5.6 shows $NR_i$ at each site as a function of the fractional infiltration opportunity time ($t/t_o$). $NR_i$ values show a substantive reduction from the case of no enhanced infiltration and by the mid-point of the snowmelt period ($t/t_o = 0.5$) indicate ion runoff reductions ranging from 11% to 57%. The trend for all sites was for decreasing $NR_i$ with increasing time. By the end of the melt period, the reduction in $NR_i$ ranged from 14% to 60%. The rank in terms of $NR_i$ was Tundra > Boreal Forest $\approx$ Mountain Forest > Prairie reflecting the substantially larger infiltration for Prairie as previously discussed. Ranking in terms of reduction in $NR_i$ from a value of 1 (no enhanced infiltration effect) was Prairie > Boreal Forest $\approx$ Tundra > Mountain Forest with the greatest reductions being roughly double the smallest reductions.
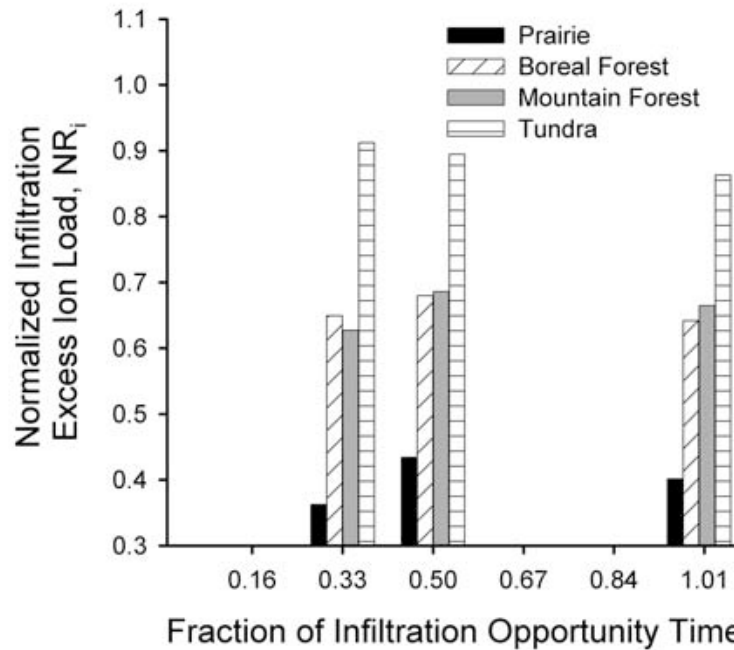


Figure 5.6. Normalized infiltration excess ion load, $NR_i$, at four sites.

## 5.1.2 Discussion

A model is proposed in which the cumulative load of an ion that infiltrates into frozen unsaturated soil can be estimated from the ion concentration in the meltwater and infiltration rate. The model shows that the fate of the preferentially eluted ions released at the base of the snowpack during spring freshet might not be as straightforward as previously thought. That the snowmelt ion load ending up in infiltration excess water will become reduced due to enhanced infiltration might help clarify previously unexplained changes in soil and flowpath chemistry (e.g. Jones and Pomeroy, 2001).

Both eluted ion concentration and infiltration rate decrease rapidly with time, but their association is non-linear and positive. In order to use time-averaged values of ion concentration and infiltration rate in calculating the infiltrating ion load a covariance term must be added. The covariance represents the excess of ion load that infiltrates during snowmelt and is termed the enhanced infiltration of meltwater ions into frozen soil. It is largest in the early stages of infiltration, due to the association between the early timing of both high ion concentration and infiltration rate.

The model suggests that enhanced infiltration is governed by initial snow water equivalent, average melt rate, and the ion concentration factor, which is strongly influenced by a leaching coefficient. A sensitivity analysis of these parameters showed the leaching coefficient to be the most sensitive; increasing it by 0.01 caused an increase in cumulative enhanced infiltration of $\leq 25\%$ and in cumulative ion infiltration of $\leq 13\%$. The importance of initial conditions on the impact of enhanced infiltration rank: $M > SWE$ and $C_0(t)$.

Assessment of the sensitivity of this model to soil, snow, and melt properties, showed that 16-50% more ion load infiltrates during the initial third of the snowmelt period because of enhanced ion infiltration. For the whole melt period, 55-160% more ion load infiltrates as a result of enhanced infiltration. Conservation of mass specifies that enhanced infiltration ions are not available for infiltration excess and therefore runoff. The reduction of ion load in runoff water due to enhanced infiltration varied with site. Generally, it was reduced by 11% to 57% after the initial half of the melt period; increasing slightly (~3%) over the rest of the melt period.

In general, the regional demonstration of the model suggested that cumulative infiltration of ion load was greatest for the Prairie environment and a ranking order of Prairie > Mountain Forest > Boreal Forest > Tundra. This was a result of inter-site variation in snow water equivalent, initial ion concentration, and melt rate, which all influenced the initial concentration factor, in addition to initial soil moisture and the location coefficient, which at the Prairie site was twice that of the other sites.

The normalized enhanced infiltration, however, showed that enhanced infiltration will have the greatest impact on the Tundra environment; the sites were ranked Tundra > Prairie > Boreal Forest > Mountain Forest in terms of ion infiltration enhancement. The reason for the greater influence in the Tundra environment was a combination of the reduced amount of mass infiltrating and the synchronicity between the timing of the highest ion concentration and infiltration rate. Overall, the demonstration showed that the Mountain Forest environment was influenced the least by enhanced infiltration.

The model suggests that calculations of the partitioning of snowmelt ions into infiltration and runoff need to consider enhanced infiltration effects due to temporal covariance between ion concentration and infiltration rate during melt.

## 5.2 Laboratory Experiments

The objective of the laboratory experiments is to examine whether enhanced infiltration can be identified in a controlled laboratory experiment. It is hypothesized that average initial soil saturation will not influence enhanced infiltration in a limited infiltration regime but the distribution of initial soil moisture may. Thus, soil columns with different initial soil moisture contents were used. It was assumed that the solutions released to the soil surface were conservative, fully mixed within each time step, and that mass and energy were conserved. The laboratory experiment data is listed in Appendix D.

### 5.2.1 Results

The experimental conditions of the nine soil column experiments are listed in Table 5.1. Differences in initial soil saturation were large for the three experiments. Differences in average porosity (<0.04), dry bulk density (~125 kg m$^{-3}$), average room temperature

*Table 5.1. Summary of experimental setup for each soil column. Soil temperatures and precipitation rates are averages for the total experimental time.*

| Experiment | Dry | | | Unsaturated | | | Saturated | | |
|---|---|---|---|---|---|---|---|---|---|
| Column # | 1 | 2 | 3 | 1 | 2 | 3 | 1 | 2 | 3 |
| Soil saturation, $S_l$ ($mm^3\ mm^{-3}$) | 0.06 | 0.06 | 0.06 | 0.85 | 0.83 | 0.81 | 0.97 | 0.95 | 0.98 |
| Soil porosity, $\phi$ | 0.46 | 0.47 | 0.47 | 0.42 | 0.45 | 0.42 | 0.43 | 0.43 | 0.43 |
| Dry bulk density ($kg\ m^{-3}$) | 1441 | 1400 | 1407 | 1528 | 1463 | 1525 | 1514 | 1502 | 1513 |
| Soil temperature (ºC ±stdev) | -1.4 ±1.1 | -0.9 ±0.8 | -0.9 ±0.8 | -1.2 ±1.2 | -0.9 ±0.6 | -0.8 ±0.6 | -0.9 ±0.9 | -0.7 ±0.4 | -0.8 ±0.5 |
| Precipitation rate ($kg\ s^{-1}\ m^{-2}$) | 0.011 | 0.010 | 0.011 | 0.009 | 0.009 | 0.010 | 0.009 | 0.008 | 0.010 |
| ($mm\ h^{-1}$) | 38.5 | 37.6 | 40.2 | 32.9 | 31.6 | 36.4 | 32.0 | 30.2 | 36.2 |

(0.1 ºC), and average precipitation rates ($<0.003$ kg s$^{-1}$ m$^{-2}$; 11 mm h$^{-1}$) were relatively minor. The rates of precipitation were generally higher than those found in nature. However, the overflow valve ensured a constant head (10 mm), which was comparable to natural conditions, and minimized the influence of the high and highly variable precipitation rates on the infiltration rate. The greatest inter-column variability was observed for average soil temperatures ranging between –0.7 and –1.4 ºC, with standard deviations ranging between 0.4 and 1.2 ºC. This variability was likely a result of the delay in additions of solute to columns 2 and 3, which allowed these columns to adjust to the room temperature increase for longer than did column 1. However, studies have shown that the effect of the soil temperature on infiltration is secondary to that of initial soil moisture (e.g. Komarov and Makarova, 1973; Granger *et al*., 1984; Zhao and Gray, 1997). In addition, the temperature of an advancing wetting front has been found to be independent of the initial temperature of a frozen soil (Zhao *et al*., 1997). Though, temperature variability may influence the supply of latent heat as water refreezes, being greater in a colder soil, causing the soil temperature to increase faster (Zhao *et al*., 1997). In general, soil temperatures were all within the range of melt period soil temperatures observed in many seasonally frozen soils.

Ponding occurred after approximately two hours during the dry experiment (saturation $\approx$ 0.06 mm$^3$ mm$^{-3}$), whereas it occurred instantly during the saturated

experiment (saturation $\approx$ 0.97 mm$^3$ mm$^{-3}$). In the unsaturated experiment (saturation $\approx$ 0.83 mm$^3$ mm$^{-3}$), ponding took place almost instantaneously for two of the columns (1 and 3), and after 25 minutes for column 2. The mass of water added to the soil surface, $P$ [kg m$^{-2}$], and the mass of infiltration excess water, $R$ [kg m$^{-2}$], were recorded throughout the experiment. The mass of infiltrated water, $F$, was estimated by difference (Equation 5.1; $F = P - R$). The largest $F$ was observed for the dry soil, averaging 119.7 kg m$^{-2}$ (Table 5.2); average $F$ was 25.2 kg m$^{-2}$ for the unsaturated soil and 8.7 kg m$^{-2}$ for the saturated soil.

Chloride concentrations in $P$ and $R$ confirmed the conservative behaviour of the solution; differences between concentrations were <10% and were assumed to be a result of instability in electrode readings. The ion load infiltrating the frozen soil, $F_i$, was imposed by conservation of mass, $F_i = P_i - R_i$ (Equation 5.11), where $P_i$ and $R_i$ are the ion load in precipitation and infiltration excess water, respectively. All columns showed a rapid initial increase in $F_i$ followed by a quasi-steady state, as described by Zhao *et al*. (1997) (Figure 5.7). The transition occurred after ~0.5 h for the saturated soil, after ~1.5 h for the unsaturated soil, and after ~2.0 h for the dry soil. The greatest $F_i$ was observed for the dry soil, with an average for the three columns of 5900 meq m$^{-2}$; the lowest $F_i$ was observed for the saturated soil, with an average of 750 meq m$^{-2}$. $F_i$

Table 5.2. Summary of infiltration results for each column.

| Experiment | Dry | | | Unsaturated | | | Saturated | | |
|---|---|---|---|---|---|---|---|---|---|
| Column # | 1 | 2 | 3 | 1 | 2 | 3 | 1 | 2 | 3 |
| Cumulative mass infiltrating, $F$ (kg s$^{-1}$ m$^{-2}$) | 119.7 | 119.3 | 120.0 | 19.4 | 39.6 | 16.7 | 12.2 | 6.3 | 7.7 |
| Cumulative ion load infiltrating, $F_i$ (meq m$^{-2}$) | 5953 | 6189 | 5643 | 870 | 2375 | 1174 | 1172 | 478 | 600 |
| – If no covariance (meq m$^{-2}$) | 2625 | 2721 | 2387 | 477 | 931 | 406 | 310 | 143 | 167 |
| Normalized enhanced infiltration, NEI ((meq m$^{-2}$)(meq m$^{-2}$)$^{-1}$) | 1.27 | 1.27 | 1.37 | 0.87 | 1.56 | 1.92 | 2.90 | 2.21 | 2.42 |
| Normalized infiltration excess ion load, NR$_i$ ((meq m$^{-2}$)(meq m$^{-2}$)$^{-1}$) | 0.55 | 0.53 | 0.56 | 0.95 | 0.81 | 0.92 | 0.90 | 0.96 | 0.96 |
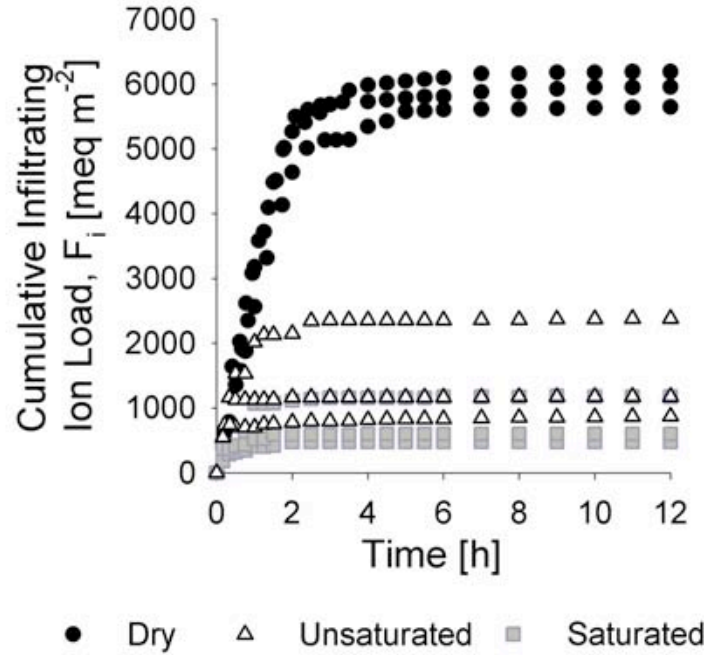
*Figure 5.7. Cumulative ion load infiltrating, $F_i$, for each soil column.*

ranged between 870 mand 2400 meq m$^{-2}$ for the unsaturated soil with an average of 1500 eq m$^{-2}$.

To assess the magnitude of enhanced infiltration, the normalized enhanced infiltration, *NEI* [(meq m$^{-2}$) (meq m$^{-2}$)$^{-1}$], was calculated for each column (Equation 5.10). Figure 5.8A shows how *NEI* increased almost linearly with infiltration time. The average rate of change was greatest for the saturated soil columns (slope = 0.22 h$^{-1}$) and least for the dry soil columns (slope = 0.12 h$^{-1}$). The average rate of change for the unsaturated soil columns was only slightly higher than that of the dry soil (slope = 0.14 h$^{-1}$). Consequently, the greatest *NEI* were obtained for the saturated soil, with values ranging between 2.2 and 2.9 (Figure 5.8A) indicating that, on average, 2.5 times more ion load infiltrated than if calculated from time-averaged ion concentration and cumulative infiltration alone (no covariance). For the dry soil, *NEI* ranged between 1.3 and 1.4 at the end of the experiment and for the unsaturated soil, *NEI* ranged between 0.9 and 1.9; average *NEI* were 1.3 and 1.5, respectively. One of the columns in the unsaturated soil experiment changed slope after approximately 6 h, ending up with the lowest cumulative *NEI* of all the experiments (0.9).
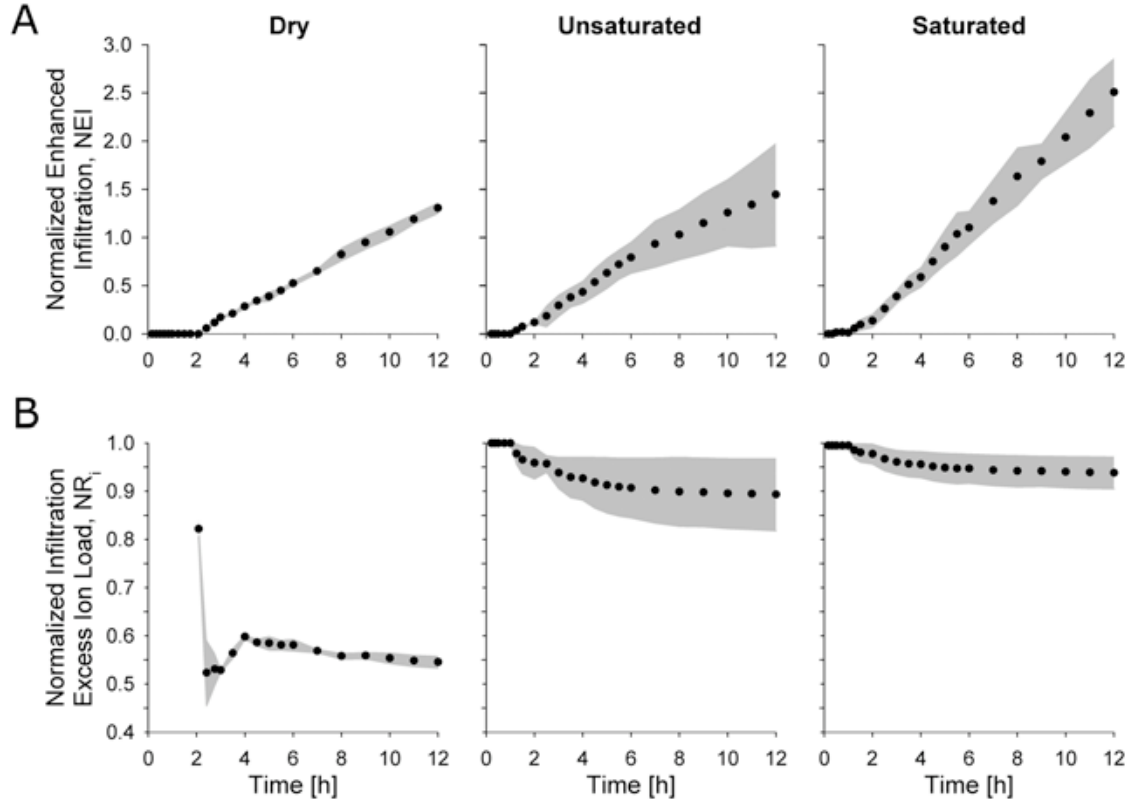
*Figure 5.8. Variation with time of A) average normalized enhanced infiltration, NEI, and B) average normalized infiltration excess ion load, NR$_i$, for each experiment. The grey area represents the range for the three columns.*

The impact of enhanced infiltration on infiltration excess ion load, $R_i$ [meq m$^{-2}$] was assessed by normalizing the infiltration excess ion load, $NR_i$ [(meq m$^{-2}$) (meq m$^{-2}$)$^{-1}$] (Equation 5.13). This showed that after the initial one-third of the experimental period (4 h), the ion load in the infiltration excess water was reduced due to enhanced infiltration ($1-NR_i$) by ~40% in the dry soil experiment, between 4% and 12% in the unsaturated soil experiment, and between 3% and 8% in the saturated soil experiment (Figure 5.8B). A slight increase in the reduction (between 1% and 7%) was observed over the rest of the period. In general, ion loads in infiltration excess water over the dry soil columns increased the most and over the saturated soil columns the least. The variation in total $R_i$ between columns was 3% in the dry soil experiment, 14% in the unsaturated soil experiment, and 6% in the saturated experiment.

## 5.2.2 Discussion

Three experiments were conducted, each in three replicates, to assess whether enhanced ion infiltration to frozen soil could be recognized in controlled laboratory settings in addition to determining its magnitude. Each experiment differed from the others with respect to initial soil saturation; differences in porosities, average room and soil temperatures, and average precipitation rates were minor (Table 5.1). The results show that enhanced infiltration of a conservative ion takes place once partitioning of meltwater added to a frozen mineral surface occurs.

It has previously been suggested that the cumulative mass that infiltrates frozen soil is inversely related to the initial moisture content of the soil (e.g. Gray *et al.*, 2001) and that the effect of soil temperature on the cumulative infiltration is secondary (e.g. Komarov and Makarova, 1973; Granger *et al.*, 1984). This was also observed for the experiments carried out in this study. The greatest cumulative infiltrating mass was observed for the dry soil and the least for the saturated soil. The inter-column variation in cumulative infiltrating mass could not be correlated with the inter-column variation in soil temperature indicating that it was of little importance for the general observations in this study. From the three experiments it was demonstrated that there is a similar relationship between initial soil moisture content and cumulative infiltrating ion load; cumulative infiltrating ion load increased with decreasing initial soil moisture (Table 5.2). General ranking order for infiltration of snowmelt ions with respect to soil moisture was: dry >> unsaturated > saturated soil conditions. Over the course of the infiltration, about 60% of the total ion load added to the soil surface of the dry soil infiltrated, varying little (~1%) between the columns; only 10% to 28% of the added ion load infiltrated the unsaturated soil, and between 6% and 13% infiltrated the saturated soil.

The impact of enhanced infiltration was shown to increase with increasing initial soil moisture content. The largest normalized enhanced infiltration (*NEI* = 2.90) was calculated for the first column in the saturated experiment with ~50% difference to the other two saturated columns. This was most likely a result of the cumulative infiltrating mass being twice that of the other columns and that most of it infiltrated during the beginning of the experiment, while solute concentrations were high. The presence of soil

macropores (i.e. cracks, worm holes, roots, and burrows) could account for the difference in infiltration, as the transport deeper into the ground would be more rapid than matrix flow alone (e.g. Beven and Germann, 1982). Consequently, the presence of macropores will enhance the effect of enhanced infiltration due to this fast transfer of water deeper into the soil. However, no visual observations of macropores were made in any of the soil columns in either experiment.

On average, *NEI* in the saturated experiment was close to twice that of the other experiments, with 250% more ion load infiltrating compared to only 131% when the soil was initially dry and 145% when the soil was unsaturated. Overall, *NEI* with respect to initial soil moisture ranked the experiments: saturated >> unsaturated > dry soil conditions.

The change in slope of *NEI* for column 1 in the unsaturated experiment (Figure 5.8A) was a result of the timing between high infiltration rate and meltwater ion concentration. During the second half of the experiment, the cumulative infiltrated mass increased by roughly 50% for this column, compared to only 10% for the other two columns. This continuous infiltration throughout the experiment, even though at a very low rate ($\sim 1$ mm h$^{-1}$), causes the cumulative ion load to increase continuously throughout the experiments. For the other columns, the infiltration rates became 0.0 mm h$^{-1}$ during parts of this period, limiting the ion load infiltration.

Even though enhanced infiltration had the greatest impact on the saturated soil, the reduction in normalized infiltration excess ion load ($1–NR_i$) was almost negligible ($\sim 5\%$) (Figure 5.8B). In contrast, enhanced infiltration had the least impact on the dry soil ($NEI \approx 1.31$) but the reduction in infiltration excess ion load was almost 10 times greater than that of the saturated columns with a reduction between 44% and 47% (Figure 5.8B). General ranking order for the reduction in infiltration excess ion load with respect to initial soil moisture content was: dry >> unsaturated > saturated soil. An implication of enhanced infiltration is that formation of a basal ice layer will result in an alteration of both meltwater ion pathway and concentration. When basal ice is present, all meltwater runs off and further ion concentration enrichment occurs (demonstrated in Chapter 6). Conversely, when partitioning occurs, enhanced infiltration of meltwater ion load can result in relatively dilute runoff water.

The unsaturated soil experiment showed the greatest inter-column variability in infiltration results (Table 5.2). Cumulative infiltrating mass for the second column (39.6 kg m$^{-2}$) was twice that of the other columns, resulting in the greatest cumulative infiltrating ion load (2400 meq m$^{-2}$) as well as greatest reduction in infiltration excess ion load (19%). Nevertheless, the third column had a cumulative infiltration ion load that was half that of the second column (1200 meq m$^{-2}$), with less than half the cumulative mass infiltrating (16.7 kg m$^{-2}$). The lowest cumulative infiltrating ion load was observed in the first column (870 meq m$^{-2}$), even though its cumulative infiltrating mass was higher than that of the third column (19.4 kg m$^{-2}$). This experiment showed the greatest range in normalized enhanced infiltration and normalized infiltration excess ion load (Figure 5.8), demonstrating the importance of timing between high meltwater ion concentration and infiltration rate.

A factor that may have influenced the experimental results was the high solute concentration in the water, because solute lowers the freezing temperature of the solution compared to the pure water (e.g. Masterton and Hurley, 1997). The freezing point depression, $\Delta T_f$ [ºC], can be calculated for any solution as

$$\Delta T_f \quad = \quad k_f \cdot m \cdot i \tag{5.14}$$

where $k_f$ is the molal freezing point constant [ºC kg mol$^{-1}$], which is 1.86 ºC kg mol$^{-1}$ for water, $m$ is the molality of the dissolved solute [mol kg$^{-1}$], and $i$ is the 'Van't Hoff factor' that is equal to the number of moles of ions per mole of electrolyte (e.g. Masterton and Hurley, 1997). For NaCl, $i$ is ~2 for dilute solutions, decreasing as the molality of the solution increases, e.g $i$ is ~1.8 for $m = 0.5$.

As water infiltrate a frozen soil, some refreezing occurs. As ice forms, ion exclusion takes place, relocating some of the ions to a quasi-liquid layer on the surface of the ice (Davis, 1991). This leads to a further depression of the freezing point, as the brine concentration is greater than the initial infiltrating solution. Figure 5.9 shows how the depression of the freezing point increases for each of the six solutions used in the experiments, as the volume of liquid water decreases. The calculations assume that all Na$^+$ and Cl$^-$ in solution are excluded from the ice lattice, as the solubility of ions in ice is much less than in water, almost negligible (e.g. Smith and Haymet, 2004; Blackford *et*

*al*., 2007). This assumption seems reasonable as reported solubility of HCl in ice range from 1 to $10^4$ mmol m$^{-3}$ (e.g. Dominé *et al*., 1994); a very small amount compared to the concentration of Cl$^-$ used herein.

In this study, the solute concentrations added to the soils were greater than those typical of snowmelt water and rain; consequently, their freezing point depressions ranged from 0.03 ºC for the 145 ppm Cl solution to 0.6 ºC for the 2890 ppm Cl solution. These depressions are larger than what will normally be observed in nature and unfrozen water was most likely present within the soils even though the soil temperatures were below zero; however, no measurements were made to confirm this. With an average soil temperature of –1.0 ºC, the freezing point depressions was most pronounced, and therefore of greatest influence, during the initial third of the experiment (Figure 5.9). The result of this will be a greater mass infiltrating the soil and thereby increasing the impact of enhanced infiltration. However, it was believed that the influence of the increased freezing point depression would be most pronounced for the dry soil where
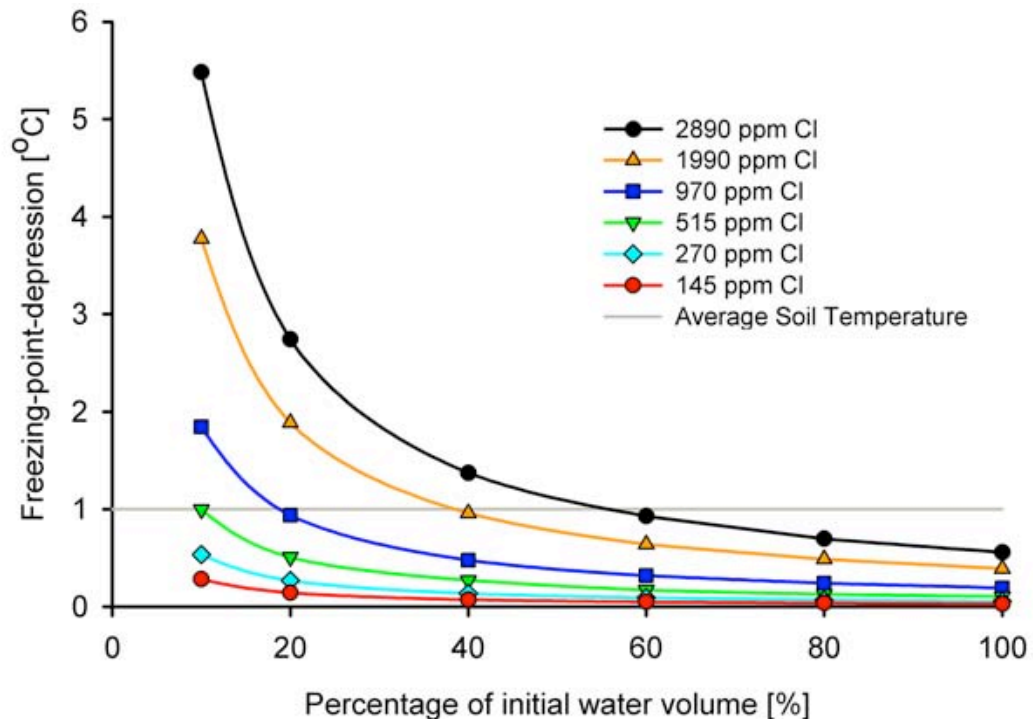


*Figure 5.9. The change in freezing point depression as the volume of water decreases. The change is shown for each of the solute concentrations used in the experiments. The horizontal line represents average soil temperature during the here presented experiments.*

infiltration was assumed unlimited as refreezing would have been limited within the soil and thereby formation of limiting ice layers. The high initial saturations of the soils in the unsaturated and saturated experiments were believed to minimize the effect of the freezing point depression on cumulative infiltration.

## 5.3    Evidence of Enhanced Infiltration

The temporal association between infiltration rate, $f(t)$ [kg s$^{-1}$ m$^{-2}$], and meltwater ion concentration, $C_i(t)$ [meq m$^{-3}$], is highly non-linear even though both decline rapidly with time. Cumulative infiltration of snowmelt ions is enhanced by initially higher ion concentration in meltwater and infiltration rate. However, time-averaged ion concentration, $\overline{C_i}$, and infiltration, $\overline{f}/\rho_w$, where $\rho_w$ [kg m$^{-3}$] is the solution's density, are far easier and more reliable to estimate than are concentrations and infiltration rates at any one time. Thus, in order to reliably calculate the cumulative ion load infiltrating a frozen soil, $F_i$ [meq m$^{-2}$], the covariance between the instantaneous values of $C_i(t)$ and $f(t)$ has to be added to the mean terms (Equation 5.8 and 5.9). This covariance term is labelled *enhanced infiltration* and represents the additional load of ion that infiltrates during snowmelt due to the combination of initially rapid infiltration rate and higher ion concentration in meltwater.

A model is proposed in which cumulative load of an ion infiltrating into frozen unsaturated soil can be estimated as a function of meltwater ion concentration and infiltration rate. Assumptions of the model are that the meltwater solution released to the soil surface is conservative, fully mixed within each time step, and that mass and energy are conserved. Infiltration and meltwater concentration are estimated using relationships developed by Gray and Stein, respectively.

Meteorological observations and soil parameters from four sites in western Canada were used to assess the sensitivity of the model to conditions at a prairie site, a boreal forest site, a mountain forest site, and a shrub tundra site. Model results showed the greatest cumulative infiltration of ion load for the Prairie site; the general ranking was: Prairie > Mountain Forest > Boreal Forest > Tundra. However, the greatest impact of enhanced infiltration was found for the Tundra site. At this site enhanced infiltration

caused up to 50% more ion load to infiltrate within the initial third of the melt period compared to infiltration estimates not accounting for this effect. Over the whole melt period, enhanced infiltration caused 55%-160% more ion load to infiltrate than estimates based solely on mean depth of infiltration and ion concentration. Sensitivity analysis showed that enhanced infiltration varies most strongly with initial snow water equivalent, average melt rate during the snowmelt period, and the snowpack ion elution concentration factor.

Laboratory experiments were carried out to examine whether enhanced infiltration to frozen soil can be recognized under controlled settings and to what extent its impact varies with soil moisture. Three experiments were carried out in triplicates: one with dry soil (0%), one with saturated soil (100%), and one with unsaturated soil (85%). Chloride solution was added to the surface of frozen soil columns; the concentration decreased exponentially over time to simulate snow meltwater. Infiltration excess water was collected and chloride concentration and volume were determined. Ion load infiltrating the frozen soil was dictated by mass conservation.

The results demonstrated that the impact of enhanced infiltration was related to initial soil moisture content, with the greatest impact on saturated and near-saturated soil. Normalized enhanced infiltration showed that 250% more ion load may infiltrate during saturated conditions than if calculated from time-averaged ion concentration and infiltration rate; only 131% more infiltrated during the dry conditions and 149% during unsaturated. However, infiltration into dry soil may result in enhanced infiltration as well and, in the presented experiment, it was shown to cause the greatest reduction in infiltration excess water ion load (45%). Least reduction in infiltration excess ion load due to enhanced infiltration was observed for the saturated soil (6%). Generally, the reduction in infiltration excess ion load increased only slightly (2–5%) over time.

The laboratory results also showed that synchronicity between the timing of high ion concentration and infiltration rate greatly influences enhanced infiltration and therefore the flowpath of snowpack ions during the melt and spring runoff periods. The importance of timing between high ion concentration and high infiltration rate was best illustrated in the unsaturated experiment, which showed greatest inter-column variation in enhanced ion infiltration and impact hereof.

# CHAPTER 6

# CHANGES IN CHEMICAL COMPOSITION
# WITH FLOWPATH

Knowledge of the changes to meltwater's chemical composition during travel along flowpaths is important as this impacts nutrient and contaminant delivery to the terrestrial and aquatic ecosystems. Overland flow and organic interflow tend to contribute rapidly to the hydrological network, while mineral interflow is more likely to replenish soil water reserves. The objective is to identify, in a controlled setting, the compositional change in runoff water chemistry for three flowpaths: i) runoff water that had sustained contact with a basal ice layer, ii) runoff water that had sustained contact with an organic layer, and iii) runoff water that had sustained contact with a mineral soil layer. Experiments were carried out in the cryospheric environmental laboratory using an insulated box with a cooling system at the base. The experimental data is listed in Appendix E.

## 6.1 Basal Ice Layer

Three experiments (termed BI-1, -2, and -3) were carried out using snow from within the city limits of Saskatoon, SK, Canada, (BI-1) and from a hay meadow outside of the city limits (BI-2 and BI-3). Snow used in BI-1 and BI-2 was collected 2-3 days after each snowfall event, but metamorphism was not pronounced (Table 6.1). Fresh snow, collected <12 hours after a snowfall event, was used in BI-3. In all experiments, the snow was composed of loose 1-2 mm crystals. The chemical compositions of the parent snow were dominated by magnesium and calcium (Table 6.2).

The initial densities of the snowpacks were 350 kg m$^{-3}$ in BI-1, 410 kg m$^{-3}$ in BI-2, and 215 kg m$^{-3}$ in BI-3. The snow reached thermal equilibrium ($T \approx -2$ ºC) prior to

*Table 6.1. Summary of snow and melt conditions for each experiment. BW refers to the runoff water that had sustained contact with basal ice; SW is the meltwater.*

| Experiment | | BI-1 | BI-2 | BI-3 |
|---|---|---|---|---|
| *Snow* | Origin | Within city | Rural area | Rural area |
| | Storage [d] | 0 | 90 | 0 |
| | Initial depth [m] | 0.45 | 0.46 | 0.46 |
| | Initial density [kg m$^{-3}$] | 350 | 410 | 215 |
| *Temperature* | Room [ºC] | +5 | +5 | +5 |
| | Coolant, initially [ºC] | –5 | –4 | –3 |
| | Base of snowpack [ave ºC] | –2 | –0.5 | –0.2 |
| *Experiment duration [d]* | | 6.2 | 11.3 | 5.1 |
| *Timing of first sample [days after initiation]* | Runoff water, BW | 2.9 | 1.7 | 1.0 |
| | Meltwater, SW | 3.9 | 5.8 | 3.2 |
| *Basal ice thickness [mm]* | | 80 | 40 | 30 |

*Table 6.2. Ion concentrations [meq m$^{-3}$] in the parent snowpacks.*

| Experiment | H$^+$ | Cl$^-$ | SO$_4^{2-}$ | NO$_3^-$ | NH$_4^+$ | Na$^+$ | K$^+$ | Mg$^{2+}$ | Ca$^{2+}$ | ICB |
|---|---|---|---|---|---|---|---|---|---|---|
| *BI-1* | 0.009 | 12.7 | 11.5 | n.d. | 16.2 | 5.5 | 6.2 | 22.8 | 73.7 | +0.67 |
| *BI-2* | 0.077 | 25.3 | 35.4 | 4.0 | 26.3 | 15.1 | 11.0 | 30.9 | 84.5 | +0.44 |
| *BI-3* | 0.428 | 9.8 | 11.5 | n.d. | 13.8 | 3.1 | 8.4 | 25.0 | 13.0 | +0.49 |

n.d. = below detection limit

initiation of each experiment; coolant temperature was set at –5 °C, –4 °C, and –3 °C in each experiment, respectively. Once thermal equilibrium was reached, the room temperature was increased to +5 °C.

For the duration of snowmelt, changes in snow depth and the volume of melt- and runoff water eluted from the box were recorded. Based on this, estimates of snow water equivalent (*SWE*) could be made since direct measurements would cause disturbance of the snowpack; differences in *SWE* were taken as the melt rate, assuming evaporation was negligible. Experiments were terminated once the depth of the snowpack had decreased by >55%. At this point, melting from the sides of the box was pronounced, revealing a direct view of the basal ice.

## 6.1.1 Results

The three experiments differed with respect to snowpack density, snowmelt rate, and temperature at the base of the snowpack (Table 6.1). In all of the experiments both density and melt rate increased as melt progressed (Figure 6.1). The greatest increase in snowpack density was observed in BI-1 with ~56 kg m$^{-3}$ d$^{-1}$. This experiment showed the lowest average melt rate (3.6 mm d$^{-1}$), the coldest base conditions, and the smallest cumulative reduction in snow water equivalent, *SWE* (7.4 mm), of all the experiments. The greatest daily melt rate was observed in BI-2 at 17.6 mm d$^{-1}$. Average melt rate was 6.8 mm d$^{-1}$ resulting in a cumulative loss of 25.4 mm *SWE*, the greatest of all experiments. The density increase rate in BI-2 was about one-fifth of the other
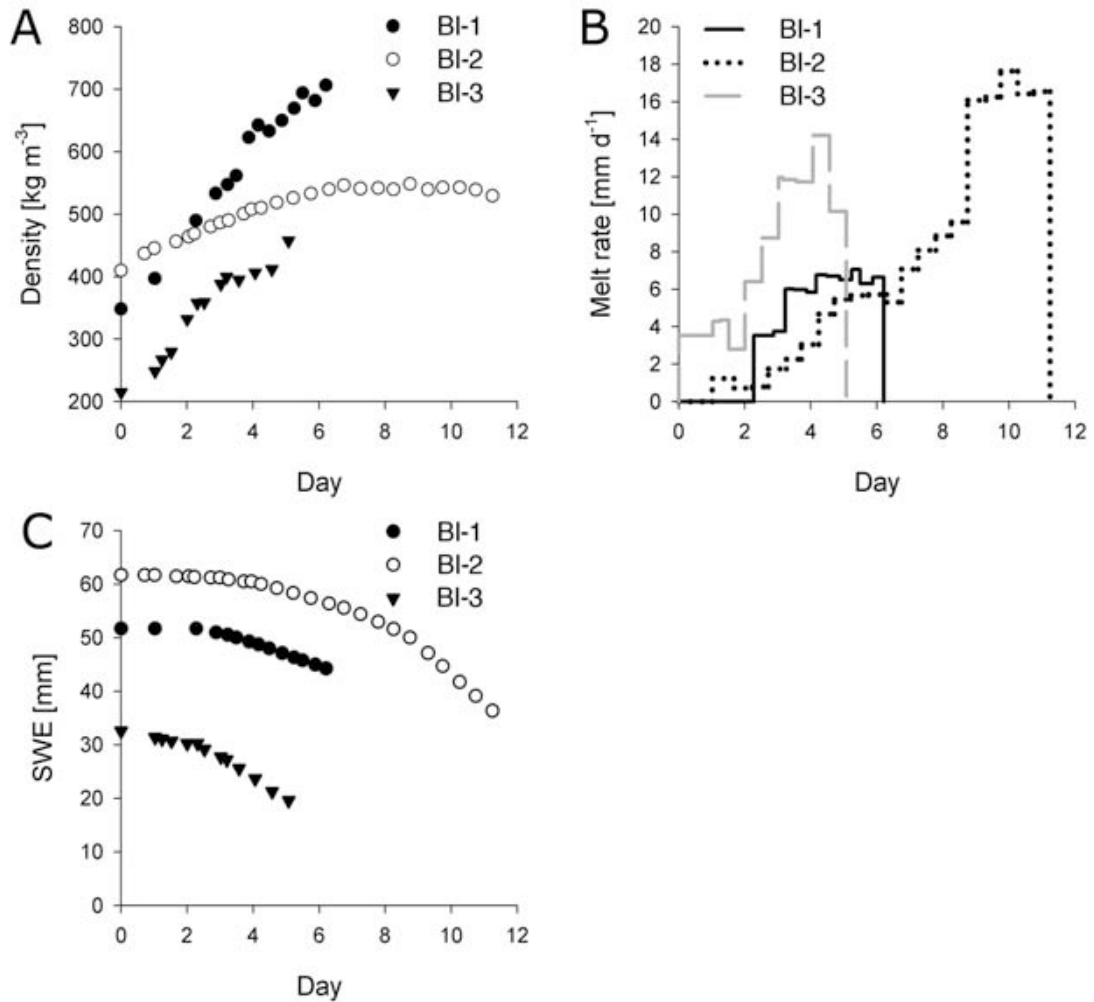


*Figure 6.1. Change in A) density [kg m$^{-3}$], B) melt rate [mm d$^{-1}$], and C) snow water equivalent [mm] as melt progressed.*

experiments; ~11 kg m$^{-3}$ d$^{-1}$. In BI-3 the rate of increase in density was almost the same as in BI-1; ~50 kg m$^{-3}$ d$^{-1}$. The average melt rate was the highest observed (7.8 mm d$^{-1}$) and the total change in *SWE* was about half that of BI-2; 13 mm.

The average base temperature throughout melt was –2 ºC in BI-1, –0.5 ºC in BI-2, and –0.2 ºC in BI-3 (Table 6.1). This range was chosen as it represents a range of melt period soil temperatures observed in many seasonally frozen soils. After termination of the experiment, the residual snow was removed from the box exposing the basal ice layer. The thickness of the basal ice varied from 80 mm in the first experiment to respectively 40 and 30 mm in the following two experiments (Table 6.1). Analyses of the chemical composition of the ice layers were not possible, as the experimental setup did not allow its intact removal without contamination.

The timing of the presence of the first water for collection varied among experiments. Snowpack structure causes instability of the meltwater wetting front, which results in formation of flow fingers and preferential flowpaths within the snowpack (Wankiewicz, 1978). The preferential flowpaths are an important mechanism for rapid delivery of meltwater to the bottom of the snowpack while it is still below 0 ºC (Woo *et al*., 1982). The ion mass flux in these flow fingers is higher than that in the matrix flow (Marsh and Pomeroy, 1999); implying that basal ice will be primarily comprised of enriched water from preferential flowpaths.

In each of the experiments, runoff water with basal ice contact (BW) was collected at the base before meltwater with no basal ice contact (SW) was present for collection. The first BW was collected after ~3 days in BI-1, ~2 days in BI-2, and ~1 day in BI-3. SW was collected 1-4 days after the initial BW sample; after 1 day in BI-1, 4 days in BI-2, and 2 days in BI-3 (Table 6.1). A reason for this delay could be that the SW extraction tube was snow-filled and so had to be saturated and melting before it could transmit water for collection outside of the box. It is also possible that the preferential flowpaths provided water to the base before they intersected with the extraction tube. However, given the relatively large collection area (10%), the extraction tube likely received preferential flowpath water at most times. Preferential flow along the sides of the box was not considered a possible explanation for this delay, as melting from the

sides was not visually pronounced until later in melt. Total melt period was shortest for BI-3 (~5 days) followed by BI-1 (~6 days) and then by BI-2 (~11 days).

The ion concentrations in the BW and SW were normalized to the corresponding ion concentration in the parent snowpack. This was done to minimize the influence that difference in origin of the snowpack and therefore parent snow composition may have on the results. The normalized value is the concentration factor, *CF* (Johannessen and Henriksen, 1978), and shows enriched conditions when *CF*>1 and depleted conditions when *CF*<1.

The variations in *CF* during melt for both BW and SW are shown in Figure 6.2. General for all experiments were that BW showed more irregular curves than SW. The figure also shows that the *CFs* for the BW were predominantly greater than or similar to the SW; most significant in BI-1 but also for most ions in BI-2. The variations in $H^+$ concentrations showed contrasting behaviour compared to the other ions. The only distinct differences between the *CFs* of BW and SW were observed in BI-1. In BI-2 and BI-3 similar *CFs* were observed for both BW and SW throughout melt; for the majority of the melt period, the *CF* was less than 1, increasing to just above 1 by the end of the melt. The curves for $NO_3^-$ and $NH_4^+$ showed an irregular *CF* evolution in BI-1. In BI-2 and BI-3 the variations in *CFs* corresponded more with the behaviour of most other ions. For most ions, the highest *CFs* were obtained within the initial third of the melt period. Table 6.3 shows that in general the highest *CFs* were obtained in BI-1 and the lowest values in BI-3. Most of these max *CFs* are within the range of values reported in

*Table 6.3. The greatest concentration factors, $CF_{max}$ [(meq $m^{-3}$)(meq $m^{-3})^{-1}$], in the runoff water, BW, and meltwater, SW, for each ion in each experiment.*

| Experiment | | $H^+$ | $Cl^-$ | $SO_4^{2-}$ | $NO_3^-$ | $NH_4^+$ | $Na^+$ | $K^+$ | $Mg^{2+}$ | $Ca^{2+}$ |
|---|---|---|---|---|---|---|---|---|---|---|
| BI-1 | BW | 8.7 | 19.8 | 9.8 | 16.6 | 4.2 | 40.7 | 1.7 | 5.5 | 8.0 |
| | SW | 15.7 | 8.0 | 3.8 | 4.5 | 2.1 | 19.5 | 0.6 | 2.5 | 2.8 |
| BI-2 | BW | 1.9 | 7.3 | 8.2 | 10.4 | 5.7 | 5.7 | 20.9 | 5.2 | 8.2 |
| | SW | 1.4 | 22.2 | 2.2 | 3.5 | 2.4 | 2.4 | 21.8 | 2.9 | 3.5 |
| BI-3 | BW | 1.1 | 5.1 | 3.5 | n.a. | 3.1 | 9.4 | 1.6 | 1.0 | 5.2 |
| | SW | 1.1 | 4.0 | 2.7 | n.a. | 2.3 | 8.0 | 2.0 | 1.7 | 5.3 |

n.a. = not applicable as concentrations were below detection limits in the parent snowpack.

*Figure 6.2. Fractionation curves showing change in concentration factors, CF, during melt for runoff water (BW, closed circles) and the snowpacks' meltwater (SW, open circles). The horizontal grey line represents CF=1.*

*Figure 6.2 (continued). Fractionation curves showing change in concentration factors, CF, during melt for runoff water (BW, closed circles) and the snowpacks' meltwater (SW, open circles). The horizontal grey line represents CF=1.*

previous studies (*CF* = 2-10; e.g. Tranter, 1991); however, *CFs* >20 have also been reported (e.g Tsiouris *et al.*, 1985; Bales *et al.*, 1989).

Normalizing the ion concentration in the BW with the corresponding concentration in the SW (BW/SW = *ER*, enrichment ratio) indicates the relative enrichment of runoff water. If *ER* >1 then BW is enriched, if *ER* <1 then BW is depleted, compared to the SW. Figure 6.3 shows the variations in the enrichment ratio throughout melt for each ion. A total of 24 samples were suitable for calculating the enrichment ratio for the nine ions. A total of 10 ratios were undefined and so not plotted in Figure 6.3 since either the BW or SW had an ion concentration below detection limit.The range of enrichment ratio observations for an individual ion in Figure 6.3 indicates the change in ratio during melt.

BI-1 showed the least variation in *ER* throughout melt for all ions. The *ER* for the $H^+$ concentration indicated depletion (~0.5) whilst that for the other ions indicated enrichment (~2). The greatest scatter in the ratio was observed in BI-2, where it initially increased and then decreased. Only $SO_4^{2-}$ showed continuous enrichment throughout melt. In the last experiment (BI-3), *ER* was very close to 1 during the whole melt period. Small variations in ratio were seen for $H^+$, $Cl^-$, $SO_4^{2-}$, $NO_3^-$, and $NH_4^+$; for the rest of the ions, the ratio increased slightly over time.
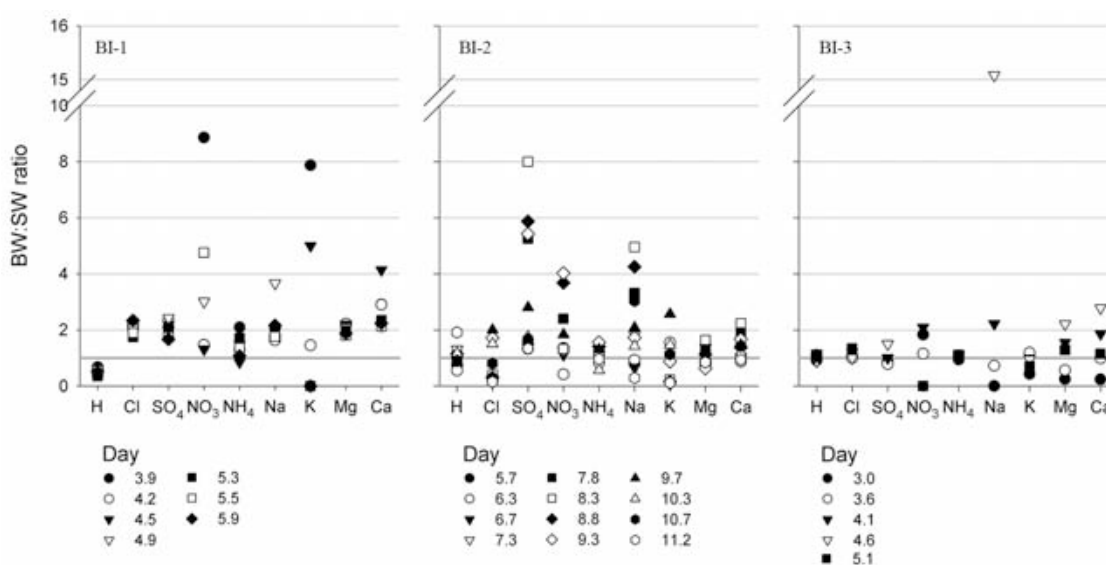


*Figure 6.3. Variation in the ion ratio between runoff water, BW, and snow meltwater, SW. The horizontal line represents ER=1.*

*Table 6.4. Mean differences between CF values for runoff, BW, and meltwater, SW, in each experiment. Positive values refer to BW enrichment compared to SW; negative values the opposite.*

| Experiment | $H^+$ | $Cl^-$ | $SO_4^{2-}$ | $NO_3^-$ | $NH_4^+$ | $Na^+$ | $K^+$ | $Mg^{2+}$ | $Ca^{2+}$ | Overall |
|---|---|---|---|---|---|---|---|---|---|---|
| *BI-1* | -6.6 | 4.3 | 1.9 | 3.9 | 0.6 | 7.6 | 0.2 | 2.4 | 2.9 | 1.9 |
| *BI-2* | 0.1 | -4.7 | 1.2 | 0.7 | 0.1 | 0.6 | -7.6 | 0.1 | 0.7 | -1.0 |
| *BI-3* | 0.0 | 0.2 | 0.0 | 0.0 | 0.1 | -1.0 | -0.3 | -0.2 | 0.1 | -0.1 |

*Table 6.5. Calculated root mean square deviation for the differences between CF values for runoff, BW, and meltwater, SW, in each experiment.*

| Experiment | $H^+$ | $Cl^-$ | $SO_4^{2-}$ | $NO_3^-$ | $NH_4^+$ | $Na^+$ | $K^+$ | $Mg^{2+}$ | $Ca^{2+}$ | Overall |
|---|---|---|---|---|---|---|---|---|---|---|
| *BI-1* | 2.1 | 2.4 | 1.4 | 4.6 | 0.7 | 5.1 | 0.4 | 0.4 | 1.5 | 4.5 |
| *BI-2* | 0.3 | 5.2 | 1.2 | 1.1 | 0.3 | 1.1 | 8.6 | 0.8 | 0.8 | 4.5 |
| *BI-3* | 0.1 | 0.1 | 0.3 | n.a. | 0.1 | 3.8 | 0.5 | 0.7 | 2.3 | 1.6 |

The mean difference between the *CF* for BW and SW is given in Table 6.4; both for each ion and overall (simple average of all ions) for each experiment. Positive values indicate enriched runoff water compared to meltwater. Positive differences were found for $SO_4^{2-}$, $NO_3^-$, $NH_4^+$, and $Ca^{2+}$ in all three experiments. Generally, the largest mean differences in *CF* were observed for the individual ions in BI-1. The mean differences in BI-3 were all close to zero, indicating similar concentrations in both runoff water and meltwater.

The dispersion of mean differences for each ion and overall, by experiment, is shown in Table 6.5; the dispersion was calculated as root mean square deviation, RMSD. For the individual ions, the largest RMSD values were observed for $H^+$ (2.1), $SO_4^{2-}$ (1.4), $NO_3^-$ (4.6), and $NH_4^+$ (5.1) in BI-1, $Cl^-$ (5.2), $K^+$ (8.6), and $Mg^{2+}$ (0.8) in BI-2, and $Ca^{2+}$ (2.3) in BI-3. Generally, BI-3 showed the least dispersion (<1).

## 6.1.2 Discussion

The influence of a basal ice layer on runoff chemistry was examined through three snowmelt experiments differing in snowpack density, melt rate, and basal cooling conditions. Ion concentrations in runoff water that had sustained basal ice contact were

compared to ion concentrations in meltwater without basal ice contact. The results showed that contact with the basal ice layer sometimes enriched the ion concentrations in runoff water compared to fractionation happening solely within the snowpack; especially during the initial half of melt.

Based on the soil surface infiltrability of frozen ground three infiltration regimes have been defined (Gray *et al*., 1985b): 'unlimited infiltrability' where all water released at the soil's surface infiltrates; 'limited infiltrability' where a partitioning of the water between infiltration and surface runoff takes place; and 'restricted infiltrability' where infiltration is negligible and water in excess ends up as runoff or evaporates. Formation of a basal ice layer acts analogous to a switch in the flow pathway, causing an unlimited or limited infiltrability regime to become a restricted infiltrability regime. Consequently, the implications of basal ice formation are that it will not only alter the flowpath but also the concentration of the ion load released from the snowpack. When no basal ice is present and infiltration is limited, but not restricted, a non-linear relationship between meltwater ion load and infiltration rate into frozen soil results in enhanced infiltration, which causes a dilution of the runoff water (Chapter 5). When basal ice is present, infiltration is restricted and all meltwater runs off (e.g. Jones and Pomeroy, 2001); in this case, further ion concentration enrichment is possible. Thus, frozen soils with variable infiltrability may exhibit great variance in soil and flowpath chemistry during snowmelt.

The experiments exhibited a large variation in the timing of water collection. This was believed to be a result of variations in initial snowpack density, melt rate, flowpaths, and base temperature. Preferential flowpaths (or finger flow) initially feed the base of the snowpack with meltwater (e.g. Wankiewicz, 1979), where it refreezes and basal ice is formed. The base temperature influenced the thickness of the growing ice layer. Experiment BI-1 had the coldest base temperature throughout melt (–2 ºC) and grew the thickest basal ice layer (80 mm). The base temperatures were higher in the other two experiments (~ –0.5 ºC) and their basal ice layers were approximately half that of BI-1 (30-40 mm). These basal ice layers all compare in thickness to those found in nature (Woo *et al*., 1982; Marsh and Woo, 1984a).

At some point, refreezing of meltwater released enough latent heat to increase the temperature of the surrounding snow to the melting point and runoff initiated. The combination of the thick basal ice layer, high initial snowpack density, and slower average melt rate in BI-1 resulted in a later collection of initial runoff water compared to the other experiments. The small variation in timing between BI-2 and BI-3 was probably a result of similar base temperatures and melt rates. The delay between initial runoff water and initial meltwater was hypothesized to be a function of the extraction tube's ability to transmit meltwater to the front of the box, the arrival of the matrix flow to the lower part of the snowpack, and the thermal state of the basal ice.

The scatter observed in the runoff water ion concentrations is probably a function of the flow rate, base temperature, and the rate of growth of the basal ice layer. In the first experiment it is hypothesized that the basal ice increased in thickness throughout melt, causing continuous ion exclusion and thereby enrichment of the runoff water. In the warmer experiments (BI-2 and BI-3), it is hypothesized that the basal ice layer stopped growing during melt. The undulating pattern of the runoff ion concentrations in BI-2 is thought to be a result of the basal ice layer growth having reached a limit. At this stage the basal ice layer may alternate between enriching the runoff water due to refreezing of percolating meltwater and diluting it as a result of melting of the ice layer itself causing the runoff water to have ion concentrations close to those in the meltwater itself. The lack of runoff water enrichment in BI-3 is most likely explained by a late formation of the basal ice layer.

The *CFs* of both BW and SW were greatest in BI-1 and lowest in BI-3 (Table 6.3). *CF* peaked early in melt and then decayed exponentially with time (Figure 6.2). *CF* for BW usually peaked after the first few samples during each experiment. Extrapolating the SW *CF* observations backward to the first observations sometimes resulted in correspondence between these extrapolations and the BW *CF* values. The delay in peak and possible commonality of first ion concentrations may provide some evidence of ion uptake early in the basal ice formation. However, further investigations of this mechanism are required. For instance, an alternative explanation for this delayed peak in *CF* could be that the initial water released at the base of the box originated primarily from relatively dilute preferential flow (Marsh and Pomeroy, 1999), whereas matrix

flow dominated by the time that meltwater collection was possible using the collection tubes.

Overall, the *CF* for SW showed little scatter. However, the BW *CF* showed abrupt increases in enrichment followed by concentrations that were slightly depleted or equal to the meltwater. The exception was in the relatively cold BI-1 where BW remained enriched compared to SW throughout melt.

Preferential flow is normally depleted compared to matrix flow (Marsh and Pomeroy, 1999); SW was likely to have been dominated by matrix flow, and basal ice formation was dominated by preferential flow. If the basal ice did not influence the BW chemistry, then the enrichment ratio would be less than 1. However, 81% of the 63 enrichment ratios in BI-1 were enriched compared to meltwater; only $H^+$ was consistently depleted. Average enrichment was near 2.0 overall for BI-1. In BI-2, 61% of the 108 ratios were enriched with an overall average enrichment of ~1.5; 38% of the ratios were depleted or near 1. The enrichment ratios in BI-3 showed an enrichment for 56% of the 45 ratios, with an overall average enrichment of ~1.2; 40% were depleted. That the enrichment ratios were near to or greater than 1 and hence overcame depletionary effects due to preferential flow demonstrates the substantial effect of basal ice contact in enhancing concentrations of runoff water compared to the meltwater leaving the snowpack.

The mean difference between the *CFs* for BW and SW supports the observations from the enrichment ratios (Table 6.4). For BI-1, the only negative mean difference was found for $H^+$; thus, the overall mean difference is positive. A negative overall mean difference was observed for BI-2 even though a majority of the ions showed positive values. This was caused by the large negative values for $Cl^-$ and $K^+$, which were a result of the depletion of BW compared to SW. This behaviour is believed to be associated with road salt contamination of snow used in this experiment with higher than natural concentrations of $Cl^-$ and $K^+$. Excluding these ions from the calculation of the overall mean difference in BI-2 reveals a positive tendency and the overall mean difference becomes equal to 0.5. In BI-3, the mean differences were all close to zero indicating similar concentrations in both BW and SW, which correspond with the observations shown in Figure 6.2.

The overall dispersion of the difference between *CF* in the BW and SW, calculated as root mean square deviation (RMSD), was 4.5 for each of BI-1 and BI-2 (Table 6.5). These values were strongly influenced by the behaviour of $NO_3^-$ (RMSD = 4.6) and $Na^+$ (RMSD = 5.1) in BI-1 and $Cl^-$ (RMSD = 5.2) and $K^+$ (RMSD = 8.6) in BI-2. In BI-3 most ions had RMSD <1 with the overall dispersion value (1.6) strongly influenced by $Na^+$ (RMSD = 3.8) and $Ca^{2+}$ (RMSD = 2.3). In all three experiments approximately half the ions had dispersion values <1, but $NH_4^+$ and $Mg^{2+}$ were the only ions for which all dispersion values were <1. No ion showed high dispersion values in all three experiments. Statistical dispersion results are consistent with the trends observed from the enrichment ratios, in that BI-1 runoff water was most enriched, with lower enrichment for BI-2 and little enrichment for BI-3. In all measures, the enrichment and degree of difference between snowmelt water and runoff water increased with increasing thickness of basal ice layer and decreased with increasing basal temperature during melt. This suggests that the thickness of the basal ice layer and the rapidity of its formation may have an important role in regulating runoff water ion concentrations.

## 6.2    Organic Base Layer

Three snowmelt experiments were conducted with an organic layer underlying the snowpack. Snow for the first two experiments (OIF-1 and -2) was collected within city limits; for the third experiment (OIF-3) snow was collected outside of city limits, at a hay meadow. The snow was collected <24 hrs after a snow event and stored at –20 ºC until used; storage times were respectively 27, 14, and 12 days for OIF-1, OIF-2, and OIF-3 (Table 6.6).

Snow was sieved into the box to a final depth between 0.41 and 0.44 m, giving a total snow volume of ~0.14 $m^3$. The snow consisted of loose 1-2 mm crystals with chemical compositions that were dominated by $Cl^-$, $Mg^{2+}$, and $Ca^{2+}$ (Table 6.7). Initial snowpack densities were ~300 kg $m^{-3}$ in OIF-1 and OIF-2 and 400 kg $m^{-3}$ in OIF-3. Thermal equilibrium of the snowpacks was reached at a room temperature of –2 ºC and a coolant temperature of –4 ºC in OIF-1 and OIF-2 and –2 ºC in OIF-3. Room temperature was then increased to +5 ºC in OIF-1 and OIF-2 and +7.5 in OIF-3.

*Table 6.6. Summary of snow and melt conditions for each experiment. OW is the runoff water that had sustained contact with an organic layer; SW is the meltwater.*

| Experiment | | OIF-1 | OIF-2 | OIF-3 |
|---|---|---|---|---|
| *Snow* | Origin | Within city | Within city | Rural area |
| | Storage [d] | 27 | 14 | 12 |
| | Initial depth [m] | 0.40 | 0.41 | 0.44 |
| | Initial density [kg m$^{-3}$] | 290 | 297 | 400 |
| *Gravimetric moisture content of base layer* | Initial [g g$^{-1}$] | 0.05 | ~2.7 | ~2.8 |
| | Final [g g$^{-1}$] | ~2.7 | ~2.8 | ~6.1 |
| *Temperature* | Room [ºC] | +5 | +5 | +7.5 |
| | Coolant (initially) [ºC] | –4 | –4 | –2 |
| | Base of snowpack [ave ºC] | –0.8 | –0.7 | ~0 |
| *Experiment duration [d]* | | 9.9 | 8.8 | 9.7 |
| *Timing of first sample [days after initiation]* | Runoff water, OW | 0.9 | 1.0 | 0.8 |
| | Meltwater, SW | 5.3 | 2.6 | 3.0 |

*Table 6.7. Ion concentrations [meq m$^{-3}$] in the parent snowpacks; DOC concentrations are in g m$^{-3}$.*

| Experiment | H$^+$ | Cl$^-$ | SO$_4$$^{2-}$ | NO$_3$$^-$ | NH$_4$$^+$ | Na$^+$ | K$^+$ | Mg$^{2+}$ | Ca$^{2+}$ | DOC | ICB |
|---|---|---|---|---|---|---|---|---|---|---|---|
| *OIF-1* | 0.188 | 22.5 | 15.6 | n.d. | 24.3 | 13.0 | 9.6 | 31.1 | 43.7 | 1.8 | +0.52 |
| *OIF-2* | 0.217 | 35.2 | 12.5 | 2.6 | 15.4 | 19.3 | 8.2 | 31.7 | 65.9 | 1.8 | +0.47 |
| *OIF-3* | 0.041 | 26.7 | 12.5 | 6.4 | 9.1 | 11.3 | 9.9 | 30.9 | 170.9 | 1.8 | +0.67 |

n.d. = below detection limits

Adjustments in coolant temperature were only done in OIF-3. During the first four days the temperature was decreased gradually to –6 ºC to ensure frozen conditions at the base of the organic layer.

Gravimetric moisture content [g g$^{-1}$] of the organic layer was equal to the hygroscopic water content (~ 0.05 g g$^{-1}$) prior to the first experiment. Knowing total depth within the box (snow and organic layer) and total water volume eluted from the box made it possible to estimate changes in total water equivalent (*SWE* as well as water stored in the organic layer) as melt progressed. Estimates of snowpack densities alone were not possible as the volume of water stored in the organic layer during melt was unknown. Direct measurements of snow density would cause disturbance of the

snowpack. Approximations of the organic layer's moisture content were made at the end of each experiment based on the total collected water volume. The approximated content was used as the initial moisture content in the following experiment as they immediately succeeded each other.

Sampling of meltwater, SW, was concluded once only a small patch (<50 mm) of snow was left on top of the organic layer. At this point the room temperature was increased to +10 ℃ and circulation of coolant was turned off to allow collection of water stored within the frozen organic layer. Only samples from OIF-1 and OIF-3 were analysed for their chemical composition. Experiments were terminated when all snow had melted.

## 6.2.1  Results

The experiments differed with respect to initial snowpack density, melt rate, base temperature, and initial moisture content of the organic layer (Table 6.6). All experiments showed an increase in total density and melt rate and a decrease in water equivalent as melt progressed (Figure 6.4). OIF-1 and OIF-2 were similar in setup (room temperature, average base temperature, and initial snow density) resulting in similar changes in densities (~26 kg m$^{-3}$ d$^{-1}$) and average melt rates (~8.6 mm d$^{-1}$). The difference between their initial water equivalents (40 and 50 mm, respectively) was a result of the moisture content of the organic layer at the beginning of each experiment.

The organic layer was initially air-dry in OIF-1 compared to the estimated initial gravimetric moisture content of 2.7 g g$^{-1}$ in OIF-2. Total reduction in water equivalent (snow + soil) over the melt period was 30 mm in OIF-1 and 40 mm in OIF-2. The greatest daily melt rate was observed in OIF-3 at 31.9 mm d$^{-1}$; average melt rate was 11.8 mm d$^{-1}$. This experiment was carried out at a higher room and average base temperature; 7.5 ℃ and ~0 ℃, respectively. Average density change was ~2.5 times greater than in the other experiments (65 mm d$^{-1}$); this combined with the higher initial snow density resulted in a final density almost twice that of OIF-1 and OIF-2 (~1320 kg m$^{-3}$). The high initial water equivalent (snow + soil) in OIF-3 was due to a high initial snow density (400 kg m$^{-3}$) and high gravimetric moisture content in the organic layer (2.8 g g$^{-1}$). However, total change and average change in water equivalent (46 mm and
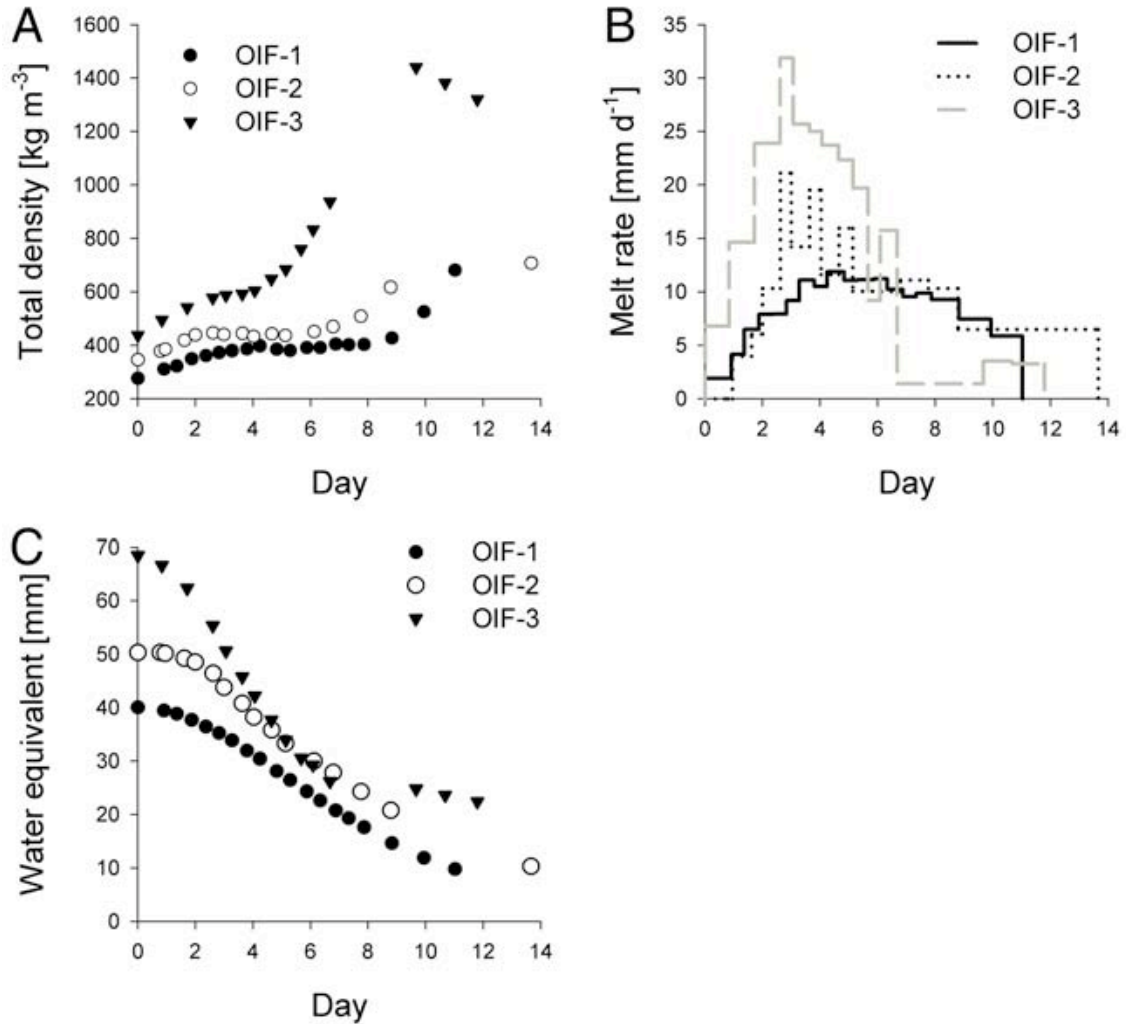
*Figure 6.4. Change in A) density [kg m$^{-3}$], B) melt rate [mm d$^{-1}$], and C) water equivalent [mm] as melt progressed.*

3.9 mm d$^{-1}$, respectively) were similar to those of OIF-2. Final gravimetric moisture content of the organic layer was estimated to 6.1 g g$^{-1}$.

Throughout melt, the average base temperature was –0.8 ºC in OIF-1, –0.7 ºC in OIF-2, and ~0 ºC in OIF-3 (Table 6.6). The low base temperatures in OIF-1 and OIF-2 resulted in ice layer formation at the base of the organic layer. The ice layers were observed along the opening at the front of the box after approximately one day in both experiments. In OIF-3, the initial decrease in coolant temperature is hypothesized to have caused a refreezing of all infiltrating meltwater, resulting in a solid frozen organic

layer by the end of the experiment. Since the ice was not visible at the front of the box, precautions could not be taken.

Organic runoff water (OW) was collected at the base before meltwater with no organic layer contact (SW) was present for collection. In each of the experiments the first OW was collected approximately one day after the room temperature was increased; 0.9 day in OIF-1, 1.0 day in OIF-2, and 0.8 day in OIF-3. SW collection was delayed by 4.4 days in OIF-1, 1.8 days in OIF-2, and 2.2 days in OIF-3 (Table 6.6). Similar to the basal ice experiments a reason for this delay could be that the SW extraction tube was snow-filled and had to be saturated and melting before it could transmit water for collection outside the box. Total melt period varied between 11 and 13.7 days; shortest during OIF-1 and longest during OIF-2. However, during OIF-2 collection of water samples only took place for 8.8 days, after which the organic layer was allowed to drain for a few days to prevent a solid frozen layer from forming prior to initiation of the last experiment. The last two samples in OIF-3 consisted solely of OW; no snow remained on the surface.

Both SW and OW were normalized using the concentrations in the parent snowpack for comparison of results among experiments and to evaluate the evolution of the waters. Figure 6.5 shows the variation in *CF* as melt progressed for all major ions and dissolved organic carbon (DOC). All curves show similar trends; a *CF* decrease as melt progressed. The curves for OW were generally more irregular than for SW. In OIF-3, the *CF* decrease was often followed by a *CF* increase for the last two samples, which were collected after the snow had fully melted. Maximum $NO_3^-$ concentration was 16.5 meq m$^{-3}$ and half of the samples had concentrations below detection limit (1.0 meq m$^{-3}$). The *CFs* obtained for the first two samples are enhanced by the very low concentration in the parent snowpacks (Table 6.7). For the rest of the ions, *CFs* generally were higher for the OW than for the SW; except for $Mg^{2+}$, for which concentrations were higher for the SW than for the OW. *CF$_{max}$* was usually obtained within the initial third of the melt period. Table 6.8 shows that the largest *CF$_{max}$* for OW were obtained in OIF-1; except for $NH_4^+$, which was obtained in OIF-3. For SW, *CF$_{max}$* were obtained in OIF-2; except for $H^+$, which was highest in OIF-3. All SW samples had *CFs* within the range of values reported in previous studies (e.g. Tranter, 1991).
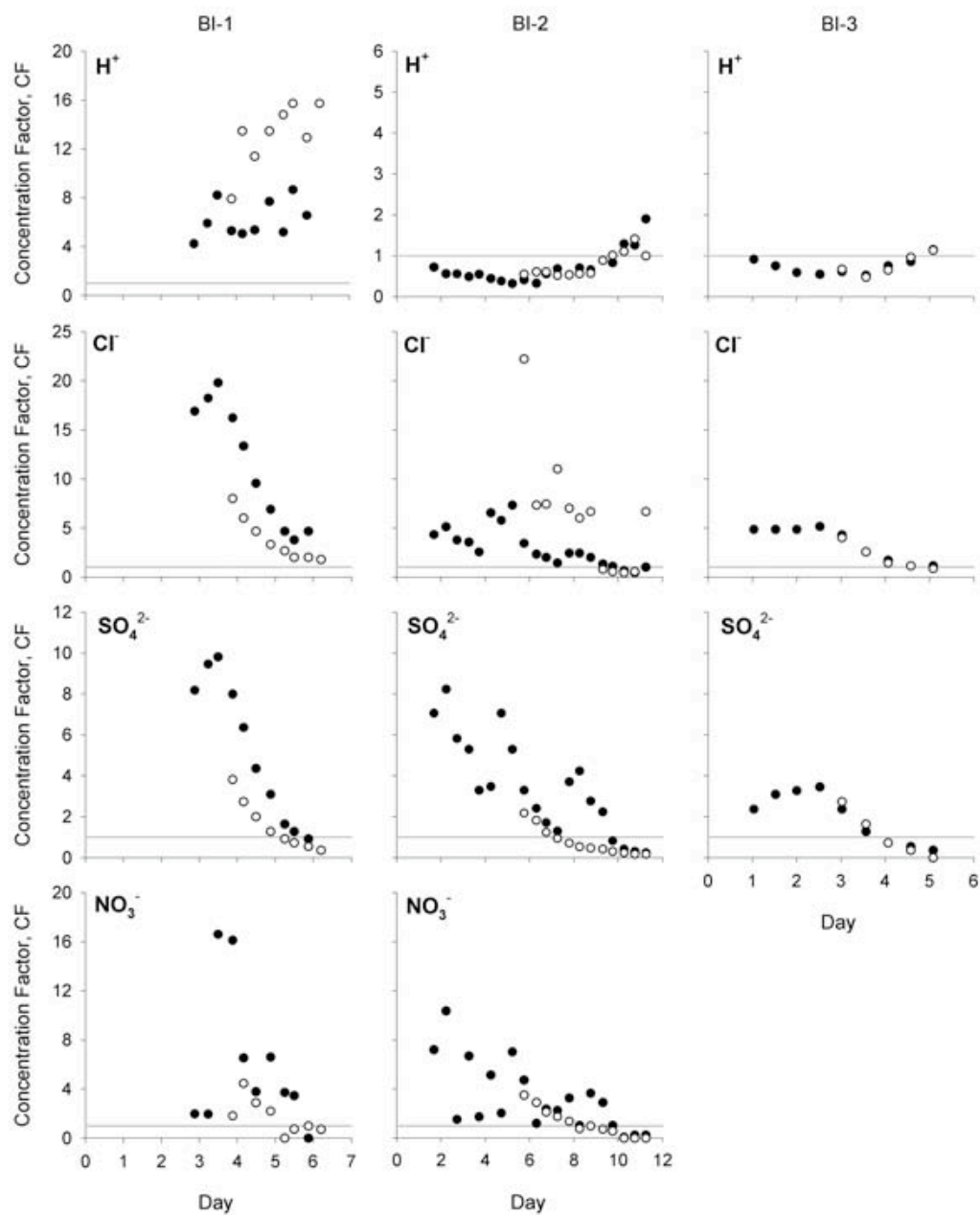
*Figure 6.5. Fractionation curves showing change in concentration factors, CF, during melt for organic interflow (OW, closed circles) and the snowpacks' meltwater (SW, open circles). The horizontal grey line represents CF=1.*
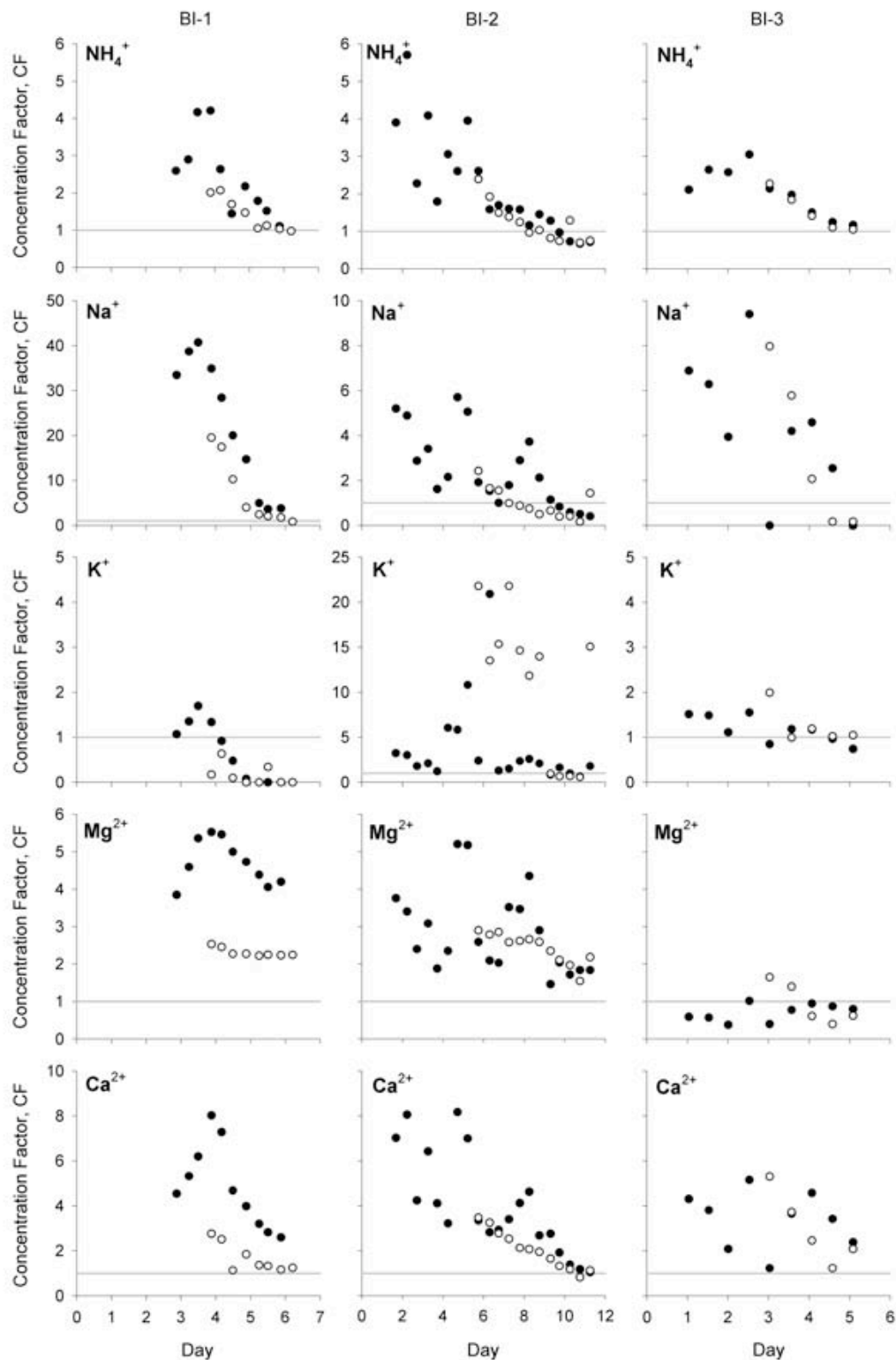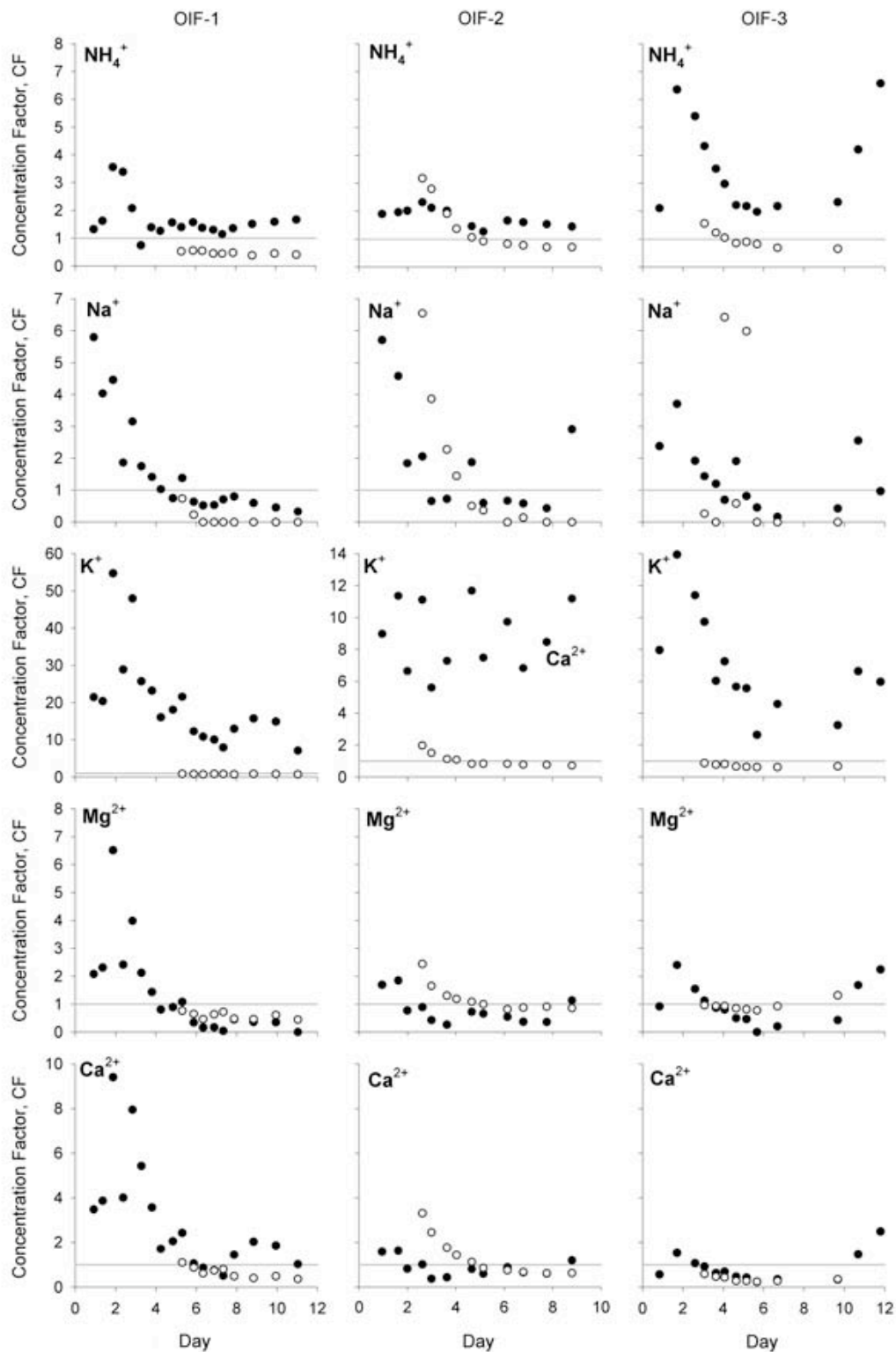
*Figure 6.5 (continued). Fractionation curves showing change in concentration factors, CF, during melt for organic interflow (OW, closed circles) and the snowpacks' meltwater (SW, open circles). The horizontal grey line represents CF=1.*

*Table 6.8. The greatest concentration factors, $CF_{max}$ $[(meq\ m^{-3})(meq\ m^{-3})^{-1}]$, in the runoff water, OW, and meltwater, SW, for each ion in each experiment.*

| Experiment | | $H^+$ | $Cl^-$ | $SO_4^{2-}$ | $NO_3^-$ | $NH_4^+$ | $Na^+$ | $K^+$ | $Mg^{2+}$ | $Ca^{2+}$ | DOC |
|---|---|---|---|---|---|---|---|---|---|---|---|
| OIF-1 | OW | 18.2 | 9.3 | 9.9 | 31.4 | 3.6 | 5.8 | 54.7 | 6.5 | 9.4 | 30.9 |
| | SW | 2.0 | 0.8 | 0.5 | 4.1 | 0.6 | 0.7 | 0.8 | 0.8 | 1.1 | n.a. |
| OIF-2 | OW | 2.0 | 3.9 | 6.5 | 3.6 | 2.3 | 5.7 | 11.7 | 1.8 | 1.6 | 6.9 |
| | SW | 1.0 | 4.3 | 7.2 | 5.2 | 3.2 | 6.5 | 2.0 | 2.4 | 3.3 | n.a. |
| OIF-3 | OW | 9.6 | 3.7 | 3.6 | 2.3 | 6.6 | 3.7 | 14.0 | 2.4 | 2.5 | 23.4 |
| | SW | 5.2 | 0.6 | 0.8 | 0.7 | 1.6 | 6.4 | 0.9 | 1.3 | 0.6 | n.a. |

n.a. = not applicable
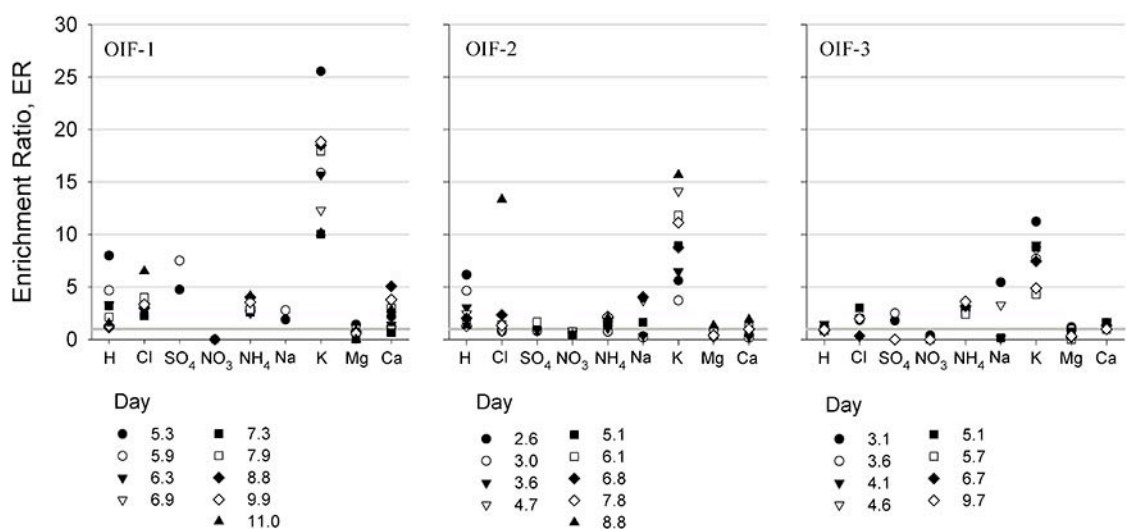


*Figure 6.6. Variation in the ion ratio between organic interflow, OW, and snow meltwater, SW. The horizontal line represents ER=1.*

The variations in enrichment ratio ($ER$ = OW/SW) as melt progressed were determined for each ion (Figure 6.6). A total of 9 ratios, $n$, were determined in OIF-1 and -2 and 8 in OIF-3. The $ER$ for DOC was not determined in any of the experiments as the evolution of DOC in the meltwater was unknown. A total of 42 ratios were not plotted because either OW or SW had an ion concentration below detection limit. Missing ratios were for $SO_4^{2-}$, $NO_3^-$, and $Na^+$.

In each of the experiments, all ions showed enriched ratios except $NO_3^-$ and $Mg^{2+}$, which were generally depleted. On average, OW had a 4.6 times higher concentration than SW in OIF-1, 2.5 in OIF-2, and 2.2 in OIF-3. For all of the experiments, $K^+$ $ER$ had

the largest range. For $SO_4^{2-}$, $NO_3^-$, $NH_4^+$, $Mg^{2+}$, and $Ca^{2+}$ the range was <2 in each experiment.

Table 6.9 shows the mean difference between the *CF* of OW and SW for each ion and overall (simple average of all ions) for each experiment. Half of the individual ions' mean differences showed positive values (>0.2) indicating that contact with the organic layer caused enrichment of ion concentrations in the interflow water compared to the meltwater. About a fifth of the values were close to zero ($\pm$0.2) indicating similar concentrations in both interflow water and meltwater; the rest of the values showed an average depletion (<–0.2). Nitrate and $Mg^{2+}$ were the only ions that showed depletion in all three experiments. Sodium changed from being enriched in the first experiment to deplete in the following two. For the individual ions, the greatest mean differences were generally found in OIF-1; there was no trend for the smallest differences. The overall tendency was positive with OIF-1 having an average mean difference more than twice that of the other experiments.

The dispersion of the mean differences was calculated as root mean square deviation, RMSD, for the individual ions and overall (Table 6.10). Seventy percent of the ions had RMSD $\leq$1.0. The greatest dispersions were observed for $H^+$ (1.7), $NO_3^-$ (1.5), and $K^+$ (4.1) in OIF-1, $Cl^-$ (1.0), $SO_4^{2-}$ (1.8), $NH_4^+$ (0.6), $Mg^{2+}$ (0.5), and $Ca^{2+}$

Table 6.9. Mean differences between CF of organic interflow, OW, and meltwater, SW, in each experiment. Positive values refer to OW being enriched compared to SW; negative values the opposite.

| Experiment | $H^+$ | $Cl^-$ | $SO_4^{2-}$ | $NO_3^-$ | $NH_4^+$ | $Na^+$ | $K^+$ | $Mg^{2+}$ | $Ca^{2+}$ | Overall |
|---|---|---|---|---|---|---|---|---|---|---|
| OIF-1 | 2.0 | 1.1 | 1.7 | –1.8 | 1.0 | 0.6 | 11.8 | –0.3 | 0.7 | 1.9 |
| OIF-2 | 0.8 | 0.2 | 0.3 | –0.7 | 0.3 | -0.4 | 7.8 | –0.6 | –0.6 | 0.8 |
| OIF-3 | –0.1 | 0.2 | 0.4 | –0.1 | 1.7 | -0.8 | 4.9 | –0.4 | 0.1 | 0.7 |

Table 6.10. Calculated root mean square deviation for the differences between CF of organic interflow, OW, and meltwater, SW, in each experiment.

| Experiment | $H^+$ | $Cl^-$ | $SO_4^{2-}$ | $NO_3^-$ | $NH_4^+$ | $Na^+$ | $K^+$ | $Mg^{2+}$ | $Ca^{2+}$ | Overall |
|---|---|---|---|---|---|---|---|---|---|---|
| OIF-1 | 1.7 | 0.3 | 0.2 | 1.7 | 0.2 | 0.1 | 4.1 | 0.3 | 0.6 | 4.0 |
| OIF-2 | 0.5 | 1.0 | 1.8 | 0.7 | 0.6 | 2.2 | 2.1 | 0.5 | 1.0 | 2.8 |
| OIF-3 | 0.9 | 0.2 | 0.3 | 0.2 | 0.5 | 2.7 | 2.0 | 0.4 | 0.1 | 2.0 |

(1.0) in OIF-2, and only $Na^+$ (2.7) in OIF-3. The overall dispersion of the mean differences was greatly influenced by $K^+$ in all experiments due to having the greatest RMSD throughout the experiments. The overall dispersion was 4.0 in OIF-1, decreasing to 2.8 in OIF-2 and 2.0 in OIF-3.

## 6.2.2  Discussion

Three experiments were carried out to examine the compositional changes in water chemistry as a result of meltwater infiltrating a frozen organic layer. The main differences between the experiments were initial snowpack density, melt rate, basal cooling, and initial moisture content of the organic layer. Organic interflow ion concentrations were compared to ion concentrations in meltwater without organic layer contact. The results showed that infiltration to a frozen organic layer, either as interflow or overland flow, causes significant compositional changes. The severity of the change was strongly influenced by the frozen moisture content of the organic layer as well as repeated flow through the layer.

The timing of OW collection was similar among the three experiments. The first OW sample was collected within 0.8-1.0 days after increasing the room temperature; slightly faster for OIF-3, which was carried out at a higher room temperature. The combination of unsaturated conditions and high porosity, resulting in a high infiltrability of the organic layer, allowed for fast transmission of infiltrating meltwater to the front of the box and therefore early collection of OW.

The frozen moisture content of the organic layer did not seem to influence the timing of collection, but it did influence the volume of flow. Experimental setup was similar for OIF-1 and OIF-2 differing only in initial soil moisture content (Table 6.6). The difference in timing of OW between the experiments was <2.5 hours. However, the flow rate for the initial sample was slower druing OIF-2 (0.6 mm $d^{-1}$) than during OIF-1 (1.92 mm $d^{-1}$). The early arrival of OW in OIF-3 was believed to be a combination of the higher room and base temperatures, which resulted in the highest initial flow rate (6.8 mm $d^{-1}$) even though the frozen moisture content of the layer was initially similar to that of OIF-2.

The timing of initial SW collection varied greatly between experiments. Similar timing was expected for OIF-1 and OIF-2 due to their similar experimental setup. Nevertheless, SW was collected 4.4 days after initial OW in OIF-1 but only 1.7 days later in OIF-2. In OIF-3, SW collection was delayed 1.8 days; similar to OIF-2. This variability was believed to be a result of the ability of the snow filled extraction tube to transmit meltwater to the outside of the box, the arrival of matrix flow to the lower part of the box and the thermal state of the base layer.

The *CF* varied more for the OW samples than for the SW samples. Both OW and SW *CFs* decreased exponentially as melt progressed. For SW, the decrease was a result of fractionation; for OW, it indicated that a washout of ions from the organic layer took place. With each experiment the degree of OW enrichment decreased; $CF_{max}$ was highest during OIF-1. These decreases were believed to be a result of the differences in flow rate and initial frozen moisture content between experiments. Increased frozen moisture content blocks pore spaces and limit the area of organic contact for the infiltrating meltwater and therefore contact time with increasing flow rate. The result is a decrease in ion concentrations in the organic interflow. Repeated flushing through this limited pore space may cause a washout of ions. However, from the last two samples in OIF-3, which were collected after all the snow had melted, it would appear that the organic layer recovers quickly after snowmelt. A general increase in ion concentrations was observed for these samples; except for $NO_3^-$, which continued to be less than the detection limit.

If contact with the organic layer did not alter the chemical composition of infiltrating meltwater, *ER* should be ~1. However, 77% of the 81 enrichment ratios in OIF-1 showed an average enrichment of 4.6; 17% of the ratios indicated that the SW was enriched compared to the OW. In OIF-2, only 52% of the 81 ratios indicated enrichment (average was 2.5) and 44% showed depletion. *ER* in OIF-3 showed enrichment for 63% of the 72 ratios, with an average enrichment of 2.2; 25% were depleted. The mean differences between the *CFs* for OW and SW (Table 6.9) confirm this, as half of the differences were positive. The greatest range in mean differences was observed in OIF-1 from −1.8 ($NO_3^-$) to 11.8 ($K^+$). The only ions that showed a positive mean difference in all three experiments were $Cl^-$, $SO_4^{2-}$, $NH_4^+$, and $K^+$. Nitrate and

$Mg^{2+}$ were the only ions that showed higher CF for SW than OW in all experiments. In general, a decrease in mean difference with each experiment was observed for $H^+$, $Cl^-$, $SO_4^{2-}$, $NO_3^-$, $K^+$, and overall. The dispersion of the mean differences was generally small ($\leq 1.0$). The overall dispersions were greatly influenced by $K^+$ in addition to $Na^+$ in OIF-2 and OIF-3. Ammonium and $Mg^{2+}$ were the only ions that had RMSD values $<1.0$ in all experiments, followed by $Cl^-$ and $Ca^{2+}$, which both had one RMSD value equal to 1.0.

## 6.3    Mineral Base Layer

Two experiments (termed MIF-1 and MIF-2) were carried out using snow from a hay meadow outside of the city of Saskatoon. The snow was collected <48 hours after a snowfall event and stored for five months at –20 ºC. Metamorphism had taken place during storage resulting in a hard crust around loose snow with a ~2 mm crystal size. The loose snow was sieved into the box to a total depth of 0.46 m in MIF-1 and 0.43 m in MIF-2 giving snow volumes of 0.12 $m^3$ and 0.13 $m^3$. Initial snowpack densities were almost the same in each experiment; ~430 kg $m^{-3}$ in MIF-1 and ~440 kg $m^{-3}$ in MIF-2 (Table 6.11). This slight difference resulted in initial *SWE* for both experiments of 60 mm.

Both snowpacks reached thermal equilibrium at room temperature –2ºC and coolant temperature –3 ºC. Once equilibrium was reached, the room temperature was increased to +5 ºC in MIF-1 and +7.5 ºC in MIF-2. Adjustments in coolant temperature were ±2 ºC in MIF-1 and –4 ºC in MIF-2. Calcium, $Cl^-$, and $NH_4^+$ dominated the chemical composition of the parent snowpack (Table 6.12).

The gravimetric moisture content of the mineral soil prior to snowmelt was 0.2 g $g^{-1}$ in MIF-1 and 0.3 g $g^{-1}$ in MIF-2. The volume of water stored in the mineral soil during melt was unknown, as direct measurements of snow density would cause disturbance of the snowpack. Consequently, estimates of total density and water equivalent within the box were made based on observations of snow depth and total water volume eluted from the box. Experiments were terminated once all snow had melted. After termination of MIF-2, the gravimetric soil moisture content was 0.3 g $g^{-1}$. In addition, estimates of the soil's dry bulk density and porosity were made; dry bulk

*Table 6.11. Summary of snow and melt conditions for each experiment.*

| Experiment | | MIF-1 | MIF-2 |
|---|---|---|---|
| *Snow* | Origin | Rural area | Rural area |
| | Storage [d] | 128 | 186 |
| | Initial depth [m] | 0.39 | 0.36 |
| | Initial density [kg m$^{-3}$] | 430 | 440 |
| *Temperature* | Room [ºC] | +5 | +7.5 |
| | Coolant, initially [ºC] | −3 (±2) | −3 (−4) |
| | Base of snowpack [ave ºC] | −0.2 | −0.1 |
| *Experiment duration [d]* | | 19 | 11 |
| *Timing of first sample [days after initiation]* | Runoff water, *MW* | 1.3 | 0.7 |
| | Meltwater, *SW* | 5.3 | 4.7 |

*Table 6.12. Ion concentrations [meq m$^{-3}$] in the parent snowpack.*

| Experiment | H$^+$ | Cl$^-$ | SO$_4^{2-}$ | NO$_3^-$ | NH$_4^+$ | Na$^+$ | K$^+$ | Mg$^{2+}$ | Ca$^{2+}$ | ICB |
|---|---|---|---|---|---|---|---|---|---|---|
| *MIF* | 0.029 | 30.9 | 22.9 | 7.5 | 29.7 | 20.2 | 4.0 | 22.1 | 113.7 | +0.51 |

density was 1.26 g cm$^{-3}$ and porosity was 0.53. These values corresponded well with the values of the soil at the observation site at Marmot Creek Research Basin (see section 4.5).

## 6.3.1 Results

The two experiments had similar initial *SWE* (60 mm) and average base temperature (~ −0.2 ºC) but varied with respect to room temperature, melt rate, and initial soil moisture (Table 6.11). In both experiments, total density increased as melt progressed; average daily change was 43 kg m$^{-3}$ in MIF-1 and 78 kg m$^{-3}$ in MIF-2 (Figure 6.7). Melt rate peaked during the initial third of melt and was faster during MIF-2 (33.4 mm d$^{-1}$) than during MIF-1 (16.7 mm d$^{-1}$). Average melt rate was 8.2 mm d$^{-1}$ during MIF-1 and 14.2 mm d$^{-1}$ during MIF-2. Total change in water equivalent was the same for both experiments (~51 mm) but the average change in water equivalent was only 2.7 mm d$^{-1}$ during MIF-1 compared to 4.8 mm d$^{-1}$ during MIF-2.
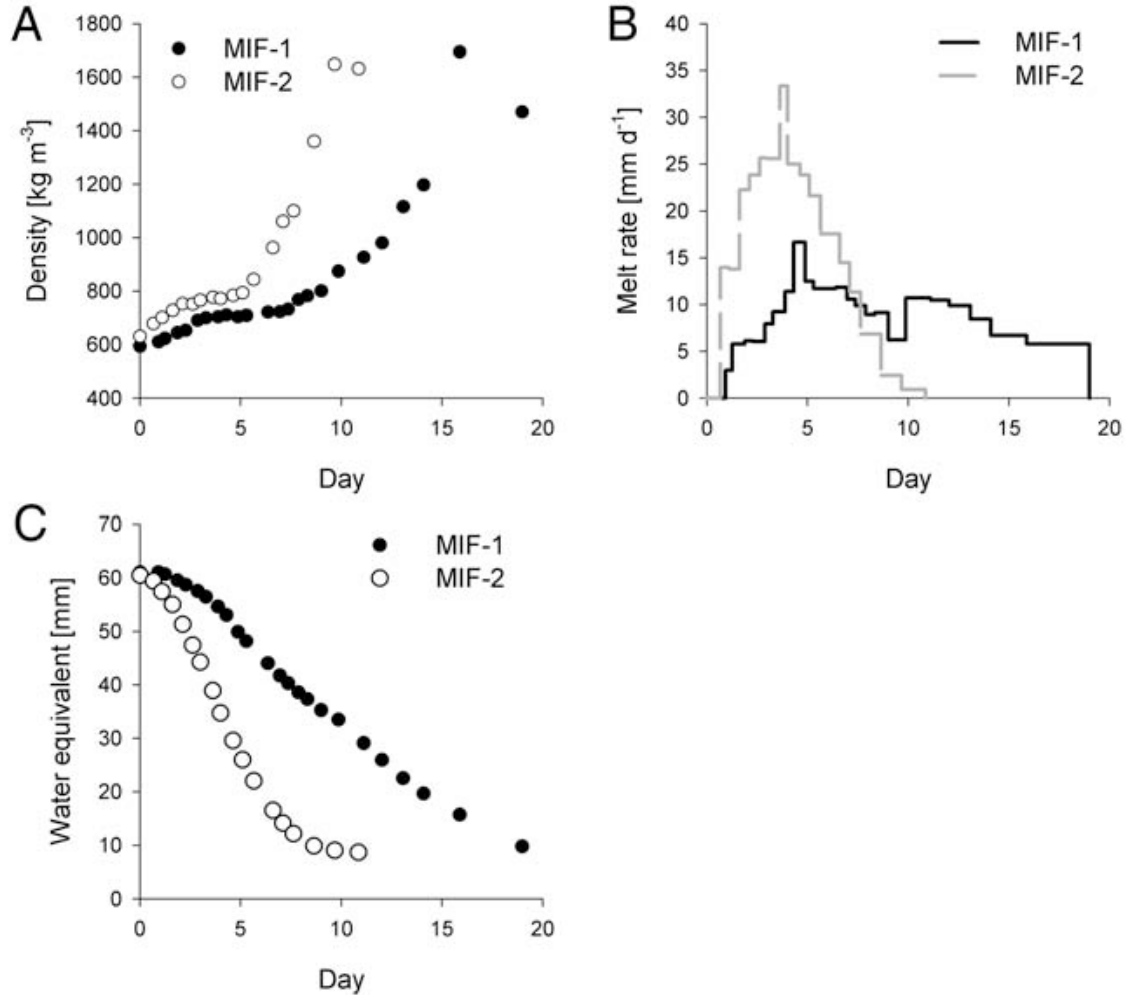
*Figure 6.7. Change in A) density [kg m$^{-3}$], B) melt rate [mm d$^{-1}$], and C) water equivalent [mm] as melt progress.*

Average temperature within the mineral soil layer, 50 mm above the base, was –0.1 ℃ in MIF-1 and +0.1 ℃ in MIF-2. The coolant temperature was decreased 4 ℃ during melt in MIF-2 to ensure frozen conditions.

The first water was present for collection 1.3 days after room temperature was increased in MIF-1 and after 0.7 day in MIF-2 (Table 6.11). In both experiments, mineral interflow water, MW, was collected at the base four days before meltwater, SW. Again, it is believed that the delay between sampling of the first MW and SW is due to the snow-filled SW extraction tube, which had to be saturated and melting before it could transmit water for collection. Total melt period was about a week shorter for MIF-2 (11 days) than for MIF-1 (19 days). Half way through each experiment melting from

- 115 -

the sides of the box revealed that ice had formed at the base of the snowpack. The extent of the ice layers (thickness and spatial distribution) was not determined, as they were mostly gone when all the snow had melted. Areas of the mineral soil layer that were not covered with ice visually appeared saturated but not frozen. The final three MW samples collected in MIF-2 were collected after all the snow had melted.

Figure 6.8 shows how MW and SW *CFs* varied as melt progressed. Enrichment of MW compared to the parent snowpack (*CF*>1) was observed throughout melt for most ions in both experiments. Chloride and $NO_3^-$ were only enriched during the initial third of melt and $NH_4^+$ was depleted continuously. In both experiments, MW *CFs* decreased during the initial part of the melt. For $Cl^-$, $SO_4^{2-}$, $Na^+$, $K^+$, $Mg^{2+}$, and $Ca^{2+}$, this decrease was followed by an increase, which was most pronounced in MIF-2. SW *CFs* showed a continuous decrease throughout melt. Depleted conditions (*CF*<1) were observed for a majority of the ions. Only $H^+$, $Mg^{2+}$, and $Ca^{2+}$ showed enrichment during melt. No trend was observed for the variations in $H^+$ in either SW or MW.

Maximum SW *CFs* were generally obtained for the first sample in both experiments and ranged between 1.6 and 4.4 in MIF-1 and 0.7 and 5.8 in MIF-2 (Table 6.13). MIF-1 had higher SW *CF_max* values than MIF-2, except for $Cl^-$. For MW, maximum *CFs* were obtained either during the initial part of melt or by the end, ranging between 1.0 and 20.9 in MIF-1 and 0.7 and 11.8 in MIF-2. Chloride, $SO_4^{2-}$, $NO_3^-$, $NH_4^+$, $Mg^{2+}$, and $Ca^{2+}$ all obtained the highest *CF_max* in MIF-1; $H^+$, $Na^+$, and $K^+$ obtained the highest *CF_max* in MIF-2. *CF_max* values for SW were all within previously reported *CF* range (e.g. Tranter, 1991).

Enrichment ratios (*ER* = MW/SW) were determined for a total of 19 sample pairs (Figure 6.9); 13 in MIF-1 and six in MIF-2. Nineteen ratios were undefined and

Table 6.13. The greatest concentration factors, $CF_{max}$ [(meq m$^{-3}$)(meq m$^{-3}$)$^{-1}$], in the runoff water, MW, and meltwater, SW, for each ion in each experiment.

| Experiment | | $H^+$ | $Cl^-$ | $SO_4^{2-}$ | $NO_3^-$ | $NH_4^+$ | $Na^+$ | $K^+$ | $Mg^{2+}$ | $Ca^{2+}$ |
|---|---|---|---|---|---|---|---|---|---|---|
| *MIF-1* | *MW* | 2.1 | 5.0 | 20.9 | 4.6 | 1.0 | 5.7 | 5.1 | 15.5 | 9.7 |
| | *SW* | 2.4 | 1.8 | 2.0 | 1.8 | 2.0 | 1.6 | 2.2 | 4.4 | 3.2 |
| *MIF-2* | *MW* | 2.9 | 3.5 | 11.8 | 2.0 | 0.7 | 6.9 | 9.9 | 10.4 | 6.5 |
| | *SW* | 1.7 | 5.8 | 0.5 | 0.7 | 1.1 | 0.5 | 1.6 | 2.8 | 1.7 |
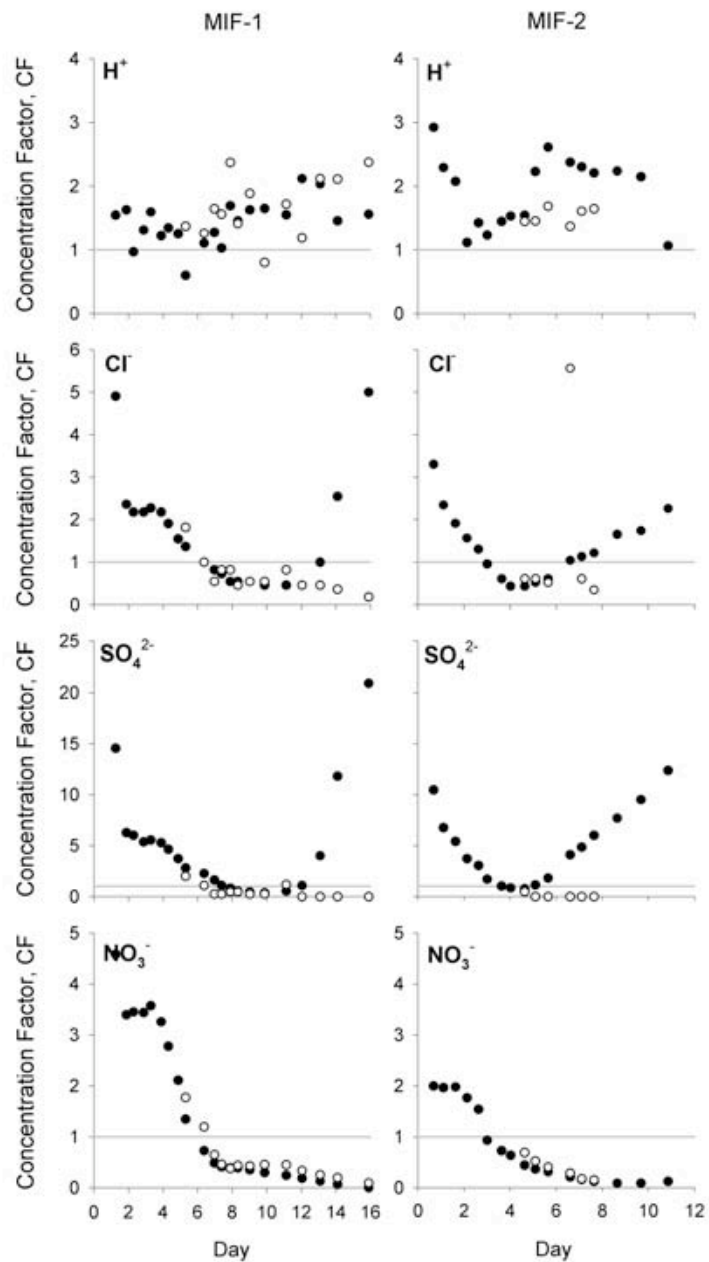
*Figure 6.8. Fractionation curves showing change in concentration factors, CF, during melt for mineral interflow (MW, closed circles) and the snowpacks' meltwater (SW, open circles). The horizontal grey line represents CF=1.*

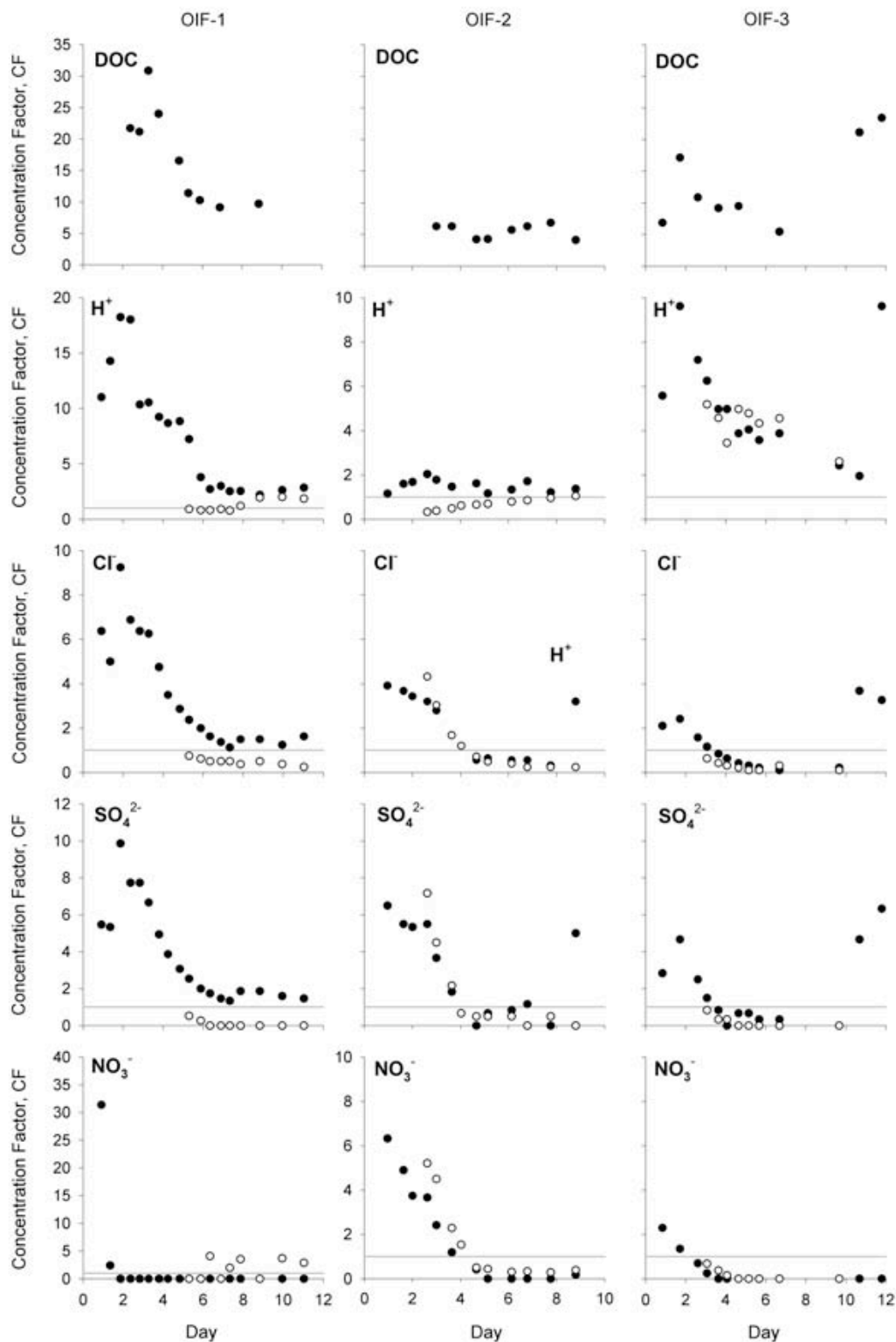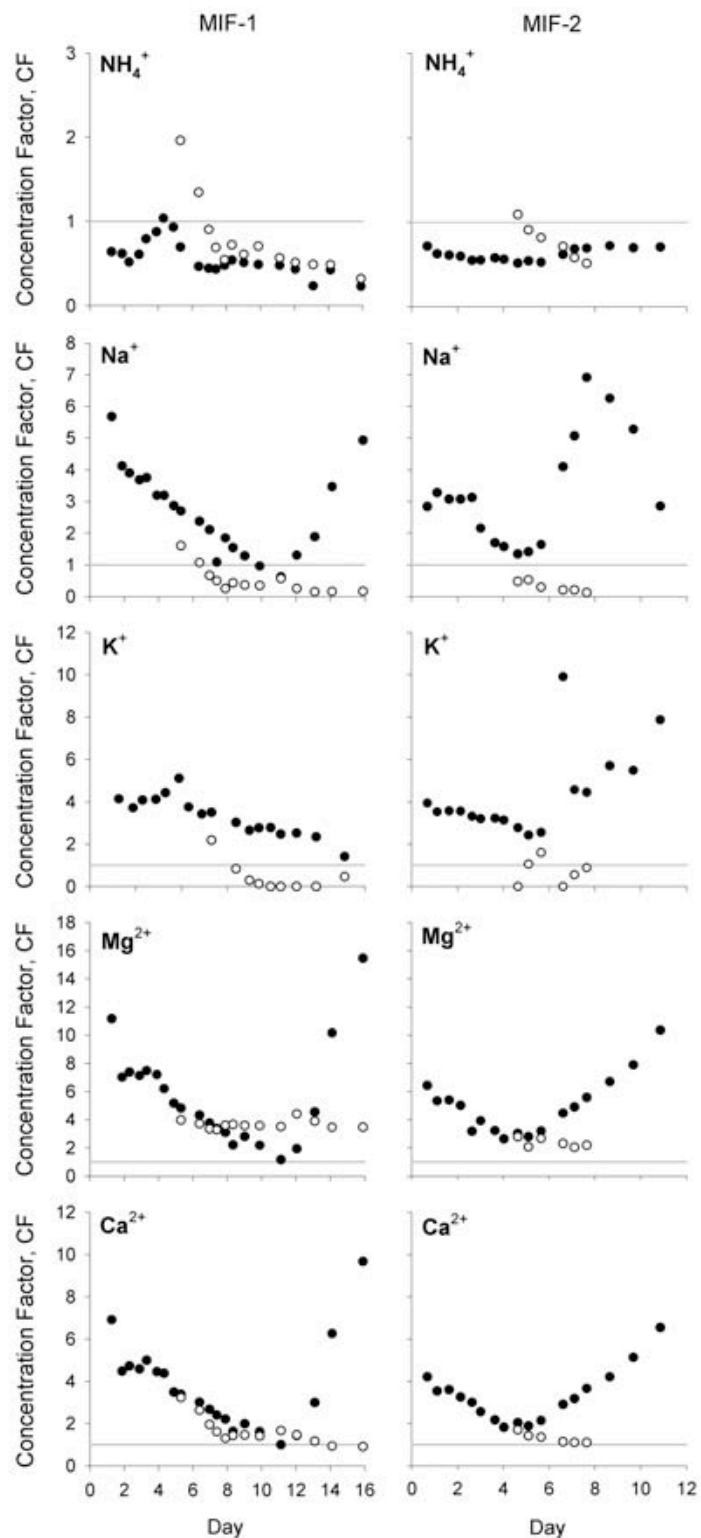*Figure 6.8 (continued). Fractionation curves showing change in concentration factors, CF, during melt for mineral interflow (MW, closed circles) and the snowpacks' meltwater (SW, open circles). The horizontal grey line represents CF=1.*
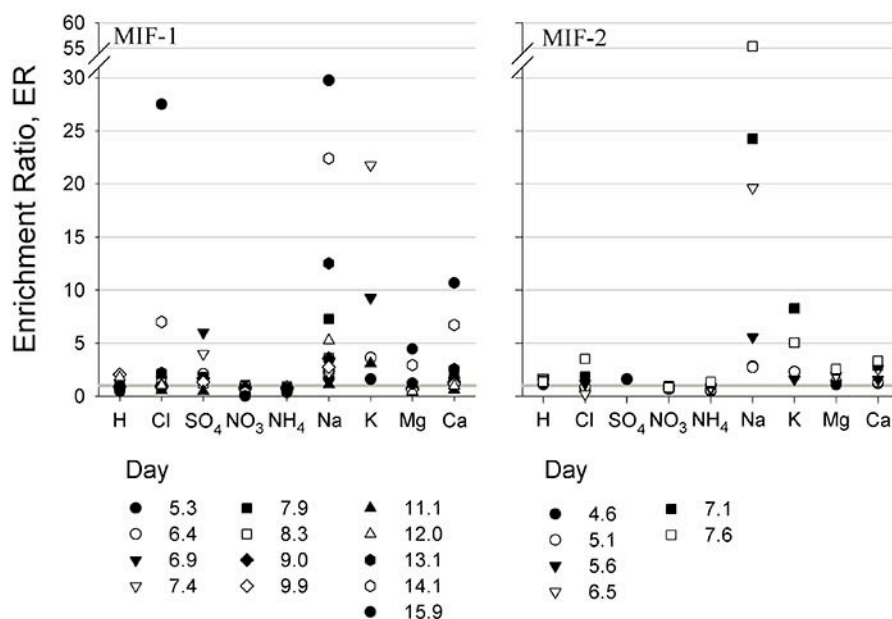
*Figure 6.9. Variation in the ion ratio between mineral interflow, MW, and snow meltwater, SW. The horizontal grey line represents ER=1.*

not plotted as the SW had ion concentrations that were below detection limit. *ER* varied for all ions as melt progressed. Sodium and $K^+$ showed enriched conditions (*ER*>1) throughout melt in MIF-1, $NH_4^+$ showed depleted conditions (*ER*<1), and the rest of the ions showed both enriched and depleted conditions. In MIF-2, enrichment was observed throughout melt for $H^+$, $SO_4^{2-}$, $Na^+$, $K^+$, $Mg^{2+}$, and $Ca^{2+}$ and depletion for $NO_3^-$. Both enriched and depleted conditions were observed for $Cl^-$ and $NH_4^+$. Overall, *ER* ranged between 0.3 and 10.

The mean differences between MW *CF* and SW *CF* for each ion and overall is shown in Table 6.14. Positive differences were found for $SO_4^{2-}$, $Na^+$, $K^+$, $Mg^{2+}$, and $Ca^{2+}$ in both experiments indicating enrichment of interflow water compared to

*Table 6.14. Mean differences between CF values for mineral interflow, MW, and meltwater, SW, in each experiment. Positive values refer to MW generally being enriched compared to the SW; negative values the opposite.*

| Experiment | $H^+$ | $Cl^-$ | $SO_4^{2-}$ | $NO_3^-$ | $NH_4^+$ | $Na^+$ | $K^+$ | $Mg^{2+}$ | $Ca^{2+}$ | Overall |
|------------|-------|--------|-------------|----------|----------|--------|-------|-----------|-----------|---------|
| *MIF-1* | -0.2 | 0.5 | 3.2 | -0.2 | -0.3 | 1.5 | 2.6 | 1.0 | 1.5 | 1.1 |
| *MIF-2* | 0.7 | -0.6 | 3.0 | -0.1 | -0.2 | 3.1 | 3.8 | 1.7 | 1.3 | 1.4 |

*Table 6.15. Calculated root mean square deviation for the differences between CF values for mineral interflow, MW, and meltwater, SW, in each experiment.*

| Experiment | $H^+$ | $Cl^-$ | $SO_4^{2-}$ | $NO_3^-$ | $NH_4^+$ | $Na^+$ | $K^+$ | $Mg^{2+}$ | $Ca^{2+}$ | Overall |
|---|---|---|---|---|---|---|---|---|---|---|
| *MIF-1* | 0.5 | 1.4 | 6.0 | 0.1 | 0.4 | 1.2 | 1.0 | 3.9 | 2.5 | 2.9 |
| *MIF-2* | 0.4 | 2.0 | 2.6 | 0.1 | 0.3 | 2.8 | 3.7 | 1.5 | 1.1 | 2.5 |

meltwater. Negative mean differences were observed in both experiments for both $NO_3^-$ and $NH_4^+$ indicating depletion of the soil water compared to the meltwater. Overall mean differences were positive showing that MW was chemically enriched compared to SW. Table 6.15 shows the dispersion of the mean differences calculated as the root mean square difference (RMSD). The dispersion of $H^+$, $NO_3^-$, and $NH_4^+$ were all ≤0.5 with little difference (<0.1) between the two experiments. Nitrate showed the least dispersion (0.1) for both experiments. The greatest dispersion was observed for $SO_4^{2-}$ (6.0), $Mg^{2+}$ (3.9), and $Ca^{2+}$ (2.5) in MIF-1 and for $Cl^-$ (2.0), $Na^+$ (2.8), and $K^+$ (3.7) in MIF-2; the dispersion of $H^+$, $NO_3^-$, and $NH_4^+$, respectively, were almost identical in the two experiments.

## 6.3.2 Discussion

Two snowmelt experiments were carried out to examine the compositional change in water chemistry as a result of meltwater infiltrating a frozen mineral soil layer. The experiments differed in melt rate and initial soil moisture content. Ion concentrations in the mineral interflow were compared to ion concentrations in meltwater without mineral soil contact. The results showed that contact with frozen mineral soil, either as interflow or overland flow, resulted in compositional changes in water chemistry.

MW was present for collection after 0.7 day of melt in MIF-2. In MIF-1, the first MW was present for collection after 1.3 days. A longer delay in initial sampling time was expected, because flow through frozen mineral soil was expected to be slower than through organic layer, unless flow occurs through macro-pores. This could indicate that the initial water comprised of overland flow, which had only been in contact with the mineral soil surface and not infiltrated the soil. Another explanation could be that the collected water was soil water that had been pushed out of the soil due to piston flow.

The delay between initial MW and initial SW, four days in both experiments, was assumed to be a result of the thermal state of the base layer. Formation of an ice layer at the base of the snowpack during the initial part of melt might have prevented the snow in the extraction tube from melting and thereby transmitting water to the front of the box. There were only ~2 hours difference in-between experiments for initial SW sampling.

Generally, the MW showed enrichment in ion concentrations compared to the parent snowpack. Chloride and $NO_3^-$ concentrations were depleted during part of the melt and $NH_4^+$ was depleted in all samples. In both experiments, MW CF decreased initially. For $Cl^-$, $SO_4^{2-}$, $Na^+$, $Mg^{2+}$, and $Ca^+$, this decrease was followed by a significant increase in both experiments and also for $K^+$ during MIF-2. The decreases' in *CFs* happened after two-thirds of the melt period during MIF-1 and one-third of the melt period in MIF-2. This shift could be a result of a shift in flowpath of the collected MW. Due to the construction of the experimental box, the formation of basal ice was not observed until the layer was well developed. The similar *CF* values for MW and SW observed about two-thirds though melt in MIF-1 and halfway through in MIF-2 indicate that the MW had not sustained substantial contact with the mineral soil; maybe the MW had only been in contact with the ice layer. The coolant temperature was increased once the presence of basal ice was observed to prevent further growth of ice, which would have blocked access to the mineral soil completely. This increase allowed the ice layer to melt and contact with the mineral layer once again, seen as an increase in ion concentrations. Variation in SW *CF* was small but except for $H^+$, ion *CFs* decreased as melt progressed. Most of the samples showed depleted ion concentrations compared to the parent snowpack. Nitrate, $NH_4^+$, and $Mg^{2+}$ had greater *CFs* in SW than MW throughout most of melt.

Enrichment of MW compared to SW was observed for a little more than half of the ratios in MIF-1; 53% of the 117 ratios. The average enrichment of these ratios was 4.8. Depleted conditions were observed for 38% of the ratios; mainly for $H^+$, $NO_3^-$, and $NH_4^+$. In MIF-2, 76% out of 53 ratios were enriched with an average enrichment of 5.0; 22% were depleted. Many of the ratios increased as melt progressed (Figure 6.9). However, the final ratios in each experiment were artificially high since the SW was

very dilute at the end of snowmelt. In both experiments, enriched conditions were observed throughout melt for $Na^+$ and $K^+$; depleted conditions were observed for $NO_3^-$ and $NH_4^+$.

The mean differences between *CFs* for MW and SW were negative for $NO_3^-$ and $NH_4^+$ in both samples, i.e. N-species were retained by the mineral soil. The mean differences for the majority of the other ions, as well as the overall mean difference, were positive indicating that MW was enriched compared to SW (Table 6.14). The difference between the two experiments' overall mean difference was minor (0.3) and were both strongly influenced by the values for $SO_4^{2-}$, $Na^+$, and $K^+$. The great increase in *CF* for MW at the end of snowmelt, while the *CF* for SW continued being very low, was the reason for the mean differences being so great for these ions. The dispersion of the mean differences did not vary significantly between experiments for $H^+$, $NO_3^-$, and $NH_4^+$ (Table 6.15). The greatest dispersions were observed for $SO_4^{2-}$, $Mg^{2+}$, and $Ca^{2+}$ in MIF-1 and for $Cl^-$, $Na^+$, and $K^+$ in MIF-2. The overall dispersion for each experiment did not vary much between experiments either.

## 6.4    Flowpath Signatures

The compositional change in runoff water chemistry as a result of contact with either a basal ice layer, a frozen forest organic layer, or a frozen mineral soil layer was examined through eight snowmelt experiments that differed in snowpack density, melt rate, and temperature at the base of the snowpack. A summary of the experiments is given in Table 6.16.

The timing of the presence of the first runoff water for collection varied between experiments and flowpaths. Generally, organic interflow was quickest with an average of 0.9 day; overland flow when basal ice was being formed was slowest with an average of 1.9 days. The structure of the snowpack, which causes instability of the wetting front (Wankiewicz, 1979), in combination with the type of base layer and its initial saturation, was believed to cause this variation in timing of initial runoff water. The delay between collection of the first runoff water with base layer contact and the first meltwater with no base layer contact varied between 1 and 4 days; generally quickest for the overland flow with basal ice contact and organic interflow. A reason for this delay was believed

*Table 6.16. Summary of experimental setup for each flowpath.*

| Flow path | | OVERLAND FLOW | | | ORGANIC INTERFLOW | | | MINERAL INTERFLOW | |
|---|---|---|---|---|---|---|---|---|---|
| Experiment | | BI-1 | BI-2 | BI-3 | OIF-1 | OIF-2 | OIF-3 | MIF-1 | MIF-2 |
| Base layer: | Type | Basal Ice Layer | | | Forest Organic Layer | | | Forest Loamy Soil | |
| Snow: | Thickness [mm] | 80 | 40 | 30 | 60 | 60 | 60 | 70 | 70 |
| | Gravimetric moisture, Initial [g g$^{-1}$] | - | - | - | 0 | ~2.7 | ~2.8 | 0.2 | 0.3 |
| | Gravimetric moisture, Final [g g$^{-1}$] | - | - | - | ~2.7 | ~2.8 | ~6.1 | 0.3 | 0.3 |
| | Origin | Within city | Rural area | Rural area | Within city | Within city | Rural area | Rural area | Rural area |
| | Storage @ -20 °C [d] | 0 | 90 | 0 | 27 | 14 | 12 | 128 | 186 |
| | Initial density [kg m$^{-3}$] | 350 | 410 | 215 | 290 | 297 | 400 | 430 | 442 |
| | Initial SWE [mm] | 52 | 62 | 33 | 40 | 50 | 69 | 61 | 61 |
| Temperature: | Room [°C] | +5 | +5 | +5 | +5 | +5 | +7.5 | +5 | +7.5 |
| | Coolant [°C]* | -5 (±2) | -4 (±2) | -3 (±2) | -4 | -4 | -2 (-5) | -3 (±2) | -3 (-4) |
| | Base, average [°C] | -2 | -0.5 | -0.2 | -0.8 | -0.7 | ~0 | -0.2 | -0.1 |
| Melt rate, average [kg m$^{-2}$ d$^{-1}$] | | 3.6 | 6.8 | 7.8 | 8.3 | 8.9 | 11.8 | 8.2 | 14.2 |
| Initial sample collection: [d$_{after\ initiation}$] | Runoff water (RW = BW, OW, MW) | 2.9 | 1.7 | 1.0 | 0.9 | 1.0 | 0.8 | 1.3 | 0.7 |
| | Meltwater (SW) | 3.9 | 5.8 | 3.2 | 5.3 | 2.6 | 3.0 | 5.3 | 4.7 |

* Values in brackets by coolant temperature refer to adjustments in coolant temperature during melt.

*Table 6.17. Mean differences between the concentration factors, CF, for runoff water, RW, and meltwater, SW, for each experiment. Values are given both for each ion and the overall average of all ions. n is the number samples that the mean differences were based on.*

| Experiment | $n$ | $H^+$ | $Cl^-$ | $SO_4^{2-}$ | $NO_3^-$ | $NH_4^+$ | $Na^+$ | $K^+$ | $Mg^{2+}$ | $Ca^{2+}$ | Overall |
|---|---|---|---|---|---|---|---|---|---|---|---|
| *BI-1* | 7 | −6.6 | 4.3 | 1.9 | 3.9 | 0.6 | 7.6 | 0.2 | 2.4 | 2.9 | 1.9 |
| *BI-2* | 12 | 0.1 | −4.7 | 1.2 | 0.7 | 0.1 | 0.6 | −7.6 | 0.1 | 0.7 | −1.0 |
| *BI-3* | 5 | 0.0 | 0.2 | 0.0 | 0.0 | 0.1 | −1.0 | −0.3 | −0.2 | 0.1 | −0.1 |
| *OIF-1* | 9 | 2.0 | 1.1 | 1.7 | −1.8 | 1.0 | 0.6 | 11.8 | −0.3 | 0.7 | 1.9 |
| *OIF-2* | 9 | 0.2 | 0.3 | −0.7 | 0.3 | −0.4 | 7.8 | −0.6 | −0.6 | 0.0 | 0.7 |
| *OIF-3* | 8 | 0.2 | 0.4 | −0.1 | 1.7 | −0.8 | 4.9 | −0.4 | 0.1 | 0.0 | 0.7 |
| *MIF-1* | 13 | −0.2 | 0.5 | 3.2 | −0.2 | −0.3 | 1.5 | 2.6 | 1.0 | 1.5 | 1.1 |
| *MIF-2* | 6 | 0.7 | −0.6 | 3.0 | −0.1 | −0.2 | 3.1 | 3.8 | 1.7 | 1.3 | 1.4 |

to be a result of the snow-filled meltwater extraction tube having to be saturated and the snow partially melted before meltwater could be transmitted.

Ion fractionation solely within the snowpack resulted in *CF* values within the range of previously reported values (*CF* = 2-10; Tranter, 1991). As melt progressed, the *CF* values generally decreased exponentially. A similar tendency was generally observed for the runoff water with *CF* generally peaking during the initial part of melt. The variations in *CF* for the runoff water were larger than for snow meltwater. Repeated flushes through the same substrate led to a further decrease in *CF* with time. For the mineral interflow, the decrease was followed by an increase for a majority of the ions. The overall tendency in mean differences between *CF* for runoff water and meltwater was positive, indicating greater *CF* for runoff water than for snow meltwater (Table 6.17). The dispersion of the mean differences calculated as root mean square deviation (RMSD) varied between 0.1 and 8.6 for the individual ions; the overall dispersion for each experiment varied between 1.6 and 4.5.

## 6.4.1 Observed Alterations

During the initial part of the melt period, runoff water that had sustained basal ice contact (experiments BI-1, BI-2, and BI-3) was most often more enriched than snowmelt water collected before surface contact. This enrichment can be attributed to ion exclusion during refreezing of meltwater into basal ice. An expected finding since

refreezing of meltwater within a snowpack has previously been shown to further enrich the meltwater percolating through the snowpack (e.g. Colbeck, 1981). The enrichment effect was most pronounced with the rapid formation of a thick basal ice layer early in melt under relatively cold experimental conditions and was small to negligible when basal ice growth occurred later in melt under relatively warmer experimental conditions.

Contact with a frozen organic layer (experiments OIF-1, OIF-2, and OIF-3) resulted in enrichment of the concentrations of DOC and all major ions in the runoff water, except $Mg^{2+}$ and $NO_3^-$. The concentrations of $NO_3^-$ quickly decreased below detection levels due to microbiological activity, i.e. denitrification (e.g. Jones, 1999). Together with the observed increase in $NH_4^+$ concentration this indicates that chemical alteration occurs in a reducing environment, causing $NH_4^+$ to increase due to mineralization. The decrease in $Mg^{2+}$ was unexpected as leaching from unfrozen litter increases the concentration (Jones and Pomeroy, 2001), as will dust deposition from exposed calcareous bedrock, present in the area. Cation exchange could account for this decrease (e.g. Borggaard and Elberling, 2004). In general, the experiments indicate that the degree of alteration was controlled mainly by initial moisture content of the organic layer and repeated flushes through the soil, which caused a washout of ions.

The alteration in chemical composition of meltwater due to contact with mineral soil (experiments MIF-1 and MIF-2) might have experienced only limited alteration due to formation of ice at the base of the snowpack in some areas. The ice was not observed as being continuous and contact with the mineral layer could still occur. The moisture content and temperature of the soil was designed to limit infiltration, which when combined with the rate of melt may have led to the formation of the ice on top of the mineral soil. Generally, the results showed slightly enriched or similar ion concentrations for most of the ions to those in the meltwater. Both experiments showed depletion of $H^+$, $NO_3^-$, and $NH_4^+$ in the runoff water compared to the meltwater. The buffering capacity of the soil most likely caused the decrease in $H^+$ concentrations. A greater decrease than observed was anticipated, due to the calcareous soils, but the presence of carbonate species, i.e. $HCO_3^-$, may have limited the buffering effect. The decrease of $NO_3^-$ and $NH_4^+$ indicate that denitrification and nitrification took place simultaneously within the soil layer; indicating the presence of microsites in the soil

(Pinay and Naiman, 1991). For this to occur, both reducing and oxidizing conditions have to be present. Nitrification may explain why $NO_3^-$ is still present for this flow path, but not for the organic interflow. Melt rate did not seem to have a large influence on the depletion of these ions, given similar variations in *CF* for both experiments except for $NO_3^-$.

Overall, the observed changes in chemical composition for the organic interflow and the mineral interflow correspond well with the expected changes (Table 2.2); different behaviours were only observed for $Cl^-$, $SO_4^{2-}$, $Mg^{2+}$, and $Ca^{2+}$ in the organic interflow and for $SO_4^{2-}$ in the mineral interflow. The observed increases in $Cl^-$ and $SO_4^{2-}$ concentrations are hypothesized to be due to dissolution of ions located on the pore walls following water evaporating from the layer prior to freeze-up (Quinton and Pomeroy, 2006); in the mineral interflow, sulphur-oxidizing bacteria could also produce the increase in $SO_4^{2-}$ concentrations (Borggaard and Elberling, 2004). The behaviour of $Mg^{2+}$ and $Ca^{2+}$ can most likely be ascribed to the cation exchange capacities of the layers. Organic layers and mineral soils typically have large cation exchange capacities, preferentially retaining $Mg^{2+}$ and $Ca^{2+}$ compared to $Na^+$ and $K^+$ (e.g. Borggard and Elberling, 2004). Cation exchange would have been observed as an increase in the concentrations of the monovalent cations combined with a decrease in the divalent cations. However, the results only show a decrease in $Mg^{2+}$ concentration in the organic interflow indicating that cation exchange is largely irrelevant. A reason for this could be that the cation exchange sites in either layer are already saturated with the divalent cations due to the base-rich parent material of the mineral layers.

### 6.4.2 Defining the Signatures

The variation in enrichment ratio, *ER*, for each flowpath is shown in Figure 6.10. Sixty-nine samples were suitable for calculation of *ER* for the major ions; 71 ratios were undefined and thus not plotted since either runoff water or snowmelt water had an ion concentration less than the detection limit. DOC ratios were not plotted, as the number of ratios was limited (<5). The percentages of enrichment ratios, which were greater than 1 (*ER*>1) are listed in Table 6.18 for each ion for each flowpath. It shows that $SO_4^{2-}$, $Na^+$, and $Ca^{2+}$ were the only ions, which were enriched in the majority of
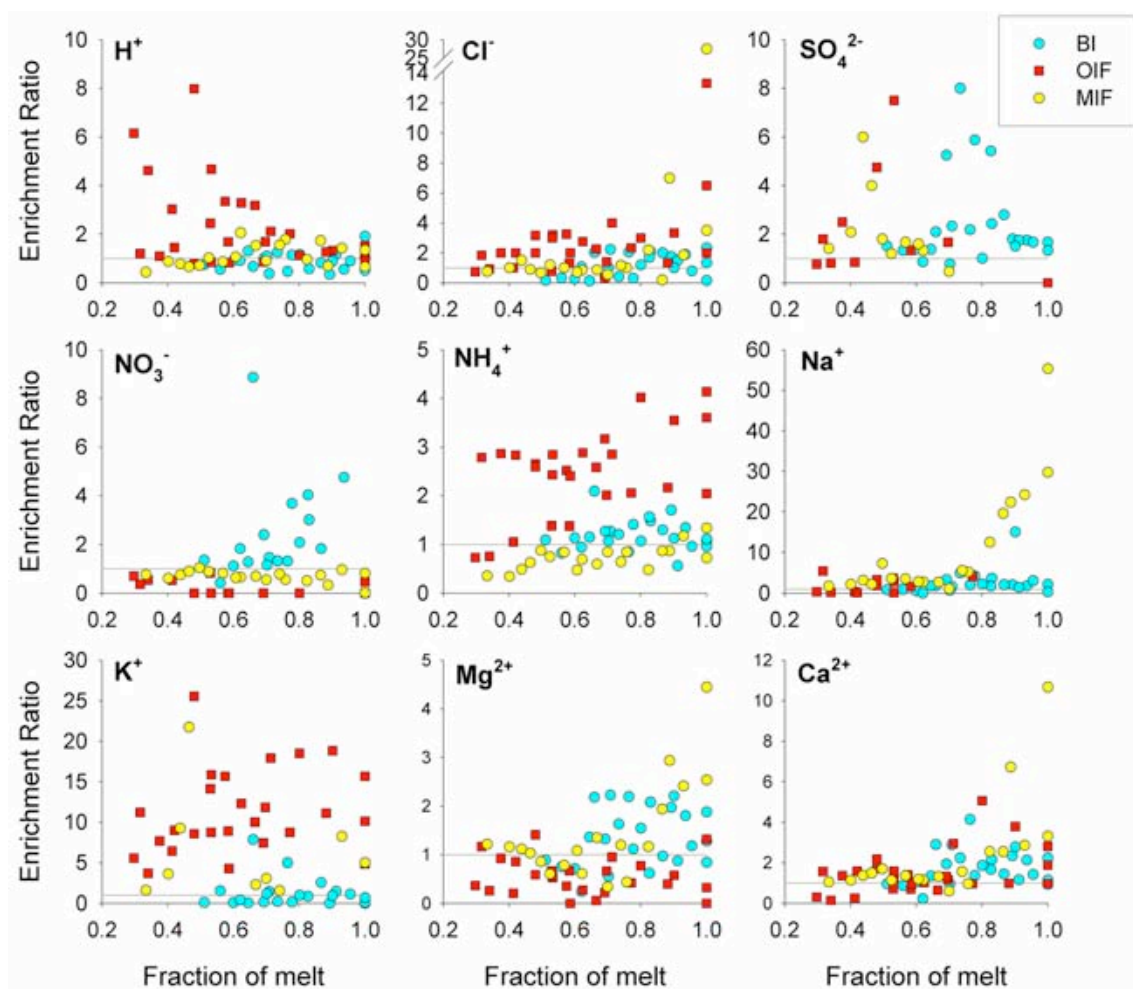
*Figure 6.10. Enrichment ratios, ER, for each of the nine ions in each flowpath.*

*Table 6.18. The percentages of enrichment ratios, ER, for each flowpath that were greater than 1 (ER>1). Green background indicates a general enrichment.*

| Flowpath | n | H⁺ | Cl⁻ | SO₄²⁻ | NO₃⁻ | NH₄⁺ | Na⁺ | K⁺ | Mg²⁺ | Ca²⁺ | DOC |
|----------|-----|------|------|-------|------|------|------|------|------|------|------|
| *BI* | 24 | 29% | 54% | **88%** | **88%** | **75%** | **71%** | 38% | **63%** | **79%** | |
| *OIF* | 26 | **81%** | **81%** | **73%** | 0% | **92%** | **81%** | **100%** | 12% | **58%** | **100%** |
| *MIF* | 19 | 42% | 42% | **95%** | 0% | 11% | **100%** | **100%** | **63%** | **89%** | |

the runoff water samples in each experiment. Average *ER* for the individual ions of each flowpath are given in Table 6.19. The green values denote enrichment in ion concentrations and red values denote depletion. Only a few values indicate that ion concentrations of runoff water were the same as those of snow meltwater.

By comparing these average enrichment ratios it was possible to identify the relative relationship in chemical composition among flowpaths (Table 6.20). The ratios among the flowpaths' average enrichment ratios were used to indicate, which flowpath had greater enrichment ratios (green values), which flowpaths had depleted ratios (red values), and which had similar ratios (black values). Based on Table 6.19 and Table 6.20 it was possible to identify ions, which displayed significant alteration in ion concentrations and can therefore be used for flowpath signatures:

- *Overland flow* (BI): Basal ice contact resulted in an overall increase in ion concentrations. In particular, $NO_3^-$ concentrations were distinctly higher for this flowpath than for the other flowpaths.

*Table 6.19. Average enrichment ratios, ER, for the individual ions in each flowpath examined. Green values indicate enrichment and red values indicate depletion; black values indicate little or no difference.*

| Flowpath | $H^+$ | $Cl^-$ | $SO_4^{2-}$ | $NO_3^-$ | $NH_4^+$ | $Na^+$ | $K^+$ | $Mg^{2+}$ | $Ca^{2+}$ | DOC |
|---|---|---|---|---|---|---|---|---|---|---|
| BI | 0.9 | 1.2 | 2.4 | 2.3 | 1.2 | 2.0 | 1.2 | 1.4 | 1.8 | – |
| OIF | 2.3 | 2.1 | 2.2 | 0.2 | 2.5 | 2.0 | 11.3 | 0.6 | 1.5 | ↑ |
| MIF | 1.1 | 1.2 | 2.2 | 0.7 | 0.7 | 10.9 | 6.3 | 1.4 | 2.4 | – |

*Table 6.20. Relative enrichment among flowpaths identified by comparing average enrichment ratios. Green values indicate larger enrichment ratios, ER, and red values indicate smaller enrichment ratios; similar ratios are indicated in black.*

| Flowpath ratio | OIF:BI | MIF:BI | OIF:MIF | Relative enrichment |
|---|---|---|---|---|
| $H^+$ | ↑ (2.6) | – (1.3) | ↑ (2.1) | BI, MIF < OIF |
| $Cl^-$ | ↑ (1.8) | – (1.0) | ↑ (1.8) | BI, MIF < OIF |
| $SO_4^{2-}$ | – (0.9) | – (0.9) | – (1.0) | BI, OIF, MIF |
| $NO_3^-$ | ↓ (0.1) | ↓ (0.3) | ↓ (0.4) | OIF < MIF < BI |
| $NH_4^+$ | ↑ (2.1) | ↓ (0.6) | ↑ (3.4) | MIF < BI < OIF |
| $Na^+$ | – (1.0) | ↑ (5.5) | ↓ (0.2) | OIF, BI << MIF |
| $K^+$ | ↑ (12.5) | ↑ (7.0) | ↑ (1.8) | BI << MIF << OIF |
| $Mg^{2+}$ | ↓ (0.4) | – (1.1) | ↓ (0.4) | OIF < BI, MIF |
| $Ca^{2+}$ | – (0.9) | ↑ (1.3) | ↓ (0.6) | OIF < BI < MIF |
| DOC[1] | ↑ | ↑ | ↑ | BI < MIF < OIF |

[1] These relative enrichment indications are given without a value, as data was limited

- *Organic interflow* (OIF): Contact with a frozen organic layer resulted in the greatest increases in $H^+$, $Cl^-$, $NH_4^+$, and DOC concentrations. The concentrations of $Mg^{2+}$ were greatly depleted and $NO_3^-$ concentrations quickly decreased below measurable levels.

- *Mineral interflow* (MIF): Contact with the mineral soil layer caused depletion in $H^+$, $NO_3^-$, and $NH_4^+$, and the greatest enrichment of $Na^+$ and $Ca^{2+}$ concentrations.

### 6.4.3 Flowpath Ion Flux

Snowmelt and runoff ion fluxes, i.e. the quantity of solute released by the meltwater or runoff water over a given time period per unit area [$\mu eq\ d^{-1}\ m^{-2}$], were calculated for all water samples to determine the impact that each flowpath may have on the receiving environment. The variations in ion flux for the meltwater and runoff water showed a general decrease as melt progressed; similar to those observed for the *CF* (section 6.4). Maximum ion fluxes were generally obtained within the first couple of samples in each experiment.

The relationships between the ion flux in the runoff water and the snowmelt water are plotted in Figure 6.11 for each of the major ions in each experiment. These give a simple overview of whether the base layer was a sink or a source for ions; points plotting below the diagonal 1:1 line indicate that the layer was a source and points plotting above the 1:1 line indicate that the layer was a sink. Combined with the differences between runoff water ion flux and meltwater ion flux (Table 6.21), it was to determine whether contact with the base layer caused an increase in ion flux (positive difference) or a decrease in ion flux (negative difference), i.e. whether the flowpaths generally were a source or a sink for the ions. Overland flow due to basal ice formation was a source for $SO_4^{2-}$, $NO_3^-$, $NH_4^+$, $Na^+$, $Mg^{2+}$, and $Ca^{2+}$ and a sink for $H^+$, $Cl^-$, and $K^+$; the organic interflow was a source for $H^+$, $Cl^-$, $SO_4^{2-}$, $NH_4^+$, $K^+$, and $Ca^{2+}$ and a sink for $NO_3^-$, $Na^+$, and $Mg^{2+}$; and mineral interflow was a source for $Cl^-$, $SO_4^{2-}$, $Na^+$, $K^+$ $Mg^{2+}$, and $Ca^{2+}$ and a sink for $NO_3^-$ and $NH_4^+$. Sulphate and $Ca^{2+}$ were the only ions for which all flowpaths were a source. Overall, contact with either of the base layers caused an increase in the runoff water's ion flux.
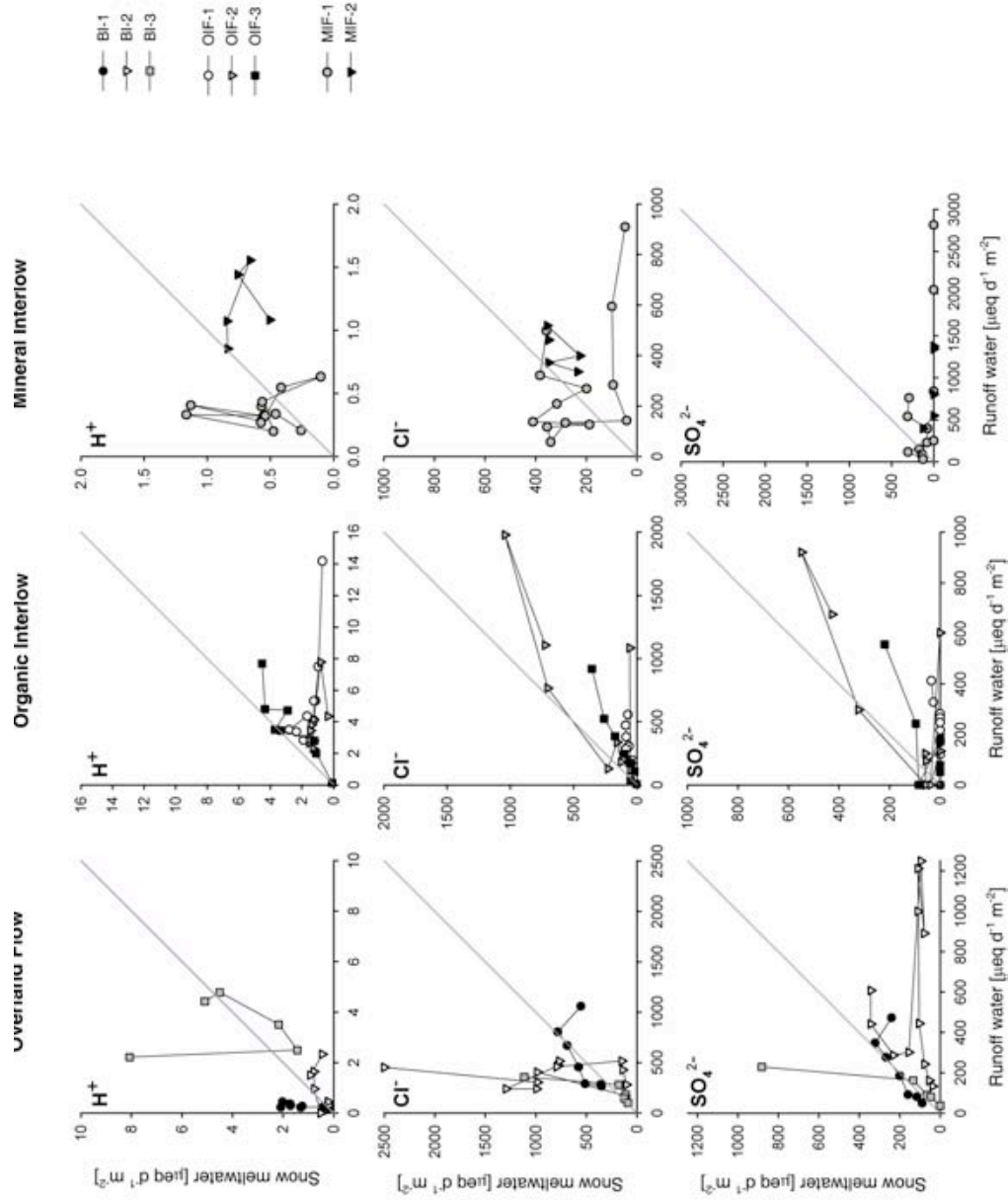
Figure 6.11. Runoff water ion flux [μeq d⁻¹ m⁻²] versus snow meltwater ion flux [μeq d⁻¹ m⁻²] for each ion in each experiment. The diagonal line represents the 1:1 ratio; points plotting below the line indicate that the base layer is a source for the ion and points plotting above the line indicate that the base layer is a sink for the ion.

Figure 6.11 (continued). Runoff water ion flux [µeq d−1 m−2] versus snow meltwater ion flux [µeq d−1 m−2] for each ion in each experiment. The diagonal line represents the 1:1 ratio; points plotting below the line indicate that the base layer is a sink for the ion and points plotting above the line indicate that the base layer is a source for the ion.

*Figure 6.11 (continued). Runoff water ion flux [μeq d−1 m−2] versus snow meltwater ion flux [μeq d−1 m−2] for each ion in each experiment. The diagonal line represents the 1:1 ratio; points plotting below the line indicate that the base layer is a source for the ion and points plotting above the line indicate that the base layer is a sink for the ion.*

*Table 6.21. Mean differences between the ion flux in the runoff water and the snow meltwater for each ion in each experiment and overall. Positive values indicate that the base layer is a source for the ion and negative values indicate that the base layer is a sink for the ion.*

| Flowpath | Experiment | $n$ | $H^+$ | $Cl^-$ | $SO_4^{2-}$ | $NO_3^-$ | $NH_4^+$ |
|---|---|---|---|---|---|---|---|
| BI | 1 | 7 | -1.2 | 3.2 | 17.3 | 6.5 | -96.6 |
| | 2 | 12 | 0.3 | -426.3 | 436.6 | 38.7 | 126.3 |
| | 3 | 5 | -0.8 | -107.6 | -104.3 | -2.0 | -76.4 |
| | *overall* | | *-0.4* | *-234.6* | *201.6* | *20.8* | *19.0* |
| OIF | 1 | 9 | 4.1 | 251.0 | 240.8 | -3.7 | 228.1 |
| | 2 | 9 | 2.6 | 303.3 | 149.5 | -2.9 | 127.4 |
| | 3 | 8 | 1.0 | 174.4 | 110.5 | -14.7 | 359.8 |
| | *overall* | | *2.6* | *245.5* | *169.1* | *-6.8* | *233.8* |
| MIF | 1 | 13 | -0.2 | 53.7 | 519.2 | -18.1 | -138.6 |
| | 2 | 5 | 0.5 | 115.1 | 868.6 | -2.4 | -72.4 |
| | *overall* | | *0.0* | *70.8* | *616.3* | *-13.8* | *-120.2* |

| Flowpath | Experiment | $n$ | $Na^+$ | $K^+$ | $Mg^{2+}$ | $Ca^{2+}$ | Overall |
|---|---|---|---|---|---|---|---|
| BI | 1 | 7 | 12.5 | 1.0 | -68.3 | 343.7 | 24.2 |
| | 2 | 12 | 120.9 | -335.7 | 289.0 | 1087.3 | 148.6 |
| | 3 | 5 | -96.1 | -71.2 | -155.9 | -163.9 | -3.2 |
| | *overall* | | *44.1* | *-182.4* | *92.1* | *609.8* | *63.3* |
| OIF | 1 | 9 | 73.4 | 1039.5 | -22.0 | 326.9 | 237.6 |
| | 2 | 9 | 6.8 | 706.2 | -102.2 | -213.4 | 108.6 |
| | 3 | 8 | -129.6 | 1068.5 | -23.0 | 888.7 | 270.6 |
| | *overall* | | *-12.1* | *933.0* | *-50.1* | *312.7* | *203.1* |
| MIF | 1 | 13 | 230.1 | 88.3 | -99.2 | 761.9 | 155.2 |
| | 2 | 5 | 794.5 | 266.3 | 616.2 | 2528.3 | 568.3 |
| | *overall* | | *386.9* | *137.7* | *99.6* | *1252.6* | *270.0* |

The dispersion of the mean differences was calculated as the root mean square difference (RMSD); the results are shown in Table 6.22. The dispersions for $H^+$ (<3) and $NO_3^-$ (<43) were very low compared to the other ions, which varied between 116 for $NH_4^+$ and 2106 for $Ca^{2+}$, both for the mineral interflow. However, the mean differences between ion fluxes for $H^+$ and $NO_3^-$ were generally much less than those for the other ions. The greatest dispersions were observed for $Cl^-$ (531.7), $NO_3^-$ (42.3), and $NH_4^+$ (193.2) in the overland flow, for $H^+$ (2.8), $Na^+$ (383.0), and $K^+$ (532.6) in the organic interflow, and for $SO_4^{2-}$ (789.6), $Mg^{2+}$ (757.6), and $Ca^{2+}$ (2105.6) in the mineral interflow; overall, the greatest dispersion values were obtained for $Ca^{2+}$ in each experiment.

*Table 6.22. The dispersion of the mean differences between the ion flux in the runoff water and the snow meltwater for each ion in each experiment and overall.*

| Flowpath | Experiment | n | H$^+$ | Cl$^-$ | SO$_4^{2-}$ | NO$_3^-$ | NH$_4^+$ |
|---|---|---|---|---|---|---|---|
| BI | 1 | 7 | 0.5 | 217.5 | 92.8 | 20.3 | 113.0 |
| | 2 | 12 | 0.6 | 646.1 | 406.0 | 50.6 | 105.7 |
| | 3 | 5 | 2.6 | 324.8 | 273.9 | 17.4 | 281.3 |
| | *overall* | | *1.5* | *531.7* | *396.9* | *42.3* | *193.2* |
| OIF | 1 | 9 | 3.8 | 113.8 | 73.4 | 3.5 | 53.2 |
| | 2 | 9 | 1.8 | 383.1 | 208.6 | 15.2 | 64.8 |
| | 3 | 8 | 1.1 | 172.1 | 120.7 | 21.0 | 233.1 |
| | *overall* | | *2.8* | *259.1* | *156.1* | *15.7* | *167.3* |
| MIF | 1 | 13 | 0.3 | 313.6 | 870.1 | 24.6 | 126.4 |
| | 2 | 5 | 0.3 | 53.9 | 433.6 | 13.4 | 60.1 |
| | *overall* | | *0.4* | *269.4* | *789.6* | *23.1* | *115.8* |

| Flowpath | Experiment | n | Na$^+$ | K$^+$ | Mg$^{2+}$ | Ca$^{2+}$ | Overall |
|---|---|---|---|---|---|---|---|
| BI | 1 | 7 | 186.1 | 18.8 | 198.3 | 811.7 | 321.4 |
| | 2 | 12 | 134.9 | 462.5 | 256.6 | 835.7 | 594.1 |
| | 3 | 5 | 303.2 | 173.4 | 468.8 | 836.3 | 393.7 |
| | *overall* | | *213.7* | *370.8* | *360.4* | *972.8* | *496.1* |
| OIF | 1 | 9 | 33.1 | 468.9 | 110.7 | 285.4 | 364.3 |
| | 2 | 9 | 286.1 | 126.6 | 145.0 | 503.2 | 356.9 |
| | 3 | 8 | 600.8 | 753.2 | 170.5 | 713.2 | 579.9 |
| | *overall* | | *383.0* | *532.6* | *148.0* | *685.8* | *445.4* |
| MIF | 1 | 13 | 187.9 | 27.2 | 803.1 | 2276.8 | 910.6 |
| | 2 | 5 | 335.5 | 179.8 | 139.7 | 480.1 | 811.7 |
| | *overall* | | *347.3* | *126.0* | *757.6* | *2105.6* | *903.4* |

In general, great agreements were observed between the calculated mean differences in ion flux and the calculated average enrichment ratios (Table 6.19) and thereby the identified chemical signatures (section 6.4.2). The ions that showed enrichment in ion concentration (*ER*>1) had an ion flux that identified the base layer as a source. Similarly, the ions that showed depletion in ion concentration (*ER*<1) had a negative mean difference in ion flux, indicating that the layer was a sink. Only two mean differences in ion fluxes did not correlate well with the calculated average enrichment ratios; these were Cl$^-$ for the overland flow and Na$^+$ for the organic interflow. The basal ice layer was observed to be a sink for Cl$^-$ even though the average enrichment ratio indicated a slight enrichment of the ion concentration (*ER*=1.2). The ion flux for Na$^+$ in the organic interflow indicated that the layer was a sink whereas the

enrichment ratio showed that a general enrichment in the ion concentration had taken place (*ER*=2.0). The reason for these differences is unknown.

Overall, these observations support the observation of the compositional change and that formation of a basal ice layer will influence not only the flowpath but also the ion load released to the surrounding environment. The ion fluxes also confirm that the buffering capacity for the base layers was high, therefore limiting the impact that the runoff water may have on the receiving environment.

# CHAPTER 7

# IDENTIFICATION OF FLOWPATHS AT A FIELD SITE

Waters from the organic layer, the mineral soil, and ponding on top of the soil and ice were sampled at an observation site in the Marmot Creek Research Basin, AB, during spring snowmelt in 2007. The objective was to compare the chemical composition of these samples to the chemical signatures of the three unmixed flowpaths (previous chapter) and based on this comparison, determine the flowpath of the individual field samples. The individual samples' chemical concentrations are listed in Appendix G.

## 7.1 Soil Conditions

Temperature and moisture content of the organic layer and mineral soil were measured continuously from early November 2006 (Julian day, JD, 305) till the end of snowmelt (JD 77; March 18 2007). Characteristics of the slope setup are shown in Figure 7.1.

Soil freeze-up initiated in early November 2006 when the air temperature dropped below 0 ºC, prior to the first snowfall (Figure 7.2A). Seasonal minimum air temperature was reached on November 28 (JD 332), –29.9 ºC, which led to temperatures < 0 ºC in the organic layer (Figure 7.2B) as well as in the top 5-10 cm of the mineral soil (Figure 7.2C). The temperature remained < 0 ºC for the rest of the winter for these layers. The temperature of the deeper mineral soil (10-20 cm) was not continuously < 0 ºC until late December (~JD 359).

Throughout the winter, the temperature of the organic layer exhibited a greater response to the air temperature, especially at the top of the slope, where tall vegetation was less abundant. February was the coldest month with an average air temperature of –7 ºC and soil temperatures averaging –2 ºC (Table 7.1). There was little variation
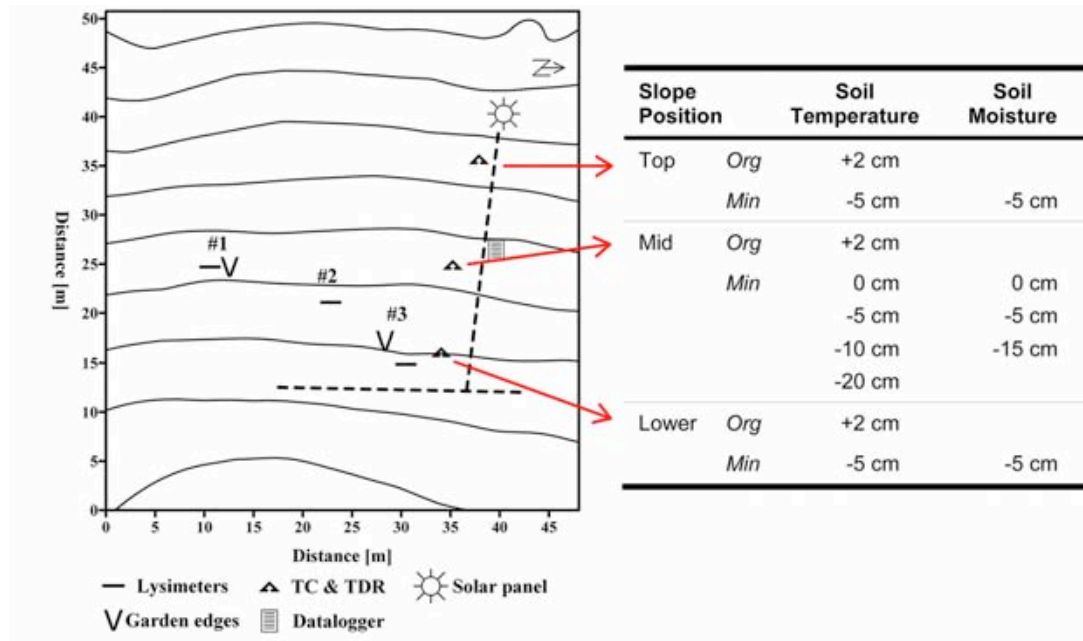
*Figure 7.1. Summary of the slope setup and instrumentation. Left) #1, #2, and #3 refers to sampling sites and the dotted lines are transects along which snow depth and density were measured. Contour interval is 2 m. Right) Measuring depths for soil temperature (TC) and moisture content (TDR).*

across the slope. Seasonal minimum temperatures for both the organic layer and the mineral soil occurred in early February (between JD 40 and 43).

At the time when the air temperature dropped below 0 ºC the first time (JD 312), the relative saturation of the mineral soil, measured by TDR, ranged from 65% at the top of the slope to ~75% at mid and lower slope; increasing with depth (Figure 7.2D). A slight decrease in the liquid moisture content (5-10%) was observed over the following two weeks. In late November (JD 329 to 334) the TDR readings indicated that the there

*Table 7.1. Average temperatures (±standard deviation) during the whole winter season (November 28 2006 to March 4 2007), the coldest month (February), and snowmelt (March 7-18).*

| Season | All Winter | February | Snowmelt |
|---|---|---|---|
| *Air temperature (ºC)* | –6.2 ±6.5 | –7.3 ±6.1 | +1.1 ±4.7 |
| *Organic layer (ºC)* | –1.6 ±1.0 | –2.2 ±1.0 | –0.2 ±0.4 |
| *Mineral soil, 0-5 cm (ºC)* | –1.2 ±0.8 | –1.9 ±0.8 | –0.2 ±0.3 |
| *Mineral soil, 10-20 cm (ºC)* | –0.8 ±0.8 | –1.6 ±0.5 | –0.2 ±0.3 |
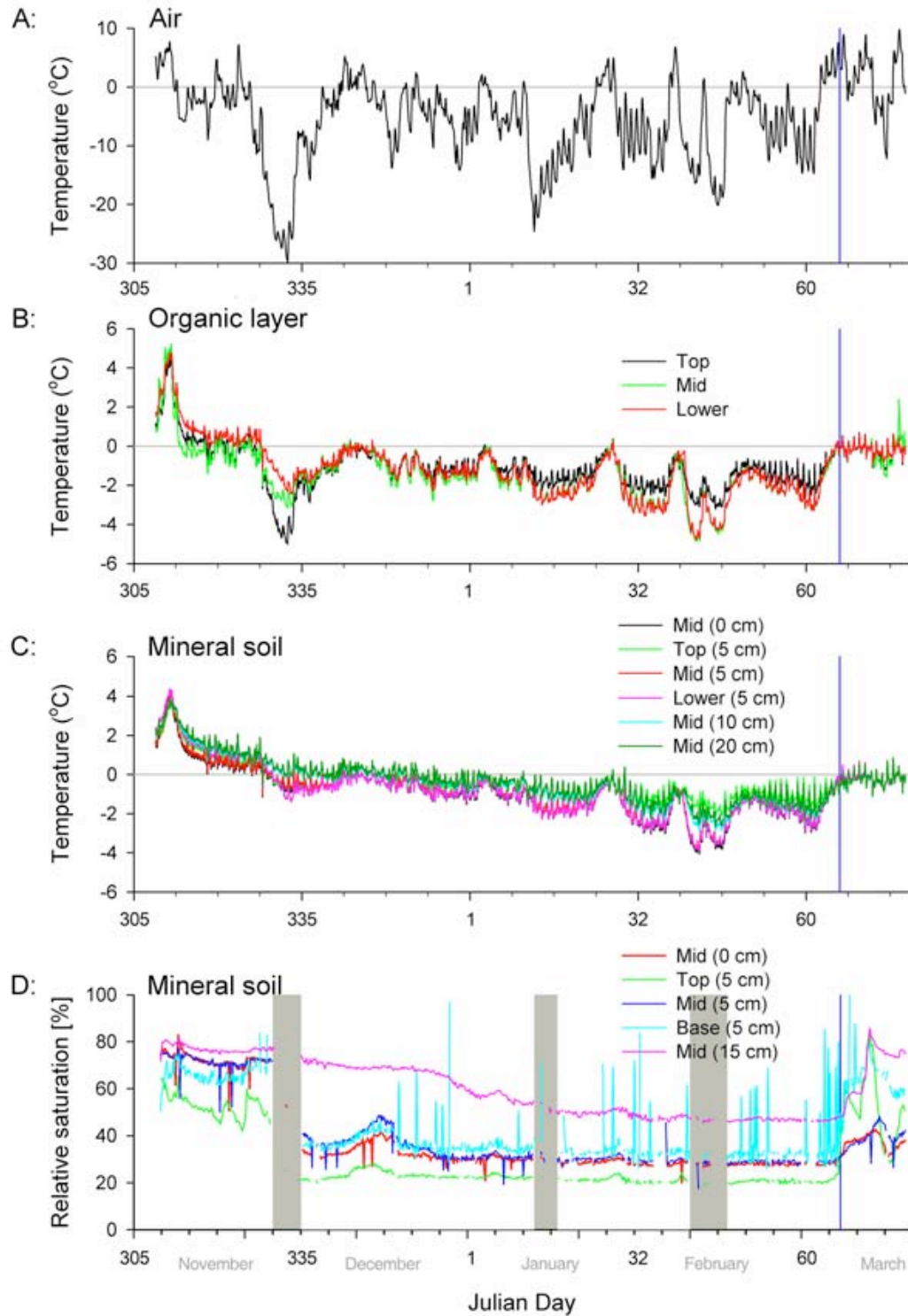
*Figure 7.2. Temperatures [ºC] A) of the air, B) in the organic layer, and C) in the mineral soil at the observation site from early November 2006 (JD 305) to mid March 2007 (JD 77). D) Relative saturation [%] in the mineral soil based on TDR; shaded areas denote frozen conditions. The vertical blue line (JD 66) denotes the beginning of snowmelt. Top, mid, and lower refers to Figure 7.1.*

was no liquid soil water present; this period coincides with the very low air temperatures. Fully frozen conditions only lasted for five days; after which the TDR readings show a liquid water content of ~30% in the top-most part of the soil (+3.75 to –8.75 cm) and a similar moisture content for the deeper soil (–11.25 to –18.75 cm) as was observed prior to freeze-up. During December and January, the relative saturation of the deeper soil decreased, reaching a minimum of 45% in mid February (JD 41). Two other episodes of soil freezing were observed during the winter; one in mid January (JD 11 to 15), which was most significant for the top part of the mineral soil, and one in mid February (JD 39 to 45), which affected the deeper soil as well.

The TDR readings during the winter might not accurately indicate the phase conditions of the soil water as the presence of both liquid and frozen water complicates TDR measurements (e.g. Evett, 2003). A change in pore-water pressures as water freezes within the soil results in a depression of the freezing point, allowing supercooled water to coexist with ice at temperatures below 0 ºC (e.g. Jame, 1972). A depression in the freezing temperature will also be caused by the solute content in the soil water (e.g. Masterton and Hurley, 1997); however, due to the dilute concentration in snowmelt and soil water the depression will only be slight (e.g. Williams and Smith, 1989).

During the first week of March (JD 63), three consecutive days with air temperatures above zero, resulted in an increase in soil temperature across the slope. Isothermal conditions (around –0.2 ºC) were present throughout the organic layer and mineral soil during melt. The soil at the top of the slope exhibited slightly higher temperatures, which was attributed to differences in vegetation cover.

Combined soil temperature and moisture observations indicate that ice was still present in the mineral soil, limiting infiltration at the time that snowmelt initiated (March 7, JD 66). This was confirmed by measurements of concrete frost, which were done along the two transects on the slope (Figure 7.1). Insertion of the graduated metal rod into the mineral soil was not possible at any time during melt; an observation that is in contrast to the statement by Barry *et al*. (1990) that concrete frost is seldom found in forested areas (section 2.2).

During the first week of melt, a rapid increase in liquid moisture content was observed, peaking around JD 71, coinciding with a rain-on-snow event. The deeper part

of the mineral soil reached a liquid moisture content similar to that prior to freeze-up (~80% saturation) while the moisture content of the top part of the soil was only about half that (~38% saturation).


## 7.2    Snowmelt

Data from a sonic snow gauge (Campbell, SR50) from a nearby site (#2 on Figure 4.6) show that snow accumulation initiated in early December (Figure 7.3A). Problems with the power supply for this station prevented data collection from mid December (JD 348) to late January (JD 20). At the time of snowmelt (March 7, JD 66), the depth of the snowpack, $d_s$ [m], at the observation site ranged between 0.07 m and 0.32 m across the slope; average snow depth was 0.16 m ±0.08 m. Surveys of snow depth were carried out daily along two transects at ~5 m intervals (Figure 7.1); all snow had melted above the collection sites after six days. Average daily change in snow depth was ~0.02 m (Figure 7.3B and C).

Wet and dry precipitation fell three times during the melt period; all values reported here are for sub-canopy precipitation. A small amount of snow fell over-night on both JD 67 (~8 mm) and JD 75 (5-10 mm); unfortunately, the latter sample was lost during storage. A rain-on-snow event started in the afternoon on March 11 (JD 70) and lasted for ~22 hours, causing most of the snow to melt (Appendix F). Upslope of the collection sites, all snow had ablated in the early morning of JD 71. Along the northern part of the area, where the snowpack was initially deeper, some patchy snow was still present (~0.09 m). Total rainfall was to 19.3 mm with an average intensity of 0.8 mm $\text{h}^{-1}$ and a peak intensity of 6 mm $\text{h}^{-1}$ on JD 71.1.

Snow densities, $\rho_s$ [kg m$^{-3}$], were measured on JD 67 and JD 68 at three places along each transect (~15 m apart). Average density was 194 kg m$^{-3}$ ±58 kg m$^{-3}$ on the first day; increasing to ~219 kg m$^{-3}$ ±68 kg m$^{-3}$ the second day. Measurements after this were not considered viable due to a very shallow snowpack (<0.07 m) in the area of the collection sites.

Snow water equivalents, $SWE$ [mm], were estimated from

$$SWE \quad = \quad \rho_s \cdot d_s$$ (7.1)
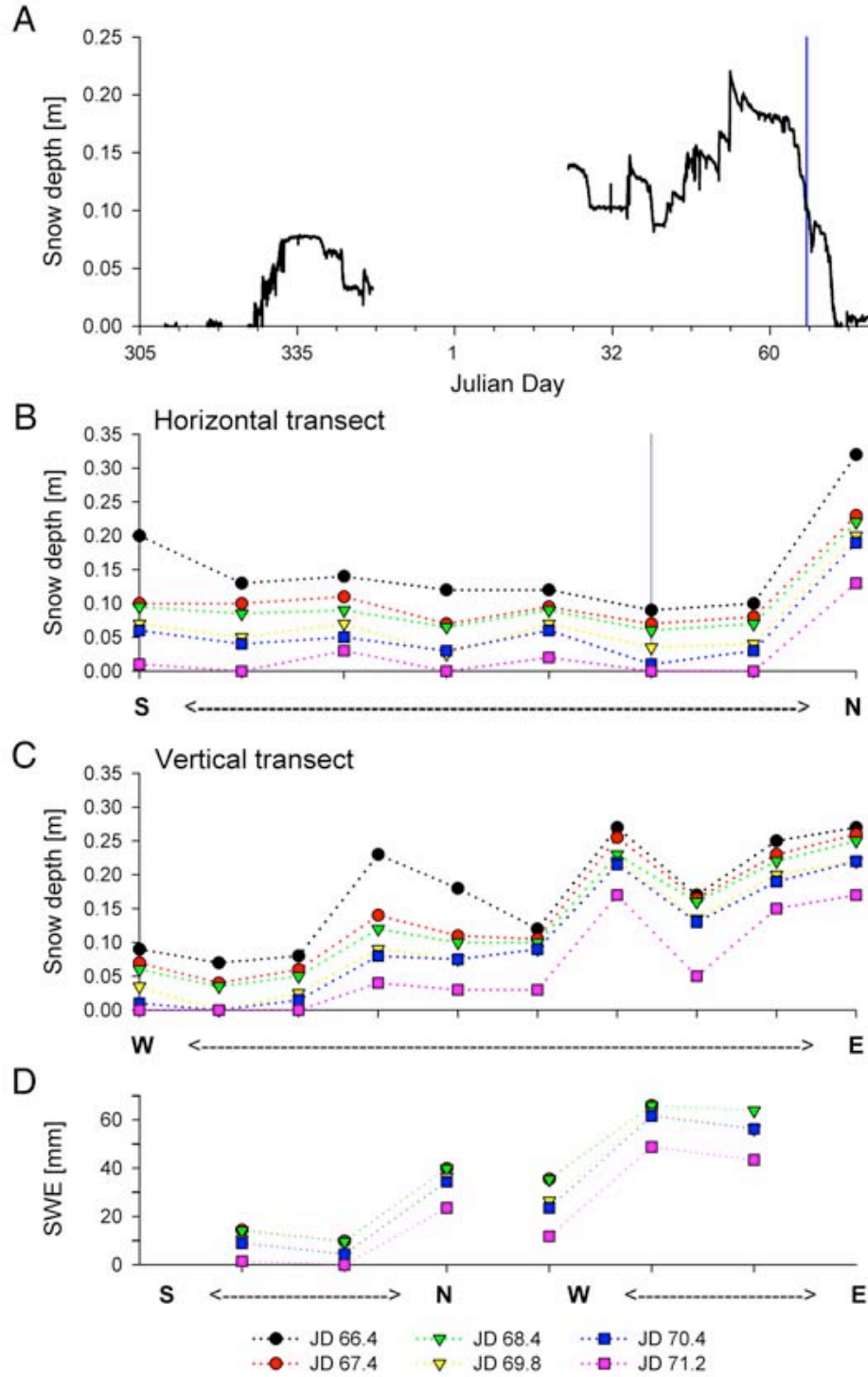
*Figure 7.3. Changes in snow depth, $d_s$ [m], (A) throughout the winter (blue line indicates snowmelt) and along the horizontal (B) and vertical (C) transect during melt; the grey line in (B) represents where the vertical transect intersect with the horizontal transect (Figure 7.1). D) Measured and estimated snow water equivalent, SWE. The left part of the plot is for the horizontal transect; the right part is for the vertical transect.*

*Table 7.2. Average melt rates for the snowpack at the observation site.*

| Julian Day | Melt rate (kg m$^{-2}$ d$^{-1}$) (average ±stdev) |
|:---:|:---:|
| 68.4 | 00.0 ±0.0 |
| 69.8 | 03.7 ±1.8 |
| 70.4 | 01.7 ±2.0 |
| 71.2 | 12.6 ±4.3 |

and showed similar *SWE* for both days; varying between 10 mm and 66 mm (Figure 7.3D). For the following three days, daily *SWE* was estimated using the depth measurements and assuming that $\rho_s$ remained constant at each site. This assumption was based on Seligman's (1936) results, which reported densities of settled snow ranging from 200 to 300 kg m$^{-3}$.

Daily melt rates were estimated based on the *SWE*, indicating that melting was limited until the morning of March 11 (JD 70.4) after which the melt rate peaked as a result of the rain-on-snow event (Table 7.2).

## 7.3    Sample Collection

A total of 41 samples were collected over a period of 10 days; six snowpack samples, three wet and dry precipitation samples, and 32 samples of organic soil water, mineral soil water, and ponding water. Figure 7.4 shows photographs of the sampling sites and Table 7.3 provides an overview of the types and number of samples collected on any given day. Sampling was not done at every site each day; some sites were collected more frequently than others.

Snowpack samples (S) were collected daily close to site #3 (Figure 7.1). On the first day of sampling, the snowpack consisted of coarse, rounded grains (~1 mm grain size). Some melting had occurred causing the lower part of the snow to be slightly wetter and denser. Wet and dry precipitation (P) was collected following each event.

Organic soil water (OSW) was collected from all three transects during melt. A total of eight samples were collected; three at each of site #1 and #2 and two at site #3 (Table 7.3). Two samples were collected on JD 67 followed by two days without any water present. The greatest volumes were collected during the rain-on-snow event with

*Figure 7.4. Photographs of sampling sites. Top row: the individual collection sites at the observation site for organic soil water (OSW) and mineral soil water (MSW). The numbers refer to position on the slope (see Figure 7.1). Centre row: overland flow installation close to site #3 where water was present during the rain-on-snow event (OSW\*). Bottom row: collection sites for ponded water; in the depression in front of the lysimeter transects (PW-site) as well as on top of snow (PW-snow) and soil (PW-soil) in the vicinity of the observation site.*

*Table 7.3. Overview of the types and number of samples collected on a given day during snowmelt.*

| March 2007, Date | 7 | 8 | 9 |  | 10 | 11 |  | 12 | 16 | 18 | Total |
|---|---|---|---|---|---|---|---|---|---|---|---|
| Julian Day | 66.4 | 67.4 | 68.4 | 68.7 | 69.8 | 70.4 | 70.7 | 71.2 | 75.4 | 77.7 |  |
| Snow, S | 1 | 1 | 1 |  | 1 | 1 |  | 1 |  |  | 6 |
| Precipitation, P |  | 1 |  |  |  |  |  | 1 | 2' |  | 3' |
| Organic soil water, OSW  #1 |  |  |  |  |  | 1 | 1 | 1 |  |  | 3 |
| #2 |  | 1 |  |  |  |  | 1 | 1 |  |  | 3 |
| #3 |  | 1 |  |  |  |  |  | 1 |  |  | 2 |
| Overland flow, OLF  #3 |  |  |  |  |  |  | 1 | 1 | 1 |  | 3 |
| Mineral soil water, MSW  #2 |  |  |  |  |  |  |  | 1 |  |  | 1 |
| #3 |  |  |  |  |  |  |  | 1 | 1 | 1 | 3 |
| Ponding water (site), PW-site  #2 |  |  |  |  | 1 | 1 | 1 | 1 |  |  | 4 |
| #3 |  |  |  |  | 1 | 1 | 1 | 1 |  |  | 4 |
| Ponding water (snow), PW-snow | 2 |  | 1 |  |  | 2 |  |  |  |  | 5 |
| Ponding water (soil), PW-soil | 2 |  | 1 |  |  | 1 |  |  |  |  | 4 |
| Total | 5 | 4 | 3 |  | 3 | 12 |  | 10 | 3' | 1 | 41 |

' Sample of snow was lost during storage.

*Table 7.4. Collected volumes (ml) of overland flow, organic soil water, and mineral soil water.*

| March 2007, Date | | 8 | 11 | | 12 | 16 | 18 | Total |
|---|---|---|---|---|---|---|---|---|
| *Julian Day* | | 67.4 | 70.4 | 70.7 | 71.2 | 75.4 | 77.7 | **volume** |
| Organic soil water, OSW | #1 | | ~200 | ~100 | ~2000 | | | ~2300 |
| | #2 | ~280 | | ~450 | ~400 | | | ~1130 |
| | #3 | ~75 | | | ~675 | | | ~750 |
| Overland flow, OSW* | #3 | | | ~3780 | ~3780 | ~300 | | ~7860 |
| Mineral soil water, MSW | #2 | | | | ~640 | | | ~640 |
| | #3 | | | | ~750 | ~100 | ~40 | ~910 |

collection site #1 eluting three to five times more than the other sites (Table 7.4). A reason for this could be that the upland area was the least obstructed by shrubs and trees. Total volumes collected were 2.3 l at site #1, 1.1 l at site #2, and 0.75 l at site #3.

During the rain-on-snow event (JD 70-71), water was present at the overland flow installation at site #3 (Figure 7.4, second row). There was no basal ice layer present or visible overland flow occurring; thus, since contact with the organic layer had occurred, samples could be labelled OSW. However, to distinguish between collection sites an asterisk (*) will be added to the label of these samples (OSW*). Three samples were collected during the rainstorm. Total collected water volume was ~7.9 l (Table 7.4); the most for all sites.

Four water samples were collected from the mineral soil horizon (MSW) during the latter part of snowmelt (Table 7.3). Three of the samples were collected at 0.05 m depth and one at 0.15 m depth. The first two samples were collected at site #2 and #3 during the rain-on-snow event on JD 71; similar volumes were collected at both sites (Table 7.4). Following the major snowmelt event (JD 75 and 77), two small samples (100 and 40 ml) were collected at site #3; the first sample was collected from the lower lysimeter.

After two days of snowmelt, on JD 69, water (PW-site) was observed to pond in the depressions in front of the lysimeter transects (Figure 7.5). There was no indication of where this water had originated from and no water was present in any of the lysimeters. The volumes of ponded water were not measured. Daily samples (~150 ml) were collected to assess the compositional change of water chemistry over time. All

*Figure 7.5. Ponded water observed in the depression in front of the lysimeter transects on JD 69 (PW-site).*

water was gone (evaporated or infiltrated) on JD 75 (Table 7.3). A total of eight samples were collected at site #2 and #3; the volume of water present at site #1 was inadequate for analyses and only present on the first day.

In the vicinity of the observation site, near site #2 on Figure 4.6, ponded water was observed on top of icy snow (PW-snow) and bare soil (PW-soil) (Figure 7.4). Sampling of these waters was attempted at the same spot on consecutive days. In total, five samples of PW-snow and four samples of PW-soil were collected between JD 66 and 70; three of each were collected at the same spot.

## 7.4    Sample Chemistry

Each sample was analysed for major anions and cations; except one (MSW on JD 77), which was not analysed for $Cl^-$ and $SO_4^{2-}$ due to an insufficient sample volume. Twenty-three samples were also analysed for DOC. Ion charge balance (*ICB*) for the individual samples varied between 0.34 and 0.94; average ion charge balance was 0.70

±0.16. These imbalances were ascribed to the presence of unmeasured carbonate species and DOC. Analyses of snow and stream water elsewhere in the Marmot Creek Research Basin showed $HCO_3^-$ concentrations of 46.8±24.0 meq m$^{-3}$ for snow and 1.7±0.4 eq m$^{-3}$ for the creek (Erin Shaw, unpublished data). Historic data from Alberta Environment reports concentrations of $HCO_3^-$ in the groundwater ranging between 4.0 and 6.0 eq m$^{-3}$. Converting the differences between anion and cation concentrations to $HCO_3^-$ concentrations, assuming that the imbalance of the *ICB* were entirely due to $HCO_3^-$, gave concentrations that corresponded well to these values.

### 7.4.1  Snowpack and Precipitation

The chemical composition of the snowpack was dominated by $Ca^{2+}$. Table 7.5 shows the concentrations of the individual ions prior to general melt. Sodium was not detected in any of the snow samples, which seemed inaccurate as the concentrations in the precipitation samples were 8.3±0.9 meq m$^{-3}$. Thus, the parent snowpack's concentration of $Na^+$ was taken as that of the first precipitation event (JD 67).

The shallow snowpack prevented the use of the installed snow lysimeter for collection of released meltwater to obtain knowledge of its chemical composition. Consequently, enrichment ratios (*ER* = RW/SW) were calculated for all ions in the collected runoff water, RW, using daily ion concentrations in the snowpack, SW. During the rain-on-snow event, weighted average concentrations of the snowpack and rainfall ion concentrations were used (Table 7.5; see Appendix H for calculations). This was considered a reasonable approximation for SW since ion fractionation within a very

*Table 7.5. Ion concentrations in the parent snow as well as the weighted average concentrations of the snow and rain during the rain-on-snow event. Concentrations are given in meq m$^{-3}$ for all major anions and cations; DOC is in g m$^{-3}$. ICB is the ion charge balance.*

| Ion | H$^+$ | Cl$^-$ | SO$_4^{2-}$ | NO$_3^-$ | NH$_4^+$ | Na$^+$ | K$^+$ | Mg$^{2+}$ | Ca$^{2+}$ | DOC | ICB |
|---|---|---|---|---|---|---|---|---|---|---|---|
| *Snow, parent* | 0.4 | 9.9 | 15.6 | 1.0 | 7.7 | 7.7 | 8.8 | 14.8 | 46.0 | 10.0 | +0.53 |
| *Snow, during rain* | 0.5 | 8.5 | 14.6 | n.d. | 8.4 | 7.7 | 18.7 | 37.8 | 79.0 | 10.0 | +0.74 |
| *Rain* | 2.6 | 8.5 | 33.3 | 0.9 | 6.8 | 7.9 | 8.3 | 23.3 | 55.2 | 10.0 | +0.42 |
| *Weighted average* | 1.8 | 8.5 | 26.1 | 0.6 | 7.4 | 7.8 | 12.3 | 28.9 | 64.3 | 10.0 | +0.55 |

n.d. = below detection limits
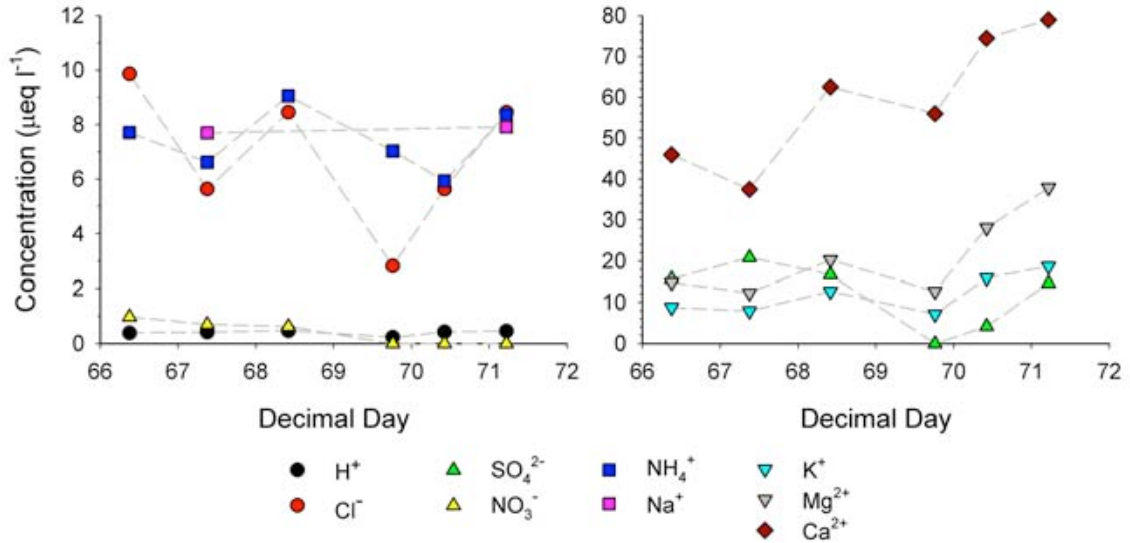
*Figure 7.6. Change in ion concentrations (meq m$^{-3}$) in the snowpack as melt progressed.*

shallow snowpack is limited (e.g. Bales *et al*., 1989). This assumption was further supported by the minor changes in snowpack ion concentrations as melt progressed (Figure 7.6). The average difference between the snowpack's chemical composition and the wet and dry precipitations chemical compositions was 8.5 meq m$^{-3}$ (±9.3 meq m$^{-3}$); a difference which was primarily affected by the differences in K$^+$, Mg$^{2+}$, and Ca$^{2+}$ concentrations. During the rain-on-snow event, the average difference increased to 10.2±10.7 meq m$^{-3}$. The smallest difference between concentrations was observed for NO$_3^-$ and NH$_4^+$ averaging <1 meq m$^{-3}$.

Samples collected on JD 75 and 77 were likely affected by the rain-on-snow event because only ~5 mm of snow fell between the rainstorm and collection. Consequently, these samples were normalized to the weighted ion concentrations from the rain-on-snow event.

*ER* were determined for a total of 308 ion concentrations; of these, 23 ratios were undefined as either RW or SW had an ion concentration below the detection limit. The majority of the undefined ratios were for NO$_3^-$ as a result of concentrations in the runoff water less than the detection limit (0.1 meq m$^{-3}$).

## 7.4.2 Organic Soil Water, OSW

Calcium dominated the chemical composition of the organic soil water samples with concentrations of 226±153 meq $m^{-3}$; few samples were high in $K^+$ and $Mg^{2+}$ concentrations, too (>100 meq $m^{-3}$). Ion charge balances ranged between 0.42 and 0.90. Average ion charge balance was 0.75±0.17.

Figure 7.7 shows the change in $ER$ for the individual ions as melt progressed. Generally, $ER$ decreased continuously with time for all ions; except for $NO_3^-$ as the concentrations in the OSW were below detection limits. The greatest depletion was observed for $K^+$ with ~25. Most of the ions showed enriched conditions throughout melt, approaching 1 during the rain-on-snow event. Excluding $NO_3^-$, the highest $ER$ for the individual ions, $ER_{max}$, ranged from 1.5 for $NH_4^+$ to 29.2 for $K^+$; generally, $ER_{max}$ occurred on JD 70.7 (Table 7.6).

Three of the samples showed similar signatures for all nine major ions: enriched conditions for all ions except $NO_3^-$. They were all collected prior to the rain-on-snow event; two were collected on JD 67 at site #2 and #3 and one was collected on JD 70 at site #1. Their signature was similar to the general trend of all OSW samples (Table 7.7). Average enrichment for the organic soil water ranged between 1.5 for $H^+$ and 8.9 for $K^+$ (Table 7.8).

### Water at the Overland Flow Installation, OSW*

The chemical compositions of the samples' collected from the overland flow installation at transect #3 (refer to Figure 7.1) were dominated by $Ca^{2+}$, too; average concentration

*Table 7.6. Maximum enrichment ratios, $ER_{max}$, obtained for each collection site.*

|  | $H^+$ | $Cl^-$ | $SO_4^{2-}$ | $NO_3^-$ | $NH_4^+$ | $Na^+$ | $K^+$ | $Mg^{2+}$ | $Ca^{2+}$ | DOC |
|---|---|---|---|---|---|---|---|---|---|---|
| **OSW** | 2.4 | 4.0 | 7.0 | <<1 | 1.5 | 10.9 | 29.2 | 7.8 | 8.5 | 8.4 |
| **OSW*** | 1.9 | 10.3 | 3.8 | <<1 | 1.0 | 11.3 | 5.6 | 10.3 | 2.8 | 4.4 |
| **MSW** | 0.7 | 1.7 | 1.3 | <<1 | 2.4 | 1.2 | 2.2 | 2.8 | 3.4 | 3.5 |
| **PW-site** | 1.9 | 13.0 | 8.0 | <<1 | 0.9 | 1.5 | 6.0 | 5.5 | 4.7 | 4.8 |
| **PW-snow** | 0.3 | 9.1 | 2.7 | >>1 | 0.9 | 1.1 | 43.9 | 12.7 | 13.1 | 3.0 |
| **PW-soil** | 0.03 | 11.1 | 3.2 | 8.8 | 1.0 | 1.7 | 42.5 | 12.5 | 14.1 | 2.6 |

>>1: concentration in snow was below detection limits.
<<1: concentration in runoff water sample was below detection limits.
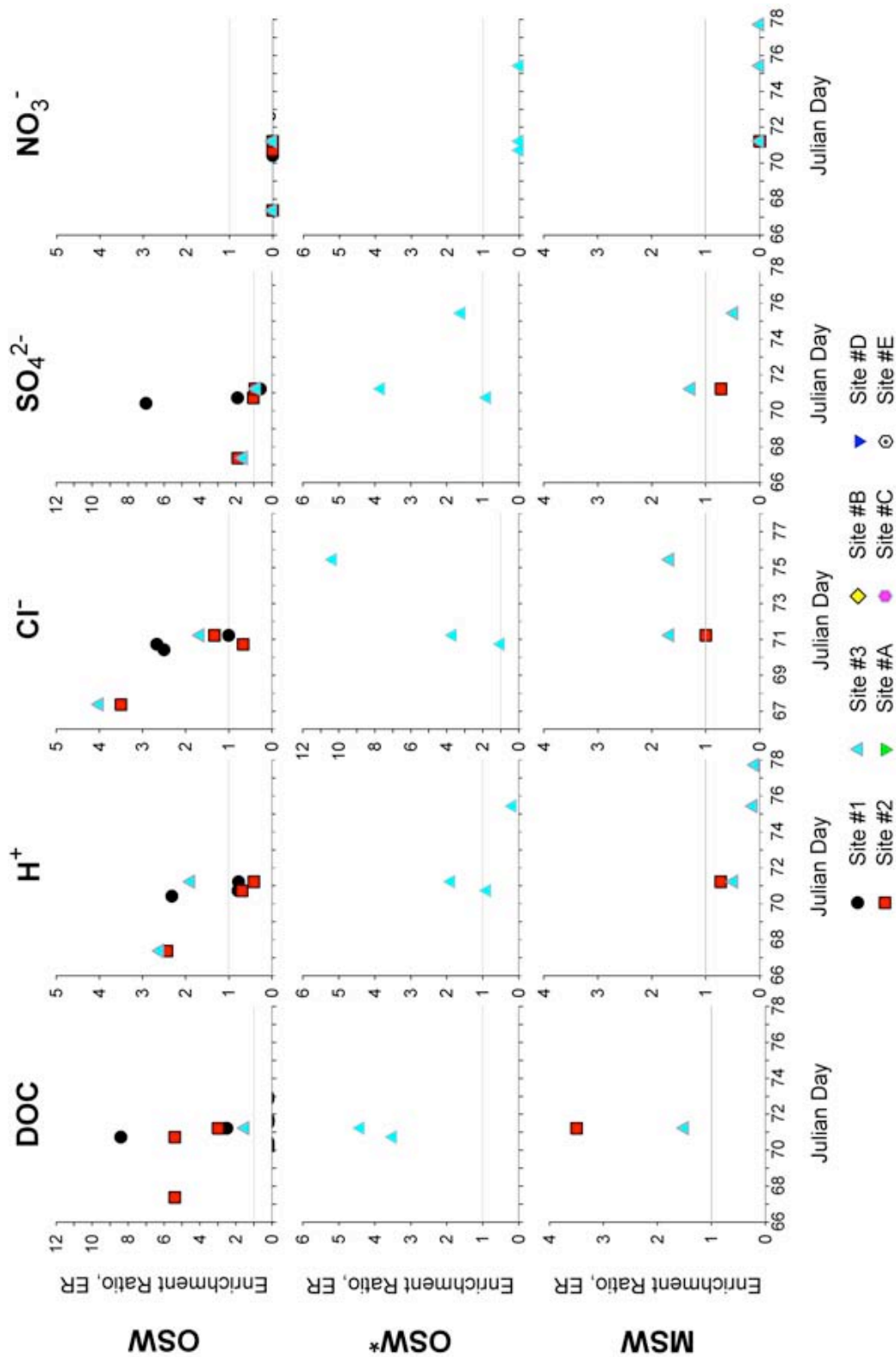
*Figure 7.7. Evolution in enrichment ratio, ER, for the individual ions in samples of organic soil water, OSW and OSW\*, and mineral soil water, MSW. The horizontal grey line represents ER=1.*
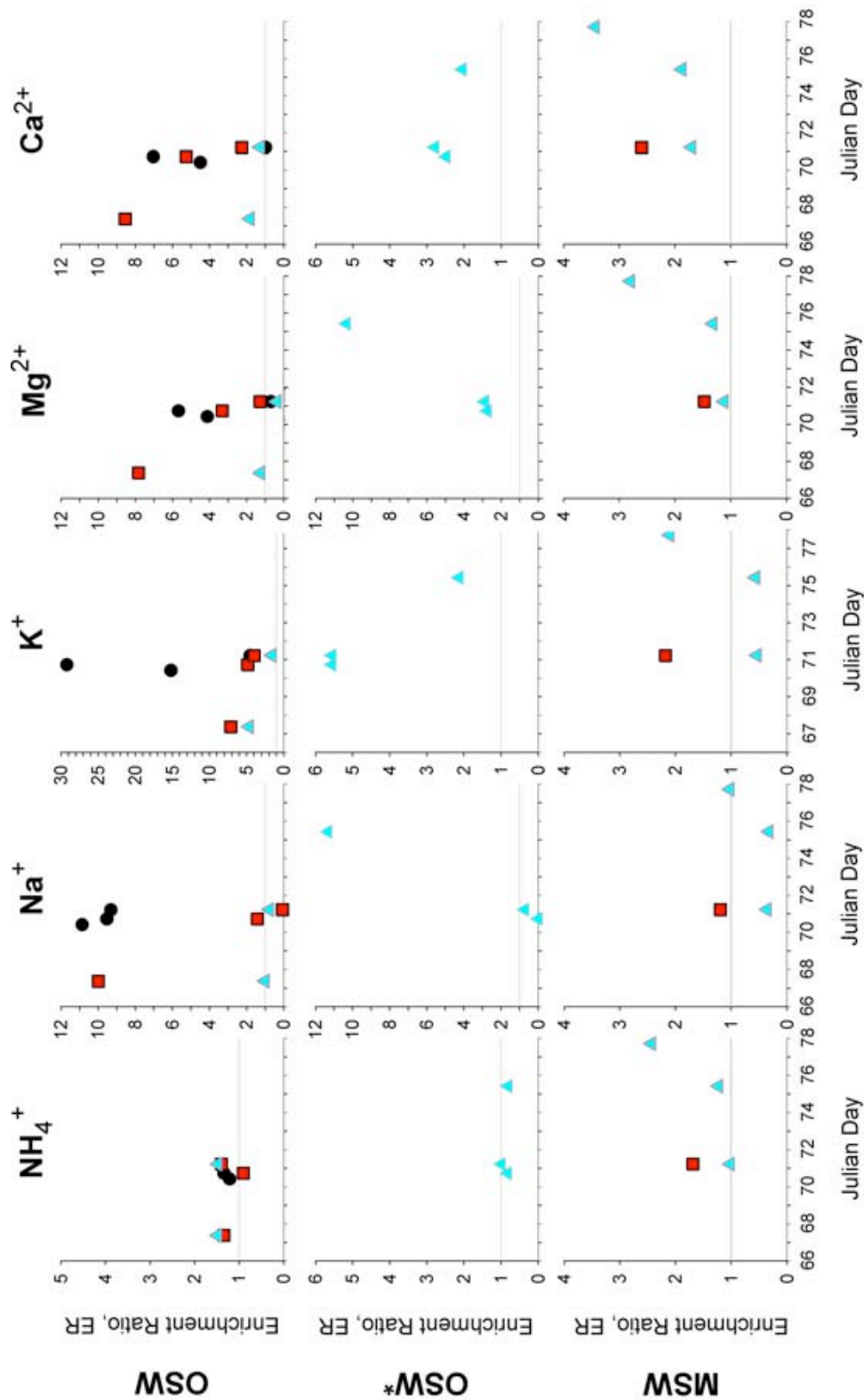
*Figure 7.7 (continued). Evolution in enrichment ratio, ER, for the individual ions in samples of organic soil water, OSW and OSW\*, and mineral soil water, MSW. The horizontal grey line represents ER=1.*

*Table 7.7. Percentage of enrichment ratios, ER, for each collection site that had ER>1. n is the number of samples at each site; values in brackets refer to the number of samples that were analysed for DOC. Green fields indicate general enrichment.*

| Collection site | n | H$^+$ | Cl$^-$ | SO$_4^{2-}$ | NO$_3^-$ | NH$_4^+$ | Na$^+$ | K$^+$ | Mg$^{2+}$ | Ca$^{2+}$ | DOC |
|---|---|---|---|---|---|---|---|---|---|---|---|
| OSW | 3 (2) | 50% | 75% | 50% | 0% | 88% | 63% | 100% | 75% | 88% | 100% |
| OSW* | 8 (6) | 33% | 67% | 67% | 0% | 0% | 33% | 100% | 100% | 100% | 100% |
| MSW | 4 (2) | 0% | 50% | 25% | 0% | 75% | 25% | 50% | 100% | 100% | 100% |
| PW-site | 8 (8) | 13% | 100% | 50% | 0% | 0% | 13% | 100% | 75% | 100% | 100% |
| PW-snow | 5 (1) | 0% | 100% | 40% | 20% | 0% | 20% | 100% | 80% | 100% | 100% |
| PW-soil | 4 (3) | 0% | 100% | 100% | 25% | 0% | 25% | 100% | 100% | 100% | 100% |

*Table 7.8. Average enrichment of the individual ions for the samples collected at the individual sites. n is the number of samples at each site; values in brackets refer to the number of samples that were analysed for DOC. – indicates that the ER could not be determined as*

| Collection site | n | H$^+$ | Cl$^-$ | SO$_4^{2-}$ | NO$_3^-$ | NH$_4^-$ | Na$^+$ | K$^+$ | Mg$^{2+}$ | Ca$^{2+}$ | DOC |
|---|---|---|---|---|---|---|---|---|---|---|---|
| OSW | 3 (2) | 1.5 | 2.2 | 2.0 | - | 1.3 | 5.4 | 8.9 | 3.1 | 4.0 | 4.4 |
| OSW* | 8 (6) | 1.0 | 5.0 | 2.1 | - | 0.9 | 4.0 | 4.4 | 5.3 | 2.4 | 4.0 |
| MSW | 4 (2) | 0.4 | 1.4 | 0.8 | - | 1.6 | 0.7 | 1.3 | 1.7 | 2.4 | 2.5 |
| PW-site | 8 (8) | 0.6 | 4.6 | 2.5 | - | 0.8 | 0.8 | 3.3 | 2.3 | 3.4 | 3.1 |
| PW-snow | 5 (1) | 0.1 | 4.3 | 1.4 | - | 0.8 | 0.8 | 13.6 | 5.1 | 6.1 | 3.0 |
| PW-soil | 4 (3) | 0.01 | 6.0 | 2.2 | 3.2 | 0.8 | 1.0 | 19.6 | 8.8 | 9.5 | 2.2 |
| Overall | 32(22) | 0.7 | 3.8 | 1.9 | 0.7 | 1.0 | 2.3 | 8.2 | 3.9 | 4.5 | 3.3 |

was 157 meq m$^{-3}$ with a standard deviation of 24 meq m$^{-3}$. Ion charge balance ranged between 0.39 and 0.82; decreasing with time.

The *ER* of Cl$^-$, Na$^+$, Mg$^{2+}$, and DOC increased over time (Figure 7.7), while *ER* for K$^+$ and Ca$^{2+}$ decreased. The greatest increase was observed for Na$^+$, increasing 11.3, followed by Cl$^-$ with a 9.3; the greatest depletion was observed for K$^+$ with 3.4. An increase in *ER* followed by a larger or similar decrease was observed for H$^+$ and SO$_4^{2-}$. Ammonium showed little variation in *ER* ($\pm 0.1$), whilst no *ER* could be calculated for NO$_3^-$ as the concentrations in the collected water were less than detection limits. Excluding NO$_3^-$, the *ER$_{max}$* ranged between 1.0 for NH$_4^+$ and 11.3 for Na$^+$ (Table 7.6).

None of the samples had identical ratios for the individual ions or even similar trends. However, all samples showed enriched conditions for DOC, $K^+$, $Mg^{2+}$, and $Ca^{2+}$ throughout melt, while $Cl^-$, $SO_4^{2-}$, and $Na^+$ went from being depleted or equal to 1 to being enriched. Hydrogen concentrations varied from being depleted to enriched to depleted again. In general, $Cl^-$, $SO_4^{2-}$, $K^+$, $Mg^{2+}$, $Ca^{2+}$, and DOC were enriched and $H^+$, $Na^+$, and $NO_3^-$ were depleted, and $NH_4^+$ was neither enriched nor depleted (Table 7.7). Average $ER$ was 0.0 for $NO_3^-$ and ~1.0 for both $H^+$ and $NH_4^+$ (Table 7.8); the rest of the ions all had average $ER>1$, ranging between 2.1 for $SO_4^{2-}$ and 5.3 for $Mg^{2+}$. The overall average $ER$ was 3.7.

### 7.4.3 Mineral Soil Water, MSW

The chemical composition of the samples collected from the mineral horizon were dominated by $Ca^{2+}$; $154.5\pm51$ meq m$^{-3}$. Ion charge balances were only assessed for the first three samples because $Cl^-$ and $SO_4^{2-}$ concentrations were not analyzed for the last sample due to the small sample size. Ion charge balances ranged between 0.54 and 0.81.

Compared to surface and organic layer waters, the ranges of the $ER$ were rather modest; excluding $NO_3^-$, $ER_{max}$ ranged between 0.7 for $H^+$ and 3.4 for DOC (Table 7.6). For $H^+$ and $SO_4^{2-}$, $ER_{max}$ were obtained on the first day of sampling (JD 71) and followed by a general decrease (Figure 7.7). The largest $ER$ decrease (0.8) was observed for $SO_4^{2-}$. An increase in $ER$ was observed for $NH_4^+$, $Na^+$, $K^+$, $Mg^{2+}$, and $Ca^{2+}$, resulting in $ER_{max}$ being obtained on the last day of sampling (JD 77). Magnesium and $Ca^{2+}$ both increased 1.7, followed closely by $K^+$ by 1.6 and $NH_4^+$ by 1.4. There was little variation in $Cl^-$ ratios and it was not possible to determine a trend for DOC because DOC was not analyzed after the first day due to small sample volume. All $NO_3^-$ concentrations were less than detection limits.

Similar trends in the $ER$ of all the ions were not observed for in any of the samples. The general chemical signature of these samples was: enrichment of $Cl^-$, $NH_4^+$, $Mg^{2+}$, $Ca^{2+}$, and DOC, depletion of $H^+$ and $SO_4^{2-}$, and removal of $NO_3^-$; $Na^+$ and $K^+$ did not show a continuous trend throughout melt (Table 7.7). Average $ER$ ranged between 0.4 for $H^+$ and 2.5 for DOC (Table 7.8).

### 7.4.4  Ponded Water at Observation site, PW-site

The chemical composition of the ponded water in the depression in front of the lysimeter transects (Figure 7.5) were all dominated by $Ca^{2+}$ with concentrations ranging from 142 to 351 meq $m^{-3}$. There were only small variations in the ion charge balances (0.75±0.07); being greatest during the rain-on-snow event.

The plots of the variation in $ER$ illustrate that the $ER$ for $H^+$, $Cl^-$, $SO_4^{2-}$, $K^+$, and $Mg^{2+}$ in the ponded water all decreased continuously with time (Figure 7.8); the greatest depletion was observed for $Cl^-$ at 11.3. The $ER$ of $Ca^{2+}$ and DOC both exhibited a slight increase from the first to the second sample, followed by a greater decrease. Ammonium and $Na^+$ showed only small variations in $ER$ over time; ±0.1 and ±0.3, respectively. Nitrate concentrations were below detection limits in all water samples. Except for $NO_3^-$, $ER_{max}$ ranged between 0.9 for $NH_4^+$ and 13.0 for $Cl^-$ (Table 7.6). $ER_{max}$ were generally obtained for the first sample (JD 69).

The general signature for the ponded water was: enrichment of $Cl^-$, $K^+$, $Mg^{2+}$, $Ca^{2+}$, and DOC, depletion of $H^+$, $SO_4^{2-}$, $NH_4^+$, and $Na^+$, and $NO_3^-$ below detection limits (Table 7.7). The average $ER$, not including $NO_3^-$, was 0.6 for $H^+$ and 0.8 for $NH_4^+$ and $Na^+$ (Table 7.8); the rest of the ions had average ratios >1, ranged between 2.3 for $Mg^{2+}$ and 4.6 for $Cl^-$. None of the samples had identical signatures for all ions; a few samples differed by just one ion.

### 7.4.5  Ponded Water in the Surroundings

The levels of $Ca^{2+}$ concentrations dominated the chemical composition of the samples; some exceeded 600 meq $m^{-3}$. Average concentration was 337.3 meq $m^{-3}$ for PW-snow and 547 meq $m^{-3}$ for PW-soil. Other dominating ions were $K^+$ and $Mg^{2+}$ with concentrations >150 meq $m^{-3}$. Ion charge balances ranged between 0.70 and 0.94.

***'PW-snow'***

For PW-snow, the $ER$ for $Cl^-$, $K^+$, $Mg^{2+}$, and $Ca^{2+}$ all decreased with time (Figure 7.8); largest for $K^+$ by 42.7. A slight increase was observed for $H^+$ (0.2) and $NH_4^+$ (0.4). The $ER$ of $SO_4^{2-}$ and $Na^+$ decreased and then increase, almost back to the initial value, over
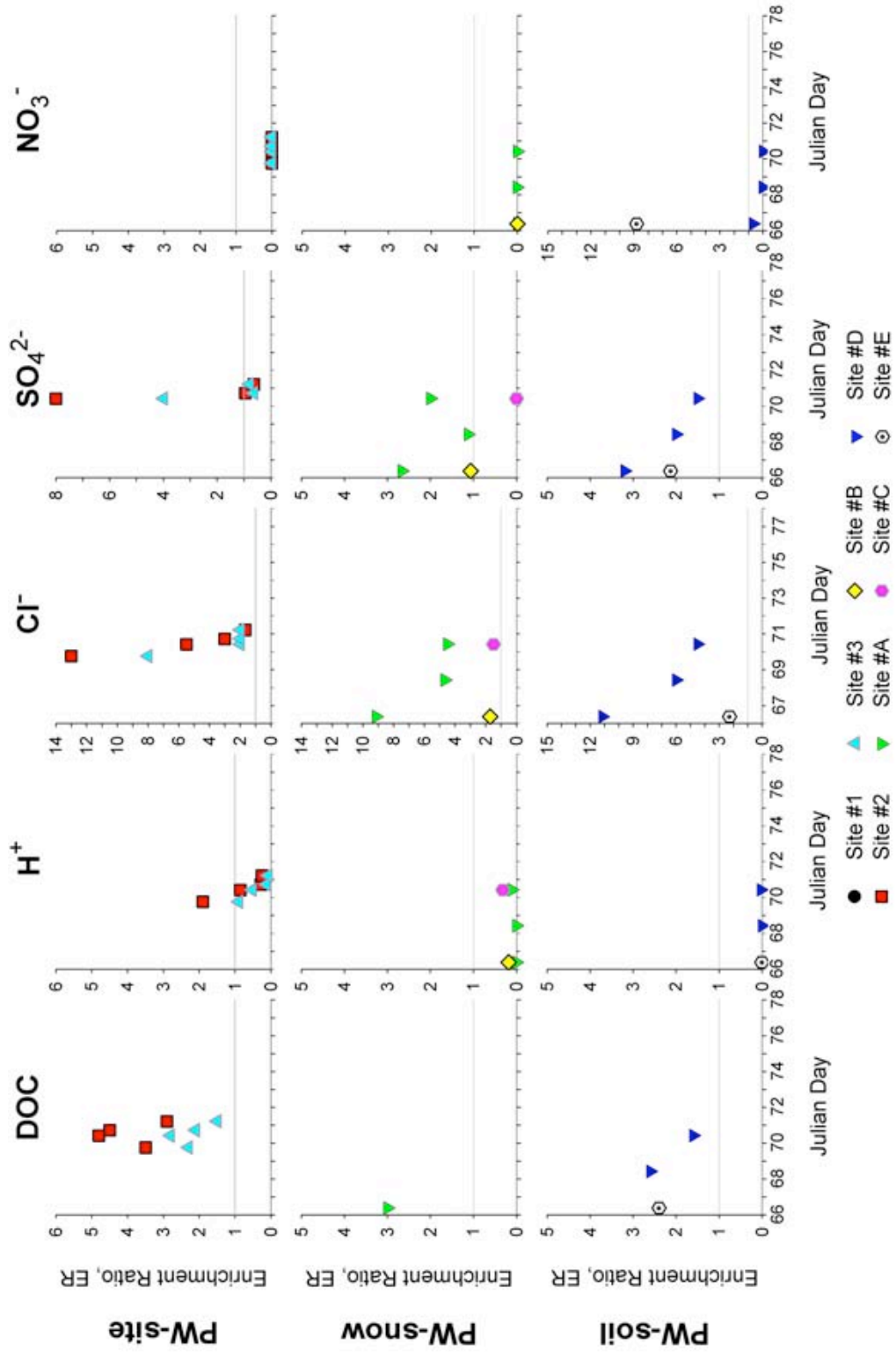
*Figure 7.8. Evolution in enrichment ratio, ER, for the individual ions in samples of ponded water at the observation site, PW-site, as well as on top of snow and ice, PW-snow, and on top of soil, PW-soil, in the vicinity. The horizontal grey line represents ER=1.*
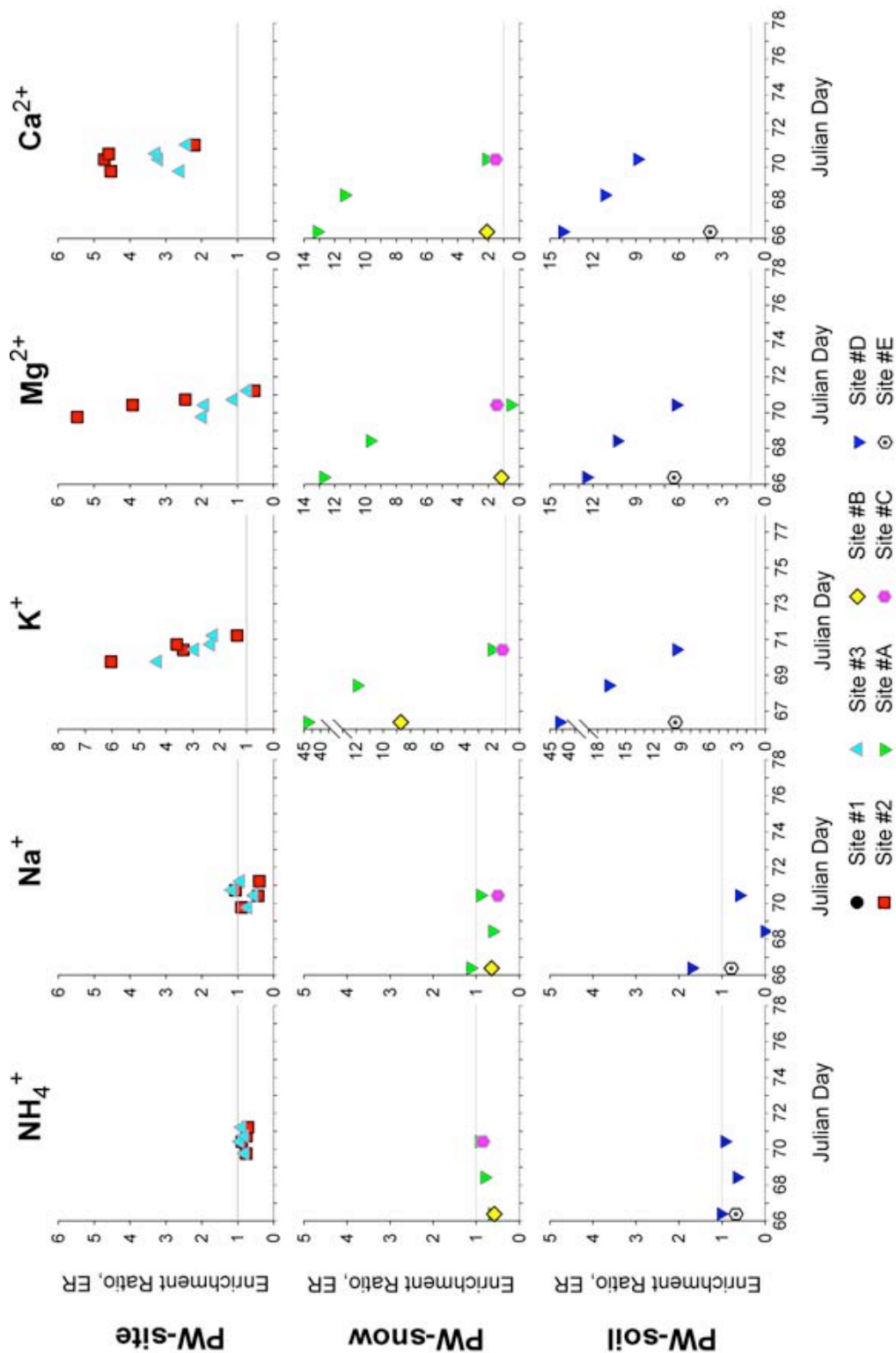
*Figure 7.8 (continued). Evolution in enrichment ratio, ER, for the individual ions in samples of ponded water at the observation site, PW-site, as well as on top of snow and ice, PW-snow, and on top of soil, PW-soil, in the vicinity. The horizontal grey line represents ER=1.*

4 days. The $ER$ of $NO_3^-$ were not measurable. DOC was only measured for one sample and was enriched. $ER_{max}$ ranged between 0.3 for $H^+$ and 43.9 for $K^+$ (Table 7.6).

The general signature for the ponded water was enrichment of $Cl^-$, $SO_4^{2-}$, $K^+$, $Mg^{2+}$, $Ca^{2+}$, and DOC, and depletion of $H^+$, $NH_4^+$, and $Na^+$ (Table 7.7). Average enrichment ranged from 0.1 for $H^+$ to 13.6 for $K^+$; $NO_3^-$ concentrations were generally below detection limits. Similar signatures for all ions were not observed for any of the samples.

### *'PW-soil'*

With high pH values of between 7.9 and 8.9 for the PW-soil samples, the $ER$ for $H^+$ remained close to zero (Figure 7.8). The $ER$ for $Cl^-$, $SO_4^{2-}$, $NO_3^-$, $K^+$, $Mg^{2+}$, $Ca^{2+}$, and DOC all decreased with time; $K^+$ decreased the most (~30). For $NH_4^+$ and $Na^+$, the $ER$ decreased initially and then increased. $ER_{max}$ ranged from 0.03 for $H^+$ to 42.9 for $K^+$ (Table 7.6). For PW-soil, $Cl^-$, $SO_4^{2-}$, $K^+$, $Mg^{2+}$, $Ca^{2+}$, and DOC were generally enriched and $H^+$, $NO_3^-$, $NH_4^+$, and $Na^+$ were depleted (Table 7.7). Average enrichment ranged from 0.01 for $H^+$ to 19.6 for $K^+$ (Table 7.8). None of the samples had similar signatures.

## 7.4.6 Comparing Sites

The $ER$ and compositional signatures of the collected samples varied markedly. This could indicate that flow is not necessarily occurring continuously through the same pore spaces. Continuous depletion or enrichment for the individual ions, depending on the flowpath and ion, was assumed an indication of this.

A comparison of the $ER$ for the individual ions at each collection site is given in Figure 7.9. The plots show that between 78% and 100% of the samples were enriched in $Cl^-$, $K^+$, $Mg^{2+}$, $Ca^{2+}$, and DOC (Table 7.9). Average enrichments were 3.8 for $Cl^-$, 8.2 for $K^+$, 3.9 for $Mg^{2+}$, 4.5 for $Ca^{2+}$, and 3.3 for DOC (Table 7.8). Only a little more than half the samples (55%) were enriched in $SO_4^{2-}$; 23% of the samples had ratios, which were close to 1. The average enrichment of $SO_4^{2-}$ was 1.9.

Depletion in $H^+$ and $Na^+$ was observed for 75% and 50% of the samples, respectively. Generally, the ponded waters and the mineral soil water were depleted in $H^+$ whilst most of the organic soil water samples were enriched; average $ER$ for all
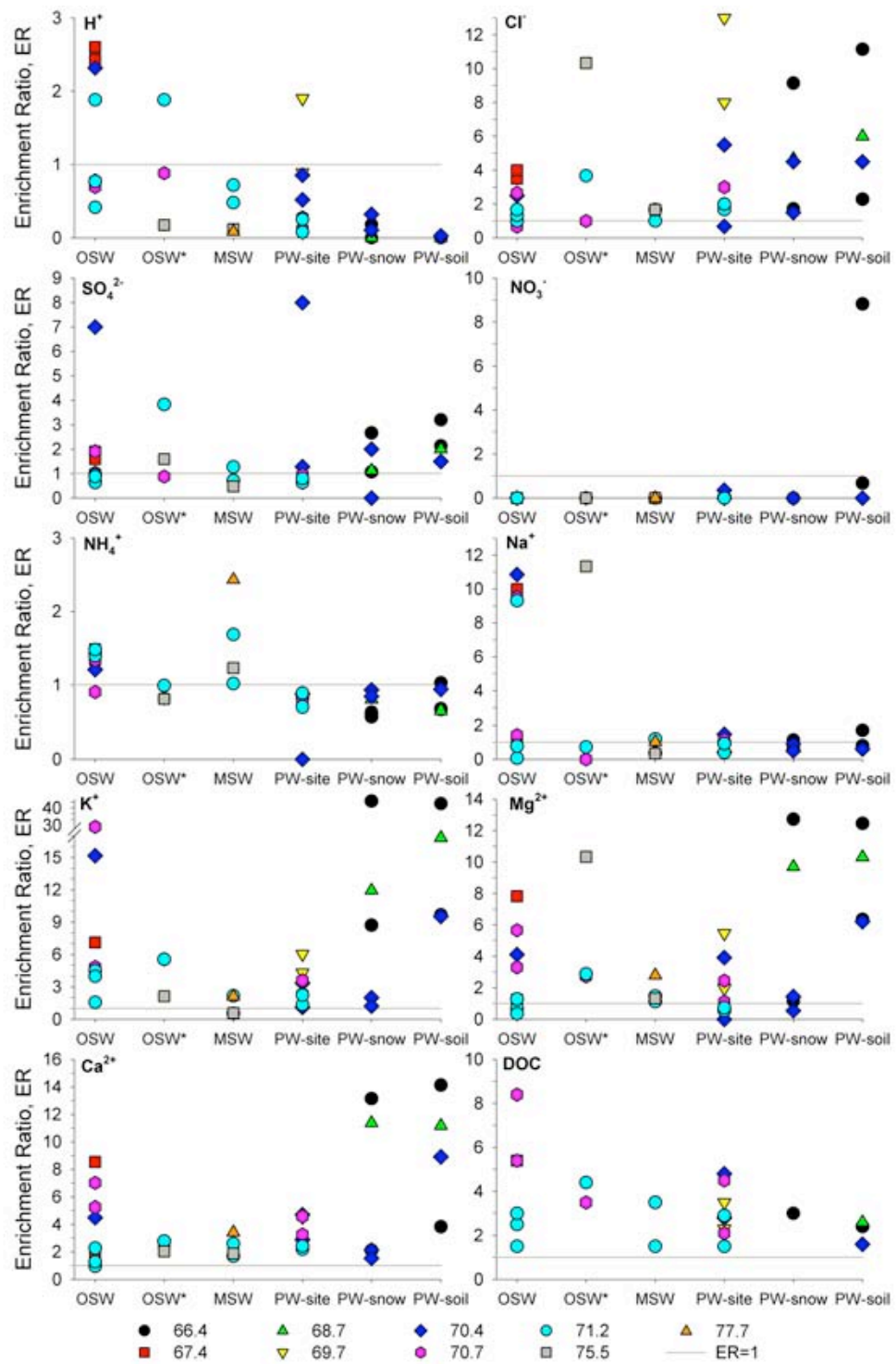
*Figure 7.9. Comparison of enrichment ratios, ER, for the samples collected at each site. The horizontal grey line represents ER=1.*

*Table 7.9. The percentage of ion ratios between runoff water (RW) and snowmelt water (SW) of all samples that were greater than 1 (ER>1), equal to 1 (ER=1), or less than 1 (ER<1). The highlighted areas illustrate the samples general trend for each ion.*

|       | $H^+$ | $Cl^-$ | $SO_4^{2-}$ | $NO_3^-$ | $NH_4^+$ | $Na^+$ | $K^+$ | $Mg^{2+}$ | $Ca^{2+}$ | DOC |
|-------|-------|--------|-------------|----------|----------|--------|-------|-----------|-----------|------|
| *ER>1* | 16% | 87% | 55% | 6% | 31% | 28% | 94% | 78% | 97% | 100% |
| *ER=1* | 9% | 10% | 23% | 0% | 28% | 22% | 0% | 6% | 3% | 0% |
| *ER<1* | 75% | 3% | 23% | 94% | 41% | 50% | 6% | 16% | 0% | 0% |
| *ER=0* | 0% | 0% | 3% | 91% | 0% | 3% | 0% | 0% | 0% | 0% |

samples was 0.7. The enrichment ratios for $Na^+$ were split in two ranges; a modest enrichment range from 0.0 to 1.7 for the majority of the samples (83%) and a much higher range from 9.3 to 11.2 for a few of the organic soil water samples. The average *ER* for all the samples was 2.2, largely controlled by the *ER* for the organic soil water; excluding the high enrichment ratios, average *ER* decreases to slightly less than 1.

There was no overall trend for $NH_4^+$; the organic soil water and mineral soil water were generally enriched, while the organic soil water collected at the overland flow site and the ponded waters were depleted. This was also reflected in the average enrichment of the samples, which was ~1.

The $NO_3^-$ concentration of most samples (91%) was less than the detection limit (0.1 meq m$^{-3}$). Only three samples of ponding water from the vicinity of the observation site contained detectable $NO_3^-$. Average *ER* was 0.3; a ratio that was largely controlled by these few samples.

The highest *ER$_{max}$* for individual ions varied among ions and site (Table 7.4). The organic soil water had the overall largest $H^+$ and $Na^+$ enrichment, 2.4 and $Na^+$ with 11.3, respectively. The mineral soil water had the largest $NH_4^+$ enrichment (2.4). The ponded water at the observation site had the largest $Cl^-$ and $SO_4^{2-}$ enrichments; 13.0 and 8.0, respectively. The ponded water in the vicinity of the observation site had largest enrichments for $NO_3^-$ (8.0), $K^+$ (43.9), $Mg^{2+}$ (12.7), and $Ca^{2+}$ (14.1); the differences in *ER$_{max}$* for the two sites were only marginal (≤1.5) compared to the other collection sites.

## 7.5   Flowpath Identification

In Chapter 6, chemical signatures for three unmixed flowpaths were evaluated. *Overland flow* (BI), which had sustained contact with a basal ice layer, showed a general enrichment in all ion concentrations with average enrichments ranging between 0.9 for $H^+$ and $K^+$ and 2.5 for $Na^+$ (Table 6.19). *Organic interflow* (OIF) was enriched in $H^+$, $Cl^-$, $NH_4^+$, and DOC, and depleted in $Mg^{2+}$; $NO_3^-$ concentrations, quickly became less than the detection limit. Average enrichments ranged between 0.2 for $NO_3^-$ and 11.3 for $K^+$. The third flowpath, *mineral interflow* (MIF), showed an enrichment of $Na^+$ and $Ca^{2+}$ and a depletion of $H^+$, $NO_3^-$, and $NH_4^+$, with average enrichments ranging between 0.7 for $NO_3^-$ and $NH_4^+$ and 10.9 for $Na^+$.

In nature, the flow pathway for snowmelt water may be more complex and runoff may consist of a mixture of several solutions. For example, (1) overland flow, which has been flowing across the surface of the ground (Figure 7.10, path a); (2) infiltration excess water, which has entered the soil at the top of the hillslope, but returned to the surface (exfiltrated) further down (path b); (3) interflow, which has infiltrated and exfiltrated several times on its way down the slope (path c), a combination of the previous flowpaths; and finally (4) exfiltration of groundwater, which originates from base flow. The latter kind is generally only important near the bottom of the slope.

Based on the change in chemical composition observed in the laboratory experiments (Chapter 6), if *ER* was >1 for all ions in the field samples, then the flowpath was assumed to be unmixed overland flow; if *ER* of $NO_3^-$ and $Mg^{2+}$ were <1,
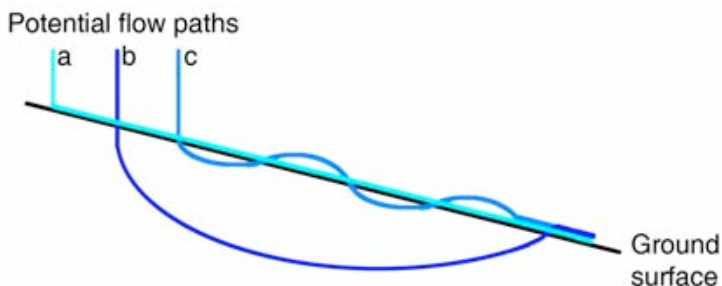


*Figure 7.10. An illustration of the different flowpaths that can contribute to the composition of surface runoff; (a) overland flow, (b) infiltration excess water and/or shallow subsurface flow, and (c) interflow, which infiltrates and exfiltrates continuously on its way down the slope.*

while the rest of the ratios were >1, then the flowpath was assumed to be unmixed organic interflow; and finally, if *ER* of $Na^+$ and $Ca^{2+}$ were >1 and <1 for $H^+$, the flowpath was assumed to be unmixed mineral interflow.

### 7.5.1  Flowpath Signatures

Approximately half of the field samples had compositional trends that were similar to at least one other sample; only five samples had a chemical trend, which was identical to at least one other sample. Three of these samples were collected from the organic layer; however, samples were collected at different sites and at different times (Table 7.10). The other two samples were of ponded water, collected in the vicinity of the slope; one sample was ponding on top of the snow, the other on top of the soil. For most samples the differences in signatures were only minor; often *ER* was 1 instead of either <1 or >1, or visa versa. However, none of the chemical signatures of the field samples matched those of the unmixed flowpaths perfectly.

For the unmixed organic interflow and mineral interflow, the most significant differences in *ER* were observed for $H^+$, $NO_3^-$, $NH_4^+$, $Mg^{2+}$, and $Ca^{2+}$. Three of these ions had opposite trends; $H^+$ and $NH_4^+$ were enriched in the organic interflow and depleted in the mineral interflow and $Mg^{2+}$ was depleted in the organic interflow and enriched in the mineral interflow. For $NO_3^-$ and $Ca^{2+}$, the mineral interflow had higher enrichments than the organic interflow (Table 6.19). Since most of the field samples had $NO_3^-$ concentrations less than the detection limit this ion proved inadequate for flowpath identification for these samples but illustrate the rapidity of denitrification by microbiological activity underneath a melting snowpack, as indicated by Jones (1999).

Focusing mainly on the behaviour of the four other ions revealed 15 samples,

*Table 7.10. Enrichment ratios, ER, for the sample with similar chemical trends.*

| Sample # | Julian Day | $H^+$ | $Cl^-$ | $SO_4^{2-}$ | $NO_3^-$ | $NH_4^+$ | $Na^+$ | $K^+$ | $Mg^{2+}$ | $Ca^{2+}$ | DOC |
|---|---|---|---|---|---|---|---|---|---|---|---|
| *PW-site (#3)* | 70.4 | 0.5 | 2.0 | 4.0 | 0.0 | 0.9 | 0.5 | 2.9 | 1.9 | 3.2 | 2.8 |
| *PW-soil (#D)* | 70.4 | 0.03 | 4.5 | 1.5 | 0.0 | 0.9 | 0.6 | 9.5 | 6.2 | 8.9 | 1.6 |
| *OSW (#2)* | 67.4 | 2.4 | 3.5 | 1.9 | 0.0 | 1.3 | 10.0 | 7.1 | 7.8 | 8.6 | 5.4 |
| *OSW (#3)* | 67.4 | 2.6 | 4.0 | 1.6 | 0.0 | 1.5 | 1.0 | 4.7 | 1.3 | 1.8 | 2.6 |
| *OSW (#1)* | 70.4 | 2.3 | 2.5 | 7.0 | 0.0 | 1.2 | 10.9 | 15.2 | 4.1 | 4.5 | - |

which could be interpreted as either unmixed organic interflow or unmixed mineral interflow (Table 7.11). Three samples' compositional change indicated an organic interflow origin; one was collected at the beginning of melt (JD 67) and two were collected shortly after the peak intensity of the rain-on-snow event (JD 71). They were all collected from the organic horizon. Only one of the samples had a signature that fully matched organic interflow. The two other samples only matched partially; one sample had an *ER* for $Mg^{2+}$ that resembled those of overland flow due to basal ice formation and the other had an *ER* for $H^+$ that was slightly too low, indicating that some buffering had occurred. However, neither of these deviations were significant enough to be caused by extensive contact with the mineral layer. The behaviour of the rest of the ions and DOC for these samples did not contradict the identification of the flowpaths as organic interflow.

Twelve samples had the signature of mineral interflow; the *ER* of $NO_3^-$ did not match the signature, however, most samples had concentrations below detection limits, indicating removal from the solution by microbial contact and/or contact with the organic layer. These samples consisted of two organic soil water samples, three samples of ponded water on the slope, and seven samples of ponded water in the vicinity of the observation site (Table 7.11). Most of these samples had $NO_3^-$ concentrations below detection limits, which was attributed to biological consumption due to a lack of inorganic N in the soil (e.g. Jones, 1991). This consumption may initiate within the snowpack once liquid water is present, which may explain the decrease in snowpack concentrations after a few days (Figure 7.6). Only three out of all 32 samples had detectable $NO_3^-$ present; two of which had a flowpath signature that could be assigned mineral interflow. The presence of $NO_3^-$ in these samples could be a result of a flowpath with limited contact with the organic layer while the soil was still frozen. The *ER* for the rest of the anions and cations displayed values for $Cl^-$ and $K^+$ of up to 12.1 and 43.9, respectively, and slightly depleted or *ER* ~1 for $Na^+$, which could indicate that some organic contact had taken place organic contact had taken place. Nevertheless, the high *ER* for $Mg^{2+}$ and $Ca^{2+}$ for all these samples indicate substantial contact with the mineral soil layer.

*Table 7.11. Enrichment ratios, ER, for the individual samples and associated flowpath. OIF refers to unmixed organic interflow, MIF refers to unmixed mineral interflow, and MIF\* indicates mixed mineral interflow.*

|  | Time | Site | $H^+$ | $NO_3^-$ | $NH_4^+$ | $Mg^{2+}$ | $Ca^{2+}$ | Flowpath |
|---|---|---|---|---|---|---|---|---|
| **OSW** | 67.4 | *#2* | 2.4 | depleted | 1.3 | 7.8 | 8.5 | **MIF\*** |
|  | 67.4 | *#3* | 2.6 | depleted | 1.5 | 1.3 | 1.8 | **OIF** |
|  | 70.4 | *#1* | 2.3 | – | 1.2 | 4.1 | 4.5 | **MIF\*** |
|  | 70.7 | *#1* | 0.8 | – | 1.3 | 5.7 | 7.0 | **MIF\*** |
|  | 70.7 | *#2* | 0.7 | – | 0.9 | 3.3 | 5.3 | **MIF** |
|  | 71.2 | *#1* | 0.8 | depleted | 1.4 | 0.7 | 1.0 | **OIF** |
|  | 71.2 | *#2* | 0.4 | depleted | 1.4 | 1.3 | 2.3 | **MIF\*** |
|  | 71.2 | *#3* | 1.9 | depleted | 1.5 | 0.4 | 1.3 | **OIF** |
| **OSW\*** | 70.7 | *#3* | 0.9 | – | 0.8 | 2.7 | 2.5 | **MIF\*** |
|  | 71.2 | *#3* | 1.9 | depleted | 1.0 | 2.9 | 2.8 | **MIF\*** |
|  | 75.4 | *#3* | 0.2 | depleted | 0.8 | 1.4 | 2.0 | **MIF** |
| **MSW** | 71.2 | *#2* | 0.7 | depleted | 1.7 | 1.5 | 2.6 | **MIF\*** |
|  | 71.2 | *#3* | 0.5 | depleted | 1.0 | 1.1 | 1.7 | **MIF\*** |
|  | 75.4 | *#3* | 0.1 | depleted | 1.2 | 1.3 | 1.9 | **MIF\*** |
|  | 77.7 | *#3* | 0.1 | depleted | 2.4 | 2.8 | 3.4 | **MIF\*** |
| **PW-site** | 69.4 | *#2* | 1.9 | depleted | 0.8 | 5.5 | 4.5 | **MIF\*** |
|  | 69.4 | *#3* | 0.9 | depleted | 0.8 | 2.0 | 2.6 | **MIF\*** |
|  | 70.4 | *#2* | 0.9 | – | 0.9 | 3.9 | 4.7 | **MIF\*** |
|  | 70.4 | *#3* | 0.5 | – | 0.9 | 1.9 | 3.2 | **MIF** |
|  | 70.7 | *#2* | 0.3 | – | 0.7 | 2.5 | 4.6 | **MIF** |
|  | 70.7 | *#3* | 0.1 | – | 0.8 | 1.1 | 3.3 | **MIF** |
|  | 71.2 | *#2* | 0.3 | depleted | 0.7 | 0.5 | 2.2 | **MIF\*** |
|  | 71.2 | *#3* | 0.1 | depleted | 0.9 | 0.7 | 2.4 | **MIF\*** |
| **PW-snow** | 66.4 | *#A* | 0.001 | 0.3 | 0.6 | 12.7 | 13.1 | **MIF** |
|  | 66.4 | *#B* | 0.2 | depleted | 0.6 | 1.2 | 2.1 | **MIF** |
|  | 68.4 | *#A* | 0.001 | depleted | 0.8 | 9.7 | 11.4 | **MIF** |
|  | 70.4 | *#A* | 0.1 | – | 0.9 | 0.6 | 2.1 | **MIF\*** |
|  | 70.4 | *#C* | 0.3 | enriched | 0.8 | 1.5 | 1.5 | **MIF\*** |
| **PW-soil** | 66.4 | *#D* | 0.0003 | 0.7 | 1.0 | 12.5 | 14.1 | **MIF** |
|  | 66.4 | *#E* | 0.01 | 8.8 | 0.7 | 6.3 | 3.8 | **MIF** |
|  | 68.4 | *#D* | 0.0008 | depleted | 0.7 | 10.3 | 11.2 | **MIF** |
|  | 70.4 | *#D* | 0.03 | – | 0.9 | 6.2 | 8.9 | **MIF** |

Orange color refers to *ER* similar to that in MIF. Green color refers to *ER* similar to that in OIF. No color refers to *ER* similar to that in BI. Depleted = RW concentration below detection limit; enriched = SW concentration below detection limit; and – = both RW and SW concentrations were below detection limits.

For most of the remaining samples (15 out of 17) the *ER* of $Ca^{2+}$ showed enriched conditions, indicating mineral soil contact. For nine of these samples, depletion in $H^+$ (*ER* <1) confirms that considerable contact with the mineral layer had taken place. However, for four samples the *ER* for $H^+$ was >1, indicating substantial contact with the organic layer, an observation that was supported by the enriched conditions of $NH_4^+$. Several of the samples showed enrichment or only slight depletion in $NH_4^+$. One of the ponded water samples was depleted in $H^+$ and $NH_4^+$ indicating mineral interflow, however, the *ER* for $Mg^{2+}$ and $Ca^{2+}$ implied that the flowpath had been organic interflow. Consequently, even though all these samples did not show immediately recognizable signatures, the hypothesized flowpath identification criteria's from Chapter 3 classify them all as mineral interflow. Thus, in Table 7.11 the asterisk (*) next to 'MIF' indicates that the flowpath for these samples were mixed.

One mineral soil water sample, collected on JD 71, did not show unambiguous evidence of originating from either of the flowpaths. Three of the ions had *ER* in the range for overland flow, one *ER* indicated organic interflow, and one indicated mineral interflow. The rest of the ions did not help identify the samples flowpath either. Consequently, since some contact with the organic layer and mineral soil had taken place, the sample's flowpath was marked as MIF* (Table 7.11).

Figure 7.11 shows a ternary diagram that compares the relative proportions between the enrichment ratios of $NH_4^+$, $Mg^{2+}$, and $Ca^{2+}$ for each of the field samples and their identified flowpaths (coloured symbols) to those of the unmixed flowpaths (open symbols). This kind of diagram eliminates any large changes that occur in the concentrations during melt since the proportions of the three elements are normalized to equal 1.0 (or 100%).

A distinct separation between the laboratory identified unmixed organic interflow (open circles) and the unmixed mineral interflow (open squares) can be observed in the plot, making these ions very useful for identification of similarities in the relative composition between samples as well as between flowpaths. The relative compositions of the overland flow due to basal ice formation (open triangles) plotted in-between the unmixed interflow paths. The relative composition of the field samples were plotted based on the flowpaths identified solely from their chemical signatures (Table 7.12).
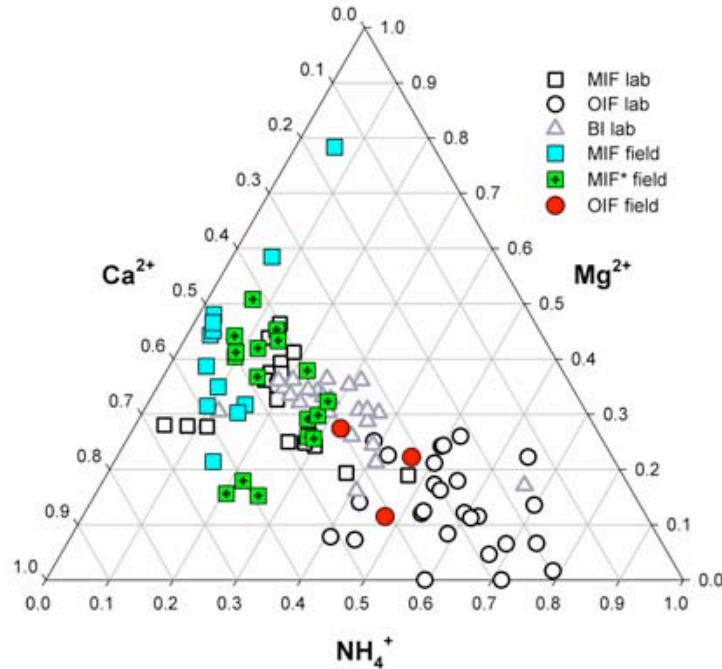
*Figure 7.11. Ternary diagram comparing the fractional percentages among $NH_4^+$, $Mg^{2+}$, and $Ca^{2+}$ for each of the unmixed flowpaths determined in the laboratory (open symbols) as well as the field samples identified flowpaths (coloured symbols).*

The agreement between the relative compositions of the unmixed organic and mineral interflow paths found in the laboratory and those observed in the field was striking. The three field samples that were identified as organic interflow based on their chemical signature showed distinctly greater relative proportion of $NH_4^+$ (>0.32) than the 12 samples identified at mineral interflow, whose relative proportion of $NH_4^+$ were <0.18.

The field samples, whose compositional signatures showed a mixed flowpath with extensive contact with both the organic layer and the mineral soil (MIF*), generally plotted in the area between the organic interflow and mineral interflow. The majority of these samples showed a relative composition that was close to those of the unmixed mineral interflow.

The other major ions did not show as distinct differences between the flowpaths' relative composition. This was believed to be partly due to the many undefined enrichment ratios as a result of concentrations less than detection limits for either the runoff water or meltwater. Subsequently, this indicates that the enrichment ratios of

$NH_4^+$, $Mg^{2+}$, and $Ca^{2+}$ are the ones best suited for flowpath identification based solely on the water sample's chemical composition.

### 7.5.2 Flowpath Development

A change in the flowpath was observed during snowmelt for the organic soil water, the ponded water on the slope, and the ponded water on top of the snow. There was no general tendency across all the sites, but rather a change at each collection site. Typically, the changes occurred during or following the rain-on-snow event.

A shift in the flowpath was observed at two of the organic soil water collection site (#1 and #2) as well as the overland flow installation (#3). At site #1, the flowpath shifted from mixed mineral interflow to organic interflow as $Mg^{2+}$ and $Ca^{2+}$ became less enriched during the rain-on-snow event. This could be a result of an increase in the flow rate of water released at the surface or that the lower part of the organic layer became saturated, limiting contact with the mineral soil surface. A change from a mixed mineral interflow to unmixed mineral interflow, back to mixed mineral interflow was observed at site #2; i.e. $H^+$ and $NH_4^+$ decreased and then $NH_4^+$ increased and finally, $Mg^{2+}$ decreased. At site #3, the organic soil water continued as organic interflow throughout melt. The organic water from the overland flow installation (OSW*) showed a shift from mixed to unmixed mineral interflow as the *ER* of $H^+$ decreased significantly. The first two samples were collected during the rain-on-snow event, whereas the third sample comprised of final part of the event as well as water from the following days. Thus, a reason for this shift could be that as soon as the rain ended the flux decreased, allowing infiltrating water to interact with the mineral soil along.

The ponded water on top of the snow showed the opposite trend of the organic soil water from the overland flow installation; the flowpath shifted from unmixed to mixed mineral interflow. This shift took place just prior to the rain-on-snow event and could be a result of dilution by the melting snow underneath. During the event the ponded water was most likely diluted directly by the rain.

A dilution of the ponded water on the slope caused the flowpath to change from mixed mineral interflow to unmixed mineral interflow and back again. The initial

change may have been caused by initial contact with the mineral soil layer; however, the ratios decreased during the rain-on-snow event, indicating that dilution took place.

The mineral soil water and the water ponded on top of the soil did not show any changes in flowpath as snowmelt progressed. The mineral soil water samples were all categorised as mixed mineral interflow due to the evidence of organic contact. Dilution of the waters occurred during the rain-on-snow event; i.e. *ER* for most ions decreased. *ER* increased for the last sample collected, which likely resulted from a longer contact time with the thawing soil. The samples of ponded water on top of the soil were all identified as unmixed mineral interflow, showing extensive contact with the mineral soil layer in form of high $Mg^{2+}$ and $Ca^{2+}$ ratios. These samples were collected close to the base of a long slope and could be comprised of exfiltrating water, which had had the opportunity of continuous contact with the mineral layer along the flowpath (path b in Figure 7.10).

## 7.6    Enhanced Infiltration

In Chapter 5 it was shown, both theoretically and in the laboratory, that enhanced infiltration occurs when partitioning of water at the mineral soil interface between infiltration and infiltration excess water occurs. Consequently, enhanced infiltration ought to take place in the field as well. In frozen ground, changes in ion concentrations along the flowpath will be also due to mixing with existing soil water and/or by dissolving dry fall-out (e.g. Stottlemyer and Toczydlowski, 1999; Weiler *et al.*, 1999) as interaction with the vegetation is limited below +5 ºC (Kimmins, 2004).

However, the shallow snowpack during the 2007 field season limited the ion fractionation within the snowpack (e.g. Bales *et al.*, 1989), preventing the examination of enhanced infiltration in the field. Nevertheless, a field study by Jones and Pomeroy (2001) revealed that as the extent of concrete frost increased so did the mass of infiltration excess water. This caused a change in routing of the meltwater, which resulted in dramatic changes in ion retention and release. The result was a correlation between considerable increases in stream water ion load as the percentage of concrete frost in the watershed increased. This implies that enhanced infiltration does take place

during infiltration to frozen ground and that it may be of great significance for the delivery of nutrients to the aquatic and terrestrial systems.

# CHAPTER 8

# CONCLUDING SUMMARY

Frozen ground underneath a melting snowpack will cause meltwater to either infiltrate the underlying stratum, run off, or pond. Ponding occurs when melt rates exceed infiltration rates and may result in the formation of a basal ice layer if there is sufficient heat flow into the soil. In areas with seasonally frozen ground or permafrost, infiltration excess water (runoff or ponding) often dominates during snowmelt.

The research presented here shows that frozen ground underneath a melting snowpack may not only alter the flowpath but also the ion load in runoff water. The presence of a basal ice layer causes all meltwater to run off and further ion concentration enrichment occurs. When no basal ice is present, enhanced infiltration causes a greater ion load to infiltrate frozen mineral soil leading to relative dilute runoff water. Consequently, basal ice formation has an important role in the disposition of snowmelt ions to the non-snow environment.

To evaluate the effect that meltwater chemistry may have on ecosystems, a better understanding of the alteration of chemical composition by flowpaths is important as this impacts nutrient and contamination delivery to the terrestrial and aquatic ecosystems. In addition, being able to infer the flowpath from chemical alterations can help to assess relative storage time, which is important to hydrograph response and has further hydrochemical impacts. In general, overland flow and organic interflow tend to contribute rapidly to streamflow whilst mineral interflow is more likely to replenish soil water reserves first.

During snowmelt, both the ion concentration of meltwater and the infiltration rate into frozen soil decrease rapidly; however, their temporal association is highly non-linear. Temporal covariance between meltwater ion concentration and infiltration rate must be compensated for in order to calculate the cumulative ion load infiltrating frozen

mineral soil using time-averaged values of these variables as time averaged ion concentrations and cumulative infiltration are much easier and more reliable to estimate than the instantaneous values. The covariance effect on infiltration of ions to frozen soil is labelled 'enhanced infiltration' and represents the additional ion load that infiltrates due to the timing of high meltwater ion concentration and infiltration rate.

A theoretical study, using relationships developed by Zhao and Gray (1999) and Stein *et al*. (1986) to estimate the cumulative ion load infiltrating unsaturated frozen soil, showed that the magnitude of enhanced infiltration is governed by initial snow water equivalent, average melt rate, and the meltwater ion concentration factor. Four demonstration sites, all located in western Canada, were used to evaluate the possible magnitude of enhanced ion infiltration due to covariance; a prairie site and a boreal forest site in Saskatchewan, a mountain forest site in Alberta, and a tundra site in the Yukon. The results showed the greatest impact of enhanced infiltration at the Tundra site; ranking the sites Tundra > Prairie > Boreal Forest > Mountain Forest. Infiltration excess ion load is the load of ions in runoff and ponded water that do not infiltrate. Enhanced infiltration reduces infiltration excess ion load and was greatest for the Prairie site and least for the Tundra site.

Three laboratory experiments were carried out on three soil columns each to assess whether enhanced infiltration could be recognized under controlled laboratory settings and to what extent its impact varies with initial soil moisture. The results showed that once partitioning of meltwater occurs, enhanced infiltration of ions take place. The magnitude of enhanced infiltration was greatest for saturated and near-saturated soils; decreasing with increasing initial soil moisture. Conversely, the impact of enhanced infiltration on infiltration excess ion load increased with increasing initial soil moisture; being greatest for the dry soil and least for the saturated soil.

The shallow snowpack during field observations of the 2007 snowmelt prevented identification of enhanced infiltration in the field. The literature shows ample evidence that enhanced infiltration takes place in nature and that it can be correlated to dramatic changes in ion retention and release observed in the ion load and concentration in snowmelt runoff over frozen soil.

Compositional changes in runoff water chemistry for three unmixed flowpaths were examined in a temperature-controlled cold room. The flowpaths were overland flow due to formation of a basal ice layer, organic interflow, and mineral interflow. The experiments simulated the melting of a warm snowpack, on top of a basal ice layer, a frozen forest organic layer, or a frozen forest mineral soil layer. Cooling from below ensured frozen conditions at the base throughout melt. A total of eight experiments were carried out, with variable initial snowpack density, melt rate, and temperature at the base of the snowpack. An enrichment ratio, defined as the ratio between the concentrations in the runoff water to that of the snow meltwater, was used to determine the change in chemical composition as meltwater came in contact with the base layers.

Results showed that it was possible to distinguish between the three flowpaths based on the chemical composition of the runoff water. Overland flow enriched ion concentrations due to ion exclusion during formation of the basal ice layer. The enrichment effect was most pronounced when a basal ice layer formed early in melt under relatively cold experimental conditions. Organic interflow increased the concentrations of $H^+$, $NH_4^+$, and DOC and depleted the concentrations of $Mg^{2+}$ and especially $NO_3^-$. Nitrate concentrations quickly dropped below measurable levels. Mineral interflow increased the concentrations of $Ca^{2+}$ and $Na^+$ and slightly decreased those of $H^+$, $NO_3^-$, and $NH_4^+$. All flowpaths rapidly caused a change in composition once contact with the underlying stratum had taken place. The alterations in ion concentrations were mainly controlled by initial moisture content in the organic and mineral soil layer and repeated flushes of meltwater through each interflow path, which caused a washout of ions. Similarly, ion concentrations were generally highest the first time meltwater was in contact with the organic layer or mineral soil.

By comparing the average enrichment ratios for the individual ions in each flowpath it was possible to identify ions whose concentrations had changed significantly as well as their relative relationship in-between flowpaths. Based on this it was possible to identify chemical signatures for each of these unmixed flowpaths. Overall, changes in ion concentrations were most significant for $H^+$, $NO_3^-$, $NH_4^+$, $Mg^{2+}$, and $Ca^{2+}$.

During snowmelt in spring 2007, water samples that had sustained contact with frozen unsaturated ground were collected at a forested observation site in the Marmot

Creek Research Basin, Alberta. Collection was carried out at seven sites that differed with respect to substrate and the presence of ponding or flowing surface water. A total of 32 samples were collected for interpretation of flowpath based on their chemical composition compared to the snowpack: 11 samples from the organic layer, four samples from the mineral soil, and 17 samples of water ponding on top of ice (5), organic material (4), and mineral soil (8).

The chemical signatures of the field samples were compared to those found in the laboratory for unmixed flowpaths. A ternary plot of the relative composition between the enrichment ratios of $NH_4^+$, $Mg^{2+}$, and $Ca^{2+}$ was found to be useful for distinguishing between the chemical signatures of organic interflow and mineral interflow.

The majority of the samples (~90%) showed that some contact with the mineral soil had taken place; high $Ca^{2+}$ and low $H^+$ concentrations indicated this. Half of these (12 samples) showed extensive contact with the mineral soil, identifying their flowpath as unmixed mineral interflow. The rest of these samples (17) showed interaction with the organic layer as well, indicating a more complex flowpath. The rapid response time between melt and sampling implies that this flowpath was along the interface between the organic and mineral soil layer. Merely three samples showed a chemical composition of unmixed organic interflow, whilst none had the signature of overland flow.

The field data presented focused on a single hillslope in the lower part of a watershed. Further experimentation is needed to obtain a better understanding of the impact of enhanced infiltration in nature. In order to generalize the flowpath for meltwater during spring melt, data from multiple sites and multiple years is needed as many watersheds show substantial year-to-year hydrological variability (e.g. Everett *et al.*, 1989). Ultimately, these results may contribute to interpreting the changes in the chemical composition of the stream water that can be observed during snowmelt. Since streamflow accumulates the compositional change of infiltration excess water within the watershed, knowledge of the major flowpath for individual parts of the watershed can help interpret these changes and identify contributing areas and runoff processes.

# REFERENCES

Abrahams PW, Tranter M, Davies TD, and Blackwood IL. 1989. Geochemical Studies in a Remote Scottish Upland Catchment. 2. Streamwater Chemistry during Snow-Melt. *Water Air and Soil Pollution* **43**: 231-248.

Alexeev GA, Kaljuzhny IJ, Kulik VYa, Pavlova KK, and Romanov VV. 1972. Infiltration of snowmelt water into frozen soil. *In: The role of snow and ice in hydrology, Symposia in Banff, Canada.* Anonymous 313-325.

Andersland OB, Wiggert DC, and Davies SH. 1996. Hydraulic conductivity of frozen granular soils. *Journal of Environmental Engineering* **122**: 212-216.

Anderson SP and Dietrich WE. 2001. Chemical weathering and runoff chemistry in a steep headwater catchment. *Hydrological Processes* **15**: 1791-1815. DOI: 10.1002/hyp.240.

Baker J. 2003. Water movement in frozen soil. *In: Encyclopedia of Water Science.* Ed: BA Stewart and TA Howell. Marcel Dekker, Inc., New York, NY, USA. 314-316.

Bales RC, Davis RE, and Stanley DA. 1989. Ion Elution through Shallow Homogeneous Snow. *Water Resources Research* **25**: 1869-1877.

Bales RC and Harrington RF. 1995. Recent Progress in Snow Hydrology. *Reviews of Geophysics* **33**: 1011-1020.

Barry R, Prevost M, Stein J, and Plamondon AP. 1990. Simulation of Snowmelt Runoff Pathways on the Lac Laflamme Watershed. *Journal of Hydrology* **113**: 103-121.

Beje GJ. 1969. *Soil of three experimental watersheds in Alberta and their hydrologic significance.* PhD thesis. Deptartment of Soil Science, University of Alberta. Edmonton, AB, Canada. p. 457.

Beven K and Germann P. 1982. Macropores and water flow in soils. *Water Resources Research* **18**: 1311-1325. DOI: 10.1029/WR018i005p01311.

Blackford JR, Jeffree CE, Noake DFJ, and Marmo BA. 2007. Microstructural evolution in sintered ice particles containing NaCl observed by low-temperature scanning electron microscope. *Proceedings of the I MECH E Part L Journal of Materials:Design and Applications* **221**: 151-156. DOI: 10.1243/14644207JMDA134.

Bodhinayake W, Si BC, and Noborio K. 2004. Determination of Hydraulic Properties in Sloping Landscapes from Tension and Double-Ring Infiltrometers. *Vadose Zone Journal* **3**: 964-970.

Bodhinayake WL. 2003. *Characterization of surface soil hydraulic properties in sloping landscapes.* M.Sc. thesis. Department of Soil Science, University of Saskatchewan. Saskatoon, SK, Canada. p. 162.

Borggaard OK and Elberling B. 2004. Weathering. *In: Pedological Biogeochemistry, part 1.* Anonymous Paritas Grafik, Brøndby, DK. Chapter 6. 277-323.

Bower H. 1986. Intake rate. Cylinder infiltrometer. *In: Methods of soil analysis.* Ed: A Klute. 2nd edition. ASA, Madison, WI, USA. Part 1: Physical and mineralogical properties. 825-843.

Brimblecombe P, Tranter M, Abrahams PW, Blackwood I, Davies TD, and Vincent CE. 1985. Relocation and preferential elution of acidic solute through the snowpack of a small, remote, high-altitude Scottish catchment. *Annals of Glaciology* **7**: 141-147.

Brimblecombe P, Tranter M, Tsiouris S, Davies TD, and Vincent CE. 1986. The Chemical Evolution of Snow and Meltwater. *In: Modelling snowmelt-induced processes.* Ed: EM Morris. (Proceedings of the Budapest Symposium, July 1986) edition. International Association Hydrological Sciences, Oxfordshire, UK. 155. 283-295.

Brown J, Ferrians OJJ, Heginbottom JA, and Melnikov ES. 1997. *International Permafrost Association Circum-Arctic Map of Permafrost and Ground Ice Conditions.* Scale 1:10,000,000. U.S. Geological Survey. USA.

Brown RD and Goodison BE. 2005. 159: Snow Cover. *In: Encyclopaedia of the Hydrological Sciences.* Ed: Malcolm G. Anderson and Jeffrey J. McDonnell. John Wiley and Sons, London, UK. 4. 2463-2473. DOI: 10.1002/0470848944.hsa165.

Burt TP and Williams PJ. 1976. Hydraulic conductivity in frozen soils. *Earth Surface Processes* **1**: 349-360.

Buttle JM and Peters DL. 1997. Inferring Hydrological Processes in a Temperate Basin Using Isotopic and Geochemical Hydrograph Separation: a Re-evaluation. *Hydrological Processes* **11**: 557-573. DOI: 10.1002/(SICI)1099-1085(199705)11:6<557::AID-HYP477>3.0.CO;2-Y.

Buttle JM, Vonk AM, and Taylor CH. 1995. Applicability of Isotopic Hydrograph Separation in a Suburban Basin during Snowmelt. *Hydrological Processes* **9**: 197-211.

Campbell DH, Muths E, Turk JT, and Corn PS. 2004. Sensitivity to acidification of subalpine ponds and lakes in north-western Colorado. *Hydrological Processes* **18**: 2817-2834.

Campbell Scientific. 2004. *TDR100 Instruction manual.* Campbell Scientific Inc., Revised: 11/04 edition. p. 56.

Campbell Scientific. 2007. *CR3000 Micrologger Operator's manual.* Campbell Scientific Inc., Revised: 09/07 edition. p. 330.

Carey SK and Woo MK. 2001. Slope runoff processes and flow generation in a subarctic, subalpine catchment. *Journal of Hydrology* **253**: 110-129.

Cary JW and Mayland HF. 1972. Salt and water movement in unsaturated frozen soil. *Soil Science Society of America Proceedings* **36**: 549-555.

Chandler DG, Seyfried M, Murdock M, and McNamara J. 2004. Field calibration of water content reflectometers. *Soil Science Society of America Journal* **68**: 1501-1507.

Christophersen N, Rustad S, Seip HM, Rosenqvist IT, Thrush BA, Sorensen NA, and Chester PF. 1984. Modelling Streamwater Chemistry with Snowmelt. *Philosophical Transactions of the Royal Society of London. Series B, Biological Sciences* **305**: 427-439.

Clapp RB and Hornberger GM. 1978. Empirical equations for some soil hydraulic properties. *Water Resources Research* **14**: 601-604.

Clow DW and Sueker JK. 2000. Relations between basin characteristics and stream water chemistry in alpine/subalpine basins in Rocky Mountain National Park, Colorado. *Water Resources Research* **36**: 49-62.

Colbeck SC. 1976. Analysis of Water-Flow in Dry Snow. *Water Resources Research* **12**: 523-527.

Colbeck SC. 1981. A simulation of the enrichment of atmospheric pollutants in snow cover runoff. *Water Resources Research* **17**: 1383-1388.

Colbeck SC. 1986. Classification of Seasonal Snow Cover Crystals. *Water Resources Research* **22**: 59S-70S.

Colbeck SC. 1987. Snow metamorphism and classification. *In: Seasonal snowcovers: Pysics, Chemistry, Hydrology.* Ed: H.G. Jones and W.J. Orville–Thomas. D. Reidel Publishing Company, NATO series. 1-35.

Colbeck SC, Akitaya E, Armstrong R, Gubler H, Lafeuille J, Lied K, McClung D, and Morris E. 1990. The international classification of seasonal snow on the ground. International Commission on Snow and Ice of the International Association of Scientific Hydrology. USA. p. pp. 23.

Colbeck SC and Davidson G. 1973. Water percolation through homogeneous snow. International Symposium: Role of snow and ice in hydrology. *IAHS publication* **107**: 242-257.

Cragin JH, Hewitt AD, and Colbeck SC. 1996. Grain-scale mechanisms influencing the elution of ions from snow. *Atmospheric Environment* **30**: 119-127.

Davies TD, Abrahams PW, Tranter M, Blackwood I, Brimblecombe P, and Vincent CE. 1984. Black acidic snow in the remote Scottish Highlands. *Nature* **312**: 58-61.

Davies TD, Brimblecombe P, Tranter M, Tsiouris S, Vincent CE, Abrahams P, and Blackwood IL. 1987. The removal of soluble ions from melting snowpacks. *In: Seasonal snowcovers: physics, chemistry, hydrology.* Ed: HG Jones and WJ Orville-Thomas. D. Reidel Publishing company, Dordrecht, Holland. 337-392.

Davies TD, Tranter M, Jickells TD, Abrahams PW, and Landsberger S. 1992. Heavily-Contaminated Snowfalls in the Remote Scottish Highlands: A Consequence of Regional-Scale Mixing and Transport. *Atmospheric Environment Part A: General Topics AEATEN* **26**: 95-112.

Davies TD, Vincent CE, and Brimblecombe P. 1982. Preferential elution of strong acids from a Norwegian ice cap. *Nature* **300**: 161-163. DOI: 10.1038/300161a0.

Davis RE. 1991. Links between snowpack physics and snowpack chemistry. *In: Seasonal snowpacks: Processes of compositional change.* Ed: Davies TD et al. Springer-Verlag, New York, USA. NATO ASI Series G 28. 116-138.

Dingman SL. 2002. Water in soils: infiltration and redistribution. *In: Physical hydrology.* Anonymous 2.ed edition. Prentice Hall, Inc., New Jersey. Chapter 6. 220-271.

Dominé F, Thibert E, Van Landeghem F, Silvente E, and Wagnon P. 1994. Diffusion and solubility of HCl in ice: preliminary results. *Geophysical Research Letters* **21**: 601-604.

Duysings JJHM, Verstraten JM, and Bruynzeel L. 1983. The Identification of Runoff Sources of a Forested Lowland Catchment - a Chemical and Statistical Approach. *Journal of Hydrology* **64**: 357-375.

Eaton AD and Franson MAH. 2005. *Standard methods for the examination of water & wastewater.* American Public Health Association, Washington, DC, USA. 21st edition.

Elrick DE, Reynolds WD, and Tan KA. 1989. Hydraulic conductivity measurements in the unsaturated zone using improved well analyses. *Ground water Monitoring review* **9**: 184-193.

Engelmark H. 1984. Infiltration in unsaturated frozen soil. *Nordic Hydrology* **15**: 243-252.

Espeby B. 1990. Tracing the Origin of Natural-Waters in a Glacial Till Slope during Snowmelt. *Journal of Hydrology* **118**: 107-127.

Everett KR, Marion GM, and Kane DL. 1989. Seasonal Geochemistry of an Arctic Tundra Drainage-Basin. *Holarctic Ecology* **12**: 279-289.

Evett SR. 2003. Soil water measurement by time domain reflectometry. *In: Encyclopedia of Water Science.* Ed: BA Stewart and TA Howell. Marcel Dekker, Inc., New York, USA. 894-898.

Ferner SJ. 1984. *A comparison of techniques used for estimating melt rates for application to the SSARR model.* M.Sc. thesis. Department of Civil Engineering, University of Saskatchewan. Saskatoon, SK, Canada.

Fetter CW. 1994. *Applied hydrology.* Prentice Hall, Upper Saddle River, New Jersey, USA. 4th edition. p. 598.

Fishman MJ and Friedman LC. 1989. Methods for determination of inorganic substances in water and fluvial sediments. *In: Techniques of Water-Resources Investigations of the United States Geological Survey.* Ed: MJ Fishman and LC Friedman. 3rd edition. United States Geological Survey, USA. Chapter A1. Book 5 - Laboratory Analysis. 466.

Fitzhugh RD, Likens GE, Driscoll CT, Mitchell MJ, Goffman PM, Fahey TJ, and Hardy JP. 2003. Role of soil freezing events in interannual patterns of stream chemistry at the Hubbard Brook Experimental Forest, New Hampshire. *Environmental Science Technology* **37**: 1575-1580.

Frazer GW, Canham CD, and Lertzman KP. 1999. *Gap Light Analyzer (GLA): Imaging software to extract canopy structure and gap light transmission indices from true-colour fisheye photographs, users manual and program documentation.* Simon Fraser University, Burnaby, British Columbia, and the Institute of Ecosystem Studies, Millbrook, New York, p. 40.

Freeze RA and Cherry JA. 1978. *Groundwater.* Prentice Hall, New Jersey, USA. p. 604.

French HK, van der Zee, S.E.A.T.M., and Leijnse A. 1999. Differences in gravity-dominated unsaturated flow during autumn rains and snowmelt. *Hydrological Processes* **13**: 2783-2800.

Gale RM. 1964. Surface water quality in the Marmot Creek project basin – a progress report for the period April – September 1964 inclusive. Department of Mines and technical surveys, Mines branch. Ottawa, ON, Canada.

Gale RM. 1965. Surface water quality in the Marmot Creek test basin – a progress report for the period October 1964 – September 1965 inclusive. Department of Mines and technical surveys, Mines branch. Ottawa, ON, Canada.

Gale RM. 1966. Chemical quality of surface and ground waters in Marmot Creek Experimental Basin, an international hydrologic decade (IHD) project/progress report for the period October 1965 to September 1966, inclusive. Department of Energy, Mines and Resources, Inland waters branch. Ottawa, ON, Canada.

George BH. 1999. *Comparison of techniques for measuring the water content of soil and other porous media.* Master's thesis, Dept. of agri. chem. and soil Sci., Uni. of Sydney, Australia.

Golding DL and Hillman GR. 1981. Forest floor characteristics of Marmot and Streeter experimental watersheds, Alberta. *Information report no. NOR-X-234.* Department of the Environmental Canadian Forestry Service, Northern Forest Research Centre. Canada. p. 22.

Granger RJ, Gray DM, and Dyck GE. 1984. Snowmelt Infiltration to Frozen Prairie Soils. *Canadian Journal of Earth Sciences* **23**: 669-677.

Grant SA. 2000. Physical and chemical factors affecting contaminant hydrology in cold environments. *ERDC/CRREL TR-00-21.* Cold Regions Research and Engineering Lab, Experimental Engineering Division. Hanover, NH, USA. p. 37.

Gray DM, Granger RJ, and Dyck GE. 1985a. Overwinter Soil Moisture Changes. *Transactions of the American Society of Agricultural Engineers* **28**: 442-447.

Gray DM, Landine PG, and Granger RJ. 1985b. Simulating infiltration into frozen prairie soils in stream flow models. *Canadian Journal of Earth Sciences* **22**: 464-474.

Gray DM, Norum DI, and Wigham JM. 1970. Infiltration and the physics of flow of water through porous media. *In: Handbook on the Principles of Hydrology.* Ed: DM Gray. Canadian National Committee of the International Hydrological Decade, Ottawa, Ontario, Canada. Chapter 5. V.1-V.58.

Gray DM, Toth B, Zhao LT, Pomeroy JW, and Granger RJ. 2001. Estimating areal snowmelt infiltration into frozen soils. *Hydrological Processes* **15**: 3095-3111.

Grimaldi C, Grimaldi M, Millet A, Bariac T, and Boulègue J. 2004. Behaviour of chemical solutes during a storm in a rainforested headwater catchment. *Hydrological Processes* **18**: 93-106. DOI: 10.1002/hyp.1314.

Groisman PY and Davies TD. 2001. Snow cover and the climate system. *In: Snow Ecology - an interdisciplinary examination of snow-covered ecosystems.* Ed: HG Jones *et al*. Cambridge University Press, USA. Chapter 1. 1-44.

Harrington RF, Bales RC, and Wagnon P. 1996. Variability of meltwater and solute fluxes from homogeneous melting snow at the laboratory scale. *Hydrological Processes* **109**: 945-953.

Havlin, J.L., J.D. Beaton, S.L. Tisdale, and W.L. Nelson. 1999. *Soil fertility and fertilizers: An introduction to nutrient management*. 6th ed. Prentice Hall, Upper Saddle River, NJ, USA.

Helliwell RC, Soulsby C, Ferrier RC, Jenkins A, and Harriman R. 1998. Influence of snow on the hydrology and hydrochemistry of the Allt a' Mharcaidh, Cairngorm mountains, Scotland. *Science of the Total Environment* **217**: 59-70.

Hillel D. 1998. *Environmental Soil Physics.* Academic Press, New York, USA. p. 771.

Hiscock K. 2005. *Hydrology: principles and practice.* Blackwell Publishing, Malden, Massachusetts, USA. p. 389.

Hoeg S, Uhlenbrook S, and Leibundgut C. 2000. Hydrograph separation in a mountainous catchment - combining hydrochemical and isotopic tracers. *Hydrological Processes* **14**: 1199-1216.

Horiguchi K and Miller RD. 1980. Experimental studies with frozen soil in an ice sandwich permeameter. *Cold Regions Science and Technology* **3**: 177-183.

Iida T, Ueki K, Tsukahara H, and Kajihara A. 2000. Point physical model of movement of ions through natural snow cover. *Journal of Hydrology* **235**: 170-182.

Ikuta K, Yada T, Kitamura S, Branch N, Ito F, Yamagichi M, Nishimura T, Kaneko T, Nagae M, Ishimatsu A, and Iwata M. 1999. Effects of acidification on fish reproduction. *UJNR Technical Report* **No. 28**: 39-45.

Jaesche P, Veit H, and Huwe B. 2003. Snow cover and soil moisture controls on solifluction in an area of seasonal frost, Eastern Alps. *Permafrost and Periglacial Processes* **14**: 339-410.

Jame YW. 1972. *Temperature effects on phase composition of a partially frozen soil.* M.Sc. University of Saskatchewan. Saskatoon, Saskatchewan, Canada.

Johannessen M and Henriksen A. 1978. Chemistry of snow meltwater: Changes in ion concentration during melting. *Water Resources Research* **14**: 615-619.

Jones HG. 1985. The chemistry of snow and meltwaters within the mesostructure of a boreal forest snow cover. *Annals of Glaciology* **7**: 161-166.

Jones HG. 1999. The ecology of snow-covered systems: a brief overview of nutrient cycling and life in the cold. *Hydrological Processes* **13**: 2135-2147.

Jones HG and Pomeroy JW. 2001. Early spring snowmelt in a small boreal forest watershed: influence of concrete frost on the hydrology and chemical composition of streamwaters during rain-on-snow events. *Proceedings of the Eastern Snow Conference, Ottawa, Ontario, Canada* **58**: 209-218.

Jones HG, Tranter M, and Davies TD. 1989. Leaching of Strong Acid Anions from Snow during Rain-on-Snow Events: Evidence for Two Component Mixing. *In: Atmospheric Deposition. Proceedings of a Symposium held during the Third Scientific Assembly of the International Association of Hydrological Sciences at Baltimore, Maryland May 1989.* Anonymous IAHS Publication, 179. 239-250.

Kachinskiy NA. 1927. Freezing, thawing and moisture content of the soil in the winter season in the forest and in open areas. *(In: Kuznik and Bezmenov 1963)*

Kahimba FC and Ranjan RS. 2007. Soil temperature correction of field TDR readings obtained under near freezing conditions. *Canadian Biosystems Engineering* **49**: 1.19-1.26.

Kane DL and Stein J. 1983. Water movement into seasonally frozen soils. *Water Resources Research* **19**: 1547-1557.

Kattlemann R. 1986. Measurements of snow layer water retention. *Proceedings of the Symposium: Cold region hydrology symposium, American Water Resources Association, Fairbanks, Alaska 1986* : 377-386.

Kimmins JP. 2004. *Forest ecology - a foundation for sustainable forest management and environmental ethics in forestry.* Prentice Hall, Upper Saddle River, NJ, USA. 3rd edition. p. 611.

Kirby CL and Ogilvie RT. 1969. The forests of Marmot Creek watershed research basin. *Report no. 1259.* Department of Fisheries and Forestry, Forest Research Branch. Canada. p. 37.

Kirkby M. 1988. Hillslope runoff processes and models. *Journal of Hydrology* **100**: 315-339. DOI: 10.1016/0022-1694(88)90190-4.

Komarov VD and Makarova TT. 1973. Effect of the ice content, temperature, cementation, and freezing depth of the soil on meltwater infiltration in a basin. *Soviet hydrology: selected papers* **3**: 243-249.

Kuznik LA and Bezmenov AL. 1963. Infiltration of meltwater into frozen soil. *Soviet Soil Science* **6**: 665-674.

LaChapelle ER. 1969. *Field guide to snow crystals.* University of Washington Press, USA. p. 101.

Langham EJ. 1981. Physics and properties of snow cover. *In: Handbook of Snow: Principles, Processes, Management & Use.* Ed: D.M. Gray and D.H. Male. Pergamon Press, USA. Chapter 7. 275-337.

Laudon H, Westling O, and Bishop K. 2000. Cause of pH decline in stream water during spring melt runoff in northern Sweden. *Canadian Journal of Fisheries and Aquatic Sciences* **57**: 1888-1900.

Ledieu J, De Ridder P, De Clerck P, and Dautrebande S. 1986. A method of measuring soil moisture by time-domain reflectometry. *Journal of hydrology* **88**: 319-328.

Leivestad H and Muniz IP. 1976. Fish kill at low pH in a Norwegian river. *Nature* **259**: 391-392.

Levitt DG and Young MH. 2008. Soils: Hygroscopic Water Content. *In: Encyclopedia of Water Science.* Ed: SW Trimble *et al*. 2nd edition. CRC Press, USA. 1136-1139. DOI: 10.1081/E-EWS2-120010269.

Lewkowicz AG and French HM. 1982. Downslope water movement and solute concentrations within the active layer, Banks Island, N.W.T. *Proceedings Fourth Canadian Permafrost Conference Calgary, Alberta. Reprint from The Roger J.E. Brown Memorial Volume. National Research Council of Canada.*

Lin W and Gray DM. 1971. Physical simulation of infiltration equations. *Water Resources Research* **7**: 1234-1240.

Lindström G, Bishop K, and Löfvenius MO. 2002. Soil frost and runoff at Svartberget, northern Sweden – measurements and model analysis. *Hydrological Processes* **16**: 3379-3392.

Male DH and Gray DM. 1981. Snowcover ablation and runoff. *In: Handbook of snow – principles, processes, management and use.* Ed: DM Gray and DH Male. Pergamon Press, UK, Chapter 9. 360-436.

Marsh P. 1991. Water flux in melting snow covers. *In: Advances in porous media.* Ed: MY Corapcioglu. Elsevier, Amsterdam, Holland. Chapter 2. 1. 61-124.

Marsh P. 2005. Water flow through snow and firn. *In: Encyclopaedia of Hydrological Sciences.* Ed: MG Anderson and JJ McDonnell. John Wiley and Co., London, UK. Chapter 161. Book 4. 2491-2504. DOI: 10.1002/0470848944.hsa167.

Marsh P and Pomeroy JW. 1999. Spatial and temporal variations in snowmelt runoff chemistry, Northwest Territories, Canada. *Water Resources Research* **35**: 1559-1567.

Marsh P and Woo MK. 1984a. Wetting front advance and freezing of meltwater within a snow cover; 1. Observations in the Canadian Arctic. *Water Resources Research* **20**: 1853-1864.

Marsh P and Woo MK. 1984b. Wetting front advance and freezing of meltwater within a snow cover: 2. A simulation model. *Water Resources Research* **20**: 1865-1874.

Masterton WL and Hurley CN. 1997. *Chemistry: Principles and Reactions: a Core Text.* Saunders College Publishing, USA. 3rd edition. p. 640+.

Maulé CP and Stein J. 1990. Hydrologic flow path definition and partitioning of spring meltwater. *Water Resources Research* **26**: 2959-2970.

Maupetit F and Davies TD. 1991. Discussion on "Chemical composition and fluxes of wet deposition at elevated sites (700-3105 masl) in the eastern Alps". *In: Seasonal snowpacks: Processes of compositional change.* Ed: Davies TD et al. Springer-Verlag, New York, USA. NATO ASI Series G 28. 299-301.

McCartney SE, Carey SK, and Pomeroy JW. 2006. Intra-basin variability of snowmelt water balance calculations in a subarctic catchment. *Hydrological Processes* **20**: 1001-1016.

McEachern P, Prepas EE, and Chanasyk DS. 2006. Landscape control of water chemistry in northern boreal streams of Alberta. *Journal of Hydrology* **323**: 303-324. DOI: 10.1016/j.jhydrol.2005.09.016.

Meijer A. 2002. Conceptual model of the controls on natural water chemistry at Yucca Mountain, Nevada. *Applied Geochemistry* **17**: 793-805.

Mertens J, Jacques D, Vanderborght J, and Feyen J. 2002. Characterisation of the field-saturated hydraulic conductivity on a hillslope: in situ single ring pressure infiltrometer measurements. *Journal of Hydrology* **263**: 217-229.

Meybeck M, Peters NE, and Chapman DV. 2005. Water Quality. *In: Encyclopedia of Hydrological Sciences.* Ed: MG Anderson and JJ McDonnell. John Wiley & Sons, Inc., New York, USA. 112. 3. 1719-1732. DOI: 10.1002/0470848944.hsa093.

Motovilov YG. 1978. Mathematical model of water infiltration into frozen soil. *Soviet hydrology: selected papers* **17**: 62-66.

Murray CD and Buttle JM. 2005. Infiltration and soil water mixing on forested and harvested slopes during spring snowmelt, Turkey Lakes Watershed, central Ontario. *Journal of Hydrology* **306**: 1-20.

Nyberg L, Stähli M, Mellander P-E, and Bishop KH. 2001. Soil frost effects on soil water and runoff dynamics along a boreal forest transect: 1. Field investigations. *Hydrological Processes* **15**: 909-926.

Obradovic MM and Sklash MG. 1986. An Isotopic and Geochemical Study of Snowmelt Runoff in a Small Arctic Watershed. *Hydrological Processes* **1**: 15-30.

Ollier C. 1975. Weathering. Ed: KM Clayton. Longman Publishing Group, London, England. Text 2. Geomorphology. 304.

Osokin NI, Samoylov RS, Sosnovskiy AV, Sokratov SA, and Zhidkov VA. 2000. Model of the influence of snow cover on soil freezing. *Annals of Glaciology* **31**: 417-421.

Peters NE and Driscoll CT. 1987. Hydrogeologic Controls of Surface-Water Chemistry in the Adirondack Region of New-York-State. *Biogeochemistry* **3**: 163-180.

Peters NE and Driscoll CT. 1989. Temporal variations in solute concentrations of meltwater and forest floor leachate at a forested site in the Adirondacks, New York. *Proceedings of 46th Eastern Snow Conference* Quebec City, Quebec, Canada: 45-56.

Pfeffer WT and Humphrey NF. 1996. Determination of timing and location of water movement and ice-layer formation by temperature measurements in sub-freezing snow. *Journal of Glaciology* **42**: 292-304.

Pfeffer WT, Illangasekare TH, and Meier MF. 1990. Analysis and modeling of melt-water refreezing in dry snow. *Journal of Glaciology* **36**: 238-246.

Philip JR. 1991. Hillslope infiltration: planar slopes. *Water Resources Research* **27**: 109-117.

Pinay G and Naiman RJ. 1991. Short-term hydrologic variations and nitrogen dynamics in beaver created meadows. *Archiv für Hydrobiologie* **123**: 187-205.

Pomeroy JW, Bewley DS, Essery RLH, Hedstrom NR, Link T, Granger RJ, Sicart JE, Ellis CR, and Janowicz JR. 2006. Shrub tundra snowmelt. *Hydrological Processes* **20**: 923-941. DOI: 10.1002/hyp.6124.

Pomeroy JW and Brun E. 2001. Physical properties of snow. *In: Snow Ecology – an interdisciplinary examination of snow-covered ecosystems.* Ed: HG Jones *et al*. Cambride University Press, USA. Chapter 2. 45-126.

Pomeroy JW, Davies TD, Jones HG, Marsh P, Peters NE, and Tranter M. 1999. Transformations of snow chemistry in the boreal forest: accumulation and volatilization. *Hydrological Processes* **13**: 2257-2273.

Pomeroy JW, Granger RJ, Pietroniro A, Elliott JE, Toth B, and Hedstrom N. 1997. Hydrological pathways in the Prince Albert Model Forest. *NHRI Contribution Series No. CS-97004.* Hydrological & Aquatic Sciences Division, National Hydrology Research Institute, Environment Canada. Saskatoon, Saskatchewan, Canada. p. 154 + appendices.

Price AG, Hendrie LK, and Dunne T. 1978. Controls on the production of snowmelt runoff. *In: Modeling of snow cover runoff. Proceedings from Hanover, New Hampshire, USA, 26-28 September 1978.* Ed: SC Colbeck and M Ray. US Army Cold Regions Research and Engineering Laboratory, Hanover, NH, USA. 257-268.

Quinton WL and Pomeroy JW. 2006. Transformations of runoff chemistry in the Arctic tundra, Northwest Territories, Canada. *Hydrological Processes* **20**: 2901-2919. DOI: 10.1002/hyp.6083.

Quinton WL, Shirazi T, Carey SK, and Pomeroy JW. 2005. Soil water storage and active-layer development in a sub-alpine tundra hillslope, southern Yukon Territory, Canada. *Permafrost and Periglacial Processes* **16**: 369-382. DOI: 10.1002/ppp.543.

Rascher CM, Driscoll CT, and Peters NE. 1987. Concentration and Flux of Solutes from Snow and Forest Floor during Snowmelt in the West-Central Adirondack Region of New-York. *Biogeochemistry* **3**: 209-224

Reynolds WD, Elrick DE, and Youngs EG. 2002. The soil solution phase. Single-ring and double- or concentric ring infiltrometers. *In: Methods of Soil Analysis. Part 4. Physical Methods.* Ed: JH Dane and GC Topp. Soil Science Society of America Inc., Madison, WI, USA. 821-826.

Roberge J and Plamondon AP. 1987. Snowmelt runoff pathways in a boreal forest hillslope, the role of pipe throughflow. *Journal of Hydrology* **95**: 39-54.

Romanov VV, Pavlova KK, and Kalyuzhnyy IL. 1974. Meltwater losses through infiltration into podzolic soils and chernozems. *Soviet hydrology: selected papers* **1**: 32-42.

Sauer TJ and Logsdon SD. 2002. Hydraulic and Physical Properties of Stony Soils in a Small Watershed. *Soil Science Society of America Journal* **66**: 1947-1956.

Schemenauer RS, Berry MO, and Maxwell JB. 1981. Snowfall formation. *In: Handbook of snow – principles, processes, management and use.* Ed: DM Gray and DH Male. Pergamon Press, Chapter 4. 129-152.

Schindler D. 1999. From acid rain to toxic snow. *Ambio* **28**: 350-355.

Schöndorf T and Herrmann R. 1987. Transport and Chemodynamics of Organic Micropollutants and Ions during Snowmelt. *Nordic Hydrology* **18**: 259-278.

Seligman G. 1936. *Snow structures and ski fields.* Macmillan, London, England.

Shanley JB and Chalmers A. 1999. The effect of frozen soil on snowmelt runoff at Sleepers River, Vermont. *Hydrological Processes* **13**: 1843-1857.

Shanley JB, Kendall C, Smith TE, Wolock DM, and McDonnell JJ. 2002. Controls on old and new water contributions to stream flow at some nested catchments in Vermont, USA. *Hydrological Processes* **16**: 589-609.

Smith EJ and Haymet ADJ. 2004. Ion Solubility in Ice: Calculation of Potentially Favorable Positions of CI- and Na+ Ions in the SPC. *Molecular Simulations* **30**: 827-830. DOI: 10.1080/08927020410001709325.

Stähli M, Nyberg L, Mellander P-E, and Bishop KH. 2001. Soil frost effects on soil water and runoff dynamics along a boreal forest transect: 2. Simulations. *Hydrological Processes* **15**: 927-941.

Stein J, Jones HG, Roberge J, and Sochanska W. 1986. The prediction of both runoff quality and quantity by the use of an integrated snowmelt model. *IAHS Publication* **155**: 347-358.

Stein J, Proulx S, and Levesque D. 1994. Forest floor frost dynamics during spring snowmelt in a boreal forested basin. *Water Resources Research* **30**: 995-1007.

Stevenson DR. 1967. *Geological and groundwater investigations in the Marmot Creek Experimental Basin of Southwestern Alberta.* M.Sc. Thesis. University of Alberta. Edmonton, AB, Canada. p. 106.

Storr D. 1967. Precipitation variations in a small forested watershed. *Proceedings of the Annual Western Snow Conference* **35**: 11-17.

Stottlemyer R and Toczydlowski D. 1999. Seasonal change in precipitation, snowpack, snowmelt, soil water, and stream water chemistry, northern Michigan. *Hydrological Processes* **13**: 2215-2231.

Stottlemyer R, Troendle CA, and Markowitz D. 1997. Change in snowpack, soil water, and streamwater chemistry with elevation during 1990, Fraser Experimental Forest, Colorado. *Journal of Hydrology* **195**: 114-136.

Sugimoto A, Naito D, Yanagisawa N, Ichiyanagi K, Kurita N, Kubota J, Kotake T, Ohata T, Maximov TC, and Fedorov AN. 2003. Characteristics of soil moisture in permafrost observed in East Siberian taiga with stable isotopes of water. *Hydrological Processes* **17**: 1073-1092. DOI: 10.1002/hyp.1180.

Swanson RH, Golding DL, Rothwell RL, and Bernier PY. 1986. Hydrologic effects of clear-cutting at Marmot Creek and Streeter Watersheds, Alberta. *Information report NOR-X-278.* Northern forestry centre, Canadian forestry service. Canada.

Tao Y and Gray DM. 1994. Prediction of snowmelt infiltration into frozen soils. *Numerical heat transfer. part A* **26**: 643-665.

Taylor S, Feng X, Williams M, and McNamara J. 2002. How isotopic fractionation of snowmelt affects hydrograph separation. *Hydrological Processes* **16**: 3683-3690.

Technicon. 1972. Nitrate & Nitrite in Water and Seawater. *Industrial method No. 158-71W/tentative (Dec.).* Technicon AutoAnalyzer II. USA.

Technicon. 1973. Ammonia in Water and Seawater. *Industrial method No. 154-71W (Feb.).* Technicon AutoAnalyzer II. USA.

Thomas JFJ. 1963. Surface water quality in the Marmot Creek project basin – a process report for the period May–September, 1963. Department of Mines and technical surveys, Mines branch. Ottawa, ON, Canada.

Topp GC, Davis JL, and Annan AP. 1980. Electromagnetic determination of soil water content: measurements in coaxial transmission lines. *Water Resources Research* **16**: 574-582.

Topp GC and Reynolds WD. 1998. Time domain reflectometry: a seminal technique for measuring mass and energy in soil. *Soil & Tillage Research* **47**: 125-132.

Tranter M. 1991. Controls on the composition of snowmelt. *In: Seasonal snowpacks: Processes of compositional change.* Ed: Davies TD et al. Springer-Verlag, New York, USA. NATO ASI Series G 28. 241-271.

Tranter M, Brimblecombe P, Davies TD, Vincent CE, Abrahams PW, and Blackwood IL. 1986. The Composition of Snowfall, Snowpack and Meltwater in the Scottish Highlands - Evidence for Preferential Elution. *Atmospheric Environment* **20**: 517-525.

Tranter M, Davies TD, Wigington PJ, and Eshleman KN. 1994. Episodic Acidification of Fresh-Water Systems in Canada - Physical and Geochemical Processes. *Water Air and Soil Pollution* **72**: 19-39.

Tranter M and Jones HG. 2001. The chemistry of snow: processes and nutrient cycling. *In: Snow Ecology – an interdisciplinary examination of snow-covered ecosystems.* Ed: HG Jones *et al*. Cambridge University Press, USA. Chapter 3. 127-167.

Tsiouris S, Vincent CE, Davies TD, and Brimblecombe P. 1985. The Elution of Ions Through Field and Laboratory Snowpacks. *Annals of Glaciology* **7**: 196-201.

UNEP/GRID-Arendal. 2007. Permafrost extent in the Northern Hemisphere. (June 2007). UNEP/GRID-Arendal Maps and Graphics Library. Retrieved April 21, 2008 from http://maps.grida.no/go/graphic/permafrost-extent-in-the-northern-hemisphere. URL: (Based on: Brown et al., 1997)

USDA. 1993. *Soil survey manual.* Soil Survey Division Staff. Soil Conservation Service, USA.

USEPA. 1995. Acid Deposition Standard Feasibility Study Report to Congress. *EPA 430-R-001a.* Office of Air and Radiation; Agency, E.P. USA.

van der Kamp G, Hayashi M, and Gallén D. 2003. Comparing the hydrology of grassed and cultivated catchments in the semi-arid Canadian prairies. *Hydrological Processes* **17**: 559-575. DOI: 10.1002/hyp.1157.

van Everdingen R. 1998. *Multi-language glossary of permafrost and related ground-ice terms.* National Snow and Ice Data Center/World Data Center for Glaciology, Boulder, CO, USA. revised 2005 edition.

Wakahama G, Kuroiwa D, Hasemi T, and Benson CS. 1976. Field observations and experimental and theoretical studies on the superimposed ice of McCall Glacier, Alaska. *Journal of Glaciology* **16**: 135-149.

Waldner PA, Schneebeli M, Schultze-Zimmermann U, and Fluehler H. 2004. Effect of snow structure on water flow and solute transport. *Hydrological Processes* **18**: 1271-1290. DOI: 10.1002/hyp.1401.

Wallach R, Steenhuis TS, and Parlange J. 1999. Modeling the movement of water and solute through preferential flow paths. *In: The Handbook of Groundwater Engineering.* Ed: JW Delleur. CRC Press, USA. Chapter 7. 7-1-7-21.

Wankiewicz A. 1979. A review of water movement in snow. *In: Proceedings: Modeling of snow cover runoff.* Ed: SC Colbeck and M Ray. US Army Cold Regions Research and Engineering Laboratory, Hanover, NH, USA. 222-252.

Watson KW and Luxmoore RJ. 1986. Estimating macroporosity in a forest watershed by use of a tension infiltrometer. *Soil Science Society of America* **50**: 578-582.

Weiler M, McDonnell JJ, Tromp-van Meerveld HJ, and Uchida T. 2005. Subsurface stormflow. *In: Encyclopedia of Hydrological Sciences.* Ed: MG Anderson and JJ McDonnell. John Wiley & Sons, Inc., New York, USA. 112. 3. 1719-1732. DOI: 10.1002/0470848944.hsa119.

Weiler M, Scherrer S, Naef F, and Burlando P. 1999. Hydrograph separation of runoff components based on measuring hydraulic state variables, tracer experiments and weighting methods. *IAHS Publication* **258**: 249-255.

Wellington BI and Driscoll CT. 2004. The episodic acidification of a stream with elevated concentrations of dissolved organic carbon. *Hydrological Processes* **18**: 2663-2680. DOI: 10.1002/hyp.5574.

White I, Zegelin AJ, Topp GC, and Fish A. 1994. Effect of bulk electrical conductivity on TDR measurement of water content in porous media. *In: Proc. time domain reflectometry in environmental, infrastructure, and mining associations. Evanston, IL. 7–9 Sept. 1994.* Ed: M O'Connor and CH Dowding. U.S. Bureau of Mines, Spec. Publ. SP 19-94, U.S. Gov. Print. Office, Washington, DC. 294-308.

Wiggert DC, Andersland OB, and Davies SH. 1997. Movement of liquid contaminants in partially saturated frozen granular soils. *Cold Regions Science and Technology* **25**: 111-117.

Wigington PJ Jr., DeWalle DR, Murdoch PS, Kretser WA, Simonin HA, Van Sickle J, and Baker JP. 1996. Episodic Acidification of Small Streams in the Northeastern United States: Ionic Controls of Episodes. *Ecological Applications* **6**: 389-407.

Williams MW and Melack JM. 1989. Effects of spatial and temporal variation in snow melt on nitrate ion and sulfate ion pulses in melt waters within an alpine basin. *Annals of Glaciology* **130**: 285-288.

Williams MW and Melack JM. 1991. Solute chemistry of snowmelt and runoff in an alpine basin, Sierra Nevada. *Water Resources Research* **27**: 1575-1588.

Williams PJ and Smith MW. 1989. *The frozen earth: fundamentals of geocryology.* Cambridge University Press, Cambridge, England. 1st paperback edition. p. 306.

Wilson GV and Luxmoore RJ. 1988. Infiltration, macroporosity, and mesoporosity distributions on two forested watersheds. *Soil Science Society of America Journal* **25**: 329-335.

Woo M. 2005. 127: Snowmelt Runoff Generation. *In: Encyclopaedia of the Hydrological Sciences.* Ed: Malcolm G. Anderson and Jeffrey J. McDonnell. 1 edition. John Wiley and Sons, London, UK. 127. Part 10. 1742-1749. DOI: 10.1002/0470848944.hsa127.

Woo M and Heron R. 1981. Occurrence of ice layers at the base of high arctic snowpacks. *Arctic and Alpine Research* **13**: 225-230.

Woo M, Heron R, and Marsh P. 1982. Basal ice in high arctic snowpacks. *Arctic and Alpine Research* **14**: 251-260.

Woo M and Steer P. 1983. Slope Hydrology as Influenced by Thawing of the Active Layer, Resolute, NWT. *Canadian Journal of Earth Sciences* **20**: 978-986.

Zhang T, Heginbottom JA, Barry RG, and Brown J. 2000. Further statistics on the distribution of permafrost and ground ice in the Northern Hemisphere. *Polar Geography* **24**: 126-131.

Zhao LT and Gray DM. 1997. A parametric expression for estimating infiltration into frozen soils. *Hydrological Processes* **11**: 1761-1775.

Zhao LT and Gray DM. 1999. Estimating snowmelt infiltration into frozen soils. *Hydrological Processes* **13**: 1827-1842.

Zhao LT, Gray DM, and Male DH. 1997. Numerical analysis of simultaneous heat and mass transfer during infiltration into frozen ground. *Journal of Hydrology* **200**: 345-363.

**APPENDICES**

# APPENDIX A: HEMISPHERICAL PHOTOS USED TO ESTIMATE LAI AND CANOPY COVERAGE

This appendix shows the images that were used to calculate leaf area index (LAI) and canopy structure (openness) using Gap Light Analyzer v. 2.0 (Frazer *et al.*, 1999). Images were recorded across the study site during uniform overcast sky conditions using a Nikon Coolpix 5000 digital camera fitted with a Nikon FC-E8 Fisheye Converter Lens with a 183º field of view. The circular images, which record the size, shape, and location of gaps in the forest canopy using a polar projection distortion, were converted into bitmaps. Image processing involves the transformation of image pixel positions into angular coordinates, the division of pixel intensities into sky and non-sky classes, and the computation of sky-brightness distributions.

A total of 13 recordings were made across the slope (Figure A.1); the numbers on the figure refer to the positions on the hill slope where each of the images (Table A.1) was recorded.
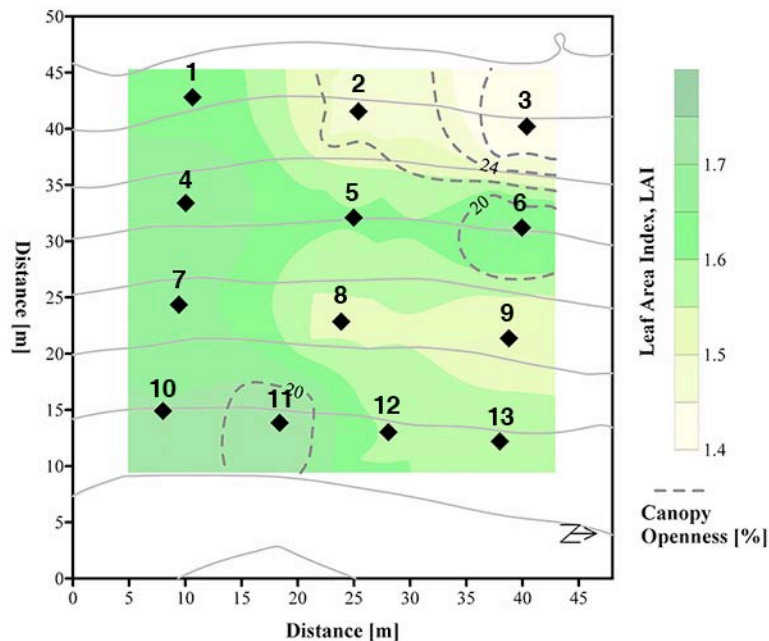


*Figure A.1. The positions where images were recorded to assess leaf area index, LAI, and canopy openness [%]. Slope contour (solid lines) interval is 2 m.*

*Table A.1. The recorded images from each position on the slope.*
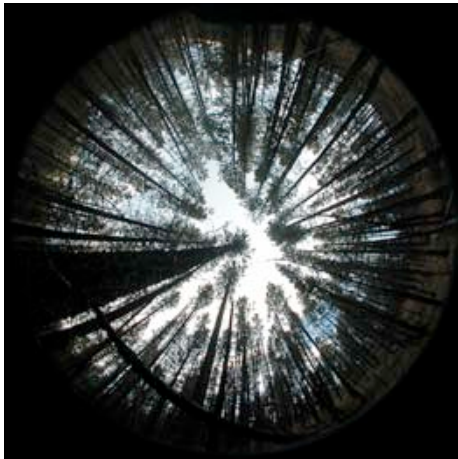
| # | Recorded image | # | Recorded image |
|---|---|---|---|
| 1 |  | 2 |  |
| 3 |  | 4 |  |
| 5 |  | 6 |  |

*Table A.1 (continued). The recorded images from each position on the slope.*
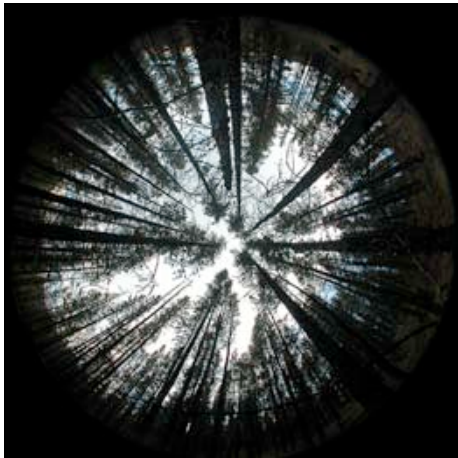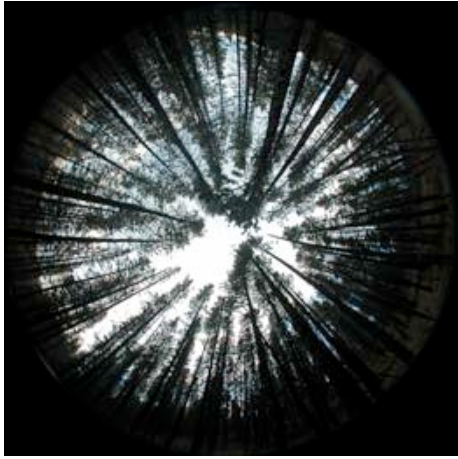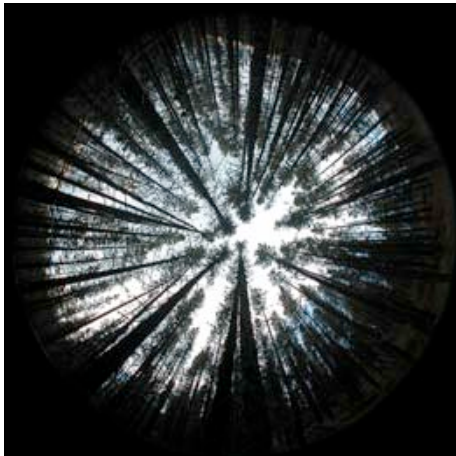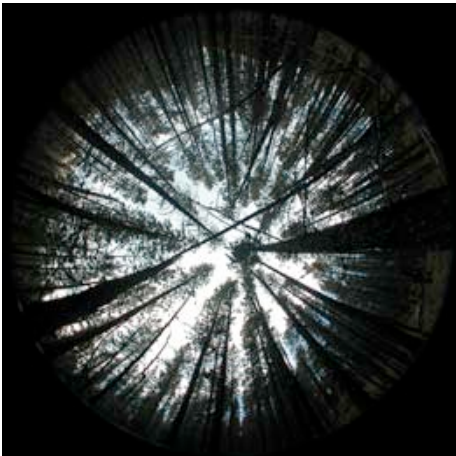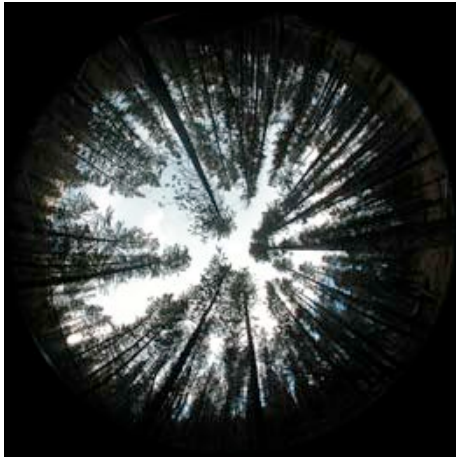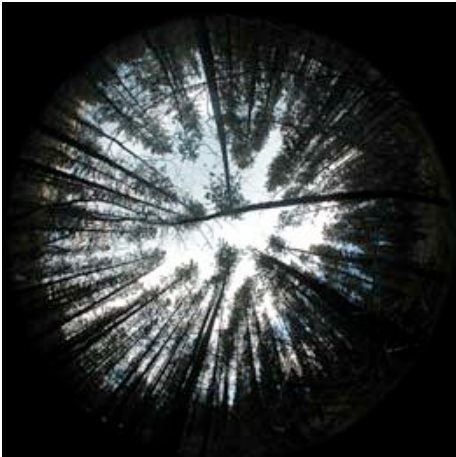
| # | Recorded image | # | Recorded image |
|---|---|---|---|
| 7 |  | 8 |  |
| 9 |  | | |

*Table A.1 (continued). The recorded images from each position on the slope.*

| # | Recorded image | # | Recorded image |
|---|---|---|---|
| 10 |  | 11 |  |
| 12 |  | 13 |  |

# APPENDIX B: METHODOLOGY FOR FIELD SATURATED HYDRAULIC CONDUCTIVITY ESTIMATIONS

This appendix describes the theory behind double-ring infiltrometers and how the calculated infiltration rate, $f(t)$ [kg s$^{-1}$ m$^{-2}$], can be used to estimate field saturated hydraulic conductivity, $K_{fs}$ [m s$^{-1}$].

### Infiltrometer Theory

Infiltrometers can be used to determine soils infiltration rate, $f(t)$ [m s$^{-1}$], in the field. Their advantages are that they require only a small surface area, measurements can be done in-situ, calculations of infiltration rates are easy, and experiments are inexpensive to construct and simple to run (e.g. Gray *et al*., 1970; Hiscock, 2005). Disadvantages are that the results only represent the plot area and great care has to be taken during installation to reduce boundary effects. Interpretation of infiltration rates can be complicated by factors such as seepage flow (lateral flow), soil heterogeneity, soil swelling and shrinkage, and soil aggregation (Hiscock, 2005).

Flooding type infiltrometers permit a direct determination of a one dimensional infiltration rate (vertical flow) and consist of either a single ring or a double-ring (Figure B.1A), which are pushed or driven a short distance into the ground (Gray *et al*., 1970; Bodhinayake, 2003). The outer ring of the double-ring infiltrometer serves to reduce the lateral flow on the inner ring so the simulated flow under the inner ring will be virtually
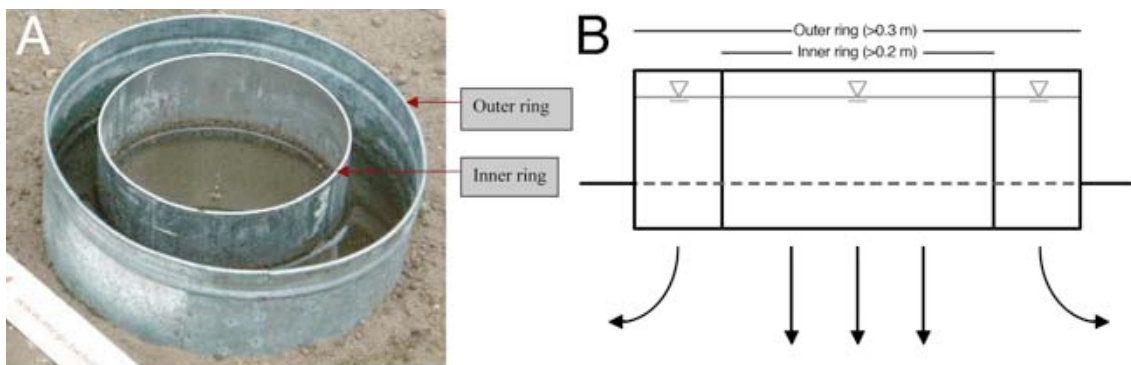


*Figure B.1. An example of installed double-ring infiltrometer (from Bodhinayake, 2003). B) Schematic drawing of the theory behind a double-ring flooding infiltrometer.*

vertical (Figure B.1B). Lateral flow will result in an overestimation of the infiltration rate. Gray *et al*. (1970) noted that results for this type of experiment should only be considered to apply for similar field conditions (i.e. ponding conditions), as it is a confined pressure induced infiltration method (Bodhinayake, 2003). Infiltration rates during normal rain conditions are normally lower as the impact of the raindrop seals the surface.

The double-ring infiltrometer is primarily designed for horizontal surfaces (Bower, 1986). Factors that affect surface soils hydraulic properties are topography (including slope gradient), the presence or absence of cover material, soil texture and structure, and type of land use (cultivated, forest, grassland etc.); slope gradient and land use influence the hydraulic properties the most (Bodhinayake 2003). However, Bodhinayake *et al*. (2004) concluded that double-ring infiltrometers are suitable for characterization of the hydraulic properties of saturated and near-saturated surface soils in landscapes with slope gradients up to 20% (11º). A theoretical study by Philip (1991) showed that infiltration normal to the slope, for slope gradients less than 30º (58%), differ relatively little from infiltration at a horizontal surface.

***Infiltration Rate***

Suggested minimum diameters of the infiltrometer rings are 20 cm for the inner and 30 cm for the outer (Bower, 1986). Three sets of rings were used; inner ring diameters were 0.31, 0.33, and 0.35 m, respectively; outer ring diameters were 0.2 m greater. The rings were made of 2 mm thick iron plates and had a general height of 0.24 m.

To install the rings, the organic layer was removed in an area corresponding to the size of the outer ring. The outer ring was installed first; it was driven into the mineral soil while trying to minimize soil disturbance. The amount of coarse gravel in the soil made it difficult to insert the rings very deeply. If the ring did not seem to be far enough into the ground, mineral soil was added along the outside edge of the ring to prevent leakage while still maintaining undisturbed soil within the experimental area. To minimize preferential infiltration along the inside walls of the rings, light tamping of the soil along the contact surface was done. The inner ring was placed as concentric inside

the bigger ring as roots and rocks allowed; installation procedure was similar to that of the outer ring.

Water was filled into the outer ring first to test for leakage. Throughout the experiments equal water levels were maintained within the two rings. One aspect to consider when using a double-ring infiltrometer on slopes is the variation in head across the sloping surface; maximum head will be found at the down-slope side of the ring, lowest head in the upslope side. Infiltration rates will therefore vary across the surface; however, according to Bodhinayake (2003) it can be assumed that the lower infiltration rate at the upslope side will be compensated for by the higher rate at the down-slope side. Thus, change in head was measured at the centre of the cylinder.

Time of measurements started once a 0.10 m head had been reached at the centre of the inner cylinder. The level of the head was measured each minute within the initial 10 minutes; hereafter, measurements continued every second minute. Once readings seemed steady, the interval of measurements was increased to every 5 minutes; this was often the case after approximately half an hour. Quasi-steady flow can be assumed once the amount of water infiltrating does not change over a period of time of approximately 30 minutes (Bodhinayake, 2003); this was obtained after 60 to 90 minutes. In one case, quasi-steady state was not reached until 120 minutes had passed. Upslope head was never less than 20 mm.

### *Field-saturated Hydraulic Conductivity*

Field-saturated hydraulic conductivity, $K_{fs}$, for the surface soil was estimated using Equation B.1 (e.g. Reynolds *et al*., 2002) where $\alpha$ [m$^{-1}$] is a soil texture-structure parameter, which is often set to 12 m$^{-1}$ for unstructured, loamy soils (Elrick *et al*., 1989); $G$ is a dimensionless factor given by Equation B.2, where $d$ is the depth [m] of ring insertion into the soil; $r$ is the radius of the inner ring [m]; $A$ is the cross-sectional area of the infiltrometers inner ring [m$^2$]; $f(t)$ is the quasi-steady infiltration rate [m s$^{-1}$] found during the field experiments; and $H_l$ is the steady pressure head of water on the infiltration surface [m], which is taken as the mean head during quasi-steady infiltration.

$$K_{fs} = \frac{\alpha \cdot G \cdot A \cdot f(t)}{\left(r\left(\alpha \cdot H_l + 1\right) + G \cdot \alpha \cdot A\right)} \tag{B.1}$$

$$G = 0.316 \cdot \left(\frac{d}{r}\right) + 0.184 \tag{B.2}$$

Measurements of infiltration rate and estimations of $K_{fs}$ were carried out at 16 points at the observation site. Figure B.2 shows where infiltration experiments were carried out and the values for the individual parameters used for estimation of $K_{fs}$ are shown in Table B.1. The infiltration rates found at the observation site correspond well to others reported in the literature for forested sites and using double-ring infiltrometers (e.g Watson and Luxmoore, 1986; Wilson and Luxmoore, 1988; Sauer and Logsdon, 2002).
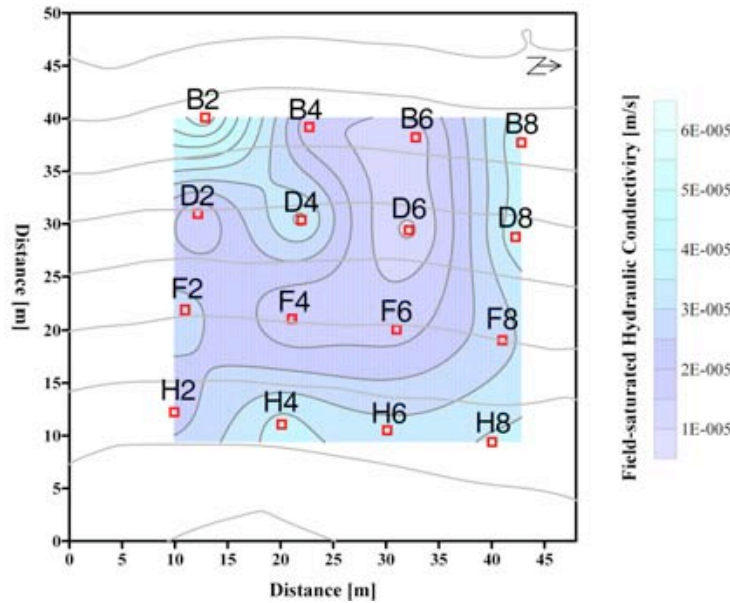


*Figure B.2. Positions (red squares) at the observation site where infiltration experiments were carried out. The labels refer to the following table (B.1).*

*Table B.1. Parameter values used for estimation of the field saturated hydraulic conductivity ($K_{fs}$) across the observation site.*

| Point in grid | B2 | B4 | B6 | B8 | D2 | D4 | D6 | D8 |
|---|---|---|---|---|---|---|---|---|
| $\alpha$ [m$^{-1}$] | 12 | 12 | 12 | 12 | 12 | 12 | 12 | 12 |
| $G$ | 0.235 | 0.229 | 0.235 | 0.229 | 0.235 | 0.229 | 0.232 | 0.232 |
| $A$ [m$^2$] | 0.075 | 0.096 | 0.075 | 0.096 | 0.075 | 0.096 | 0.086 | 0.086 |
| $f(t)$ [m s$^{-1}$] | 1.4E-04 | 3.6E-05 | 3.2E-05 | 9.9E-05 | 3.7E-05 | 8.5E-05 | 2.1E-05 | 9.8E-05 |
| $r$ [m] | 0.155 | 0.175 | 0.155 | 0.175 | 0.155 | 0.175 | 0.165 | 0.165 |
| $H_l$ [m] | 0.0795 | 0.088 | 0.098 | 0.108 | 0.09 | 0.081 | 0.085 | 0.102 |
| $d$ [m] | 0.025 | 0.025 | 0.025 | 0.025 | 0.025 | 0.025 | 0.025 | 0.025 |
| $K_{fs}$ [m s$^{-1}$] | 5.9E-05 | 1.5E-05 | 1.3E-05 | 4.0E-05 | 1.5E-05 | 3.7E-05 | 8.6E-06 | 3.9E-05 |

| Point in grid | F2 | F4 | F6 | F8 | H2 | H4 | H6 | H8 |
|---|---|---|---|---|---|---|---|---|
| $\alpha$ [m$^{-1}$] | 12 | 12 | 12 | 12 | 12 | 12 | 12 | 12 |
| $G$ | 0.235 | 0.229 | 0.232 | 0.235 | 0.235 | 0.229 | 0.232 | 0.235 |
| $A$ [m$^2$] | 0.075 | 0.096 | 0.086 | 0.075 | 0.075 | 0.096 | 0.086 | 0.075 |
| $f(t)$ [m s$^{-1}$] | 6.7E-05 | 3.4E-05 | 4.1E-05 | 6.7E-05 | 5.2E-05 | 8.3E-05 | 7.3E-05 | 8.8E-05 |
| $r$ [m] | 0.155 | 0.175 | 0.165 | 0.155 | 0.155 | 0.175 | 0.165 | 0.155 |
| $H_l$ [m] | 0.084 | 0.0795 | 0.074 | 0.075 | 0.069 | 0.0695 | 0.071 | 0.082 |
| $d$ [m] | 0.025 | 0.025 | 0.025 | 0.025 | 0.025 | 0.025 | 0.025 | 0.025 |
| $K_{fs}$ [m s$^{-1}$] | 2.7E-05 | 1.5E-05 | 1.8E-05 | 2.8E-05 | 2.3E-05 | 3.8E-05 | 3.2E-05 | 3.6E-05 |

# APPENDIX C: TIME DOMAIN REFLECTOMETRY

Time domain reflectometry (TDR) is a non-destructive method used to measure the liquid water content in any porous media and especially soil (Topp *et al.*, 1980). It is based on the dielectric constant, $K_a$ or $\varepsilon_r$, of the material, which is a measure of the molecules tendency to orientate in an electrostatic force field (e.g. Hillel, 1989). A dielectric medium is a non-conductor of electricity; it allows no flow of electric charges between two charged surfaces (capacitors) but only a displacement of charge.

Water molecules are polar by nature due to the position of the hydrogen molecules (e.g Hillel, 1989). This gives it a relatively high $K_a$ compared to other media such as air, ice, and soil (Table C.1). The value of $K_a$ for soil depends on the composition and texture of the material (Topp *et al.*, 1980). As a consequence, a soil, which consists of air, solids, and water in varying portions, the value of $K_a$ will largely be determined by the fraction of water present and it is this difference that enables the use of $K_a$ for moisture determination.

The TDR probe consists of parallel rods (2 or more), which are connected with a coaxial cable to a signal receiver (Figure C.1). Measurements are made by sending a fast-rise voltage pulse (electromagnetic wave) through the cable and rods (e.g. Topp *et al.*, 1980). The rods serve as conductors and the soil between and around the rods, serve as the dielectric medium. At the end of the rods, the signal is reflected and returned to the TDR receiver. The time between sending and receiving the pulse, $t_r$ [s], is measured and used to calculate $K_a$ as

$$K_a = \left(\frac{c \cdot t_r}{2L}\right)^2 \tag{C.1}$$

Table C.1. Dielectric constants, $K_a$, for various media (after Hillel, 1989; Evett, 2003; Kahimba and Ranjan, 2007).

| Media | Water | Air | Ice | Soil |
|-------|-------|-----|-----|------|
| $K_a$ | ~88 at 0 °C | 1.0 | 3.2 | 2-5 |
|  | ~80 at 20 °C | (defined) |  |  |
|  | ~79 at 25 °C |  |  |  |
|  | ~70 at 50 °C |  |  |  |
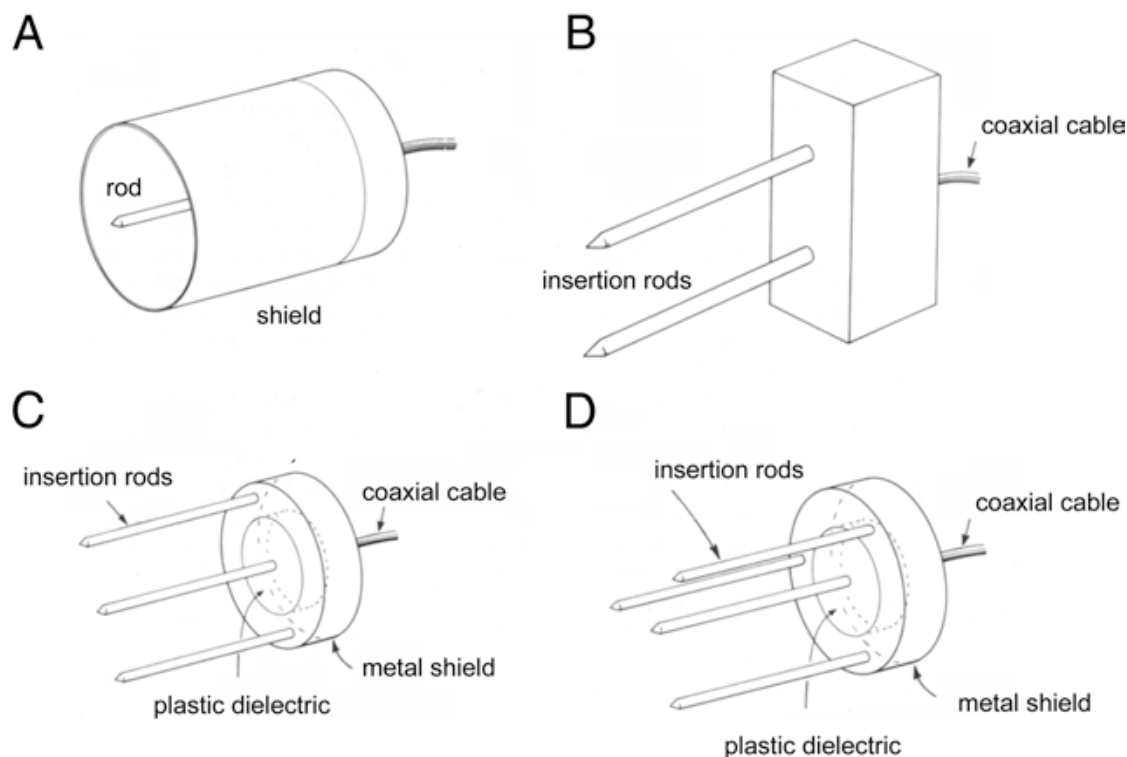
*Figure C.1. Schematic examples of commonly used TDR probe designs; A) early design used a controlled volume, B) two rod probe, C) three rod probe, and D) four rod probe (from George, 1999).*

where $c$ is the velocity of an electromagnetic wave in free space (vacuum), i.e. the speed of light [$3 \cdot 10^8$ m s$^{-1}$], and $L$ is the length of the probe's rods [m] (e.g. Topp *et al.*, 1980). The method relies on the graphical interpretation of the waveform reflected from the probe (Figure C.2).

The relationship between $K_a$ and the volumetric water content of a media, $\theta$, can be found either from empirically or physically derived models (Topp and Reynolds, 1998). Topp *et al.* derived an empirical model, a third-order polynomial, in 1980 which has been widely used and found to have a quite broad application (e.g. Topp and Reynolds, 1998)

$$\theta = -5.3 \cdot 10^{-2} + 2.92 \cdot 10^{-2} K_a - 5.5 \cdot 10^{-4} K_a^2 + 4.3 \cdot 10^{-6} K_a^3 \qquad \text{(C.2)}$$
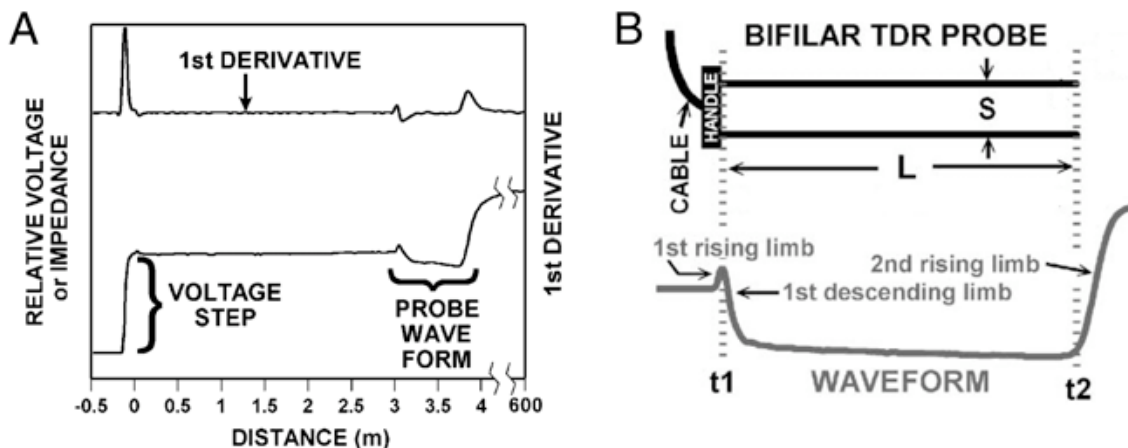
*Figure C.2. A) Schematic plot of a waveform and its first derivative from a TDR probe. The signal starts within the wave generator (the negative distance) and is connected at 3 m to a probe. Inflections in the first derivative of the waveform are used to help determine pulse travel time, t_r. B) Schematic drawing of a two rod (bifilar) TDR probe and the corresponding waveform; L is the rod length, S is the rod spacing, and t_1 and t_2 refer to the times used in the calculation of K_a (after Evett, 2003).*

Later research showed that θ is related practically linearly to the travel time of the TDR signal (e.g. Ledieu *et al.*, 1986)

$$\theta_v = 0.1138\sqrt{K_a} - 0.1758 \qquad \text{(C.3)}$$

Current research involves attempts to improve the method by using dielectric mixing models that consider the volumetric proportions of soil mineral, organic, water, and air constituents, as well as soil mineralogy, particle shapes, and packing (e.g. Evett, 2003). This could lead to a more universal calibration, but currently empirically derived models (e.g. Topp *et al.*, 1980; Ledieu *et al.*, 1986) are considered to be the standards (e.g. Topp and Reynolds, 1998; Evett, 2003).

### *Limitations*

The dielectric constant, $K_a$, as a function of the soil's volume wetness, has only been found to depend weakly on soil type, bulk density, temperature, and the electrical conductivity of pore water (e.g. Hillel, 1989; Topp and Reynolds, 1998). It is best for describing water content in non-saline, medium, and coarse-textured soils (e.g. White *et al.*, 1994; Chandler *et al.*, 2004). However, most soil water contains dissolved ionic

species and is in close contact with electrically charged surfaces. If the ionic concentrations are too high, a dielectric loss will happen, complicating the interpretation of the TDR measurements. This has been observed especially in heavy clay soils (e.g. White *et al*., 1994). In most cases, the measuring error has been found to be ~0.013 m$^3$ m$^{-3}$ (e.g. Chandler *et al*., 2004).

Topp *et al*. (1980) found that the temperature had little influence on $K_a$ between 5 ℃ and 40 ℃. However, as the temperature gets close to 0 ℃ the variation in $K_a$ becomes significant (Table C.1) and an adjustment in $K_a$ is needed in order to use Topp *et al*.'s calibration equation. A model, which adjusts $K_a$ to a standard temperature (i.e. 25 ℃), is suggested by Kahim and Ranjan (2007)

$$K_{adj} \quad = \quad K_{a-field} + 0.3572(T_s - 25) - 8.25 \cdot 10^{-4}(T_s - 25)^2 - 1.0 \cdot 10^{-6}(T_s - 25)^3 \quad \text{(C.2)}$$

where $K_{adj}$ is the adjusted $K_a$ to a temperature of 25 ℃, $K_{a-field}$ is the measured $K_a$ in the field, and $T_s$ is the soil temperature at the measured depth. Still, measurements in partly frozen soils, where water exists in both liquid and frozen conditions, pose a challenge (Evett, 2003).

### *Setup*

The measuring area of a TDR probe with two rods is cylindrical with an axis that lies midway between the rods. The diameter of the area is 1.4 times the spacing between the rods (e.g. Hillel, 1989). Hence, the volume of the measurements varies directly with the length of the rods. The probe can be inserted either vertically or horizontally into the ground. Vertical insertion measures the soil moisture of a layer with a depth equal to the length of the probe rods, whereas horizontal insertion measures the soil moisture content of a layer equal to 1.4 times the spacing between the rods.

Air gaps around the rod or across the pair of rods are potential sources of measurement error (e.g. Hillel, 1989). Hence, caution has to be taken during installation since air gaps can arise hereof. Drying of soil (and thereby shrinking) may also lead to air gaps. Installation at an angle instead of vertically may minimize this.

The probes used in this research all consisted of two stainless steel rods (0.15 m) with 50 mm spacing between them, giving a measuring volume of ~770 cm$^3$. A

Campbell Scientific TDR100 was used as the pulse generator for the signal applied to the TDR probes. A multiplexer unit (SDMX50SP, Campbell Scientific) allowed measurement for multiple TDR probes (Figure C.3).
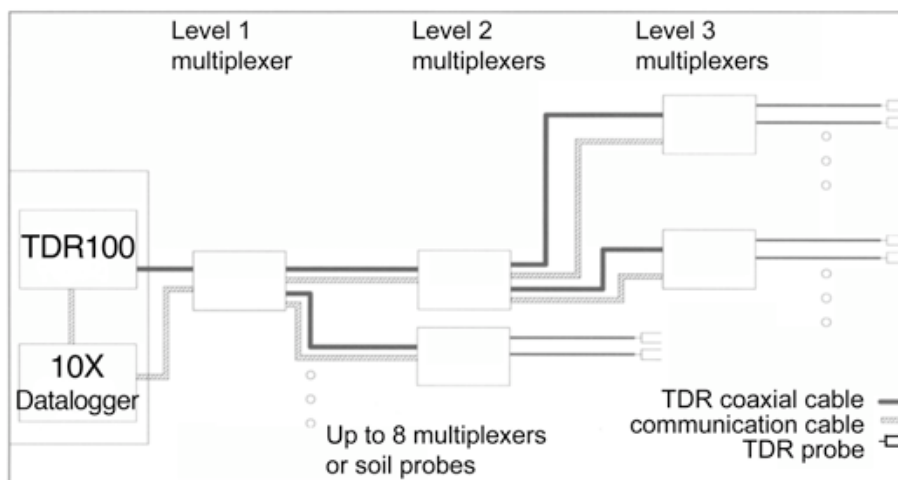


*Figure C.3. Schematic illustration of the TDR100 setup (after Campbell Scientific, 2004). At the study site only one multiplexer (level 1) was used.*

# APPENDIX D: DATA FROM ENHANCED INFILTRATION LABORATORY EXPERIMENTS

This appendix contains the data used in section 5.2 to examine whether *enhanced infiltration* can be identified in a small-scale controlled laboratory experiment as well as the impact of initial soil saturation on *enhanced infiltration.*

Columns: $F_i$ is the cumulative ion load infiltrating a frozen unsaturated soil underneath a snowpack [kg m$^{-2}$]; *NEI* [(meq m$^{-3}$)(meq m$^{-3}$)$^{-1}$] is the normalized enhanced infiltration found as the ratio between the cumulative enhanced infiltration and cumulative ion infiltration estimated from time-averaged ion concentration and cumulative infiltration (Equation 5.10); and *NR$_i$* [(meq m$^{-3}$)(meq m$^{-3}$)$^{-1}$] is the normalized infiltration excess ion load defined as the infiltration excess ion load divided by the difference between meltwater ion load and infiltrating ion load due only to time-averaged ion concentration and cumulative infiltration (Equation 5.13).

*Soil Saturation = 0.06 mm³ mm⁻³*

| Column 1 | | | | Column 2 | | | | Column 3 | | | |
|---|---|---|---|---|---|---|---|---|---|---|---|
| Time [h] | $F_i$ [kg/m²] | NEI | $NR_i$ | Time [h] | $F_i$ [kg/m²] | NEI | $NR_i$ | Time [h] | $F_i$ [kg/m²] | NEI | $NR_i$ |
| 0.0 | 0.0 | 0.00 | 0.00 | 0.0 | 0.0 | 0.00 | 0.00 | 0.0 | 0.0 | 0.00 | 0.00 |
| 0.2 | 440.5 | 0.00 | 0.00 | 0.2 | 377.5 | 0.00 | 0.00 | 0.3 | 350.0 | 0.00 | 0.00 |
| 0.2 | 593.8 | 0.00 | 0.00 | 0.3 | 782.6 | 0.00 | 0.00 | 0.5 | 1356.8 | 0.00 | 0.00 |
| 0.4 | 1636.0 | 0.00 | 0.00 | 0.5 | 1360.7 | 0.00 | 0.00 | 0.6 | 1573.1 | 0.00 | 0.00 |
| 0.6 | 2025.4 | 0.00 | 0.00 | 0.7 | 1915.2 | 0.00 | 0.00 | 0.8 | 1875.9 | 0.00 | 0.00 |
| 0.8 | 2615.3 | 0.00 | 0.00 | 0.8 | 2347.8 | 0.00 | 0.00 | 1.0 | 2564.1 | 0.00 | 0.00 |
| 1.0 | 3079.3 | 0.00 | 0.00 | 1.0 | 3177.6 | 0.00 | 0.00 | 1.3 | 3316.6 | 0.00 | 0.00 |
| 1.1 | 3582.7 | 0.00 | 0.00 | 1.3 | 3719.1 | 0.00 | 0.00 | 1.7 | 4132.9 | 0.00 | 0.00 |
| 1.4 | 4090.8 | 0.00 | 0.00 | 1.5 | 4479.8 | 0.00 | 0.00 | 2.0 | 4638.2 | 0.00 | 0.00 |
| 1.6 | 4512.9 | 0.00 | 0.00 | 1.8 | 4985.2 | 0.00 | 0.00 | 2.4 | 5009.6 | 0.03 | 0.46 |
| 1.8 | 5015.4 | 0.00 | 0.00 | 2.1 | 5495.4 | 0.00 | 0.83 | 2.9 | 5131.5 | 0.11 | 0.51 |
| 2.0 | 5266.7 | 0.01 | 0.81 | 2.4 | 5601.0 | 0.08 | 0.52 | 3.2 | 5136.0 | 0.17 | 0.53 |
| 2.3 | 5404.2 | 0.07 | 0.59 | 2.8 | 5664.1 | 0.13 | 0.52 | 3.5 | 5142.1 | 0.22 | 0.56 |
| 2.7 | 5556.2 | 0.11 | 0.57 | 3.0 | 5682.5 | 0.18 | 0.53 | 4.0 | 5343.1 | 0.26 | 0.60 |
| 3.3 | 5721.7 | 0.19 | 0.58 | 3.5 | 5898.2 | 0.22 | 0.56 | 4.5 | 5428.6 | 0.33 | 0.59 |
| 4.0 | 5724.4 | 0.30 | 0.60 | 4.0 | 5983.3 | 0.29 | 0.59 | 5.0 | 5577.7 | 0.33 | 0.60 |
| 4.5 | 5754.3 | 0.35 | 0.59 | 4.5 | 6012.8 | 0.36 | 0.58 | 5.5 | 5582.9 | 0.43 | 0.59 |
| 5.0 | 5783.3 | 0.41 | 0.58 | 5.0 | 6043.6 | 0.42 | 0.57 | 6.0 | 5606.0 | 0.50 | 0.60 |
| 5.5 | 5803.3 | 0.47 | 0.58 | 5.5 | 6073.5 | 0.45 | 0.57 | 7.0 | 5610.4 | 0.68 | 0.57 |
| 6.0 | 5805.7 | 0.54 | 0.58 | 6.0 | 6095.5 | 0.54 | 0.57 | 8.0 | 5612.7 | 0.88 | 0.57 |
| 7.0 | 5874.2 | 0.64 | 0.57 | 7.0 | 6163.5 | 0.63 | 0.57 | 9.0 | 5622.2 | 1.02 | 0.57 |
| 8.0 | 5874.8 | 0.85 | 0.55 | 8.0 | 6163.7 | 0.75 | 0.56 | 10.0 | 5631.0 | 1.13 | 0.56 |
| 9.0 | 5921.9 | 0.96 | 0.56 | 9.0 | 6180.3 | 0.88 | 0.55 | 11.0 | 5638.5 | 1.25 | 0.56 |
| 10.0 | 5949.2 | 0.99 | 0.56 | 10.0 | 6180.6 | 1.05 | 0.54 | 12.0 | 5643.3 | 1.37 | 0.56 |
| 11.0 | 5950.0 | 1.16 | 0.55 | 11.0 | 6186.9 | 1.17 | 0.54 | | | | |
| 12.0 | 5952.8 | 1.27 | 0.55 | 12.0 | 6189.1 | 1.27 | 0.53 | | | | |

*Soil Saturation = 0.83 mm³ mm⁻³*

| Column 1 | | | | Column 2 | | | | Column 3 | | | |
|---|---|---|---|---|---|---|---|---|---|---|---|
| Time [h] | $F_i$ [kg/m²] | NEI | $NR_i$ | Time [h] | $F_i$ [kg/m²] | NEI | $NR_i$ | Time [h] | $F_i$ [kg/m²] | NEI | $NR_i$ |
| 0.0 | 0.0 | 0.00 | 0.00 | 0.0 | 0.0 | 0.00 | 0.00 | 0.0 | 0.0 | 0.00 | 0.00 |
| 0.2 | 559.7 | 0.00 | 0.00 | 0.2 | 544.7 | 0.00 | 0.00 | 0.2 | 734.5 | 0.00 | 1.00 |
| 0.3 | 698.3 | 0.00 | 1.00 | 0.3 | 1164.6 | 0.00 | 0.00 | 0.4 | 739.9 | 0.00 | 1.00 |
| 0.5 | 698.5 | 0.00 | 1.00 | 0.5 | 1529.4 | 0.00 | 1.00 | 0.5 | 1126.3 | 0.00 | 1.00 |
| 0.8 | 698.7 | 0.00 | 1.00 | 0.8 | 1529.5 | 0.00 | 1.00 | 0.8 | 1126.3 | 0.00 | 1.00 |
| 1.0 | 698.9 | 0.00 | 1.00 | 1.0 | 2014.9 | 0.00 | 1.00 | 1.0 | 1126.5 | 0.00 | 1.00 |
| 1.3 | 746.8 | 0.02 | 0.99 | 1.3 | 2132.8 | 0.04 | 0.95 | 1.3 | 1126.6 | 0.04 | 0.99 |
| 1.5 | 755.0 | 0.07 | 0.99 | 1.5 | 2132.9 | 0.07 | 0.93 | 1.5 | 1126.8 | 0.08 | 0.98 |
| 2.0 | 777.4 | 0.11 | 0.98 | 2.0 | 2149.4 | 0.12 | 0.92 | 2.0 | 1162.7 | 0.13 | 0.97 |
| 2.5 | 795.6 | 0.17 | 0.98 | 2.5 | 2339.8 | 0.08 | 0.94 | 2.5 | 1162.8 | 0.30 | 0.95 |
| 3.0 | 795.7 | 0.29 | 0.97 | 3.0 | 2354.2 | 0.18 | 0.90 | 3.0 | 1162.8 | 0.41 | 0.95 |
| 3.5 | 798.1 | 0.37 | 0.96 | 3.5 | 2354.2 | 0.28 | 0.88 | 3.5 | 1162.9 | 0.48 | 0.94 |
| 4.0 | 815.8 | 0.41 | 0.96 | 4.0 | 2354.3 | 0.33 | 0.88 | 4.0 | 1163.0 | 0.56 | 0.94 |
| 4.5 | 823.5 | 0.47 | 0.96 | 4.5 | 2354.4 | 0.44 | 0.86 | 4.5 | 1163.0 | 0.70 | 0.94 |
| 5.0 | 828.7 | 0.54 | 0.96 | 5.0 | 2354.4 | 0.54 | 0.85 | 5.0 | 1163.1 | 0.81 | 0.93 |
| 5.5 | 828.9 | 0.63 | 0.96 | 5.5 | 2354.4 | 0.63 | 0.84 | 5.5 | 1163.1 | 0.90 | 0.93 |
| 6.0 | 831.5 | 0.67 | 0.95 | 6.0 | 2354.5 | 0.73 | 0.84 | 6.0 | 1163.1 | 0.98 | 0.93 |
| 7.0 | 841.1 | 0.70 | 0.95 | 7.0 | 2357.8 | 0.92 | 0.83 | 7.0 | 1163.1 | 1.18 | 0.93 |
| 8.0 | 849.8 | 0.74 | 0.95 | 8.0 | 2357.9 | 1.11 | 0.82 | 8.0 | 1172.0 | 1.25 | 0.93 |
| 9.0 | 854.8 | 0.80 | 0.95 | 9.0 | 2368.5 | 1.22 | 0.82 | 9.0 | 1172.0 | 1.43 | 0.92 |
| 10.0 | 857.3 | 0.88 | 0.95 | 10.0 | 2372.1 | 1.35 | 0.81 | 10.0 | 1173.3 | 1.55 | 0.92 |
| 11.0 | 865.5 | 0.86 | 0.95 | 11.0 | 2375.4 | 1.42 | 0.81 | 11.0 | 1173.6 | 1.74 | 0.92 |
| 12.0 | 869.8 | 0.87 | 0.95 | 12.0 | 2375.4 | 1.56 | 0.81 | 12.0 | 1173.6 | 1.92 | 0.92 |

*Soil Saturation = 0.97 mm$^3$ mm$^{-3}$*

| Column 1 | | | | Column 2 | | | | Column 3 | | | |
|---|---|---|---|---|---|---|---|---|---|---|---|
| Time [h] | F$_i$ [kg/m$^2$] | NEI | NR$_i$ | Time [h] | F$_i$ [kg/m$^2$] | NEI | NR$_i$ | Time [h] | F$_i$ [kg/m$^2$] | NEI | NR$_i$ |
| 0.0 | 0.0 | 0.00 | 0.00 | 0.0 | 0.0 | 0.00 | 0.00 | 0.0 | 0.0 | 0.00 | 0.00 |
| 0.2 | 301.1 | 0.01 | 0.99 | 0.2 | 183.6 | 0.00 | 1.00 | 0.2 | 370.4 | 0.00 | 1.00 |
| 0.3 | 357.0 | 0.03 | 0.99 | 0.3 | 290.7 | 0.00 | 1.00 | 0.3 | 370.7 | 0.00 | 1.00 |
| 0.5 | 397.5 | 0.04 | 0.99 | 0.5 | 319.1 | 0.00 | 1.00 | 0.5 | 416.0 | 0.00 | 1.00 |
| 0.8 | 553.3 | 0.05 | 0.99 | 0.8 | 347.6 | 0.00 | 1.00 | 0.8 | 437.0 | 0.00 | 1.00 |
| 1.0 | 1071.7 | 0.04 | 0.99 | 1.0 | 405.5 | 0.00 | 1.00 | 1.0 | 520.8 | 0.00 | 1.00 |
| 1.3 | 1073.4 | 0.11 | 0.97 | 1.3 | 408.8 | 0.03 | 1.00 | 1.3 | 526.0 | 0.04 | 0.99 |
| 1.5 | 1075.2 | 0.16 | 0.96 | 1.5 | 421.0 | 0.09 | 0.99 | 1.5 | 589.8 | 0.04 | 0.99 |
| 2.0 | 1114.8 | 0.22 | 0.95 | 2.0 | 473.0 | 0.09 | 0.99 | 2.0 | 589.9 | 0.10 | 0.99 |
| 2.5 | 1138.2 | 0.35 | 0.94 | 2.5 | 474.2 | 0.20 | 0.98 | 2.5 | 590.0 | 0.24 | 0.98 |
| 3.0 | 1155.6 | 0.46 | 0.93 | 3.0 | 474.3 | 0.33 | 0.98 | 3.0 | 590.1 | 0.37 | 0.97 |
| 3.5 | 1157.8 | 0.61 | 0.93 | 3.5 | 474.4 | 0.42 | 0.97 | 3.5 | 590.1 | 0.50 | 0.97 |
| 4.0 | 1157.9 | 0.71 | 0.92 | 4.0 | 474.5 | 0.52 | 0.97 | 4.0 | 599.6 | 0.53 | 0.97 |
| 4.5 | 1157.9 | 0.91 | 0.92 | 4.5 | 474.5 | 0.66 | 0.97 | 4.5 | 599.6 | 0.68 | 0.97 |
| 5.0 | 1158.0 | 1.11 | 0.91 | 5.0 | 474.5 | 0.77 | 0.97 | 5.0 | 599.6 | 0.83 | 0.97 |
| 5.5 | 1158.0 | 1.30 | 0.91 | 5.5 | 474.6 | 0.88 | 0.97 | 5.5 | 599.7 | 0.94 | 0.96 |
| 6.0 | 1172.1 | 1.30 | 0.91 | 6.0 | 475.9 | 0.96 | 0.97 | 6.0 | 599.7 | 1.04 | 0.96 |
| 7.0 | 1172.1 | 1.63 | 0.91 | 7.0 | 477.1 | 1.19 | 0.96 | 7.0 | 599.7 | 1.31 | 0.96 |
| 8.0 | 1167.3 | 1.97 | 0.90 | 8.0 | 477.1 | 1.40 | 0.96 | 8.0 | 599.8 | 1.53 | 0.96 |
| 9.0 | 1181.4 | 1.99 | 0.91 | 9.0 | 477.1 | 1.64 | 0.96 | 9.0 | 599.8 | 1.74 | 0.96 |
| 10.0 | 1176.0 | 2.34 | 0.90 | 10.0 | 477.5 | 1.81 | 0.96 | 10.0 | 599.8 | 1.98 | 0.96 |
| 11.0 | 1169.9 | 2.69 | 0.90 | 11.0 | 477.5 | 2.01 | 0.96 | 11.0 | 599.8 | 2.18 | 0.96 |
| 12.0 | 1171.5 | 2.90 | 0.90 | 12.0 | 477.5 | 2.21 | 0.96 | 12.0 | 599.8 | 2.42 | 0.96 |

# APPENDIX E: CHEMICAL COMPOSITION OF LABORATORY SAMPLES

This appendix contains the chemical composition for the individual samples used in Chapter 6 to examine the compositional change in water chemistry for three unmixed flowpaths: overland flow due to formation of a basal ice layer (BI-1, -2, and -3), organic interflow (OIF-1, -2, and -3), and mineral interflow (MIF-1 and -2). *Day* refers to the time in days after experiment was initiated; BS refers to parent snow; BW, OW, and MW refer to runoff water; and SW refers to meltwater without contact to either of the base layers. Ion concentrations for all major ions are given in meq m$^{-3}$; DOC concentrations are given in g m$^{-3}$. Hyphens (–) indicate that no data is available.

*Basal Ice Layer Experiment 1 (BI-1)*

| Day | Sample | H$^+$ | Cl$^-$ | SO$_4^{2-}$ | NO$_3^-$ | NH$_4^+$ | Na$^+$ | K$^+$ | Mg$^{2+}$ | Ca$^{2+}$ | DOC |
|-----|--------|-------|--------|-------------|----------|----------|--------|-------|-----------|-----------|-----|
| 0.0 | T3-BS-1 | 0.006 | 14.1 | 12.5 | n.d. | 11.4 | 7.1 | 6.2 | 25.2 | 78.6 | - |
| 0.0 | T3-BS-2 | 0.013 | 11.3 | 10.4 | 1.4 | 21.0 | 3.8 | 6.2 | 20.3 | 68.7 | - |
| 2.9 | T3-BW-1 | 0.039 | 213.8 | 93.7 | 1.4 | 42.1 | 182.8 | 6.6 | 87.6 | 334.4 | - |
| 3.2 | T3-BW-2 | 0.055 | 230.7 | 108.3 | 1.4 | 47.0 | 211.3 | 8.4 | 104.5 | 392.1 | - |
| 3.5 | T3-BW-3 | 0.076 | 250.4 | 112.4 | 11.7 | 67.5 | 222.3 | 10.5 | 122.0 | 456.8 | - |
| 3.9 | T3-BW-4 | 0.049 | 205.3 | 91.6 | 11.4 | 68.2 | 190.7 | 8.3 | 125.7 | 591.3 | - |
| 4.2 | T3-BW-5 | 0.047 | 168.8 | 72.9 | 4.6 | 42.7 | 154.9 | 5.7 | 124.3 | 536.3 | - |
| 4.5 | T3-BW-6 | 0.050 | 121.0 | 50.0 | 2.7 | 23.4 | 109.4 | 2.9 | 113.6 | 345.2 | - |
| 4.9 | T3-BW-7 | 0.072 | 87.2 | 35.4 | 4.7 | 35.2 | 80.1 | 0.5 | 107.6 | 293.2 | - |
| 5.2 | T3-BW-8 | 0.048 | 59.1 | 18.7 | 2.6 | 29.0 | 27.2 | n.d. | 99.7 | 235.9 | - |
| 5.5 | T3-BW-9 | 0.081 | 47.8 | 14.6 | 2.4 | 24.6 | 19.8 | n.d | 92.2 | 207.8 | - |
| 5.9 | T3-BW-10 | 0.061 | 59.1 | 10.4 | n.d. | 18.0 | 20.7 | n.d | 95.5 | 191.4 | - |
| 3.9 | T3-SW-1 | 0.074 | 101.3 | 43.7 | 1.3 | 32.6 | 106.7 | 1.0 | 57.6 | 203.4 | - |
| 4.2 | T3-SW-2 | 0.125 | 75.9 | 31.2 | 3.1 | 33.5 | 95.2 | 3.9 | 55.9 | 185.1 | - |
| 4.5 | T3-SW-3 | 0.106 | 59.1 | 22.9 | 2.0 | 27.5 | 56.1 | 0.6 | 51.8 | 83.4 | - |
| 4.9 | T3-SW-4 | 0.125 | 42.2 | 14.6 | 1.5 | 23.8 | 21.9 | n.d. | 51.7 | 136.0 | - |
| 5.2 | T3-SW-5 | 0.138 | 33.8 | 10.4 | n.d. | 17.1 | 13.4 | n.d. | 50.6 | 100.7 | - |
| 5.5 | T3-SW-6 | 0.146 | 25.3 | 8.3 | n.d. | 18.2 | 11.3 | 2.1 | 51.2 | 97.5 | - |
| 5.9 | T3-SW-7 | 0.120 | 25.3 | 6.2 | n.d. | 16.8 | 9.6 | n.d. | 50.9 | 85.6 | - |
| 6.2 | T3-SW-8 | 0.146 | 22.5 | 4.2 | n.d. | 15.9 | 4.7 | n.d. | 51.1 | 92.1 | - |

n.d. = not detected

*Basal Ice Layer Experiment 2 (BI-2)*

| Day | Sample | $H^+$ | $Cl^-$ | $SO_4^{2-}$ | $NO_3^-$ | $NH_4^+$ | $Na^+$ | $K^+$ | $Mg^{2+}$ | $Ca^{2+}$ | DOC |
|-----|--------|-------|--------|-------------|----------|----------|--------|-------|-----------|-----------|-----|
| 0.0 | T4-BS-1 | 0.077 | 25.3 | 35.4 | 3.2 | 26.9 | 11.0 | 9.5 | 23.5 | 59.8 | - |
| 0.0 | T4-BS-2 | 0.077 | 25.3 | 35.4 | 4.8 | 25.7 | 19.1 | 12.6 | 38.4 | 109.1 | - |
| 1.7 | T4-BW-1 | 0.055 | 109.7 | 249.8 | 28.8 | 102.6 | 78.3 | 35.7 | 116.3 | 593.3 | - |
| 2.2 | T4-BW-2 | 0.043 | 129.4 | 291.5 | 41.5 | 150.1 | 73.5 | 33.4 | 105.4 | 681.2 | - |
| 2.7 | T4-BW-3 | 0.042 | 95.6 | 206.1 | 6.1 | 59.8 | 43.3 | 19.9 | 74.3 | 358.8 | - |
| 3.3 | T4-BW-4 | 0.037 | 90.0 | 187.4 | 26.7 | 107.6 | 51.3 | 23.2 | 95.5 | 542.9 | - |
| 3.7 | T4-BW-5 | 0.041 | 64.7 | 116.6 | 6.9 | 47.0 | 24.4 | 13.5 | 58.2 | 347.8 | - |
| 4.2 | T4-BW-6 | 0.034 | 166.0 | 122.8 | 20.6 | 80.4 | 32.4 | 66.9 | 72.7 | 272.1 | - |
| 4.7 | T4-BW-7 | 0.029 | 146.3 | 249.8 | 8.1 | 68.5 | 85.8 | 64.6 | 161.0 | 690.2 | - |
| 5.2 | T4-BW-8 | 0.024 | 185.7 | 187.4 | 28.1 | 104.0 | 76.2 | 119.4 | 160.2 | 591.3 | - |
| 5.7 | T4-BW-9 | 0.031 | 87.2 | 116.6 | 18.9 | 68.7 | 28.9 | 26.4 | 80.1 | 282.7 | - |
| 6.3 | T4-BW-10 | 0.025 | 59.1 | 85.4 | 4.8 | 41.5 | 23.1 | 230.8 | 64.8 | 238.2 | - |
| 6.7 | T4-BW-11 | 0.042 | 50.6 | 60.4 | 9.4 | 44.6 | 15.2 | 14.4 | 62.9 | 248.4 | - |
| 7.3 | T4-BW-12 | 0.052 | 36.6 | 45.8 | 9.0 | 42.0 | 27.0 | 16.7 | 109.0 | 287.7 | - |
| 7.8 | T4-BW-13 | 0.041 | 61.9 | 131.2 | 13.1 | 41.5 | 43.6 | 26.1 | 107.3 | 348.3 | - |
| 8.3 | T4-BW-14 | 0.054 | 61.9 | 149.9 | 4.1 | 30.5 | 56.0 | 28.6 | 134.6 | 391.2 | - |
| 8.8 | T4-BW-15 | 0.050 | 50.6 | 97.9 | 14.6 | 38.1 | 32.0 | 23.0 | 89.9 | 226.7 | - |
| 9.3 | T4-BW-16 | n.a. | 33.8 | 79.1 | 11.6 | 33.6 | 17.2 | 9.1 | 45.2 | 232.7 | - |
| 9.7 | T4-BW-17 | 0.063 | 28.1 | 29.1 | 4.2 | 25.4 | 12.4 | 18.1 | 63.3 | 162.2 | - |
| 10.3 | T4-BW-18 | 0.099 | 16.9 | 14.6 | n.d. | 19.1 | 8.7 | 10.7 | 53.2 | 116.9 | - |
| 10.7 | T4-BW-19 | 0.097 | 11.3 | 10.4 | n.d. | 17.5 | 7.7 | 7.1 | 56.9 | 100.0 | - |
| 11.2 | T4-BW-20 | 0.146 | 25.3 | 8.3 | n.d. | 18.8 | 6.1 | 19.8 | 56.9 | 88.9 | - |
| 5.7 | T4-SW-1 | 0.042 | 562.6 | 77.0 | 14.0 | 62.8 | 36.6 | 240.5 | 89.9 | 293.9 | - |
| 6.3 | T4-SW-2 | 0.046 | 185.7 | 64.5 | 11.6 | 50.5 | 24.8 | 149.1 | 86.2 | 274.9 | - |
| 6.7 | T4-SW-3 | 0.046 | 188.5 | 43.7 | 8.5 | 39.3 | 23.3 | 169.2 | 88.4 | 234.7 | - |
| 7.3 | T4-SW-4 | 0.040 | 278.5 | 33.3 | 7.0 | 36.4 | 14.9 | 240.5 | 80.1 | 214.5 | - |
| 7.8 | T4-SW-5 | 0.041 | 177.2 | 25.0 | 5.5 | 32.7 | 13.2 | 161.4 | 81.1 | 179.8 | - |
| 8.3 | T4-SW-6 | 0.043 | 151.9 | 18.7 | 3.1 | 25.3 | 11.3 | 130.7 | 82.5 | 175.1 | - |
| 8.8 | T4-SW-7 | 0.044 | 168.8 | 16.7 | 4.0 | 27.1 | 7.5 | 153.9 | 80.1 | 165.1 | - |
| 9.3 | T4-SW-8 | 0.068 | 19.7 | 14.6 | 2.9 | 21.5 | 10.0 | 10.4 | 72.7 | 139.8 | - |
| 9.7 | T4-SW-9 | 0.077 | 14.1 | 10.4 | 2.3 | 19.5 | 6.0 | 7.1 | 65.2 | 111.8 | - |
| 10.3 | T4-SW-10 | 0.085 | 11.3 | 8.3 | n.d. | 33.9 | 6.2 | 7.3 | 61.0 | 100.0 | - |
| 10.7 | T4-SW-11 | 0.108 | 14.1 | 6.2 | n.d. | 18.3 | 2.5 | 6.2 | 48.0 | 70.1 | - |
| 11.2 | T4-SW-12 | 0.076 | 168.8 | 6.2 | n.d. | 19.6 | 21.6 | 166.2 | 67.6 | 95.1 | - |

n.d. = not detected

*Basal Ice Layer Experiment 3 (BI-3)*

| Day | Sample | H$^+$ | Cl$^-$ | SO$_4$$^{2-}$ | NO$_3$$^-$ | NH$_4$$^+$ | Na$^+$ | K$^+$ | Mg$^{2+}$ | Ca$^{2+}$ | DOC |
|------|---------|-------|------|------|------|------|------|------|------|------|-----|
| 0.00 | T5-BS-1 | 0.428 | 11.3 | 14.6 | n.d. | 13.5 | n.d. | 8.5 | 24.5 | 13.0 | - |
| 0.00 | T5-BS-2 | 0.428 | 8.4 | 8.3 | n.d. | 14.1 | 3.1 | 8.3 | 25.5 | 13.0 | - |
| 1.03 | T5-BW-1 | 0.391 | 47.8 | 27.1 | n.d. | 29.0 | 21.3 | 12.7 | 14.8 | 55.9 | - |
| 1.52 | T5-BW-2 | 0.321 | 47.8 | 35.4 | 6.1 | 36.4 | 19.4 | 12.5 | 14.4 | 49.4 | - |
| 2.00 | T5-BW-3 | 0.252 | 47.8 | 37.5 | 6.5 | 35.4 | 12.2 | 9.3 | 9.5 | 26.9 | - |
| 2.52 | T5-BW-4 | 0.233 | 50.6 | 39.6 | 7.8 | 42.0 | 29.1 | 13.1 | 25.4 | 66.9 | - |
| 3.02 | T5-BW-5 | 0.261 | 42.2 | 27.1 | 5.0 | 29.5 | n.d. | 7.2 | 10.0 | 16.0 | - |
| 3.57 | T5-BW-6 | 0.223 | 25.3 | 14.6 | 3.1 | 27.2 | 13.0 | 9.9 | 19.4 | 47.4 | - |
| 4.07 | T5-BW-7 | 0.321 | 16.9 | 8.3 | 1.1 | 20.7 | 14.2 | 9.9 | 23.6 | 59.4 | - |
| 4.58 | T5-BW-8 | 0.366 | 11.3 | 6.2 | n.d. | 17.1 | 7.9 | 8.1 | 21.8 | 44.4 | - |
| 5.08 | T5-BW-9 | 0.489 | 11.3 | 4.2 | n.d. | 16.0 | n.d. | 6.2 | 20.0 | 30.9 | - |
| 3.15 | T5-SW-1 | 0.286 | 39.4 | 31.2 | 2.7 | 31.3 | 24.7 | 16.8 | 41.3 | 68.9 | - |
| 3.57 | T5-SW-2 | 0.202 | 25.3 | 18.7 | 2.7 | 25.3 | 17.9 | 8.4 | 35.0 | 48.4 | - |
| 4.07 | T5-SW-3 | 0.277 | 14.1 | 8.3 | n.d. | 19.4 | 6.4 | 10.0 | 15.3 | 31.9 | - |
| 4.58 | T5-SW-4 | 0.411 | 11.3 | 4.2 | n.d. | 15.1 | 0.5 | 8.6 | 9.9 | 16.0 | - |
| 5.08 | T5-SW-5 | 0.483 | 8.4 | n.d. | n.d. | 14.4 | 0.5 | 8.8 | 15.6 | 26.9 | - |

n.d. = not detected

*Organic Base Layer Experiment 1 (OIF-1)*

| Day | Sample | H$^+$ | Cl$^-$ | SO$_4$$^{2-}$ | NO$_3$$^-$ | NH$_4$$^+$ | Na$^+$ | K$^+$ | Mg$^{2+}$ | Ca$^{2+}$ | DOC |
|---|---|---|---|---|---|---|---|---|---|---|---|
| 0.0 | T6-BS-1 | 0.188 | 22.5 | 16.7 | n.d. | 24.2 | 12.7 | 10.0 | 34.6 | 49.4 | 2.0 |
| 0.0 | T6-BS-2 | 0.188 | 22.5 | 14.6 | n.d. | 24.4 | 13.4 | 9.2 | 27.6 | 37.9 | 1.5 |
| 0.9 | T6-OW-1 | 2.070 | 143.5 | 85.4 | 9.3 | 32.0 | 75.6 | 205.6 | 64.5 | 152.0 | - |
| 1.4 | T6-OW-2 | 2.685 | 112.5 | 83.3 | n.d. | 39.4 | 52.6 | 195.2 | 71.8 | 168.9 | - |
| 1.9 | T6-OW-3 | 3.428 | 208.2 | 154.1 | n.d. | 86.5 | 58.2 | 524.3 | 202.5 | 410.5 | - |
| 2.4 | T6-OW-4 | 3.388 | 154.7 | 120.8 | n.d. | 82.3 | 24.4 | 276.5 | 74.9 | 174.9 | 38.0 |
| 2.8 | T6-OW-5 | 1.945 | 143.5 | 120.8 | n.d. | 50.4 | 41.1 | 459.5 | 123.8 | 346.9 | 37.0 |
| 3.3 | T6-OW-6 | 1.982 | 140.6 | 104.1 | n.d. | 18.0 | 22.8 | 246.5 | 66.0 | 236.9 | 54.0 |
| 3.8 | T6-OW-7 | 1.734 | 106.9 | 77.0 | n.d. | 33.8 | 18.5 | 222.7 | 44.5 | 155.8 | 42.0 |
| 4.2 | T6-OW-8 | 1.629 | 78.8 | 60.4 | n.d. | 30.7 | 13.4 | 154.0 | 25.1 | 74.8 | - |
| 4.8 | T6-OW-9 | 1.663 | 64.7 | 47.9 | n.d. | 38.0 | 9.8 | 173.3 | 27.8 | 89.3 | 29.0 |
| 5.3 | T6-OW-10 | 1.358 | 53.4 | 39.6 | n.d. | 34.0 | 18.0 | 206.4 | 33.6 | 105.9 | 20.0 |
| 5.9 | T6-OW-11 | 0.714 | 45.0 | 31.2 | n.d. | 38.0 | 8.3 | 117.7 | 10.6 | 46.5 | 18.0 |
| 6.3 | T6-OW-12 | 0.512 | 36.6 | 27.1 | n.d. | 33.3 | 6.8 | 103.8 | 5.1 | 37.8 | - |
| 6.9 | T6-OW-13 | 0.562 | 30.9 | 22.9 | n.d. | 31.5 | 7.0 | 96.7 | 5.3 | 33.2 | 16.0 |
| 7.3 | T6-OW-14 | 0.473 | 25.3 | 20.8 | n.d. | 27.8 | 9.3 | 75.9 | 1.2 | 22.5 | - |
| 7.9 | T6-OW-15 | 0.479 | 33.8 | 29.1 | n.d. | 32.9 | 10.5 | 124.3 | 14.2 | 63.4 | - |
| 8.8 | T6-OW-16 | 0.413 | 33.8 | 29.1 | n.d. | 36.7 | 7.8 | 150.6 | 11.1 | 88.5 | 17.0 |
| 9.9 | T6-OW-17 | 0.497 | 28.1 | 25.0 | n.d. | 38.6 | 6.0 | 143.0 | 10.9 | 81.3 | - |
| 11.0 | T6-OW-18 | 0.536 | 36.6 | 22.9 | n.d. | 40.6 | 4.3 | 68.2 | n.d. | 45.0 | - |
| 5.3 | T6-SW-1 | 0.170 | 16.9 | 8.3 | n.d. | 12.8 | 9.6 | 8.1 | 23.8 | 48.4 | - |
| 5.9 | T6-SW-2 | 0.153 | 14.1 | 4.2 | n.d. | 13.4 | 3.0 | 7.4 | 20.2 | 38.4 | - |
| 6.3 | T6-SW-3 | 0.153 | 11.3 | n.d. | 1.2 | 13.2 | n.d. | 6.6 | 14.3 | 26.9 | - |
| 6.9 | T6-SW-4 | 0.171 | 11.3 | n.d. | n.d. | 10.9 | n.d. | 7.9 | 19.6 | 32.4 | - |
| 7.3 | T6-SW-5 | 0.149 | 11.3 | n.d. | n.d. | 10.8 | n.d. | 7.6 | 22.4 | 34.9 | - |
| 7.9 | T6-SW-6 | 0.226 | 8.4 | n.d. | 1.0 | 11.5 | n.d. | 6.9 | 14.9 | 21.5 | - |
| 8.8 | T6-SW-7 | 0.367 | 11.3 | n.d. | n.d. | 9.1 | n.d. | 8.1 | 14.4 | 17.5 | - |
| 9.9 | T6-SW-8 | 0.376 | 8.4 | n.d. | 1.1 | 10.9 | n.d. | 7.6 | 19.0 | 21.5 | - |
| 11.0 | T6-SW-9 | 0.349 | 5.6 | n.d. | n.d. | 9.8 | n.d. | 6.7 | 13.8 | 16.0 | - |

n.d. = not detected

*Organic Base Layer Experiment 2 (OIF-2)*

| Day | Sample | H$^+$ | Cl$^-$ | SO$_4^{2-}$ | NO$_3^-$ | NH$_4^+$ | Na$^+$ | K$^+$ | Mg$^{2+}$ | Ca$^{2+}$ | DOC |
|-----|--------|-------|--------|-------------|----------|----------|--------|-------|-----------|-----------|-----|
| 0.0 | T7-BS-1 | 0.217 | 33.8 | 12.5 | 2.9 | 15.5 | 20.6 | 8.1 | 34.0 | 73.4 | - |
| 0.0 | T7-BS-2 | 0.217 | 36.6 | 12.5 | 2.2 | 15.3 | 18.0 | 8.2 | 29.4 | 58.4 | - |
| 1.0 | T7-OW-1 | 0.251 | 137.8 | 81.2 | 16.3 | 29.3 | 110.1 | 73.4 | 53.7 | 104.6 | - |
| 1.6 | T7-OW-2 | 0.347 | 129.4 | 68.7 | 12.6 | 30.2 | 88.3 | 92.8 | 58.5 | 107.3 | - |
| 2.0 | T7-OW-3 | 0.365 | 121.0 | 66.6 | 9.7 | 31.1 | 35.6 | 54.2 | 24.4 | 54.1 | - |
| 2.6 | T7-OW-4 | 0.443 | 112.5 | 68.7 | 9.4 | 35.8 | 39.7 | 90.8 | 28.2 | 67.2 | - |
| 3.0 | T7-OW-5 | 0.387 | 98.5 | 45.8 | 6.2 | 32.7 | 12.7 | 45.8 | 13.7 | 25.0 | 11.0 |
| 3.6 | T7-OW-6 | 0.319 | 59.1 | 22.9 | 3.1 | 31.1 | 14.1 | 59.5 | 8.5 | 29.3 | 11.0 |
| 4.7 | T7-OW-8 | 0.352 | 19.7 | 0.0 | 1.1 | 22.5 | 36.2 | 95.5 | 23.0 | 53.1 | 7.4 |
| 5.1 | T7-OW-9 | 0.254 | 22.5 | 8.3 | n.d. | 19.5 | 11.6 | 61.2 | 21.0 | 39.4 | 7.5 |
| 6.1 | T7-OW-10 | 0.290 | 19.7 | 10.4 | n.d. | 25.6 | 13.0 | 79.5 | 17.2 | 58.8 | 10.0 |
| 6.8 | T7-OW-11 | 0.373 | 19.7 | 14.6 | n.d. | 24.7 | 11.3 | 55.8 | 11.6 | 43.8 | 11.0 |
| 7.8 | T7-OW-12 | 0.266 | 11.3 | n.d. | n.d. | 23.6 | 8.3 | 69.2 | 11.4 | 40.3 | 12.0 |
| 8.8 | T7-OW-13 | 0.297 | 112.5 | 62.5 | n.d. | 22.3 | 56.1 | 91.4 | 36.0 | 79.1 | 7.2 |
| 2.6 | T7-SW-1 | 0.072 | 151.9 | 89.5 | 13.5 | 49.0 | 126.3 | 16.2 | 77.2 | 218.1 | - |
| 3.0 | T7-SW-2 | 0.084 | 106.9 | 56.2 | 11.6 | 43.2 | 74.5 | 12.4 | 52.3 | 161.2 | - |
| 3.6 | T7-SW-3 | 0.105 | 59.1 | 27.1 | 5.9 | 29.5 | 43.9 | 9.2 | 41.3 | 116.8 | - |
| 4.0 | T7-SW-4 | 0.136 | 42.2 | 8.3 | 4.0 | 21.1 | 27.9 | 8.8 | 37.7 | 94.8 | - |
| 4.7 | T7-SW-5 | 0.144 | 25.3 | 6.2 | 1.3 | 16.3 | 9.8 | 6.8 | 34.4 | 74.4 | - |
| 5.1 | T7-SW-6 | 0.151 | 16.9 | 6.2 | 1.1 | 14.2 | 7.1 | 6.9 | 31.4 | 56.4 | - |
| 6.1 | T7-SW-7 | 0.172 | 14.1 | 6.2 | n.d. | 12.8 | n.d. | 6.7 | 25.9 | 50.4 | - |
| 6.8 | T7-SW-8 | 0.185 | 8.4 | n.d. | n.d. | 12.0 | 2.8 | 6.4 | 27.6 | 44.9 | - |
| 7.8 | T7-SW-9 | 0.209 | 8.4 | 6.2 | n.d. | 10.9 | n.d. | 6.2 | 28.8 | 40.9 | - |
| 8.8 | T7-SW-10 | 0.228 | 8.4 | n.d. | 1.0 | 10.9 | n.d. | 5.8 | 27.2 | 41.9 | - |

n.d. = not detected

*Organic Base Layer Experiment 3 (OIF-3)*

| Day | Sample | H$^+$ | Cl$^-$ | SO$_4$$^{2-}$ | NO$_3$$^-$ | NH$_4$$^+$ | Na$^+$ | K$^+$ | Mg$^{2+}$ | Ca$^{2+}$ | DOC |
|-----|--------|-------|--------|---------------|------------|------------|--------|-------|-----------|-----------|-----|
| 0.0 | T8-BS-1 | 0.041 | 25.3 | 12.5 | 6.8 | 8.9 | 10.7 | 9.8 | 30.8 | 168.7 | 2.0 |
| 0.0 | T8-BS-2 | 0.041 | 28.1 | 12.5 | 6.1 | 9.2 | 12.0 | 10.0 | 31.1 | 173.2 | 1.5 |
| 0.8 | T8-OW-1 | 0.231 | 56.3 | 35.4 | 14.7 | 19.1 | 27.0 | 78.9 | 28.5 | 97.7 | 12.0 |
| 1.7 | T8-OW-2 | 0.398 | 64.7 | 58.3 | 8.7 | 57.7 | 42.0 | 138.3 | 74.3 | 262.1 | 30.0 |
| 2.6 | T8-OW-3 | 0.298 | 42.2 | 31.2 | 4.5 | 49.1 | 21.8 | 112.9 | 47.8 | 183.8 | 19.0 |
| 3.1 | T8-OW-4 | 0.259 | 30.9 | 18.7 | 1.6 | 39.3 | 16.3 | 96.4 | 34.7 | 157.7 | - |
| 3.6 | T8-OW-5 | 0.206 | 22.5 | 10.4 | n.d. | 32.0 | 13.6 | 59.8 | 26.7 | 108.0 | 16.0 |
| 4.1 | T8-OW-6 | 0.206 | 16.9 | n.d. | n.d. | 27.0 | 7.9 | 71.9 | 24.8 | 119.9 | - |
| 4.6 | T8-OW-7 | 0.160 | 11.3 | 8.3 | n.d. | 20.1 | 21.7 | 56.1 | 15.5 | 79.7 | 9.5 |
| 5.1 | T8-OW-8 | 0.167 | 8.4 | 8.3 | n.d. | 19.8 | 9.2 | 55.1 | 14.3 | 73.4 | - |
| 5.7 | T8-OW-9 | 0.148 | 5.6 | 4.2 | n.d. | 18.0 | 5.2 | 26.2 | n.d. | 39.8 | - |
| 6.7 | T8-OW-10 | 0.160 | 2.8 | 4.2 | n.d. | 19.8 | 1.9 | 45.4 | 6.3 | 61.6 | 6.2 |
| 9.7 | T8-OW-11 | 0.100 | 5.6 | n.d. | n.d. | 21.1 | 4.8 | 32.3 | 13.2 | 59.2 | - |
| 10.7 | T8-OW-12 | 0.081 | 98.5 | 58.3 | n.d. | 38.2 | 29.0 | 65.8 | 51.9 | 252.0 | 37.0 |
| 11.8 | T8-OW-13 | 0.398 | 87.2 | 79.1 | n.d. | 59.7 | 11.0 | 59.2 | 69.4 | 426.4 | 41.0 |
| 3.1 | T8-SW-1 | 0.215 | 16.9 | 10.4 | 4.3 | 14.1 | 3.0 | 8.6 | 29.7 | 100.3 | - |
| 3.6 | T8-SW-2 | 0.189 | 11.3 | 4.2 | 2.4 | 11.2 | n.d. | 7.8 | 28.9 | 79.3 | - |
| 4.1 | T8-SW-3 | 0.143 | 8.4 | 4.2 | n.d. | 9.5 | 72.8 | 8.0 | 28.9 | 75.9 | - |
| 4.6 | T8-SW-4 | 0.206 | 5.6 | n.d. | n.d. | 7.8 | 6.6 | 6.5 | 26.2 | 46.4 | - |
| 5.1 | T8-SW-5 | 0.198 | 2.8 | n.d. | n.d. | 8.1 | 67.8 | 6.3 | 25.1 | 46.4 | - |
| 5.7 | T8-SW-6 | 0.179 | 2.8 | n.d. | n.d. | 7.5 | n.d. | 6.1 | 24.0 | 41.4 | - |
| 6.7 | T8-SW-7 | 0.188 | 8.4 | n.d. | n.d. | 6.2 | n.d. | 6.1 | 28.7 | 46.4 | - |
| 9.7 | T8-SW-8 | 0.108 | 2.8 | n.d. | n.d. | 5.9 | n.d. | 6.6 | 40.7 | 61.4 | - |

n.d. = not detected

*Mineral Soil Base Layer Experiment 1 (MIF-1)*

| Day | Sample | $H^+$ | $Cl^-$ | $SO_4^{2-}$ | $NO_3^-$ | $NH_4^+$ | $Na^+$ | $K^+$ | $Mg^{2+}$ | $Ca^{2+}$ | DOC |
|-----|--------|-------|--------|-------------|----------|----------|--------|-------|-----------|-----------|-----|
| 0.0 | T9-BS-1 | 0.029 | 33.8 | 22.9 | 7.4 | 27.0 | 20.6 | 4.9 | 18.2 | 113.8 | - |
| 0.0 | T9-BS-2 | 0.029 | 28.1 | 22.9 | 7.5 | 32.4 | 19.8 | 3.1 | 25.9 | 113.5 | - |
| 1.3 | T9-MW-1 | 0.045 | 151.9 | 333.1 | 34.2 | 19.0 | 114.7 | 16.6 | 246.7 | 786.0 | - |
| 1.9 | T9-MW-2 | 0.048 | 73.1 | 143.7 | 25.3 | 18.3 | 83.3 | 14.9 | 154.9 | 509.2 | - |
| 2.3 | T9-MW-3 | 0.029 | 67.5 | 137.4 | 25.8 | 15.4 | 78.7 | 16.4 | 162.9 | 536.4 | - |
| 2.9 | T9-MW-4 | 0.039 | 67.5 | 122.8 | 25.7 | 18.1 | 74.5 | 16.5 | 157.4 | 520.9 | - |
| 3.3 | T9-MW-5 | 0.047 | 70.3 | 127.0 | 26.7 | 23.5 | 75.9 | 17.8 | 165.2 | 568.4 | - |
| 3.9 | T9-MW-6 | 0.036 | 67.5 | 120.8 | 24.3 | 26.1 | 64.5 | 20.5 | 159.0 | 506.3 | - |
| 4.3 | T9-MW-7 | 0.040 | 59.1 | 106.2 | 20.7 | 30.9 | 64.5 | 15.1 | 136.9 | 497.6 | - |
| 4.9 | T9-MW-8 | 0.037 | 47.8 | 85.4 | 15.8 | 27.7 | 57.9 | 13.7 | 114.4 | 397.0 | - |
| 5.3 | T9-MW-9 | 0.018 | 42.2 | 64.5 | 10.1 | 20.7 | 54.6 | 14.1 | 106.6 | 385.5 | - |
| 6.4 | T9-MW-10 | 0.033 | 30.9 | 52.0 | 5.4 | 13.8 | 48.1 | 12.1 | 95.3 | 342.8 | 7.7 |
| 7.0 | T9-MW-11 | 0.037 | 25.3 | 37.5 | 3.7 | 13.2 | 42.7 | 10.7 | 82.9 | 303.7 | - |
| 7.4 | T9-MW-24 | 0.030 | 22.5 | 25.0 | 3.1 | 12.9 | 21.9 | 11.1 | 74.7 | 274.2 | - |
| 7.9 | T9-MW-13 | 0.050 | 16.9 | 18.7 | 2.9 | 14.2 | 37.4 | 11.2 | 68.4 | 251.7 | - |
| 8.3 | T9-MW-14 | 0.043 | 16.9 | 12.5 | 2.9 | 16.0 | 31.2 | 9.9 | 48.7 | 185.8 | - |
| 9.0 | T9-MW-15 | 0.048 | 16.9 | 10.4 | 2.6 | 15.2 | 26.0 | 10.2 | 62.0 | 226.7 | 4.2 |
| 9.9 | T9-MW-16 | 0.048 | 14.1 | 8.3 | 2.2 | 14.5 | 19.4 | 9.4 | 48.1 | 184.4 | - |
| 11.1 | T9-MW-17 | 0.045 | 14.1 | 12.5 | 1.8 | 14.2 | 12.7 | 5.7 | 26.1 | 113.9 | - |
| 12.0 | T9-MW-18 | 0.062 | 14.1 | 25.0 | 1.4 | 12.9 | 26.4 | 11.5 | 42.8 | 162.9 | - |
| 13.1 | T9-MW-19 | 0.060 | 30.9 | 91.6 | 1.0 | 7.0 | 38.1 | 9.6 | 100.4 | 340.8 | - |
| 14.1 | T9-MW-20 | 0.043 | 78.8 | 270.7 | n.d. | 12.6 | 70.1 | 17.1 | 224.2 | 711.6 | - |
| 15.9 | T9-MW-21 | 0.046 | 154.7 | 478.8 | n.d. | 6.9 | 99.6 | 19.0 | 341.0 | 1099.8 | - |
| 5.3 | T9-SW-1 | 0.040 | 56.3 | 45.8 | 13.2 | 58.3 | 32.4 | 8.8 | 87.7 | 366.8 | - |
| 6.4 | T9-SW-2 | 0.037 | 30.9 | 25.0 | 8.9 | 40.0 | 21.7 | 3.4 | 82.0 | 300.4 | - |
| 7.0 | T9-SW-3 | 0.048 | 16.9 | 6.2 | 4.9 | 26.9 | 13.5 | 1.2 | 74.1 | 221.7 | - |
| 7.4 | T9-SW-4 | 0.046 | 25.3 | 6.2 | 3.4 | 20.5 | 10.0 | 0.5 | 72.5 | 183.6 | - |
| 7.9 | T9-SW-5 | 0.070 | 25.3 | 10.4 | 2.8 | 16.2 | 5.1 | n.d. | 79.5 | 148.0 | - |
| 8.3 | T9-SW-6 | 0.041 | 14.1 | 10.4 | 3.3 | 21.4 | 8.7 | n.d. | 80.6 | 163.5 | - |
| 9.0 | T9-SW-7 | 0.055 | 16.9 | 6.2 | 3.2 | 18.0 | 7.3 | n.d. | 79.2 | 166.8 | - |
| 9.9 | T9-SW-8 | 0.023 | 16.9 | 6.2 | 3.4 | 21.0 | 7.0 | n.d. | 79.0 | 160.2 | - |
| 11.1 | T9-SW-9 | 0.050 | 25.3 | 27.1 | 3.4 | 16.8 | 11.5 | 1.8 | 77.4 | 190.0 | - |
| 12.0 | T9-SW-10 | 0.035 | 14.1 | n.d. | 2.5 | 15.2 | 5.0 | n.d. | 97.3 | 166.6 | - |
| 13.1 | T9-SW-11 | 0.062 | 14.1 | n.d. | 1.9 | 14.5 | 3.0 | n.d. | 86.1 | 133.5 | - |
| 14.1 | T9-SW-12 | 0.062 | 11.3 | n.d. | 1.5 | 14.5 | 3.1 | n.d. | 76.4 | 105.9 | - |
| 15.9 | T9-SW-13 | 0.070 | 5.6 | n.d. | n.d. | 9.5 | 3.3 | n.d. | 76.7 | 103.0 | - |

n.d. = not detected

*Mineral Soil Base Layer Experiment 2 (MIF-2)*

| Day | Sample | H$^+$ | Cl$^-$ | SO$_4^{2-}$ | NO$_3^-$ | NH$_4^+$ | Na$^+$ | K$^+$ | Mg$^{2+}$ | Ca$^{2+}$ | DOC |
|---|---|---|---|---|---|---|---|---|---|---|---|
| 0.0 | T10-BS-1 | 0.029 | 33.8 | 22.9 | 7.4 | 27.0 | 20.6 | 4.9 | 18.2 | 113.8 | - |
| 0.0 | T10-BS-2 | 0.029 | 28.1 | 22.9 | 7.5 | 32.4 | 19.8 | 3.1 | 25.9 | 113.5 | - |
| 0.7 | T10-MW-1 | 0.086 | 106.9 | 229.0 | 14.9 | 21.3 | 57.4 | 15.8 | 141.9 | 478.9 | - |
| 1.1 | T10-MW-2 | 0.067 | 75.9 | 147.8 | 14.7 | 18.6 | 66.2 | 14.2 | 117.8 | 402.6 | - |
| 1.6 | T10-MW-3 | 0.061 | 61.9 | 118.7 | 14.8 | 18.2 | 62.1 | 14.4 | 119.2 | 408.9 | - |
| 2.1 | T10-MW-4 | 0.033 | 50.6 | 81.2 | 13.2 | 17.7 | 62.1 | 14.3 | 110.8 | 369.7 | - |
| 2.6 | T10-MW-5 | 0.042 | 42.2 | 66.6 | 11.5 | 16.3 | 63.1 | 13.3 | 70.4 | 342.0 | - |
| 3.0 | T10-MW-6 | 0.036 | 30.9 | 37.5 | 7.0 | 16.4 | 43.6 | 12.8 | 86.6 | 290.9 | - |
| 3.6 | T10-MW-7 | 0.043 | 19.7 | 22.9 | 5.5 | 17.2 | 34.3 | 13.0 | 71.3 | 247.8 | - |
| 4.0 | T10-MW-8 | 0.045 | 14.1 | 18.7 | 4.8 | 16.8 | 31.8 | 12.6 | 58.2 | 206.7 | - |
| 4.6 | T10-MW-9 | 0.045 | 14.1 | 16.7 | 3.3 | 15.3 | 27.2 | 11.1 | 66.9 | 232.4 | - |
| 5.1 | T10-MW-10 | 0.065 | 16.9 | 25.0 | 2.7 | 16.2 | 28.6 | 9.7 | 61.6 | 214.7 | - |
| 5.6 | T10-MW-11 | 0.077 | 19.7 | 39.6 | 2.3 | 15.6 | 33.2 | 10.3 | 70.8 | 243.7 | - |
| 6.6 | T10-MW-24 | 0.070 | 33.8 | 89.5 | 1.6 | 18.5 | 82.8 | 39.8 | 98.7 | 330.5 | - |
| 7.1 | T10-MW-13 | 0.068 | 36.6 | 106.2 | 1.3 | 20.3 | 102.3 | 18.4 | 108.4 | 362.1 | - |
| 7.6 | T10-MW-14 | 0.065 | 39.4 | 131.2 | n.d. | 20.6 | 139.7 | 17.9 | 123.3 | 416.0 | - |
| 8.6 | T10-MW-15 | 0.066 | 53.4 | 168.6 | n.d. | 21.4 | 126.4 | 22.9 | 147.9 | 478.7 | - |
| 9.7 | T10-MW-18 | 0.063 | 56.3 | 208.2 | n.d. | 20.7 | 106.7 | 22.0 | 174.2 | 583.2 | - |
| 10.9 | T10-MW-16 | 0.031 | 73.1 | 270.7 | n.d. | 21.0 | 57.7 | 31.6 | 228.7 | 743.3 | - |
| 4.6 | T10-SW-1 | 0.042 | 19.7 | 10.4 | 5.2 | 32.4 | 9.7 | 0.0 | 61.7 | 194.4 | - |
| 5.1 | T10-SW-2 | 0.043 | 19.7 | n.d. | 3.9 | 27.1 | 10.6 | 4.2 | 45.7 | 162.5 | - |
| 5.6 | T10-SW-3 | 0.049 | 16.9 | n.d. | 3.0 | 24.3 | 6.0 | 6.4 | 58.9 | 155.2 | - |
| 6.6 | T10-SW-4 | 0.040 | 180.0 | n.d. | 2.1 | 21.2 | 4.2 | 0.0 | 50.9 | 129.9 | - |
| 7.1 | T10-SW-5 | 0.047 | 19.7 | n.d. | 1.3 | 17.3 | 4.2 | 2.2 | 44.8 | 126.4 | - |
| 7.6 | T10-SW-6 | 0.048 | 11.3 | n.d. | 1.1 | 15.3 | 2.5 | 3.6 | 48.5 | 125.5 | - |

n.d. = not detected

# APPENDIX F: RAIN-ON-SNOW DATA

The rain-on-snow event that started in the afternoon of March 11, 2007 lasted a total of 22 hours and resulted in the greatest number of samples being collected at any one time during snowmelt. The grey line represents average intensity.

*Figure F.1. Hyetograph for the rain-on-snow event that started on March 11, 2007 (JD 70). The grey line represents the average rainfall intensity.*

# APPENDIX G: CHEMICAL COMPOSITION OF SNOW AND WATER SAMPLES FROM THE FIELD

This appendix contains the chemical composition of the individual samples collected at the forested observation site at Marmot Creek Research Basin, AB, during the 2007 snowmelt (Chapter 7).

      Columns: *Sample* is the code for the individual samples; *Julian Day* refers to the date and time of collection (JD 66 = March 7); the following columns show the ion concentrations for all major anions and cation in meq m$^{-3}$; DOC concentrations are in g m$^{-3}$; hyphens (–) indicate that no data is available; and *ICB* is the Ion Charge Balance for each sample (Equation 4.1).

## Snow (S)

| Sample | Julian Day | H$^+$ | Cl$^-$ | SO$_4$$^{2-}$ | NO$_3$$^-$ | NH$_4$$^+$ | Na$^+$ | K$^+$ | Mg$^{2+}$ | Ca$^{2+}$ | DOC | ICB |
|--------|-----------|-------|--------|--------|--------|--------|--------|-------|------|------|-----|-----|
| 7A | 66.4 | 0.509 | 11.3 | 14.6 | 0.7 | 7.9 | n.d. | 10.5 | 19.4 | 55.0 | - | 0.56 |
| 7B | 66.4 | 0.270 | 8.5 | 16.7 | 1.3 | 7.6 | n.d. | 7.1 | 10.2 | 37.0 | - | 0.40 |
| 8 | 67.4 | 0.415 | 5.6 | 20.8 | 0.7 | 6.6 | n.d. | 7.9 | 12.3 | 37.5 | - | 0.41 |
| 9 | 68.4 | 0.465 | 8.5 | 16.7 | 0.6 | 9.1 | n.d. | 12.6 | 20.3 | 62.5 | - | 0.61 |
| 10 | 69.8 | 0.229 | 2.8 | n.d. | 0.3 | 7.0 | n.d. | 7.2 | 12.6 | 56.0 | - | 0.93 |
| 11 | 70.4 | 0.424 | 5.6 | 4.2 | n.d. | 5.9 | n.d. | 15.9 | 28.1 | 74.5 | - | 0.85 |
| 12 | 71.2 | 0.453 | 8.5 | 14.6 | n.d. | 8.4 | n.d. | 18.7 | 37.8 | 79.0 | - | 0.72 |
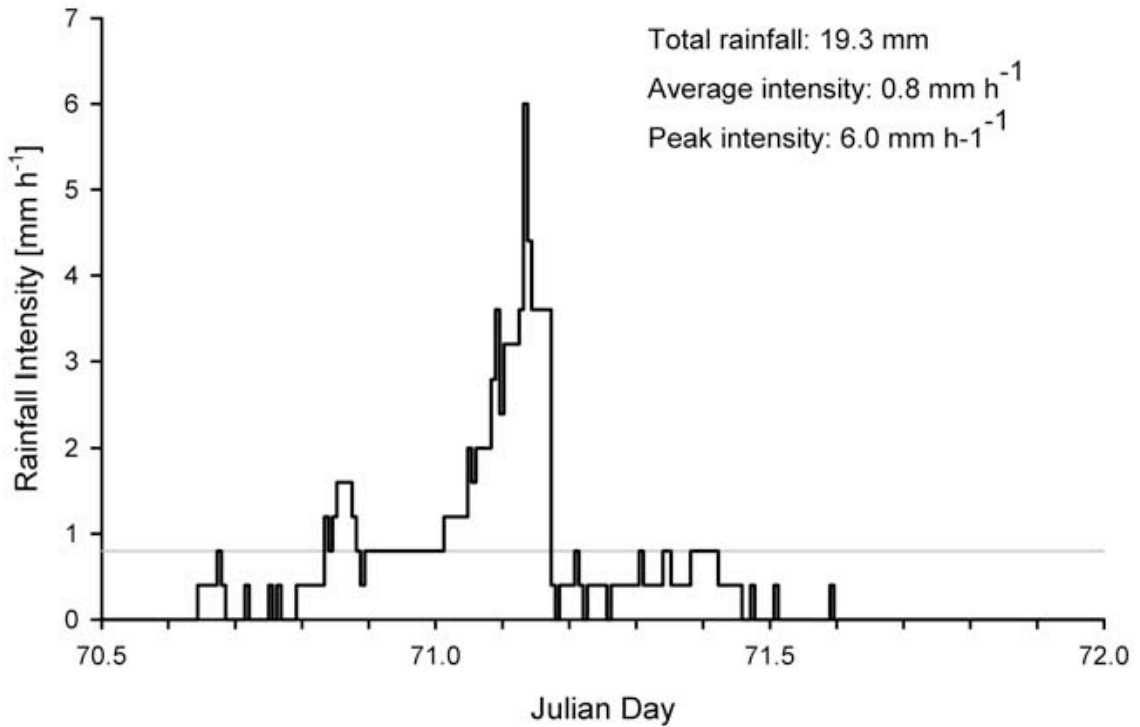
    n.d. = below detection limit

## Precipitation (P)

| Sample | Julian Day | H$^+$ | Cl$^-$ | SO$_4$$^{2-}$ | NO$_3$$^-$ | NH$_4$$^+$ | Na$^+$ | K$^+$ | Mg$^{2+}$ | Ca$^{2+}$ | DOC | ICB |
|--------|-----------|-------|--------|--------|--------|--------|--------|-------|------|------|-----|-----|
| 8 (snow) | 67.4 | 0.400 | 14.1 | 14.6 | 1.2 | 7.4 | 7.7 | n.d. | 8.2 | 49.6 | - | 0.42 |
| 12 (rain) | 71.2 | 2.582 | 8.5 | 33.3 | 0.9 | 6.8 | 7.9 | 8.3 | 23.3 | 55.2 | 10 | 0.42 |
| 16 (rain) | 75.4 | 0.407 | 16.9 | 6.3 | 0.2 | 6.7 | 9.3 | 6.3 | 12.9 | 44.1 | - | 0.55 |

    n.d. = below detection limit

## Organic Soil Water (OSW)

| Sample | Julian Day | H$^+$ | Cl$^-$ | SO$_4^{2-}$ | NO$_3^-$ | NH$_4^+$ | Na$^+$ | K$^+$ | Mg$^{2+}$ | Ca$^{2+}$ | DOC | ICB |
|--------|-----------|-------|--------|-------------|----------|----------|--------|-------|-----------|-----------|-----|-----|
| #1-11A | 70.4 | 0.982 | 14.1 | 29.2 | n.d. | 7.2 | 83.5 | 240.7 | 115.7 | 334.7 | - | 0.90 |
| #1-11B | 70.7 | 1.380 | 22.5 | 50.0 | n.d. | 9.9 | 74.6 | 359.3 | 163.8 | 452.0 | 84.0 | 0.87 |
| #1-12 | 71.2 | 1.361 | 8.5 | 16.7 | n.d. | 10.5 | 72.9 | 55.5 | 19.8 | 62.2 | 25.0 | 0.80 |
| #2-8 | 67.4 | 1.009 | 19.7 | 39.6 | n.d. | 8.9 | 76.9 | 56.1 | 95.8 | 320.5 | 54.0 | 0.81 |
| #2-11B | 70.7 | 1.225 | 5.6 | 27.1 | n.d. | 6.7 | 11.1 | 59.7 | 95.8 | 338.1 | 54.0 | 0.88 |
| #2-12 | 71.2 | 0.736 | 11.3 | 25.0 | n.d. | 10.3 | 0.5 | 49.0 | 37.1 | 146.1 | 30.0 | 0.74 |
| #3-8 | 67.4 | 0.108 | 22.5 | 33.3 | n.d. | 9.8 | 7.7 | 36.6 | 15.3 | 68.6 | - | 0.42 |
| #3-12 | 71.2 | 3.319 | 14.1 | 22.9 | n.d. | 10.9 | 6.0 | 19.3 | 10.3 | 82.3 | 15.0 | 0.56 |

n.d. = below detection limit

## Overland Flow (OSW*)

| Sample | Julian Day | H$^+$ | Cl$^-$ | SO$_4^{2-}$ | NO$_3^-$ | NH$_4^+$ | Na$^+$ | K$^+$ | Mg$^{2+}$ | Ca$^{2+}$ | DOC | ICB |
|--------|-----------|-------|--------|-------------|----------|----------|--------|-------|-----------|-----------|-----|-----|
| #3-11 | 70.7 | 1.556 | 8.5 | 22.9 | n.d. | 6.0 | 0.0 | 68.3 | 79.1 | 159.8 | 35.0 | 0.82 |
| #3-12 | 71.2 | 3.319 | 31.0 | 100.0 | n.d. | 7.3 | 5.6 | 68.4 | 83.5 | 179.5 | 44.0 | 0.45 |
| #3-16 | 75.4 | 0.307 | 87.3 | 41.7 | n.d. | 6.0 | 88.7 | 26.2 | 41.2 | 131.7 | - | 0.39 |

n.d. = below detection limit

## Mineral Soil Water (MSW)

| Sample | Julian Day | H$^+$ | Cl$^-$ | SO$_4^{2-}$ | NO$_3^-$ | NH$_4^+$ | Na$^+$ | K$^+$ | Mg$^{2+}$ | Ca$^{2+}$ | DOC | ICB |
|--------|-----------|-------|--------|-------------|----------|----------|--------|-------|-----------|-----------|-----|-----|
| #2-12 | 71.2 | 1.271 | 8.5 | 18.8 | n.d. | 12.4 | 9.3 | 26.8 | 42.7 | 167.3 | 35.0 | 0.81 |
| #3-12 | 71.2 | 0.847 | 14.1 | 33.3 | n.d. | 7.5 | 2.8 | 6.6 | 32.3 | 109.5 | 15.0 | 0.54 |
| #3-16 | 75.4 | 0.211 | 14.1 | 12.5 | n.d. | 9.1 | 2.6 | 6.9 | 38.2 | 120.7 | - | 0.74 |
| #3-18 | 77.7 | 0.149 | - | - | n.d. | 18.0 | 8.0 | 25.9 | 80.9 | 220.8 | - | - |

n.d. = below detection limit

*Ponding Water, site (PW-site)*

| Sample | Julian Day | H⁺ | Cl⁻ | SO₄²⁻ | NO₃⁻ | NH₄⁺ | Na⁺ | K⁺ | Mg²⁺ | Ca²⁺ | DOC | ICB |
|--------|-----------|------|------|-------|------|------|-----|------|-------|-------|------|------|
| #2-10  | 69.76 | 0.436 | 36.6 | 31.3 | n.d. | 5.4 | 6.9 | 43.2 | 68.8  | 254.1 | 35.0 | 0.70 |
| #2-11A | 70.42 | 0.362 | 31.0 | 33.3 | n.d. | 5.2 | 3.3 | 53.3 | 110.1 | 351.2 | 48.0 | 0.78 |
| #2-11B | 70.72 | 0.491 | 25.4 | 25.0 | n.d. | 5.5 | 8.3 | 44.3 | 71.1  | 295.4 | 45.0 | 0.79 |
| #2-12  | 71.22 | 0.445 | 14.1 | 16.7 | n.d. | 5.2 | 3.1 | 16.7 | 15.6  | 141.6 | 29.0 | 0.71 |
| #3-10  | 69.76 | 0.205 | 22.5 | 22.9 | n.d. | 5.6 | 5.5 | 30.8 | 24.8  | 145.6 | 23.0 | 0.65 |
| #3-11A | 70.42 | 0.220 | 11.3 | 16.7 | n.d. | 5.5 | 4.2 | 46.5 | 53.8  | 237.8 | 28.0 | 0.85 |
| #3-11B | 70.72 | 0.216 | 16.9 | 16.7 | n.d. | 6.0 | 9.0 | 28.7 | 32.2  | 210.6 | 21.0 | 0.79 |
| #3-12  | 71.22 | 0.137 | 16.9 | 20.8 | n.d. | 6.5 | 7.2 | 27.6 | 20.9  | 155.8 | 15.0 | 0.70 |

n.d. = below detection limit

*Ponding Water, snow (PW-snow)*

| Sample | Julian Day | H⁺ | Cl⁻ | SO₄²⁻ | NO₃⁻ | NH₄⁺ | Na⁺ | K⁺ | Mg²⁺ | Ca²⁺ | DOC | ICB |
|--------|-----------|--------|------|-------|------|------|-----|-------|-------|-------|------|------|
| 2#1-7  | 66.4 | 0.0004 | 90.1 | 41.7 | 0.3  | 4.9 | 8.7 | 385.3 | 188.3 | 604.9 | 30.0 | 0.80 |
| 2#1-9  | 68.4 | 0.001  | 39.4 | 18.8 | n.d. | 7.3 | 4.8 | 150.9 | 196.5 | 711.1 | -    | 0.90 |
| 2#1-11 | 70.4 | 0.045  | 25.4 | 8.3  | n.d. | 5.5 | 7.0 | 31.7  | 15.5  | 159.2 | -    | 0.73 |
| 2#3-7  | 66.4 | 0.071  | 16.9 | 16.7 | n.d. | 4.5 | 5.0 | 76.4  | 17.3  | 97.0  | -    | 0.71 |
| 2#6-11 | 70.4 | 0.136  | 8.5  | n.d. | 4.3  | 5.0 | 3.8 | 19.5  | 40.8  | 114.4 | -    | 0.87 |

n.d. = below detection limit

*Ponding Water, soil (PW-soil)*

| Sample | Julian Day | H⁺ | Cl⁻ | SO₄²⁻ | NO₃⁻ | NH₄⁺ | Na⁺ | K⁺ | Mg²⁺ | Ca²⁺ | DOC | ICB |
|--------|-----------|--------|-------|-------|------|------|------|-------|-------|-------|------|------|
| 2#2-7  | 66.4 | 0.0001 | 109.9 | 50.0 | 0.7  | 7.9 | 13.1 | 372.5 | 184.3 | 649.9 | -    | 0.77 |
| 2#2-9  | 68.7 | 0.0004 | 50.7  | 33.3 | n.d. | 6.0 | n.d. | 212.6 | 209.0 | 698.8 | 26.0 | 0.86 |
| 2#2-11 | 70.4 | 0.012  | 25.4  | 6.3  | n.d. | 5.6 | 4.6  | 151.4 | 174.4 | 663.7 | 16.0 | 0.94 |
| 2#5-7  | 66.4 | 0.004  | 22.5  | 33.3 | 8.6  | 5.2 | 6.1  | 84.7  | 93.9  | 176.2 | 24.0 | 0.70 |

n.d. = below detection limit

# APPENDIX H: WEIGHTED AVERAGE CONCENTRATION

The weighted ion concentrations of snow and rain, $C_{ave}$, used in section 7.3 were calculated using following equation

$$C_{ave} = \frac{\left(\left(C_{snow} \cdot V_{snow}\right) + \left(C_{rain} \cdot V_{rain}\right)\right)}{V_{snow} + V_{rain}} \qquad (H.1)$$

where $C_{snow}$ and $C_{rain}$ are the ion concentrations measured in the snow and the rain, respectively, and $V_{snow}$ and $V_{rain}$ are the intensities of snowmelt and rainfall, respectively.

The concentrations of the individual ions in the snow and rain are given in the following table

| Ion | $H^+$ | $Cl^-$ | $SO_4^{2-}$ | $NO_3^-$ | $NH_4^+$ | $Na^+$ | $K^+$ | $Mg^{2+}$ | $Ca^{2+}$ | DOC |
|-----|-------|--------|-------------|----------|----------|--------|-------|-----------|-----------|-----|
| Snow | 0.5 | 8.5 | 14.6 | n.d. | 8.4 | 7.7 | 18.7 | 37.8 | 79.0 | 10.0 |
| Rain | 2.6 | 8.5 | 33.3 | 0.9 | 6.8 | 7.9 | 8.3 | 23.3 | 55.2 | 10.0 |

All major anion and cation concentrations are given in meq $m^{-3}$; DOC concentrations are given in g $m^{-3}$. Nitrate concentrations were all less than the detection limit (n.d; 1.0 meq $m^{-3}$). Average intensities of snowmelt and rainfall were 0.5 kg $m^{-2}$ $h^{-1}$ and 0.8 kg $m^{-2}$ $h^{-1}$, respectively (Appendix F).

Calculation example for $H^+$ concentration:

$$C_{H^+ \, ave} = \frac{\left(\left(0.5 \cdot 0.5\right) + \left(2.6 \cdot 0.8\right)\right)}{\left(0.5 + 0.8\right)} = \frac{\left(0.25 + 2.1\right)}{1.3} = 1.8 \; meq \; m^{-3}$$

The resulting weighted average concentrations are:

| Ion | $H^+$ | $Cl^-$ | $SO_4^{2-}$ | $NO_3^-$ | $NH_4^+$ | $Na^+$ | $K^+$ | $Mg^{2+}$ | $Ca^{2+}$ | DOC |
|-----|-------|--------|-------------|----------|----------|--------|-------|-----------|-----------|-----|
| Weighted average | 1.8 | 8.5 | 26.1 | 0.6 | 7.4 | 4.9 | 12.3 | 28.9 | 64.3 | 10.0 |